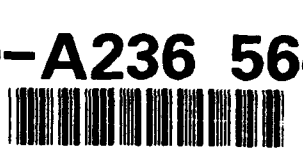

(2)

WRDC-TR-89-2031

IMPROVED BORON FOR ENHANCED COMBUSTION

ALLIED-SIGNAL ENGINEERED
MATERIALS RESEARCH CENTER
50 EAST ALGONQUIN ROAD
DES PLAINES IL 60017-5016

JUNE 1990

Interim Report for Period February 1986 - December 1988

Approved for public release; distribution unlimited.

AERO PROPULSION AND POWER LABORATORY
WRIGHT RESEARCH AND DEVELOPMENT CENTER
AIR FORCE SYSTEMS COMMAND
WRIGHT-PATTERSON AIR FORCE BASE, OHIO 45433-656

NOTICE

When Government drawings, specifications, or other data are used for any purpose other than in connection with a definitely Government-related procurement, the United States Government incurs no responsibility or any obligation whatsoever. The fact that the government may have formulated or in any way supplied the said drawings, specifications, or other data, is not to be regarded by implication, or otherwise in any manner construed, as licensing the holder, or any other person or corporation; or as conveying any rights or permission to manufacture, use, or sell any patented invention that may in any way be related thereto.

THIS REPORT HAS BEEN REVIEWED BY THE OFFICE OF PUBLIC AFFAIRS (ASD/PA) AND IS RELEASABLE TO THE NATIONAL TECHNICAL INFORMATION SERVICE (NTIS). AT NTIS IT WILL BE AVAILABLE TO THE GENERAL PUBLIC INCLUDING FOREIGN NATIONS.

This technical report has been reviewed and is approved for publication.

Charlotte R. Eigel

CHARLOTTE R. EIGEL
Fuels Branch
Fuels and Lubrication Division
Aero Propulsion and Power Laboratory

Charles L. Delaney

CHARLES L. DELANEY, Chief
Fuels Branch
Fuels and Lubrication Division
Aero Propulsion and Power Laboratory

FOR THE COMMANDER

L. S. Harootyan Jr

LEO S. HAROOTYAN, JR, Chief
Fuels and Lubrication Division
Aero Propulsion and Power Directorate

If your address has changed, if you wish to be removed from our mailing list, or if the addressee is no longer employed by your organization please notify WRDC/POSF, WPAFB, OH 45433-6563 to help us maintain a current mailing list.

Copies of this report should not be returned unless return is required by security considerations, contractual obligations, or notice on a specific document.

REPORT DOCUMENTATION PAGE

Form Approved
OMB No. 0704-0188

1a. REPORT SECURITY CLASSIFICATION UNCLASSIFIED	1b. RESTRICTIVE MARKINGS
2a. SECURITY CLASSIFICATION AUTHORITY	3. DISTRIBUTION/AVAILABILITY OF REPORT APPROVED FOR PUBLIC RELEASE: DISTRIBUTION UNLIMITED
2b. DECLASSIFICATION/DOWNGRADING SCHEDULE	
4. PERFORMING ORGANIZATION REPORT NUMBER(S)	5. MONITORING ORGANIZATION REPORT NUMBER(S) WRDC-TR-89-2031
6a. NAME OF PERFORMING ORGANIZATION ALLIED-SIGNAL ENGINEERED MATERIAL RES. CNTR.	6b. OFFICE SYMBOL (If applicable)
7a. NAME OF MONITORING ORGANIZATION WRIGHT RESEARCH & DEVELOPMENT CENTER AEROPROPULSION & POWER LAB (WRDC/POSF)	
6c. ADDRESS (City, State, and ZIP Code) 50 E. ALGONQUIN ROAD DES PLAINES IL 60017-5016	7b. ADDRESS (City, State, and ZIP Code) WRIGHT-PATTERSON AFB OH 45433-6563
8a. NAME OF FUNDING/SPONSORING ORGANIZATION	8b. OFFICE SYMBOL (If applicable)
9. PROCUREMENT INSTRUMENT IDENTIFICATION NUMBER F33615-85-C-2550	
8c. ADDRESS (City, State, and ZIP Code)	10. SOURCE OF FUNDING NUMBERS

PROGRAM ELEMENT NO	PROJECT NO	TASK NO	WORK UNIT ACCESSION NO
62203	3048	05	49

11. TITLE (Include Security Classification)
IMPROVED BORON FOR ENHANCED COMBUSTION

12. PERSONAL AUTHOR(S)
MILLER, STEVEN (CALLERY CHEMICAL CO) & MEZZA, THOMAS M. (ALLIED-SIGNAL EMRC)

13a. TYPE OF REPORT	13b. TIME COVERED	14. DATE OF REPORT (Year, Month, Day)	15. PAGE COUNT
INTERIM	FROM FEB 86 TO DEC 88	June 1990	257

16. SUPPLEMENTARY NOTATION
This report was prepared as Task 3 of the Scholarly Research Program (Contract F33615-86C-2633) with UOP since funding for its preparation was redirected from this contract

17. COSATI CODES		
FIELD	GROUP	SUB-GROUP
21	02	
07	02	

18. SUBJECT TERMS (Continue on reverse if necessary and identify by block number)
BORON, BORON PRODUCTION, BORON RAMJET FUELS, BORON OXIDE, BORON IGNITION

19. ABSTRACT (Continue on reverse if necessary and identify by block number)

The objective of this effort was to develop a domestic commercial process for producing pure, spherical, amorphous boron particles with diameters in the range of 0.5 to 3 microns. Such particles could offer improved combustion and processing properties over present commercial boron powders when incorporated into slurry and solid fuels. The approach was to start with the Callery process for making high-purity, submicron size boron, then change process variables and add a recycle in an attempt to increase particle size. Pure, spherical particles approaxhing 0.1 micron were achieved. Allied-Signal EMRC provided the overall program management, boron analysis and characterization.

20. DISTRIBUTION/AVAILABILITY OF ABSTRACT	21. ABSTRACT SECURITY CLASSIFICATION
☒ UNCLASSIFIED/UNLIMITED ☐ SAME AS RPT ☐ DTIC USERS	UNCLASSIFIED
22a. NAME OF RESPONSIBLE INDIVIDUAL CHARLOTTE R. FIGEL	22b. TELEPHONE (Include Area Code) (513)255-7405
	22c. OFFICE SYMBOL WRDC/POSF

DD Form 1473, JUN 86 Previous editions are obsolete SECURITY CLASSIFICATION OF THIS PAGE

TABLE OF CONTENTS

TABLE OF CONTENTS (Concluded)

LIST OF FIGURES

LIST OF TABLES

I. PHASE I SUMMARY

Due to processing and combustion difficulties experienced when using high levels of elemental boron for fuel preparations, a need has arisen for improved boron particle design. The particle characteristics sought in this Phase I work have been determined by others to be: (1) spherical shape, (2) particle diameters in the range of 0.5 to 3 micrometers, (3) purity greater than 99 wt. %, and (4) producible by United States facilities and materials. A further desirable trait would be economically attractive cost, although there is no present domestic supplier capable of supplying this type of boron. Other important considerations for a source of fuel-quality boron include a manufacturing process capable of reliable scale-up to the product quantities required, and a product particle that exhibits low tendencies of self-agglomeration into masses.

The work in this report is pursuant to the prime contract executed February 28, 1986 between Signal Research Center and the Department of the Air Force, Improved Boron for Enhanced Combustion (F33615-85-C-2550), and the subcontract executed between Signal Research Center and Callery Chemical Company on April 18, 1986. Callery's effort began on April 28, 1986 with the formulation of a construction work schedule. Assembly of the experimental system (Task 1.1) was completed on September 22, 1986, and proveout of this system combined with training of the operating staff (Task 1.2) concluded on October 23, 1986. The experimental studies of the variables (Task 1.3) commenced on November 12, 1986, and in March, 1987 a no-cost extension to September 30, 1987 was granted to allow completion of Task 1.3.

Approximately two-thirds of the original variable study was conducted before an oral progress review was held by Signal and Callery at Wright-Patterson Air Force Base on July 15, 1987. Upon review of the data, certain modifications to the experimental study were proposed so that a potentially useful alternative of boron particle recycle could be explored for the benefit of the Air Force. These modifications were allowed, as "modified Task 1.4", in lieu of the original Task 1.4 entitled "Scale-up Demonstration". Subsequently, Task 1.3 experimental studies were completed on September 30, 1987, and the modified Task 1.4 recycle studies were completed, at no additional cost to the Air Force, on November 24, 1987.

Signal Research Center's experimental effort during Phase I has consisted of Task 1.5, "Particle Characterization", in which both the physical and chemical properties of Callery's boron particles have been determined. Certain methods of analysis, especially the photomicrographic technique leading to measurement of particle size, have required some development work by Signal and are discussed in the appropriate section of this report. The concluding task of Phase I is Task 1.6 "Final Report", which is contained herein and is a complete record of the Phase I program. Phase II effort, "Particle Protection, Demonstration, and Evaluation," was not performed because of a redirection of Air Force funds and priorities.

II. HYPOTHESIZED MECHANISM OF PARTICLE FORMATION

A. Theoretical Basis

The general mechanism hypothesized for boron particle formation in the Callery process has been hypothesized to be:

(1) Thermal decomposition (irreversible dehydrogenation) of boron hydride, at a kinetic rate limited by the heat transfer rate;

(2) Nucleation and condensation of an intermediate boron/hydrogen species vapor into a glassy or tarry fluid particle as a result of homogeneous nucleation. This is likely to occur near the adiabatic combustion temperature (T_a);

(3) Continuing thermal decomposition of the particle during growth via collision and deposition, and

(4) Escape from the "Reaction Zone" after being fully dehydrogenated.

Particles may agglomerate downstream in regions of lower temperature; this is distinct from growth of individual particles which only occurs in the reaction zone. There is considerable support for this type of mechanism from the field of crystallization, combustion, and air quality management, where nucleation and growth of crystalline materials, soot, and aerosols have been extensively studied.

It is helpful to visualize a flame similar to a propane torch when considering the particle formation mechanism: the combustion process in a flame occurs at the edges of the fuel gas jet emanating from the nozzle, and for turbulent flow conditions the flame length does not change appreciably with fuel flow variations although the heat released increases [1]. The borane feedstream in the boron reactor behaves in a like manner: with turbulent flow conditions in the feed nozzle, a gas free-jet (called the "Reaction Zone" for this work) is formed downstream of the nozzle exit that has a length controlled by nozzle diameter. Changes in feedrate (= feed velocity) affect the rate of mixing of this jet with the surrounding hot nitrogen stream, but the jet length remains unchanged. This general relationship is shown in Figure 1. Under laminar flow nozzle conditions, the "Reaction Zone" resembles more of a cylinder than a free jet, and its length is controlled by the feedrate.

To arrive at an experimental program, it is necessary to establish means of control of the various rates comprising the mechanism and to then vary the control parameters to cause changes in those rates. The means of control are discussed in this section. The independent variables providing that control, and the ranges of control available, are discussed in the "Process Design" section.

Part one of the mechanism, thermal decomposition, is an irreversible gas-phase dehydrogenation of boron hydride. The overall reaction mechanism is unknown and is probably nonelementary. However, it is believed valid, but unsupported by experimental evidence, that the initial portion of the thermal decomposition is a unimolecular first-order reaction [2,3]. Feed concentration therefore has no effect on this part of the particle formation mechanism, although it does have

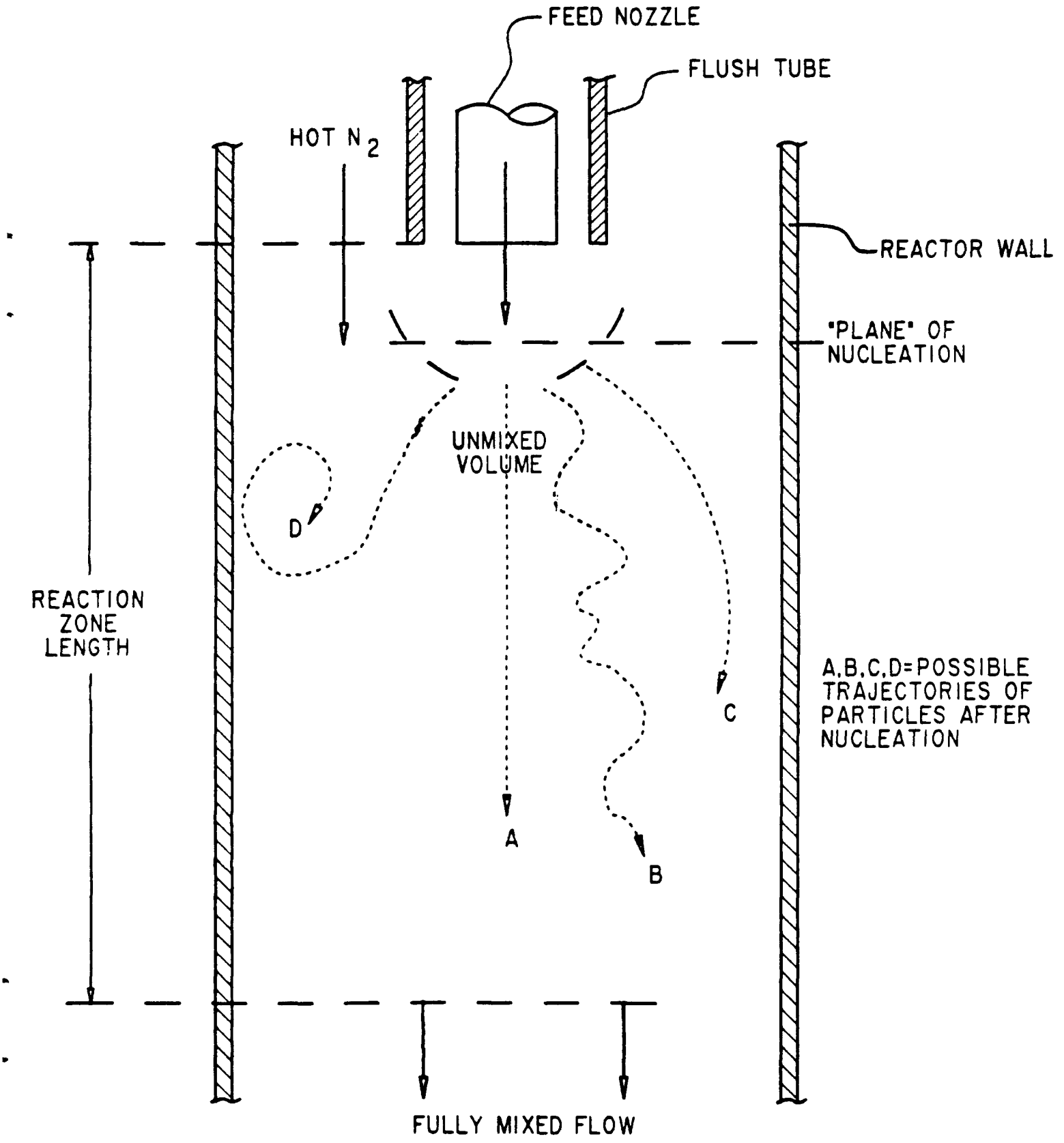

Figure 1. Schematic Representation of Reactor Zone

an effect on Part 2. The rate of decomposition is controlled by the rate of heat input to the feed, and by the activation energy required by the feed to achieve reaction. Heat input to the feed is from three sources; externally from the hot nitrogen stream and transferred to the feed via mixing; externally from the hot reactor walls and transferred directly to the feed by radiation; and internally from the exothermic decomposition reaction and controlled by feedrate of reactant. The thermal environment for the reaction has been approximated by the use of the "adiabatic combustion temperature" (T_a) concept, which is basically a heat balance around the entire reaction $B_2H_6 \xrightarrow{N_2} 2B + 3H_2$. Use of this concept allows the thermal environment to be compared among runs so that the contribution of Part 1 of the particle formation mechanism may be judged. (Due to the difficulty in establishing the emissivity of the hot reactor wall, and the efficiency of conductive/convective heat transfer from the wall to the nitrogen component of the reaction flowstream, the radiant heat transfer portion of external heat input has been omitted from T_a calculations).

Part 2 of the mechanism, nucleation and condensation, is a heterogeneous process that occurs before complete reaction to boron is achieved. The decomposition reaction produces a intermediate vapor species whose partial pressure at any particular location remains essentially constant, while the species' vapor pressure constantly decreases due to ongoing decomposition. This situation creates supersaturation which, upon reaching a critical level, is almost instantaneously relieved via homogeneous nucleation [4,5] and accompanying condensation. Thus, fluid particles are formed; it is likely that this process occurs near T_a, since much of the reaction system is presumed to be at that temperature. Control of Part 2 of the particle formation mechanism therefore is provided by: the continuing rate of decomposition, as in Part 1; system

pressure, which affects the condensing species' partial pressure; and feed concentration (dilution with nitrogen), which affects the location in the reaction zone at which nucleation occurs. Additional control of Part 2 may be provided by control of feedrate (synonymous with feed velocity) which also affects the location of nucleation [5] in the reaction zone.

Part 3 of the mechanism, particle growth, is a possibly heterogeneous process that occurs via deposition (condensation) of any remaining vapor species onto particles through heterogeneous nucleation, and/or by collisions between particles while still in the fluid state. Control of Part 3 is partially already established by the prior control of Parts 1 and 2, as follows: the continuing rate of decomposition; system pressure; system temperature, which additionally affects the outcome of particle collisions; turbulence, which affects the frequency of particle collisions and also the momentum of particles; and feedrate, which controls the total mass of nuclei available for growth, and is likely to control the actual population of nuclei.

Part 4 of the mechanism, escape, is by definition the termination of all the preceding processes. Escape from the "Reaction Zone" may coincide with the end of the heated-wall portion of the reactor, or it may occur earlier within the reactor.

A summary of the control opportunities for manipulating the overall particle formation mechanism is given below:

Part 1 (Thermal Decomposition):	Mixing, radiant heat transfer, feedrate, T_a
Part 2 (Nucleation/Condensation):	Mixing, radiant heat transfer, feedrate, T_a, system pressure, feed concentration
Part 3 (Growth):	Mixing/turbulence, radiant heat transfer, feedrate, T_a, system pressure
Part 4 (Escape):	Dependent on control of Parts 1 to 3, and on reactor length.

A further description of the mixing and nucleation processes is necessary to adequately portray the mechanism. Mixing occurs in the process system, in turbulent flow conditions, due to molecular diffusion among small rotating parcels of fluid called eddies. The size of the eddies is called the "scale of turbulence", and is determined by a characteristic length in the system; in the boron process system, the feed nozzle diameter determines the scale of turbulence in the feed jet, and the reactor diameter determines the scale of turbulence in the bulk mixed flow. The rotational velocity of the eddies is called "intensity of turbulence", and is determined by the average bulk velocity of the particular stream. Thus, mixing and turbulence are complimentary processes; the term "mixing" is more properly used when a particular degree of uniformity, in blending components together, is the desired result of turbulence. By definition in laminar flow conditions, these eddies are not formed, and mixing is

effected by molecular diffusion only. The process of homogeneous nucleation is thermodynamically driven by supersaturation of a vapor species. Simply stated, nucleation occurs when the formation of clusters of molecules (nuclei) reduces the molecules' total energy below that required to maintain the vapor phase. The process is quite complex and is not completely understood. Literature reference [4,5,6] indicate that the rate of homogeneous nucleation is a very steep function of supersaturation, changing from a negligible to an extremely large (up to $\approx 10^{17}$ nuclei/cm^3-sec) rate with temperature changes of only a few degrees. The nucleation rate is considered to be therefore very difficult to control in the boron process. Once nuclei are available the remaining vapor phase molecules condense on these nuclei, driven by the continuing reduction in their vapor pressure by ongoing thermal decomposition. It has been postulated that quantities of molecules on the order of 100 or so are required [4] for the formation of nuclei; in the boron process system, the nuclei formed would therefore be very roughly on the order of 20 Å. For various borane feedrates, the number of nuclei formed and the vapor mass available for condensation are likely to have a rather constant ratio, which would cause no change in particle size with feedrate. The historically observed proportionality (Q.V.) of feedrate and particle size in the Callery boron process therefore believed to arise from collisions between particles, which would be more frequent at higher feedrates due to more nuclei being formed. Based on 20 Å particles at 10^{17} particles/cm^3 concentration, the mean free path for particles with Maxwell-Boltzmann velocity distribution would be on the order of 5600 Å. The intent in the control of Part 2 of the particle formation mechanism is to manipulate the location where nucleation occurs, so that collision probabilities are enhanced.

B. Prior Experimental Evidence

The Callery boron reactor system has been operated for a number of years and has generated considerable operating data. Since the system has been used almost exclusively for production, however, the available data are grouped in a narrow range of process conditions, which limits its utility. The most significant available data are particle size, feedrate, operating temperatures, and product analyses.

Prior measurements of particle size have been subject to the difficulties described in Section V. B.2, "Size Determination Method", of this report. To provide a consistent basis for comparison of prior and new data, a composite sample of selected Callery production lots has been subjected to the size measurement procedure given in Section V. B.1. The mean particle size was determined to be 616 Å. Prior measurements of similar production lots by various techniques had shown varying sizes up to 1500 Å; it is now believed that these larger sizes are in error, and that those results did not include the typical large quantities of smaller particles seen in the composite sample. A smaller mean size tends to confirm the hypothesized particle formation mechanism: prior data at 1 lb/hr. borane feedrates gave mean particle diameters of about 400 Å. A 3 lb/hr feedrate gives a (revised) mean diameter of 616 Å. If the hypothesis is correct, particle growth occurs by the addition of mass to already nucleated seed particles. The mass available and the resulting particle volume are linearly proportional to feedrate, and any single dimension of the particle is proportional to the cube root of the feedrate. For the case of a 3 x feedrate change: $\left[\frac{3 \text{ lb/hr}}{1 \text{ lb/hr}}\right]^{1/3} \times 400 \text{ Å} = 577 \text{ Å}$.

Operating temperatures during production runs have normally been held to 1380°F - 1650°F inert gas feed, and 1800°F reactor walls. Operation at lower temperature had frequently led to plugging of the reactor in the vicinity of the feed nozzle. It was observed that the reactor could be operated with as much as the lower 40% of length unheated, before incompletely reacted material was produced; however, operability was poor. It was also concluded that direct measurements of gas temperatures within the reactor were unreliable due to the tendency of boron powder to adhere to any exposed surfaces, creating an insulating layer. A prime operating rule was that inert gas feed ("Heater N_2") temperatures had to be above a certain minimum, approximately 1300°F, to ensure sufficient heating downstream in the reactor so that complete reaction occurred.

Product analyses by wet chemistry have normally shown 97.5 to 99+ wt.% boron. The balance of the composition has been determined, by fusion in LECO and similar equipment, to be adsorbed nitrogen, hydrogen, and oxygen gases; the adsorbed oxygen is directly related to the degree to which the boron is handled in air. Trace element analyses by various spectrographic methods generally show less than 200 ppm total metallic impurities, with 70 elements scanned.

C. Particle Dynamics

Ultrafine particles on the order of 0.01 to 0.1 micron diameter are known to exhibit dynamic behavior considerably different from the classical models of "hard-sphere" Newtonian mechanics. The extremely low individual particle mass causes behavior somewhat similar to gas molecules, in that the particles are subject to Brownian motion, show response to phoretic forces (e.g., thermophoresis), and have very short relaxation times after perturbations [7]. Of the four major regimes of particle dynamic behavior, these ultrafine particles are classified in the "transition" regime. The equations governing particle motion in this regime are imprecise, and are best used for qualitative purposes only. For these reasons, study of the variables controlling boron ultrafine particle formation is best done by actual experimentation, rather than by mathematical modeling.

Ultrafine particles up to approximately 0.1 micron in diameter tend to have unequilibrated surface energy [7,8,9,10]. This is particularly true for amorphous boron particles, which contain 0.9 kcal/mole higher internal energy than the crystalline state. The residual energy causes the individual particles to agglomerate into masses, a phenomenon distinct from agglomeration due to static electrical surface charge and from fusion due to collisions of molten particles. This agglomeration tendency subsides at larger particle diameter, where lower unit surface area and increased mass are available to disperse this energy.

III. PROCESS DESIGN

A. Available Variables and Practical Limitations

The Callery boron process reaction is a three-phase heterogeneous irreversible reaction, and undergoes a volume increase in the reaction zone due to hydrogen release from the thermal decomposition of the feed. The reactor stream is plug flow, although some amount of backmixing may occur in the vicinity of the feed nozzle. Adequate control of the major process variables has already been demonstrated during commercial production in a process system completely similar to that used for this contract.

The means of control discussed in Section II. A. is exercised through manipulations of the appropriate independent variables. These variables and the expected effects of changes are described in detail in the following text and are summarized in Figure 2.

1. Mixing and Feedrate

Control of mixing affects the outcome of all parts of the particle formation mechanism. Two distinct mixing processes occur in the reactor - mixing of the feed gas jet with the surrounding hot nitrogen, and mixing of the particle-laden reaction stream with itself. The length of the turbulent-flow feed gas jet is determined by the diameter of the feed nozzle, which may be varied between the minimum diameter needed to deliver sufficient flow at ΔP = 30 PSI and the maximum diameter able to fit inside the reactor pipe. The range of feed nozzle diameters to be studied has thus been calculated to be 18 gauge to 3/8

inch, with inside diameters of 0.0028 to 0.028 feet. Commercially available tubing sizes are limited; with this in mind, nominal feed nozzle diameters of 18 ga., 14 ga., 3/16 inch, 1/4 inch, and 3/8 inch have been chosen for study. The intensity of feed gas jet mixing is controlled by the feed velocity which, at constant composition, is the borane feedrate. This feedrate should be varied across as wide a range as possible, so that laminar flow conditions and near-sonic velocities may be studied. Two constraints on this range are that minimum feedrates should not be so low that excessively lengthy runs are required, and maximum feedrates should not be so high that excessive borane is consumed. (The minimum duration of a run should be at least 45-60 minutes so that sufficient steady-state operation is achieved). Within these constraints, the feedrate range is established as 0.6 to 5.0 lb/hr of diborane.

Mixing of the reaction stream itself is controlled by the reactor diameter and the bulk flow velocity. At the very outset of this work, it was recognized that changes in reactor diameter would require considerable downtime and capital cost; the reactor diameter has therefore been held constant. The bulk flow velocity, aside from the contribution of the feed and the effect of temperature on gas density, is mainly a function of heater nitrogen flowrate. This flow is adjustable within the minimum necessary to convey the boron particles through the system, and the maximum that can be adequately heated by the N_2 heater section. These extremes have been estimated and yield a heater nitrogen flowrate range of 3.7 to 17.0 lb/hr.

2. Radiant Heat Transfer

It is known that boranes and particles will absorb infrared radiation, whereas nitrogen and hydrogen do not. It is also known that radiant heat flux from a surface is dependent on temperature of that surface and the extent to which it resembles a black body. The absorption of this energy is dependent on the area of absorber exposed, the absorptivity or ability to absorb radiation for that absorber, and, for clouds or particles, the opacity of the cloud. For the boron process system, much of this information is extremely difficult to quantify, although radiant heat transfer may be quite important to the process. Since the fluid and solid particles in the process are subject to thermophoresis, it is considered necessary to have reactor wall temperatures hotter than the particles, which are approximated to be at T_a. For these reasons, the general intent for the reactor wall temperature variable is to maintain it at historical settings of 1700° to 1900°F while simpler variables are explored, and then investigate reductions of wall temperatures to the extent suggested by the previous data. The potential range of wall temperatures is approximately 500°F to 2,000°F, with the minimum at the lowest anticipated T_a and the maximum limited by the structural strength of the reactor alloy.

3. Adiabatic Combustion Temperature (T_a)

The actual thermal environment of the decomposition reaction is very difficult to assess, but since mixing is a fundamental aspect of the reaction, it is appropriate to use a mixed-stream temperature as an indicator of that environment. The T_a calculation combines the enthalpies of all incoming streams with the heat of reaction from the borane decomposition to determine the resulting

mixed-stream temperature. Heat transfer across the reactor walls is not accounted for. The largest component of the T_a calculation is the heater nitrogen enthalpy; the heater N_2 flowrate has been described under "Mixing", and its temperature is established by the stream enthalpy required to yield the desired T_a at the chosen borane feedrate. The range of T_a to be studied has as a minimum temperature at which literature reference imply a change in reaction order for various boranes [2,3]; this is at approximately 250°C (482°F). The range maximum is established by limitations of heater N_2 maximum temperature and the minimum diborane feedrate of 0.6 lb/hr, which gives maximum T_a of about 1400°F. The heater N_2 temperature available range is 70°F to about 1950°F depending on flowrate.

4. Other Independent Variables

Reactor diameter and length are independently variable, but to keep the scope of this work manageable, these will be held constant. Feed dilution with nitrogen may be varied, within the constraint of desired feed velocity, to any limit. However, it is believed that the best opportunity for particle size enlargement is obtained with high borane feed concentrations. Therefore, borane feed will be diluted to no more than 50 mole % nitrogen. Flush nitrogen flowrate, used for cooling the feed nozzle to avoid plugging, is normally as low as possible and is not expected to have much influence on particle size. A flow of 1.08 lb/hr has historically provided sufficient cooling at various operating conditions, and will therefore be used here. System pressure is a potentially major variable, since higher pressure would increase the condensing species' partial pressure and thereby accelerate the onset of nucleation. A major drawback to the use of pressure is that substantial increases would be necessary to

cause pronounced effects, and the system cannot withstand both higher pressures and high temperatures combined. Also, higher borane feed pressures would be required, which is highly undesirable from a safety viewpoint. Since other variables will also give increases in partial pressure (e.g., feedrate), system pressure will be held constant.

In summary, the following parameters are important to the particle formation mechanism:

Independent Variables	Dependent Variables	Constants
(Diborane Feed Concentration)	Turbulence/Mixing Rate	Reactor Diameter
Diborane Feedrate	Residence Time	Reactor Length
Feed Nozzle Diameter	Collision Frequency	System Pressure
Reactor Wall Temperature	Collision Intensity	
T_a	Mean Particle Diameter	
Heater Nitrogen Flowrate	Particle Size Distribution	
(Flush Nitrogen Flowrate)	Decomposition Rate	
	Heater N_2 Temperature	
	Nucleation Rate	
	Dilution N_2 Flowrate	
	Heat Transfer Flux Across Reactor Wall	

B. Experimental Design

The overall plan of experimentation is to study each independent variable separately, holding all others constant, and to modify subsequent run conditions to the extent suggested by prior particle size results. The variables will be studied in decreasing order of estimated importance to the particle size. Due to the number of variables for study and the effort required per run, there will be very little duplication of run conditions. This of course creates the risk of faulty data being undetected, but allows a greater range of process conditions to be studied. The risk is minimized by achieving steady-state conditions for sufficient time (45-60 minutes minimum) during each run and by strict adherence to a standard operating procedure so that the effects of operator technique and bias are eliminated. Cross-contamination of each run's product from preceding runs has historically been less than 10% by weight in Callery's production experience; a material balance will be done for each experimental run to check for cross-contamination.

The experimental effort has been divided into groups, within which the results of particle size are related. The different variables' ranges and the group divisions are shown in Figure 2. The specific conditions for each run are tabulated in Section V.A.2., Table of Run Conditions".

MAJOR VARIABLES BY GROUP, FOR TASK 1.3

GROUP 1: 18 GA,14 GA,3/16",1/4",3/8" NOZZLES
Ta 842°F B_2H_6 1 AND 5 LB/HR

GROUP 2: FEED VELOCITIES 11.5-528 FT/SEC
2 NOZZES, Ta 842°F

GROUP 3: Ta 570-1252°F
WALLS 1300-1900°F

GROUP 4: WALLS 1100/1500-1300/1775°F
Ta 582°F

GROUP 5: HEATER N_2 3.7-8.3 LB/HR
Ta 480-580°F
WALLS 1100-1300/1700°F

GROUP 6: HEATER N_2 3.7-17 LB/HR
B_2H_6 1.7-5 LB/HR
Ta 580°F

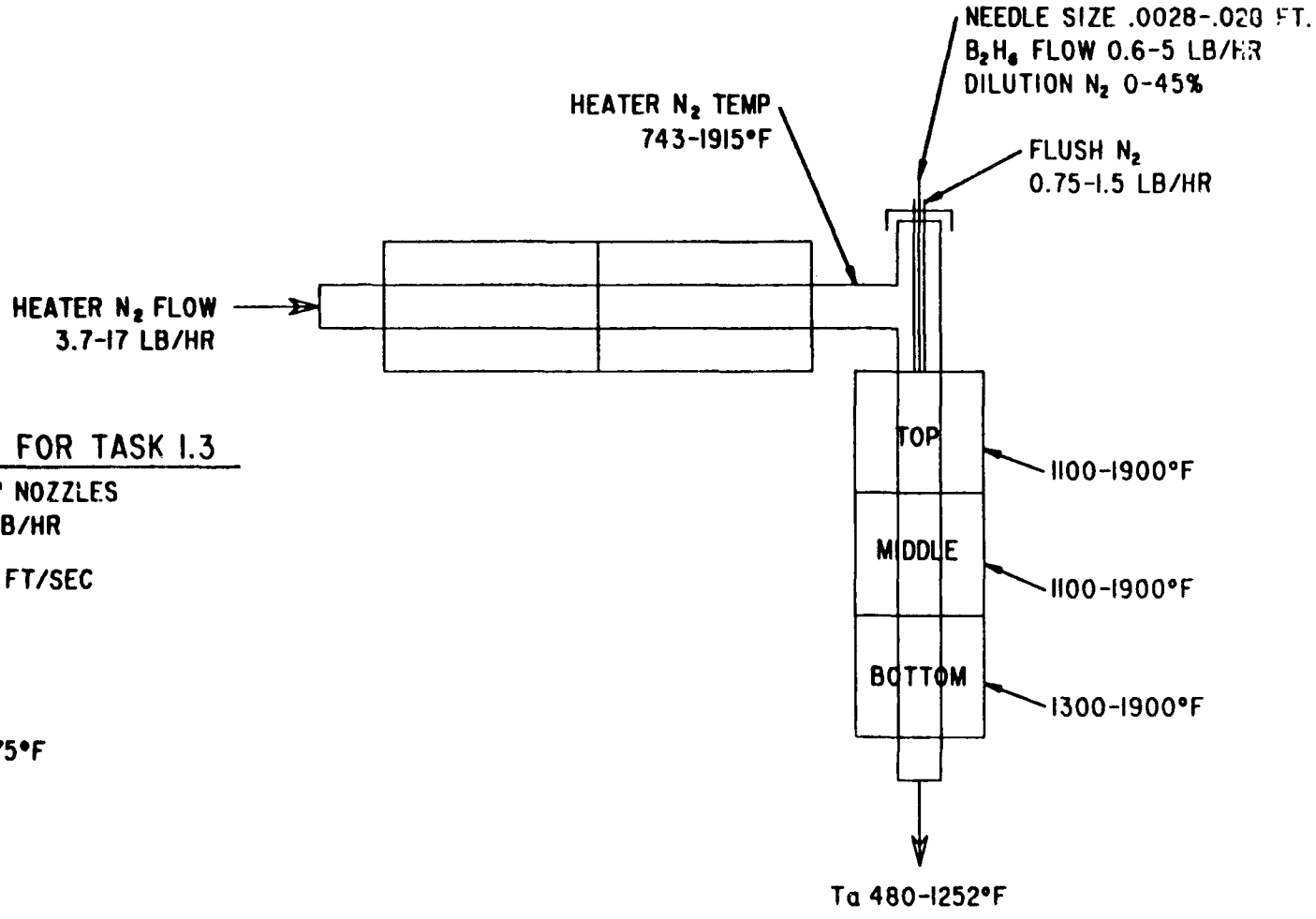

Figure 2.

MAJOR VARIABLES
OF THE BORON PROCESS,
AND RANGES AVAILABLE

C. Special Considerations for Particle Recycle

The hypothesized particle formation mechanism in Section II.A. states that homogeneous nucleation from the supersaturated vapor phase creates particles which then undergo size growth by collision and/or deposition. If particles (Seed Nuclei) were present in the reaction zone before the onset of homogeneous nucleation, the supersaturated condition of the vapor phase would be equilibrated by condensation only, which is a much lower-energy path to equilibrium than homogeneous nucleation. Certain parameters of the particle growth mechanism could thus be studied in a simplified manner. In fact, there is considerable commercial use of this phenomenon in such applications as fluidized-bed combustion and semiconductor device fabrication ("Chemical Vapor Deposition"), among others.

The boron process system easily lends itself to introduction of a dispersed powder-in-nitrogen stream into the reaction zone. This stream would be mixed with the borane feed jet, and thereby provide the seed nuclei for vapor deposition. The major variables expected to control the amount of deposition are (1) feedrate of borane, which controls the partial pressure of condensing species and also the mixing rate of the feed streams; (2) T_a and reactor wall temperature, which control the vapor pressure of condensing species and the rate of decomposition of the feed and the deposited species, and (3) the number of seed nuclei present, which controls the surface area available for deposition.

Due to the relatively few number of runs planned for recycle study, T_a and reactor wall temperature will be held constant at values in the middle of the range described previously. Also, since it is desirable to investigate both

"once-through" and consecutive recycle, the minimum useful number of three diborane feedrates and three particle feedrates should be studied. Accordingly, diborane feedrates will be 1.68, 3.0, and 5.0 lb/hr. Particle feedrates should be low, so that maximum deposition per particle is achieved; the equipment described later in Section IV.A. lends itself to particle feedrates of 12, 24, and 30 grams powder/hour. After the combinations of diborane and particle feedrates have been conducted, a series of runs, each using recycled boron powder from the previous run, will be conducted while holding all independent variables constant. It is expected that conditions of minimum particle feedrates and maximum diborane feedrate will yield the highest quantity of deposition per particle and consequently the largest increase in particle size.

The total recycle effort is necessarily limited in scope, but is designed to provide sufficient data to reliably assess the utility of recycle for boron particle enlargement.

IV. EQUIPMENT - DESIGN

A. System Integration

The equipment specified for the experimental boron system closely resembles the Callery production system, with additional flexibility provided for exploration of wide ranges of variables. Safety is of prime importance when working with boron hydrides, and therefore good ventilation, robust equipment, simplicity, and reliability are extremely important considerations.

The overall system, shown in Figures 3 and 4, utilizes diborane from refrigerated gas cylinders at -80°C and 30 to 300 PSIG, and nitrogen from an 80 PSIG supply header. The diborane cylinders (up to 3 in number) are connected to a manifold which leads to a 30 PSIG step-down regulator; the cylinder stations and header are completely contained within an open-face fume hood with induced-draft negative pressure ventilation. Each cylinder station is fully purgeable with 40 PSIG nitrogen to prevent air entry into the system when connecting cylinders. 30 PSIG regulated diborane flows to a rotameter/throttle valve assembly for precise control of flowrate, and then is routed to the reactor feed nozzle. Dilution nitrogen is introduced through a tee sufficiently upstream of the feed nozzle to allow complete mixing. All tubing carrying diborane is 304 or 316 stainless steel, to ensure adequate low-temperature ductility and to prevent contamination of the feed stream by rust; lines are generously sized so that plugging from diborane degradation products (BHx, B_2O_3) is prevented. Valving and purge connections are arranged such that any section of diborane piping can be isolated and/or purged to the reactor or to the vent line.

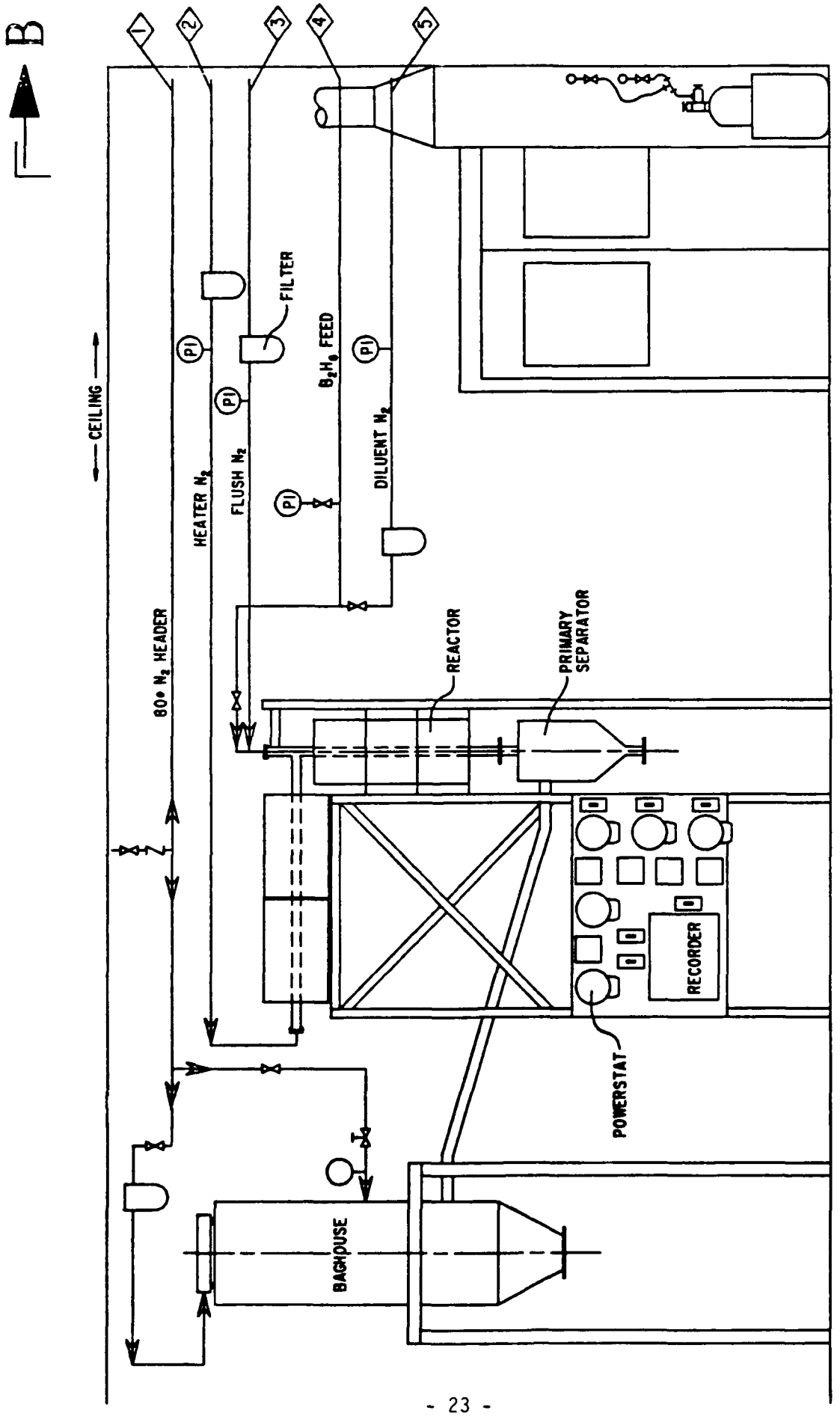

FIGURE 3. ELEVATION VIEW OF EXPERIMENTAL BORON SYSTEM VIEW A-A

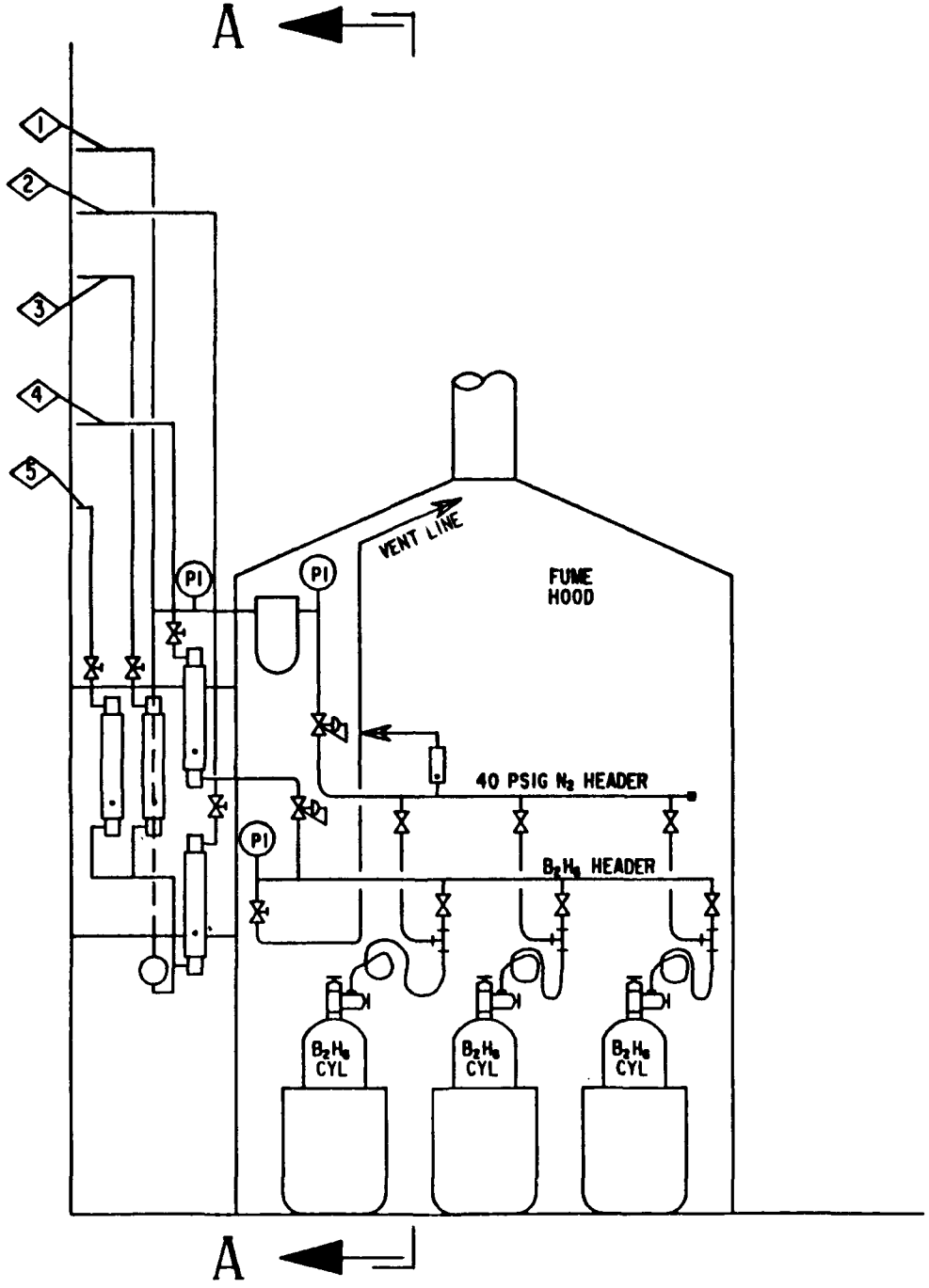

FIGURE 4. ELEVATION VIEW OF EXPERIMENTAL BORON SYSTEM VIEW B-B

The process nitrogen for diluent, heater, and flush stream is regulated at 30 PSIG and flowrates are precisely controlled by individual rotameter/throttle valve assemblies. Each stream is filtered through a 0.45 μ cartridge filter to prevent migration of rust/dust particles into the reactor, which could act as seed nuclei.

The reactor itself is an L-shaped welded fabrication, with one branch of the "L" filled with 1/4 inch Inconel 600 Raschig rings; this section serves as the nitrogen heater. At the joint of the "L" is a threaded pipe tee for insertion of the feed nozzle/flush tube assembly. The other side of the "L" is the reactor section. The end of the reactor is flanged for connection with the primary separator. The entire reactor/heater assembly is constructed of 1 1/4 inch schedule 40 Inconel 600 pipe., which has excellent high-temperature strength and outstanding resistance to both the external oxidizing and internal reducing conditions present during operation.

The process heaters are a "Clamshell" resistance-type design which provides for easy installation and removal. The two heaters that enclose the horizontal nitrogen heater are each of 3200 watts capacity at 2200°F maximum operating temperature. The three vertical reactor heaters are also "Clamshell" type with a rating of 2300 watts, 2200°F maximum. The five heaters and the reactor/N_2 heater assembly are all supported by a 1/4 inch carbon steel welded frame; the three reactor heaters are each on a shelf and the small gaps between the heater housings are packed with "Thermazip" ceramic insulating blanket to prevent a chimney effect. Also supported by the carbon steel frame is a control panel which holds the five variable transformers ("Powerstats") and five ammeters that control the process heaters, and holds the 12-point temperature recorder.

Process temperatures are measured with Type K (Chromel-Alumel) thermocouples banded onto the Reactor/N_2 heater pipe with stainless steel wire. The process heaters have factory-installed integral thermocouples. The temperature recorder is a digital/analog programable unit with 12 channels recorded in 6 colors, and it is capable of automatically logging the time and date on the face of the chart paper. A thermocouple burnout is indicated by full-scale deflection of the affected channel. A depiction of the thermocouple attachments to the process is given in Figure 5.

The feed nozzle/flush tube assemblies are a modular design, with the feed nozzle tube mounted concentrically inside the flush tube, and the tube delivery ends are in the same horizontal plane. The assembly is installed in the reactor in such a manner that the tube ends are in the plane of the upper edge of the top heater.

A stainless steel "Primary Separator" is connected to the bottom outlet end of the reactor pipe and serves to disengage any large particles or chunks of boron from the product stream. This separator also provides passive cooling of the product stream so that downstream temperatures are not excessive. A ball valve is connected to the outlet for purposes of isolation for leak-testing of the separator after each operating cycle.

The product baghouse is connected to the primary separator through a 1-1/2 inch stainless steel welded pipeline, and is itself of welded 304 stainless steel construction with a 2.2 PSIG maximum pressure rating. Specifically, the baghouse is a MIKRO-Pulsaire Model 2 1/2 B with 25 ft^2 of fiberglass filter

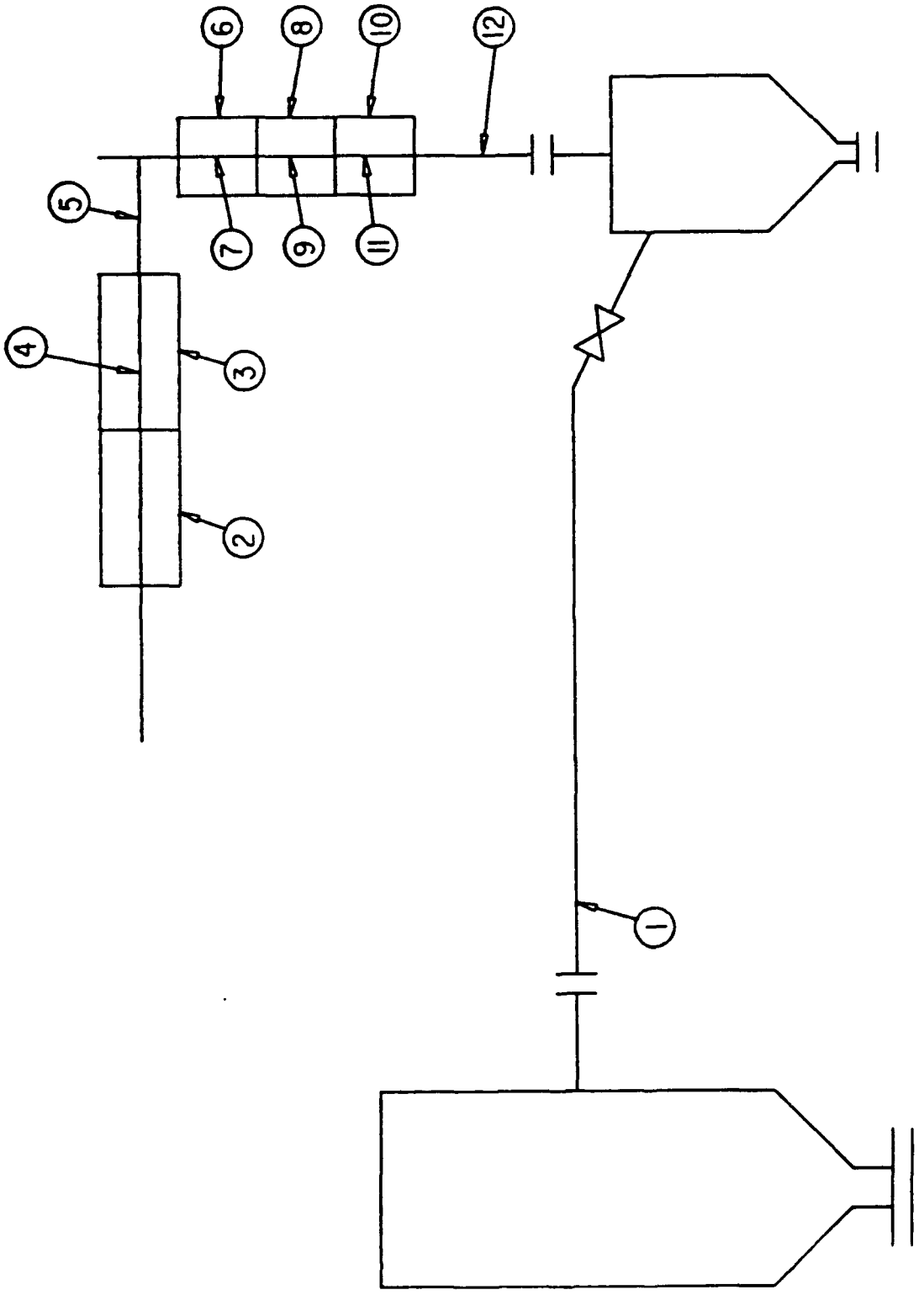

FIGURE 5.
THERMOCOUPLE
ATTACHMENT
POINTS TO
PROCESS

area, discharging by nitrogen reverse-pulse to an integral hopper having 60° cone sides and a bottom 8 inch outlet. This bottom outlet is sealed with an 8 inch nylon-11-coated butterfly valve, and is emptied into polyethylene bags which are the final boron product containers. The filled bags are stored inside open-top 55-gallon drums for protection.

The experimental boron process system constructed as described closely duplicates a proven system which has demonstrated a high percentage of availability and operability, and is designed to be repaired in minimal time should a breakdown occur. This creates benefits to the contract since funds will be expended for research results rather than hardware debugging, and since particle size increases will be due to intentional variations of operating conditions rather than hardware peculiarities.

The particle recycle effort is accomplished through the modular addition of a Model 1251 particle feeder device manufactured by the Plasmadyne Division of Miller Thermal Technologies, Inc. The feeder uses a slotted rotating wheel to discharge a precise volume of boron powder into a gas stream. In this application, the flush nitrogen stream of the process is diverted through the particle delivery end of the feeder, and conveys the boron to the reactor through the flush tube of the feed nozzle/flush tube assembly. It was briefly considered that the recycled powder should be introduced via the diborane feed stream, but this was judged to be unsafe since the particle feeder must be frequently opened for cleaning and recharging.

B. Operating Method

The assembled experimental system was first cleaned of all grease, welding slag, and general contaminants and then leak-tested by pneumatic test with nitrogen. Upon satisfactory completion of these, operational testing began with the goals of developing standard operating procedures, establishing inert conditions inside the system, and identifying any equipment or assembly deficiencies. When proper functioning of the system was obtained, two proveout runs using diborane were performed at conditions similar to commercial production, and the resulting particle sizes were shown to be sufficiently close to Callery's product for the proveout to be successful.

A typical experimental run requires that the operating conditions of diborane feedrate, nitrogen flows and temperature, reactor wall temperatures, nozzle size, and run duration be calculated prior to set-up. Then, starting with an empty baghouse and primary separator, nitrogen flow is initiated to ensure proper purging and then the process heaters are turned on. Normally a two to three-hour heatup period is required to reach temperature steady-state; during this period the operator prepares sample bottles and product bags, weighs and logs the previous run's product, and prepares the logbook for data entry. When temperatures have stabilized, the operator retrieves the diborane cylinder(s) from the storage cooler and connects them after purging the manifold. Diborane pressure is noted, and the proper flowrate is initiated. Immediately, the operator increases the amperage to the 3 reactor heaters to compensate for the drop in wall temperature that occurs upon diborane entry into the reactor. Then, during the reaction, the operator carefully monitors all flows, temperatures and pressures and adjusts as necessary to maintain steady-state.

Occasionally, deposits will form on the inside wall of the reactor which interfere with flow and cause pressure increases. Rapping on the reactor pipe usually dislodges these, but if they remain, the run sometimes must be terminated.

Upon completion of a run, the diborane cylinder(s) outlet valve is closed and a nitrogen purge is initiated on the line for 15 minutes while the reactor is at operating temperature. Then, the cylinder is disconnected, weighed, and returned to storage, and the process nitrogen flows are reduced to standby rates. The process heaters are turned down to "Idle" settings.

When the baghouse and primary separator have cooled to near-ambient (usually not until the next morning), they are emptied into the preweighed bags and the system is ready for another cycle. Normally, the feed nozzle/flush tube assembly is removed and inspected at this time to ensure it is serviceable for the next run.

The recycle runs are operated in an identical manner as above, with the additional steps of cleaning, loading, and operating the particle feeder. The feeder is loaded (if necessary) during the reactor heat-up period. When the system is up to temperature, the flush nitrogen stream is diverted into the gas inlet of the feeder, and the powder wheel motor is started and its speed adjusted to that desired for the run. Dispersed powder is now flowing into the reactor, and diborane flow is initiated. During operation, the feeder motor speed and powder chamber level are monitored; at the conclusion of a run, the diborane is shut off and then the feeder motor is stopped and the flush nitrogen flow is then bypassed around the feeder. While the process system is cooling

down, the particle feeder is cleaned out if the next run requires a different boron powder lot to be fed.

The operating method described above has resulted in generation of reliable data, and has maximized safety and reliability of the system.

V. EXPERIMENTAL METHOD

The means of control of the experimental boron process, the variables providing that control, the function of the various system components, and the general operating procedure have all been described in previous sections. This section is intended to elucidate the formulation of the operating conditions for each of the 64 experimental runs, and to explain the various methods and techniques used to obtain experimental results.

A. Calculations

1. Sample Calculations

Diborane physical and thermodynamic properties have been obtained from the "Diborane Handbook", National Aeronautics and Space Administration, Contract NAS7-769. Nitrogen, hydrogen, and boron properties have been taken from the "Advances in Chemistry Series", American Chemical Society, Number 18: Thermodynamic properties of the elements. Certain properties not available elsewhere have been found in "Handbook of Chemistry and Physics", CRC Press, 64th Edition.

Adiabatic Combustion Temperature (T_a)

The reference state for this calculation has been defined as 25°C (77°F), which is very close to the temperature of the process area and is therefore a convenient reference. The enthalpies of all streams (diborane, flush N_2 and dilution N_2) entering the process at this temperature are therefore zero.

It has been decided to treat the diborane decomposition as forming products at 25°C, and then use the thermodynamic properties of those products in the T_a calculation. The assumptions required to simplify the calculation are:

(a) The diborane decomposition is complete, i.e. $B_2H_6 \longrightarrow 2B + 3H_2$

(b) Adiabatic conditions (no heat transfer across reactor wall)

(c) No PV work or frictional energy lost by flow stream

(d) Heat capacities for boron are for the β - rhombohedral crystalline form; no values were found for amorphous boron

(e) Average values for heat capacities have been used (at 850°F). This creates a small error of ≤ 4% in some T_a values

(f) ΔH_f° at 25°C for amorphous boron is 0.9 Kcal/g mole.

The heat of reaction for diborane as in (a) above is

$$\Delta H_r\ (25^\circ C) = \Delta H_f^\circ B_2H_6 + \Delta H_f^\circ \text{ boron (am.)} = -8.5 + 2\ (0.9) \text{ Kcal/g Mole}$$
$$= -436.4 \text{ Btu/lb. } B_2H_6$$

For the calculation, as in (b) and (c) above, $\sum H_{in} = \sum H_{out}$ and $H = wC_p(T_a - T_{ref})$; if only the incoming heater nitrogen stream is at other than 25°C the $\sum H_{in} = H_{htr.N_2}$.

So $\sum H_{in} = w \Delta H_{rB_2H_6} + [(w_{N_2})(C_p) + (w_B)(C_p) + (w_{H_2})(C_p)](T_a - T_{ref})$ where w

is the weight rate of flow of the various streams. As an example, for a T_a of 842°F and B_2H_6 flow of 0.84 lb/hr, heater N_2, 10.15 lb/hr, flush N_2, 1.08 lb/hr, and dilution N_2 of zero,

$$\sum H_{in} = (0.84)(-436.4) + [(11.23)(.264) + (.66)(.470) + (.18)(3.497)](842°-77°F)$$

$$\sum H_{in} = \frac{2620.3 \text{ Btu/Hr}}{10.15 \text{ lb/hr Heater } N_2} = 258.2 \text{ Btu/lb} = 4.0 \times 10^3 \text{ cal/g mole } N_2$$

Nitrogen has this enthalpy at 1080°F, so this is the operating temperature for the heater nitrogen stream. The system enthalpy equation can be used to find the enthalpy of the heater nitrogen stream required to balance the equation, which is then used in the nitrogen thermodynamic tables to find the corresponding temperature. *Alternatively, by knowing all component enthalpies, or by* using an iterative procedure based on guesses of T_a, the adiabatic combustion temperature may be determined.

The relative turbulence in either the feed nozzle or the reactor pipe is best assessed by use of the Reynolds number N_{Re} where $N_{Re} = \frac{Du\rho}{\mu}$ and D is duct diameter, μ is velocity, ρ is fluid density, and μ is fluid viscosity. N_{Re} for the feed nozzle stream is calculated with fluid properties at 77°F and the actual feed pressure; for the reactor mixed stream it is calculated with properties at T_a and 14.7 PSIA. Feed nozzle Reynolds numbers have ranged from 970 to 59,900; reactor Reynolds numbers have ranged from 840 to 3100. (Note -

feed nozzle Reynolds numbers have been calculated only for Groups 1 and 2 runs). The calculated N_{Re} values are shown in Section VI, "Results and Discussion".

The material balance for each run is determined by

$$\frac{\text{lb. boron recovered}}{\text{lb. } B_2H_6 \text{ fed} \times 0.7814} \times 100 = \% \text{ yield},$$

and includes all boron samples, the primary separator contents, and the baghouse recovered contents.

2. Tables of Run Conditions:

TABLE 1

Variables for Study

GROUP	NUMBER OF RUNS	VARIABLE(S)	CONSTANTS	PURPOSE
P	(2)	Feedrate Heater N_2 Flow	Medium Nozzle, Flush N_2, Dilution N_2	To provide preliminary data for choosing Group 1 & 2 T_a*
1	11	Nozzle Diameter (Each at 2 Feedrates), Feed Concentration	T_a, Heater N_2 Flow, Flush N_2, Dilution N_2	Determine effect of reaction zone length on D_p**
2	12	Feedrate (Each in 2 Nozzle Diameters), Dilution N_2 flow	T_a, Feed Concentration, Heater N_2, Flush N_2	Determine effect on D_p of changing "Plane" of Nucleation
3	12	T_a, Heater N_2, Reactor Wall Temp.	Nozzle Diameter, Feedrate, Flush N_2, Dilution N_2	Determine effect on D_p of altering temperature-dependent rates
4	4	Reactor Wall Temp.	Feedrate, T_a, Heater N_2 Flush N_2, Nozzle Diameter Dilution N_2	Investigate optimum radiant heat transfer
5	6	Heater N_2, T_a	Feedrate, Reactor Wall Temp., Flush N_2, Dilution N_2, Nozzle Diameter	Investigate lower turbulence/longer residence time, low T_a
6	8	Heater N_2, Feedrate, Flush N_2	T_a, Reactor Wall Temp., Nozzle Diameter (slight changes), Dilution N_2 (slight changes)	Search for optimum combinations of turbulence and temperature
7	11	Feedrate, Flush N_2, Particle Feedrate, Seed nuclei size	T_a, Heater N_2, Nozzle Diameter, Feed Concentration	Determine maximum Deposition conditions during heterogeneous nucleation

* T_a = Adiabatic Combustion Temperature
** D_p = Mean Particle Diameter

TABLE 2

A-167 Run Conditions

GROUP	RUN NO.	NEEDLE	(°F) TEMP #5	(lb/hr) HEATER N_2 FLOW	(lb/hr) B_2H_6 FLOW	(lb/hr) FLUSH N_2 FLOW	(lb/hr) DILUENT N_2 FLOW
1	BGHS 1 & PRI	3/16" in 1/2"	1750	9.17	3.0	1.08	0.85
1	BGHS 2 & PRI	3/16" in 1/2"	1170	10.15	1.0	1.08	0.85
1	BGHS 3 & PRI	3/16" in 1/2"	1700	10.15	5.0	1.08	0.85
1	BGHS 4 & PRI	14 Ga. in 1/4	1170	10.15	1.0	1.08	0.85
1	BGHS 5	14 Ga. in 1/4	1700	10.15	5.0	1.08	0.85
1	BGHS 6	1/4" in 1/2"	1170	10.15	1.0	1.08	0.85
1	BGHS 7	1/4" in 1/2"	1700	10.15	5.0	1.08	0.85
1	BGHS 8 & PRI	3/8" in 1/2"	1700	10.15	5.0	1.08	0.85
1	BGHS 9	3/8" in 1/2"	1170	10.15	1.0	1.08	0.85
1	BGHS 10	18 Ga. in 1/4	1170	10.15	1.0	1.08	0.85
1	BGHS 11	18 Ga. in 1/4	1700	10.15	2.0	1.08	- 0 -
2	BGHS 1 & PRI	3/8" in 1/2"	1044	10.15	0.60	1.08	- 0 -
2	BGHS 2	3/8" in 1/2"	1168	10.15	1.19	1.08	0.42
2	BGHS 3	3/8" in 1/2"	1378	10.15	2.39	1.08	0.84
2	BGHS 4	3/8" x 1/2"	1585	10.15	3.58	1.08	1.26
2	BGHS 5 & PRI	3/8" x 1/2"	1789	10.15	4.77	1.08	1.68
2	BGHS 6	3/8" x 1/2"	1915	10.15	5.00	1.08	3.02
2	BGHS 7	14 Ga. in 1/4	1080	10.15	0.84	1.08	- 0 -
2	BGHS 8	14 Ga. in 1/4"	1258	10.15	1.68	1.08	0.59

TABLE 2 (Continued)

GROUP	RUN NO.	NEEDLE	(°F) TEMP #5	(lb/hr) HEATER N_2 FLOW	(lb/hr) B_2H_6 FLOW	(lb/hr) FLUSH N_2 FLOW	(lb/hr) DILUENT N_2 FLOW
2	BGHS 9 & PRI	14 Ga. in 1/4"	1404	10.15	2.52	1.08	0.89
2	BGHS 10	14 Ga. in 1/4"	1546	10.15	3.36	1.08	1.18
2	BGHS 11	14 Ga. in 1/4"	1697	10.15	4.20	1.08	1.48
2	BGHS 12 & PRI	14 Ga. in 1/4"	1828	10.15	5.00	1.08	1.75
3	BGHS 1	14 Ga. in 1/4"	1128 Walls 1700	10.15	1.68	1.08	0.59
3	BGHS 2	14 Ga. in 1/4"	945 Walls 1700	10.15	1.68	1.08	0.59
3	BGHS 3 & PRI	14 Ga. in 1/4"	757 Walls 1700	10.15	1.68	1.08	0.59
3	BGHS 4	14 Ga. in 1/4"	757 Walls 1900	10.15	1.68	1.08	0.59
3	BGHS 5 & PRI	14 Ga. in 1/4"	750 Walls 1900	10.15	1.68	1.08	- 0 -
3	BGHS 6	14 Ga. in 1/4"	757 Walls 1300	10.15	1.68	1.08	0.59
3	BGHS 7 & PRI	14 Ga. in 1/4"	1810 Walls 1300	12.00	1.68	1.08	0.59
3	BGHS 8	14 Ga. in 1/4"	1810 Walls 1700	12.00	1.68	1.08	- 0 -
3	BGHS 9	14 Ga. in 1/4"	1483 Walls 1700	10.15	1.68	1.08	0.59
3	BGHS 10	14 Ga. in 1/4"	1657 Walls 1700	10.15	1.68	1.08	0.59
3	BGHS 11	14 Ga. in 1/4"	1828 Walls 1700	10.15	1.68	1.08	0.59
3	BGHS 12 & PRI	14 Ga. in 1/4"	1810 Walls 1700	12.00	1.68	1.08	0.59

TABLE 2 (Continued)

GROUP	RUN NO.	NEEDLE	(°F) TEMP #5 TOP/MID/BOT	(lb/hr) HEATER N_2 FLOW	(lb/hr) B_2H_6 FLOW	(lb/hr) FLUSH N_2 FLOW	(lb/hr) DILUENT N_2 FLOW
4	BGHS 1	14 Ga. in 1/4"	757 1300/1300/1775	10.15	1.68	1.08	0.59
4	BGHS 2	14 Ga. in 1/4"	750 1300/1300/1775	10.15	1.68	1.08	- 0 -
4	BGHS 3	14 Ga. in 1/4"	750 1100/1100/1775	10.15	1.68	1.08	- 0 -
4	BGHS & PRI 4	14 Ga. in 1/4"	750 1100/1100/1500	10.15	1.68	1.08	- 0 -
5	BGHS 1	14 Ga. in 1/4"	779 1300/1500/1700	8.30	1.68	1.08	- 0 -
5	BGHS & PRI 2	3/16" in 1/2" & 14 Ga. in 1/4"	826 1300/1300/1700	6.50	1.68	1.08	- 0 -
5	BGHS 3	14 Ga. in 1/4"	905 1300/1300/1700	4.75	1.68	1.08	- 0 -
5	BGHS 4	14 Ga. in 1/4"	988 1300/1300/1700	3.70	1.68	1.08	- 0 -
5	BGHS 5	14 Ga. in 1/4"	828 1100/1300/1700	3.70	1.68	1.08	- 0 -
5	BGHS & PRI 6	14 Ga. in 1/4"	779 1300/1300/1700	3.70	1.68	1.08	- 0 -
		(All 1" longer except 6-7)					
6	BGHS 1	14 Ga. in 1/4"	743 1100/1100/1600	15.00	3.0	1.08	- 0 -
6	BGHS 2	14 Ga. in 1/4"	777 1100/1100/1600	15.00	4.0	1.08	- 0 -
6	BGHS & PRI 3	14 Ga. in 1/4"	788 1100/1100/1600	17.00	5.0	1.08	- 0 -
6	BGHS 4	14 Ga. in 1/4"	1063 1100/1100/1500	3.70	2.0	0.75	0.59

TABLE 2 (Continued)

GROUP	RUN NO.	NEEDLE	(°F) TEMP #5 TOP/MID/BOT	(lb/hr) HEATER N_2 FLOW	(lb/hr) B_2H_6 FLOW	(lb/hr) FLUSH N_2 FLOW	(lb/hr) DILUENT N_2 FLOW
6	BGHS & PRI 5	14 Ga. in 1/4"	1162 1300/1100/1500	3.70	2.0	1.50	0.59
6	BGHS 6	3/8" in 1/2"	747 1100/1100/1500	10.15	1.68	1.08	- 0 -
6	BGHS 7	3/16" in 1/2" (original length)	747 1100/1100/1500	10.15	1.68	1.08	- 0 -
6	BGHS 8	1/4" in 1/2"	747 1300/1100/1500	10.15	1.68	1.08	- 0 -
							(g/hr) POWDER FEEDRATE (RPM)
7	BGHS P	14 Ga. in 1/4"	1216	10.15	1.68	1.08	12 (4.00)
7	BGHS 1	13 Ga. in 1/4"	1416	10.15	3.0	1.08	12 (4.00)
7	BGHS & PRI 2	13 Ga. in 1/4"	1708	10.15	5.0	1.08	12 (4.00)
7	BGHS 3	13 Ga. in 1/4"	1416	10.15	3.0	1.08	24 (8.00)
7	BGHS 4	13 Ga. in 1/4"	1416	10.15	3.0	1.08	30 (10.00)
7	BGHS 5	13 Ga. in 1/4"	1494	10.15	3.0	2.16	24 (8.00)
7	BGHS & PRI 6	13 Ga. in 1/4"	1369	10.15	1.68	3.24	12 (4.00)

TABLE 2 (Concluded)

GROUP	RUN NO.	NEEDLE	(°F) TEMP #5 TOP/MID/BOT	(lb/hr) HEATER N_2 FLOW	(lb/hr) B_2H_6 FLOW	(lb/hr) FLUSH N_2 FLOW	(g/hr) POWDER FEEDRATE (RPM)
RECYCLE							
7	BGHS 7	13 Ga. in 1/4"	1416	10.15	3.0	1.08	12 (4.00)
7	BGHS 8 & PRI	13 Ga. in 1/4"	1416	10.15	3.0	1.08	12 (4.00)
7	BGHS 9	13 Ga. in 1/4"	1416	10.15	3.0	1.08	12 (4.00)
7	BGHS 10 & PRI	13 Ga. in 1/4"	1416	10.15	3.0	1.08	12 (4.00)

B. Particle Size Measurement

1. Sample Preparation

The method developed for reproducible sizing and analysis of the boron powder began with the sampling of the bulk powder at Callery. The bulk powder collected from each experimental run is gravity discharged from the baghouse hopper into a large polyethylene bag while excluding air. After transfer, the bag of powder is slightly pressurized so that a flow of mixed nitrogen and powder is obtained through a tube leading from inside the bag to a sample bottle. The end of the tube inside the bag is in the approximate center of the powder mass so that unrepresentative material near the edges of the mass is not sampled. Three bottles were filled in this manner- one serving as a retainer for Callery and two which were sent to Allied-Signal for subsequent analysis. Each bottle contained about 8 grams of powder.

At Allied-Signal, one bottle from each run was analyzed and the other bottle was left sealed and retained for possible future analysis. A sample from each experimental run was prepared for particle size/shape analysis. Since the amount of sample required for Scanning Electron Microscopy (SEM) is so small, a method had to be devised in order to obtain representative and reproducible sampling. The best method involves throughly mixing the powder in the bottle and dispersing 0.1 gram in 100 mL of ethanol using an ultrasonic bath. This sample was then used for particle size determination by both light scattering and SEM.

The particle size determinations by light scattering were made on a Leeds and Northrup SPA Particle Size Analyzer. This instrument has a size range of 0.3 to

40 micrometers. One mL of the boron/ethanol slurry is added to the water in the sampler and continuously recirculated through the sample cell. The instrument converts the scattered light patterns into a particle size distribution. The instrument expresses the particle size as an equivalent spherical diameter.

In order to obtain reproducible samples for the SEM analysis, we spin-coated the boron-ethanol slurry onto one inch diameter cover slips using a Headway Research Photoresist Spinner. The coverslip was cleaned and dust and lint were removed with a filtered nitrogen stream. The glass disk was labeled and spun at 1000 RPM. Ten to 20 uL of the slurry were applied with an adjustable micropipet to the center of the spinning disk. The spinning motion evenly distributes the boron particles across the disk without forming large clumps. The particles also adhere to the disk sufficiently well to allow subsequent handing without losing material. Each sample was prepared in duplicate. These disks were then gold-coated before SEM analysis to minimize distortion due to charging effects in the instrument. All of the SEM photographs were obtained on a JEOL JSM-840A Scanning Microscope.

2. Size Determination Method

Prior experience with particle size measurement of Callery's commercial products has shown that the various indirect techniques, i.e., centrifugation, light-scattering, and Coulter counter, generally cannot distinguish individual particles from agglomerates. This has been determined by comparison of photomicrographs by S.E.M. and T.E.M. methods to indirect results; the comparisons show that the particle sizes determined by indirect methods correlate closely with measurements of agglomerate dimensions from photomicrographs, but are usually 2 to 6 times larger than the individual mean particle diameters. Additionally, T.E.M. - derived photomicrographs normally show low clarity due to the physical properties of boron. Therefore, the scanning electron microscope (S.E.M.) is considered to be the best technique for providing direct measurement of boron particle sizes.

The prepared slides with the dispersed powder are examined under SEM. Several photographs, 1 lower-magnification (20,000X) and 3 higher-magnification (50,000X) photomicrographs are made. The 20,000X print is used for qualitative judgment of agglomerate structure and particle population density. The three 50,000X prints are subjectively judged for relative populations of various particle sizes, then a random but representative sample of the total particle population is measured for diameter to within 0.2 mm. Prints of different runs are not critically compared prior to measurement, to reduce bias by the measurer. A minimum of 10, and generally 15 to 20, particles are measured on each print so that the number of measurements (n) is greater than 30. The number of measurements allows the approximation of Gaussian distribution to be made; mean size (x) and standard deviation (s) of the sampled population for

each experimental run are then calculated and are reported in the "Results" section. The resolution of the individual measurements is approximately ± 40 Å. As a check on the accuracy of the method 2 runs (2-8 and 3-1) made at essentially identical conditions were compared. The x values compare at 579 Å and 552 Å, and the s values compare at 129 Å and 101 Å, and using a two-population test of hypothesis for means [11], where

n = number of particles measured
x = individual particle size (a random variable)
$\bar{x}$ = sample arithmetic mean particle size

$$s = \text{sample standard deviation, } = \left(\frac{\sum (x_i - \bar{x})^2}{n-1} \right)^{1/2}$$

μ = population mean; regarded as constant for any population in this work

F = ratio of variance = s_1^2/s_2^2

$$S_p^2 = \text{Pooled variance of 2 sample means, } = \frac{s_1^2(n_1-1) + s_2^2(n_2-1)}{(n_1-1) + (n_2-1)}$$

$$t = \frac{(\bar{x}_1 - \bar{x}_2) - (\mu_1 - \mu_2)}{\left(s_p \left[1/n_1 + 1/n_2\right] \right)^{1/2}}$$

H_0 = null hypothesis $x_1 = x_2$ (deviation of method is due to chance)

H_1 = alternative hypothesis $x_1 \neq x_2$ (deviation of method is due to defective sampling)

at significance level = α = .01

for Run 2-8: $\bar{x}_1$ = 579 Å s_1 = 129 Å n_1 = 65

Run 3-1: $\bar{x}_2$ = 552 Å s_2 = 101 Å n_2 = 60

First, testing validity of assumption of $\sigma_1^2 = \sigma_2^2$ by F distribution:

Degrees of Freedom = (n_1-1, n_2-1) = (64, 59) at 2 α the critical value from F tables [11] for F (60, 60) is 1.84:

$$\text{Sample } F = \left| \frac{129}{101} \right|^2 = 1.63 < 1.84$$

There is insufficient cause to reject the hypothesis that deviation of the method is due to chance. One hundred twenty-three degrees of freedom and a two-tailed α level of 1% gives, from the t tables [11], a critical value of t = $\pm$ 2.61. The pooled sample variance is given by

$$s_p^2 = \frac{64(129)^2 + 59\ (101)^2}{64 + 59} = 13{,}552\ \text{Å}$$

$$s_p = 116\ \text{Å}$$

$$\text{The sample } t = \frac{(579 - 552)}{116\ \left(\frac{1}{65} + \frac{1}{60}\right)^{1/2}} = 1.30$$

The decision rule is to accept H_0 if $-2.61 \leq$ sample t ≤ 2.61. Therefore at sample t of 1.30 it is accepted that the deviation of the measuring method is due only to chance.

To further check that the distribution of particle sizes measured are not unintentionally biased, Run 3-1 particle size counts were plotted to determine distribution (See Figure 6) in 5 fractions. This run was chosen since nearly all of the distinct particles in the 3 separate 50,000X prints were measured. The resulting distribution resembles Gaussian but is skewed to the left, therefore the mean particle size of the total population is somewhat less than 552 Å.

A check of distribution for a larger particle size sample was done for Run 6-2 (See Figure 7). The distribution here is bimodal with 57% of particles falling into separate extremes comprising 27% of the size range. It is clearly

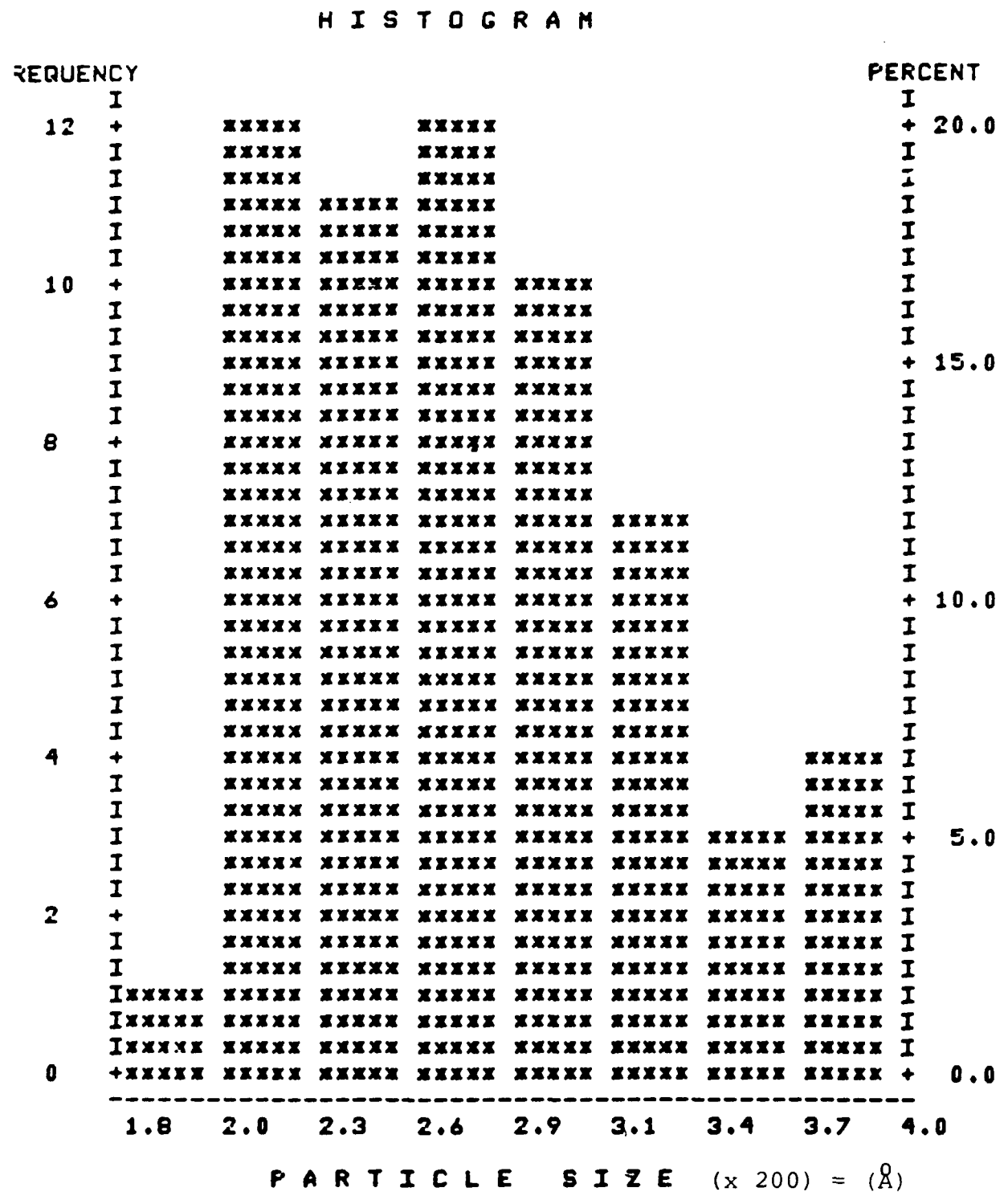

Figure 6. Particle Size Distribution for Sample 3-1B

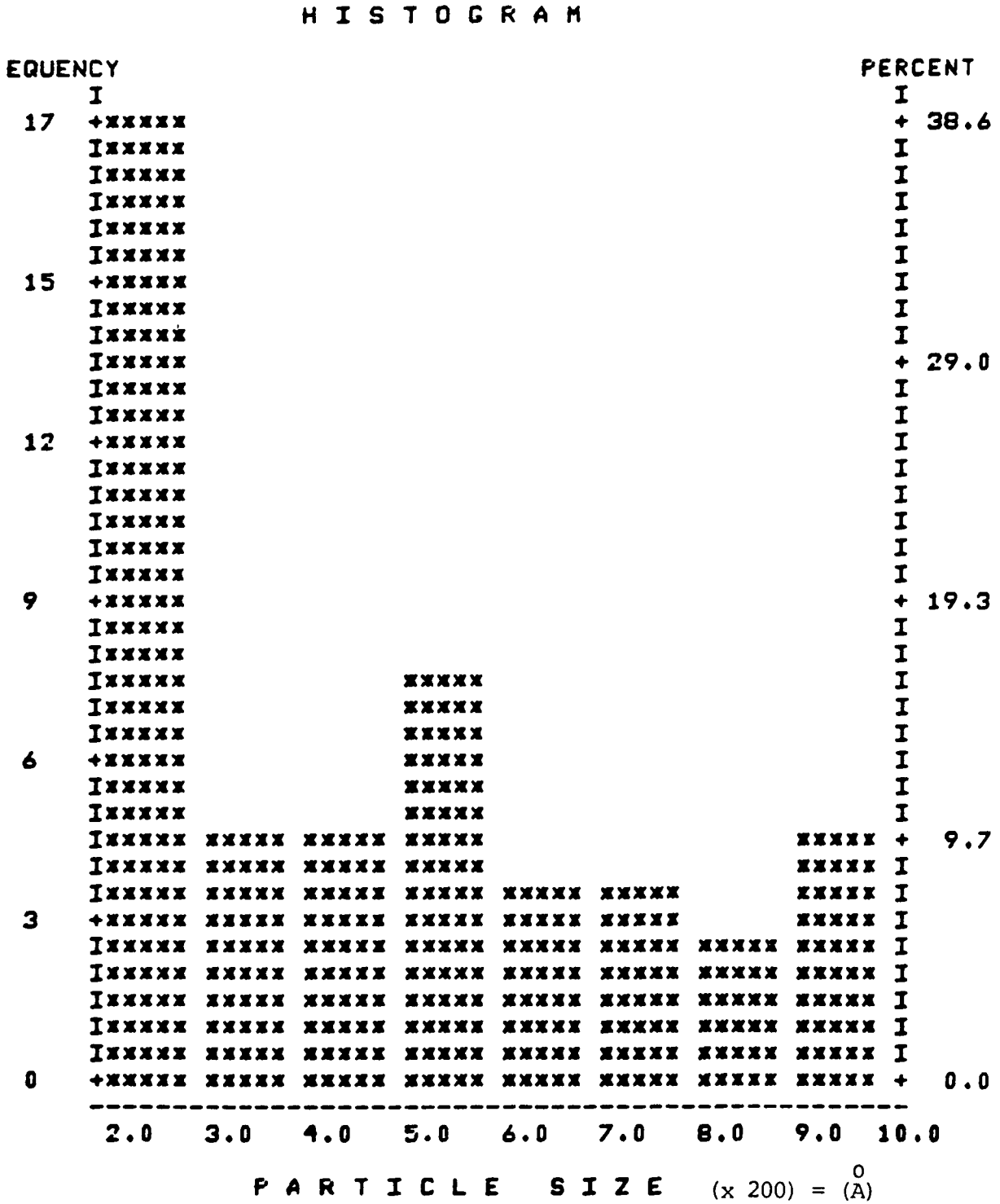

Figure 7. Particle Size Distribution for Sample 6-2B

misleading to assign a standard deviation to particle size averages with such an abnormal distribution; however, since the purpose of the work is to investigate process conditions that lead to larger particle sizes, the mean values x are still usable regardless of distribution. This is so because the effect of larger particles is to increase the mean size, whether it has occurred by increasing size of all particles, by adding large particles to an otherwise constant-size population, or by reduced numbers of small particles.

It must be kept in mind, however, when considering the mechanism of particle formation, that the process may create larger particles in discrete size ranges, or continuously. This could require a different mechanism for the different distributions of size enlargement. Generally, the runs showing mean particle diameters below approximately 700 Å have a normal but left-skewed distribution, and larger mean sizes will be reviewed on a case-by-case basis. Histograms and statistical analyses for all Groups 4, 5, and 6 Runs are available in the APPENDIX. Multiply the histogram X-Axis by 200 to obtain sizes in angstroms, since 5 mm on the 50,000X photomicrographs represents 1000 Å.

C. Chemical and Physical Analysis

In addition to the particle size/shape analysis, the boron powders produced by Callery were also subjected to a variety of physical and chemical characterization procedures. In the original project proposal, these analyses were geared toward determining the suitability of the boron for use in slurry fuels and comparing the properties of the uncoated boron with those of the coated boron produced by Allied-Signal during Phase II of this program. However, with the cancellation of Phase II, the particle characterization methods were modified to provide extensive analysis of the boron powders produced under various reactor conditions.

The analytical techniques used for the characterization of the boron powders can be divided into two main categories: physical properties and chemical composition. The physical characterization includes particle size/shape distribution (discussed in the previous Section V-B-2), surface area/porosity measurements, and particle density. The chemical analyses include a variety of techniques to determine both the bulk and surface composition of the boron powders.

1. Physical Properties

Particle Surface Area/Porosity

As the particle diameter increases, the surface area per unit mass of the particle will decrease. A spherical shape provides the minimum surface area to volume ratio of any geometrical configuration. The lowest possible surface area on the boron particles is desirable since the exposed surface impacts on

both the rheological and combustion properties of the slurry fuel. Therefore, in addition to particle size distribution, the surface area of the particles is another important parameter in determining the suitability of the boron for use in the fuel. The pore volume and distribution of pores within the particles is also important since these can significantly increase the surface area of a particle even though it is spherical. In this work, we determined particle surface areas using the B.E.T. nitrogen adsorption method.

Particle Density

Particle density is another important parameter in determining the stability of dispersions of boron particles in a fuel. The relative densities of the particles and the liquid dispersing medium control the rate of gravimetric settling. Therefore, a measure of the true particle density is required. In this case, we measured particle densities with a helium pycnometer to compare the boron powders produced at in this program with the tabulated density for boron as an indication of uniformity within the particles. If the particles were hollow inside, their density would be much lower than expected.

Heating Value

In the original proposal, measurement of the heating value of the particles was included in the physical characterization of the boron powders. These values were to be compared to those obtained for the coated particles produced in Phase II. Since Phase II was cancelled, the heating value measurements were eliminated from the characterization work.

2. Chemical Analysis

A variety of analytical techniques were used to determine both the bulk and surface chemical composition of the boron particles. The purity of the boron is the primary concern. According to the goals in the program, a minimum purity of 95% boron is required for obtaining the maximum volumetric heat content and combustion properties.

Boron Assay

Several analytical methods for the determination of boron at high concentrations were examined. We required a method that could determine boron concentrations of 95 wt% or greater with a precision of <1% RSD. The most appropriate techniques included acid-base titration in the presence of mannitol, Inductively-Coupled Plasma Atomic Emission Spectrometric (ICP-AES), and Atomic Absorption Spectroscopy (AAS).

The acid-base titration method using mannitol was examined, but we found that the titration endpoint was dependent on the ionic strength of the solution. Also, the boron concentrations determined by this method were lower than the expected values by 1 to 2 wt%. The AAS method has an upper linear working concentration range of about 500 μg/mL. This would require the use of either very small amounts of powder sample or large liquid volumes to assure representative sampling. We chose the ICP method because it involves fewer steps than the wet chemical method, allows the use of higher solution concentrations of boron than AAS, provides better precision, and allows us to simultaneously qualitatively identify most of the other elements that may be present in significant concentrations.

The following procedure was used to measure the boron content of the powders:

Sample Preparation

About 0.05 g of a boron powder sample was accurately weighed (± 0.0001 g) into a Pyrex 250 mL Erlenmeyer flask. The flasks were leached with dilute nitric acid before use. Fifteen mL of Nanopure water (Barnstead, Dubuque, IA) and 3.00 mL of ultrapure nitric acid (Seastar, Seattle, WA) were added to the flasks. The samples were carefully heated on a hotplate to dissolve the boron. There was an induction period of a few minutes before the reaction occurred and then there was a vigorous evolution of gas. The solutions were allowed to digest for about one hour with frequent additions of small volumes of water to wash down the sides of the flask. The samples were cooled, quantitatively transferred to a pre-leached, 100 mL polypropylene volumetric flasks (Nalgene, Rochester, NY), and 25.00 mL of a 1000 μg/mL scandium standard solution (Spex Industries, Edison, NJ) were added to provide a 50.0 μg/mL internal standard for the ICP measurements. The solutions were diluted to volume and thoroughly mixed just prior to analysis.

Several boron standard solutions were prepared using NBS 951 Boric Acid (National Institue of Standards and Technology, Gaithersburg, MD) which has a certified purity of 100.00 + 0.01 wt% boric acid. The 5000 μg/mL boron stock solution was diluted to make several standard solutions with concentrations that bracketed those expected for the boron powder samples (450 to 550 μg/mL). All samples were prepared in triplicate and a blank solution was prepared with each set of samples. The blank consisted of Nanopure water and nitric acid and was carried through the entire sample prep procedure.

ICP-AES Analysis

All measurement were performed on a Perkin-Elmer Plasma II Emission Spectrometer using argon as the plasma gas. Initially, four different boron emission lines were used for the analysis: 182.589, 182.640, 208.959, and 249.773 nm. The linearity of the instrument response was checked using the 5 standard solutions with concentrations of 450, 475, 500, 525, and 550 ug/mL Boron. The 249.773 nm emission line of boron was found to be the most sensitive, reproducible, and showed less effects from boron build-up. The other lines showed significant deviations from the standard values because of the large quantities of boron aspirated through the system. Generally, we found it necessary to aspirate pure water through the system for 5 to 10 minutes between each sample to prevent high background signals from boron.

The instrument was calibrated using the blank solution and three of the standard solutions-475, 500, and 525 µg/mL boron. Each of the boron powder sample batchs that were analyzed were prepared in triplicate and the emission from each solution was measured five times- a total of 15 measurements on each batch of powder. The standard solutions were frequently run between sample analyses to check the instrument calibration.

Semi-Quantitative Analysis

ICP-AES was also used to determine the levels of 67 other elements in the boron powder samples. Sample preparation was similar to that used for the boron assay procedure with a few variations. New plastic volumetrics flasks and Teflon beakers were leached with nitric acid before use to minimize contamina-

tion of the boron samples. About 1 gram of boron powder was dissolved and diluted in 50 mL volumetric flasks to increase the concentrations of any non-boron impurities for easier detection. A multi-element calibration mixture was prepared using Spex and Fisher certified ICP-AES standards, a scandium internal reference, and a matrix solution containing 2000 μg/mL boron in nitric acid. This analysis is considered semi-quantitative since the boron concentration in the sample matrix is about 10 times that in the standard multi-element calibration mixture.

Other Chemical Analyses

The boron powder samples were also analyzed by other techniques to further characterize their chemical composition. Elemental analysis for carbon, hydrogen, nitrogen, and sulfur was performed on a LECO CHN 600 and a LECO SC132, respectively. The ICP-AES method is not suitable for these elements. Infrared spectroscopy on a Perkin-Elmer 580B Infrared Spectrometer was used to identify any non-elemental boron compounds such as oxides and hydrides that may be present. X-ray diffraction (XRD) measurements on an automated Norelco Diffractometer were included to determine whether the boron powders are amorphous or have any crystalline phases present.

X-ray photoelectron spectroscopy (XPS) on a Hewlett-Packard 5950A ESCA Spectrometer with an AlKα monochromatic source was used to study the chemical composition of the surface of the boron powders. The surface composition is extremely important in determining the combustion properties of the powders. An oxide coating has been shown to reduce the combustion rate of boron in slurry fuels. XPS provides semi-quantitative information about the elements are

present at or near the surface of the boron surface. In addition, it also gives chemical information about the oxidation states of those elements. Therefore, we can distinguish boric oxide on the surface from chemically adsorbed oxygen.

The characterization techniques, the type of information obtained, and the specific instruments used are summarized in Table 3.

TABLE 3

Characterization Methods for Boron Powder Samples

Technique	Information Obtained	Instrument
Light Scattering	Agglomerate size distribution	Leeds & Northrup SPA Particle Size Analyzer
Scanning Electron Microscope	Particle size/shape distribution	JEOL JSM-840A Scanning Microscope
Helium Pycnometry	Particle density	Quantachrome Stereopycnomenter
B.E.T. Nitrogen Adsorption	Surface area/porosity	Quantachrome Autosorb-6
ICP-AES	Boron content of powders. Trace element impurities	Perkin-Elmer Plasma II Emission Spectrometer
Elemental Analysis	Carbon, hydrogen, nitrogen content, sulfur content	LECO CHN 600 LECO SC132
XPS	Composition of particle surface	HP5950A ESCA Spectrometer
IR	Identification of boron compounds	Perkin-Elmer 580B Infrared Spectrometer
XRD	Identification of chemical phases, extent of crystallinity	Automated Norelco Diffractometer

VI. EXPERIMENTAL RESULTS

The experimental run data consists partially of tabulated values for material balance, Reynolds numbers, T_a, and particle size, which are included in the text of this section. The balance of the data, consisting of SEM photomicrographs of boron samples, statistical analysis computer printouts, and particle size histograms, are attached in the Appendix, due to their bulkiness.

A. Conventional Mode

The Group 1 experiments exhibited no particularly unusual performance with the variations of nozzle size and diborane feedrate. Some "Clinker" formation (chunks of boron caused by wall deposition) was observed, particularly in Run 1-8. The use of the largest feed nozzle in the series, 3/8 inch O.D., led to some problems with nozzle plugging and tended to cause slightly erratic operation. For Run 1-11, it had been planned to operate at 5 lb/hr diborane flow, but the high pressure drop created by the 18 gauge feed nozzle limited the feedrate to 2.0 lb/hr diborane. To even achieve 2.0 lb/hr, the dilution nitrogen was eliminated for that run only. The particle size measurements range between 569 Å and 710 Å; random histograms done for Runs 1-6 and 1-11 show fairly normal distribution.

Group 2 experiments were all performed at constant mole fraction diborane feed, using 2 sizes of feed nozzle. The runs using the 3/8 inch O.D. feed nozzle continued to exhibit clinker formation, although an attempt at reducing clinkers was made in Run 2-1 by shortening the feed nozzle/flush tube by 1 inch. Runs 2-1 and 2-7 were performed with no dilution nitrogen flow, which did not

significantly increase particle size. Particle size measurements range from 514 Å to 641 Å; a comparison of Runs 1-9 and 2-2, made under similar conditions, show about a 10% variation in mean particle size, which tends to validate the measurement technique. Run 2-1 feed conditions were intended to achieve laminar flow conditions in the feed nozzle, presumably altering the nature of the feed jet structure, with no apparent benefit to particle size.

Group 3 Runs were conducted to examine the effect of T_a on particle size. All but one of the runs gave sizes similar to previous runs; Run 3-6 showed a substantial increase in size, and was incompletely dehydrogenated. This run finally provided the clues needed to find process conditions that lead to larger particles; these clues were incorporated in subsequent Group 4, 5, and 6 Runs, and basically involved lower reactor wall temperatures combined with moderate-to-low T_a values. Most of the Group 3 Runs showed slight plugging tendencies except for Run 3-6, which had some problem with clinker formation. Particle size distribution has been checked for Runs 3-1, 3-6, and 3-12; distribution is relatively normal for 3-1 and 3-12, but Run 3-6 has a distribution tending towards bimodal. Mean particle sizes for Group 3 have ranged from 494 Å to 912 Å.

Group 4 Runs were exclusively concerned with investigating lower reactor wall temperatures, and showed that this is an extremely important process variable. Clinker formation was much more prevalent, and was a constant annoyance during the runs. Run 4-4 was somewhat incompletely dehydrogenated, although less so than Run 3-6. A 1 inch longer feed nozzle/flush tube assembly was used for Run 4-4 (and also for Runs 5-3 through 5-6) which reduced somewhat the reactor plugging tendency. The Group 4 runs have provided considerable information for

assessing the particle formation mechanism; particle sizes ranged from 743 Å to 1475 Å, and the particle size distributions were anything but Gaussian. This is due to collision phenomena which are treated thoroughly in the discussion portion of this section.

Group 5 Runs were intended to explore turbulence effects on particle size, and have shown some relationship between those two. The minimum T_a of the program was used in Run 5-6. Some reactor plugging has again been experienced throughout these runs; the lower reactor wall temperatures tend to give rise to somewhat more frequent plugging, which is discussed later. Particle size ranged from 769 Å to 944 Å; particle size distribution again is quite different from Gaussian.

Group 6 Runs show some relationship between higher flow turbulence and larger particle size. Also, a pronounced effect of reactor wall temperature is displayed in this group of runs; lower wall temperatures give larger particles, and the absolute size is extremely sensitive to the zoning of wall temperatures. Again, all runs in this group were plagued with plugging, and Run 6-5 had the mildest plugging of the reactor and had one of the highest average wall temperatures. A modest trend for larger particle size when using smaller-diameter feed nozzles is evident from the results; this had not been clearly seen in Group 1 or 2 Runs since the effect had likely been masked by the higher temperatures used. Particle sizes in Group 6 ranged from 806 Å to 1288 Å, and the distribution was again quite different from normal Gaussian shapes.

B. Recycle Mode

The Group 7 Runs were all conducted with essentially no plugging during the runs; this is directly related to the higher T_a and reactor wall temperatures used for these runs, and is comparable to the experience in the Group 1 and 2 Runs. Particle feedrates were easily controllable during Runs 7-P to 7-6, but became erratic and considerably below design during the four consecutive recycle runs 7-7 to 7-10. The reason for this is unknown, but may be due to wear of the feeder or gradual plugging of the flush nitrogen lines that carried the powder.

A very surprising result is that recycle not only gave no particle size increase, but the particle sizes from the runs appears identical to those from Groups 1 and 2 Runs made at very similar conditions. For example, Run 7-4 BGHS showed 532 Å, S = 110 Å; the powder source for the run (and for all Runs 7-P through 7-6) was Run 2-12, which shows 526 Å, S = 104 Å. This unequivocally indicates that the reaction of diborane at the run temperature conditions is so rapid that non-fusible solids were formed before the diborane and powder feed streams began to mix. This was initially judged to be a disappointing result, but it actually provides some unexpected information concerning the rate of diborane decomposition, discussed further in Part "D" of this section. Since none of the Group 7 photomicrographs showed any size increases by a visual qualitative scan, no particle size measurement has been performed. The photomicrographs are included in the appendices for reference.

C. Tables of Results

The results of particle size and deviation, diborane consumption, boron produced, T_a, and Reynolds number are attached to this chapter.

TABLE 4

RUN NUMBER	lbs. BORON PRODUCED	lbs. B_2H_6 CONSUMED	B_2H_6 x .7814 MATERIAL BALANCE (%)	(°F) T_a	AVERAGE D_p* (Å)	(Å) DISTRIBUTION**
1-1	5.18	6.58	100.8	919	PRI 631 BGS 598	S-131 S-159
1-2	2.59	3.56	93.1	842	PRI 592 BGS 598	S-144 S-197
1-3	3.30	5.00	84.5	842	PRI 603 BGS 640	S-118 S-177
1-4	3.41	3.69	118.3	842	PRI 580 BGS 609	S-102 S-116
1-5	3.65	4.81	97.1	842	BGS 669	S-201
1-6	2.88	3.69	99.9	842	BGS 621	S-131
1-7	3.78	5.07	95.4	842	BGS 583	S-109
1-8	4.21	5.00	107.8	842	PRI 673 & 680 BGS 662 & 649	S-164 & 156 S-163 & 169
1-9	2.21	3.28	86.2	842	BGS 710	S-126
1-10	2.67	3.60	94.9	842	BGS 606	S-127
1-11	3.57	4.53	100.9	1083	BGS 569	S-104
2-1	1.88	2.06	116.8	842	BGS 629 PRI 623	S-98 S-109
2-2	2.64	3.38	100.0	842	BGS 641	S-129
2-3	3.64	4.66	100.0	842	BGS 624	S-133
2-4	5.04	6.13	105.2	842	BGS 598	S-105
2-5	3.58	4.75	96.5	842	BGS 637 PRI 689	S-99 S-146
2-6	3.70	5.00	94.8	842	BGS 603	S-109

* BGS = Baghouse Sample,
PRI = Primary Separator Sample

** Standard Deviation of
the sampled population

TABLE 4 (Continued)

RUN NUMBER	lbs. BORON PRODUCED	lbs. B_2H_6 CONSUMED	B_2H_6 x .7814 MATERIAL BALANCE (%)	(°F) T_a	AVERAGE D_p* (Å)	(Å) DISTRIBUTION
2-7	2.19	2.87	97.7	842	BGS 638	S-132
2-8	3.83	4.75	103.2	842	BGS 579	S-129
2-9	3.70	4.87	97.2	842	BGS 546 PRI 573	S-100 S- 90
2-10	2.53	3.31	97.8	842	BGS 514	S- 88
2-11	3.22	4.06	101.5	842	BGS 548	S-128
2-12	3.93	5.12	98.2	842	BGS 526 PRI 544	S-104 S-104
(COMPOSITE)					BGS 616	S- 91
3-1	3.65	4.62	101.1	770	BGS 552	S=101
3-2	3.62	4.43	104.6	670	BGS 518	S=108
3-3	2.50	3.32	96.4	570	BGS 610 PRI 493	S=109 S= 75
3-4	3.63	4.82	96.3	570	BGS 537	S= 97
3-5	3.72	4.69	101.4	582	BGS 558 PRI 644	S=120 S=129
3-6	3.97	4.50	110.1	570	BGS 912	S=388
3-7	3.03	3.84	101.0	1219	BGS 547 PRI 549	S= 99 S=105
3-8	3.55	4.50	101.0	1252	BGS 494	S=113
3-9	3.79	4.68	103.5	970	BGS 504	S= 83
3-10	3.05	3.76	103.8	1070	BGS 589	S= 91
3-11	3.02	3.69	104.8	1170	BGS 542	S= 89
3-12	3.26	4.00	104.4	1219	BGS 558 PRI 558	S= 97 S= 88
4-1	2.44	3.06	102.0	554	BGS 754	S-353
4-2	3.02	4.00	96.6	582	BGS 743	S-292

TABLE 4 (Continued)

RUN NUMBER	lbs. BORON PRODUCED	lbs. B_2H_6 CONSUMED	B_2H_6 x .7814 MATERIAL BALANCE (%)	(°F) T_a	AVERAGE D_p* (Å)	(Å) DISTRIBUTION
4-3	0.34	0.50	(87.0)	582	BGS 1062	S-518
4-4	3.06	4.00	97.9	582	BGS 1475 PRI 1268	S-576 S-677
5-1	1.12	1.13	(126.8)	580	BGS 769	S-417
5-2	3.43	4.62	95.0	580	BGS 916 PRI 757	S-354 S-392
5-3	3.00	3.87	99.2	580	BGS 884	S-397
5-4	2.23	2.69	106.1	580	BGS 853	S-474
5-5	2.75	3.31	106.3	530	BGS 944	S-441
5-6	3.11	4.07	97.8	480	BGS 786 PRI 821	S-324 S-520
6-1	1.45	2.00	92.8	580	BGHS 1288	S-522
6-2	2.67	3.43	99.6	580	BGHS 933	S-480
6-3	1.54	1.75	112.6	580	BGHS 963 PRI 740	S-546 S-409
6-4	0.74	1.00	(95.3)	580	BGHS 922	S-349
6-5	3.08	3.75	104.9	580	BGHS 846 PRI 810	S-360 S-389
6-6	2.89	3.56	103.7	580	BGHS 1120	S-478
6-7	1.90	2.63	92.6	580	BGHS 1185	S-629
6-8	2.88	3.37	109.5	580	BGHS 806	S-296

TABLE 4 (Continued)

RUN NUMBER	DATE	lbs. BORON PRODUCED	lbs. B_2H_6 CONSUMED	B_2H_6 x .7814 MATERIAL* BALANCE (%)	(°F) T_a	ACTUAL BORON PARTICLE FEEDRATE (g/hr)
7-P	11-10-87	2.93	3.69	101.6	842	12.9
7-1	11-11-87	3.70	4.56	103.8	842	12.9
7-2	11-12-87	2.87	3.56	103.2	842	12.9
7-3	11-13-87	3.50	4.25	105.4	842	25.8
7-4	11-16-87	3.57	4.57	100.0	842	32.2
7-5	11-17-87	3.52	4.44	101.5	842	25.8
7-6	11-18-87	3.31	4.07	104.1	842	12.9
RECYCLE						
7-7	11-19-87	3.51	4.63	97.0	842	3.3
7-8	11-20-87	3.34	4.56	93.7	842	3.3
7-9	11-23-87	3.87	4.62	107.2	842	7.3
7-10	11-24-87	3.57	4.56	100.2	842	4.7

* Boron particle feed not deducted from "lb. boron produced" column

TABLE 4 (Continued)

RUN NUMBER	FEED NOZZLE N_{Re}	REACTOR STREAM N_{Re}
1-1	15,980	1,582
1-2	7,679	1,705
1-3	24,282	1,826
1-4	16,118	1,705
1-5	50,969	1,826
1-6	5,196	1,705
1-7	16,430	1,826
1-8	9,489	1,826
1-9	3,001	1,705
1-10	31,036	1,705
1-11	33,552	1,483
2-1	973	1,575
2-2	2,620	1,651
2-3	5,222	1,745
2-4	7,833	1,840
2-5	10,444	1,934
2-6	13,055	2,127
2-7	7,335	1,582
2-8	19,822	1,690
2-9	29,776	1,757
2-10	39,643	1,822
2-11	49,598	1,890
2-12	58,941	1,951
3-1	(No Further Calculation)	1,799
3-2		1,859
3-3		1,992
3-4		1,992
3-5		1,895
3-6		1,992
3-7		1,690
3-8		1,619
3-9		1,593
3-10		1,549
3-11		1,468
3-12		1,690
4-1		1,992
4-2		1,895
4-3		1,895
4-4		1,895

TABLE 4 (Concluded)

RUN NUMBER	FEED NOZZLE N_{Re}	REACTOR STREAM N_{Re}
5-1		1,593
5-2		1,299
5-3		1,013
5-4		841
5-5		841
5-6		841
6-1		2,735
6-2		2,771
6-3		3,132
6-4		895
6-5		1,018
6-6		1,895
6-7		1,895
6-8		1,895

(7-P through 7-10 not calculated)

D. Discussion of Particle Size and Trends

Taken as a whole, the results of the various runs have provided some very unexpected information which nonetheless appears consistent and credible. Some variables expected to have a large influence on particle size, namely feedrate, feed concentration, and nozzle diameter, in fact exert little desirable control over size. The reactor wall temperature, on the other hand, is a very powerful variable which overshadows all others when high wall temperatures are used. The adiabatic combustion temperature, even at levels below those believed possible, has only a mild effect on particle size even when reactor wall temperatures are rather low. The heater nitrogen flowrate and related turbulence has an effect that would seem reasonable, across a Reynolds number range of 840 to 3100 which encompasses transition and fully turbulent flow conditions (the reactor flow stream is probably so disturbed by reaction that true laminar flow is not likely to occur).

The independent variables that do have some effect on particle size are plotted vs. mean particle diameter in Figures 10 through 13. Before those figures are discussed, other relevant results from the experimental program are that no breakdowns or mishaps occurred during the experiments, which vindicates the Air Force decision to use the Callery process as the vehicle for the investigation. Also, the overall material balance for Groups 1 to 7 Runs is 100.35%, which shows that excellent accountability has been developed and maintained for all the material handling aspects of the program.

Now, reviewing the mean particle size as a function of certain independent variables brings us to Figure 8. This shows the mean particle size for the progression of runs in the program, and demonstrates that there has been a learning curve associated with the experimentation. The bars are the bounds of the ± size distribution (even though use of the term "standard deviation" of the distribution is not exactly correct, as explained in Section V.B.2.), and the dots are the mean particle size. The figure clearly depicts that the Group 1 and 2 runs had no significant change in particle size, and that subsequent runs were frequently successful in this respect. The most striking result here is that runs having larger mean sizes always have wider distributions; this is more clearly shown in Figure 9 as a plot of mean size vs. distribution. The trend of increasing distribution with mean size is quite pronounced and consistent; this has provided a major clue to the actual particle formation mechanism, as will be explained shortly.

Figure 10 is a plot which is analogous to a standard kinetic plot. If mean particle size (y-axis) were dominated by the diborane decomposition rate, the size would be related to reaction temperature, $\bar{x}$ and T_a could be plotted as -ln (r) vs. 1/T, and the slope of the plot would be negative (T_a is used as reaction temperature, as described earlier in Section III). The actual trend shown is opposite to a kinetically-controlled trend [12], so there must be some other variable involved. At this point, the results of the recycle study are useful:

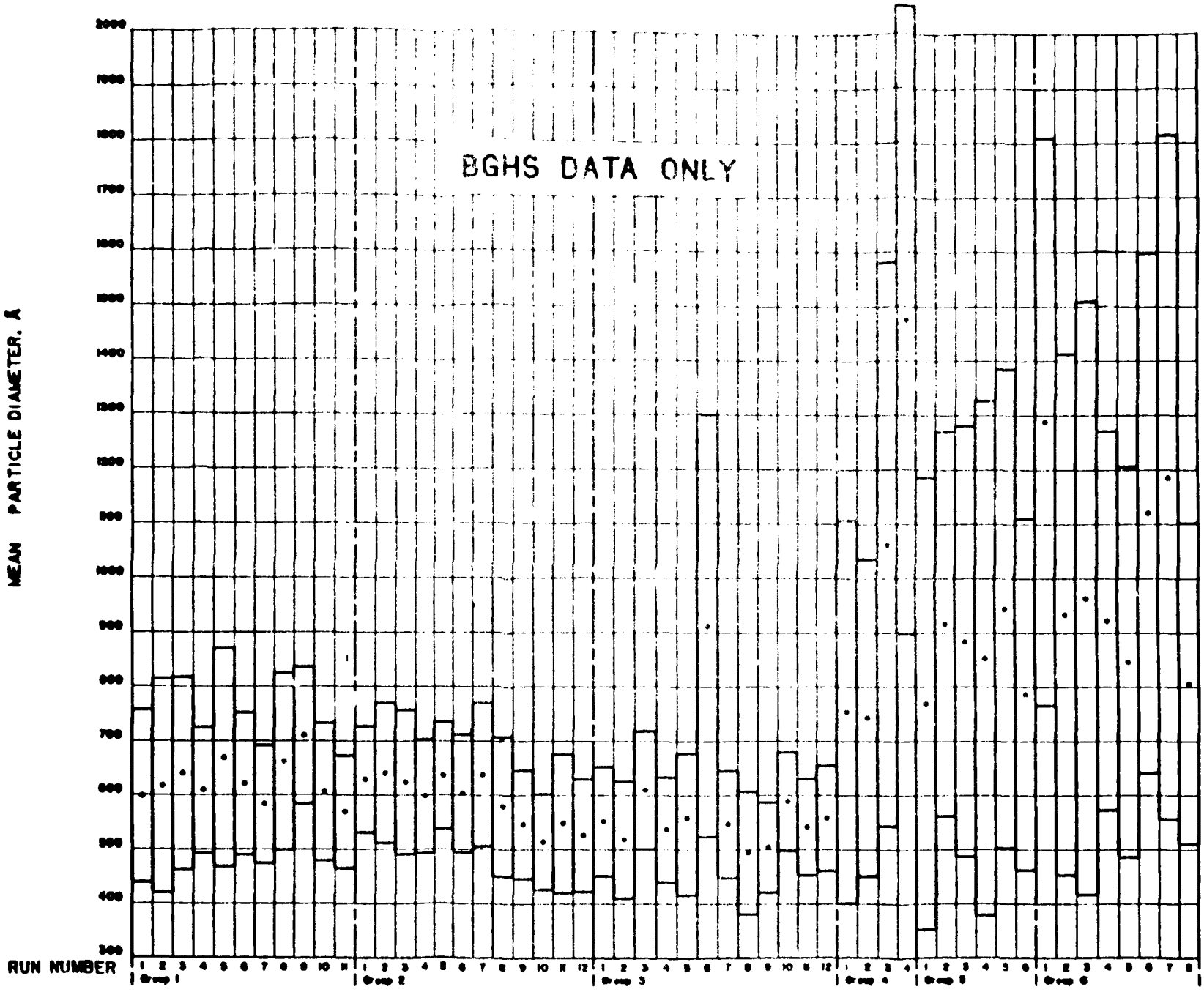

Figure 8. Mean Particle Diameters for Baghouse Samples

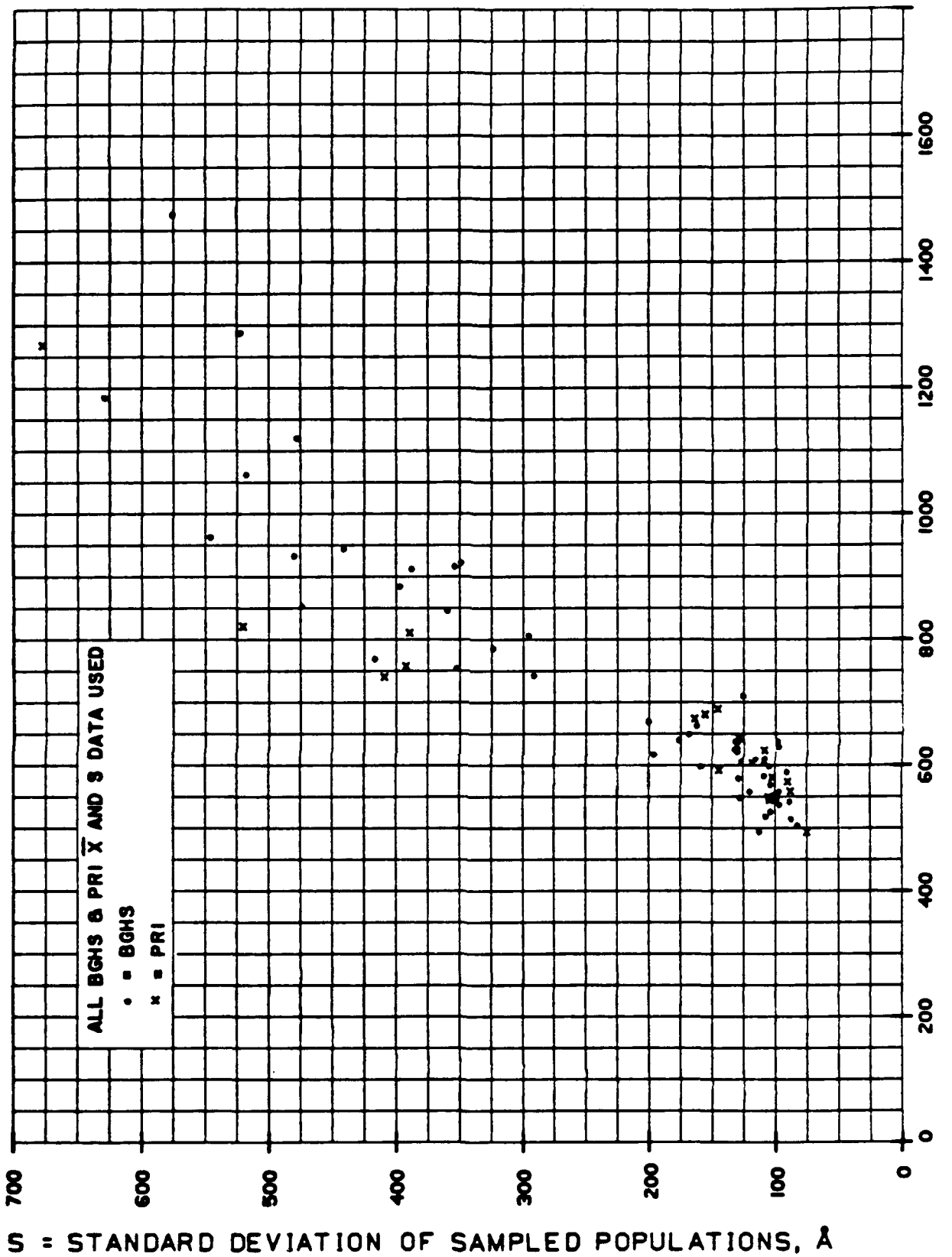

Figure 9. Standard Deviation vs. Mean Particle Size for Boron Powder Samples

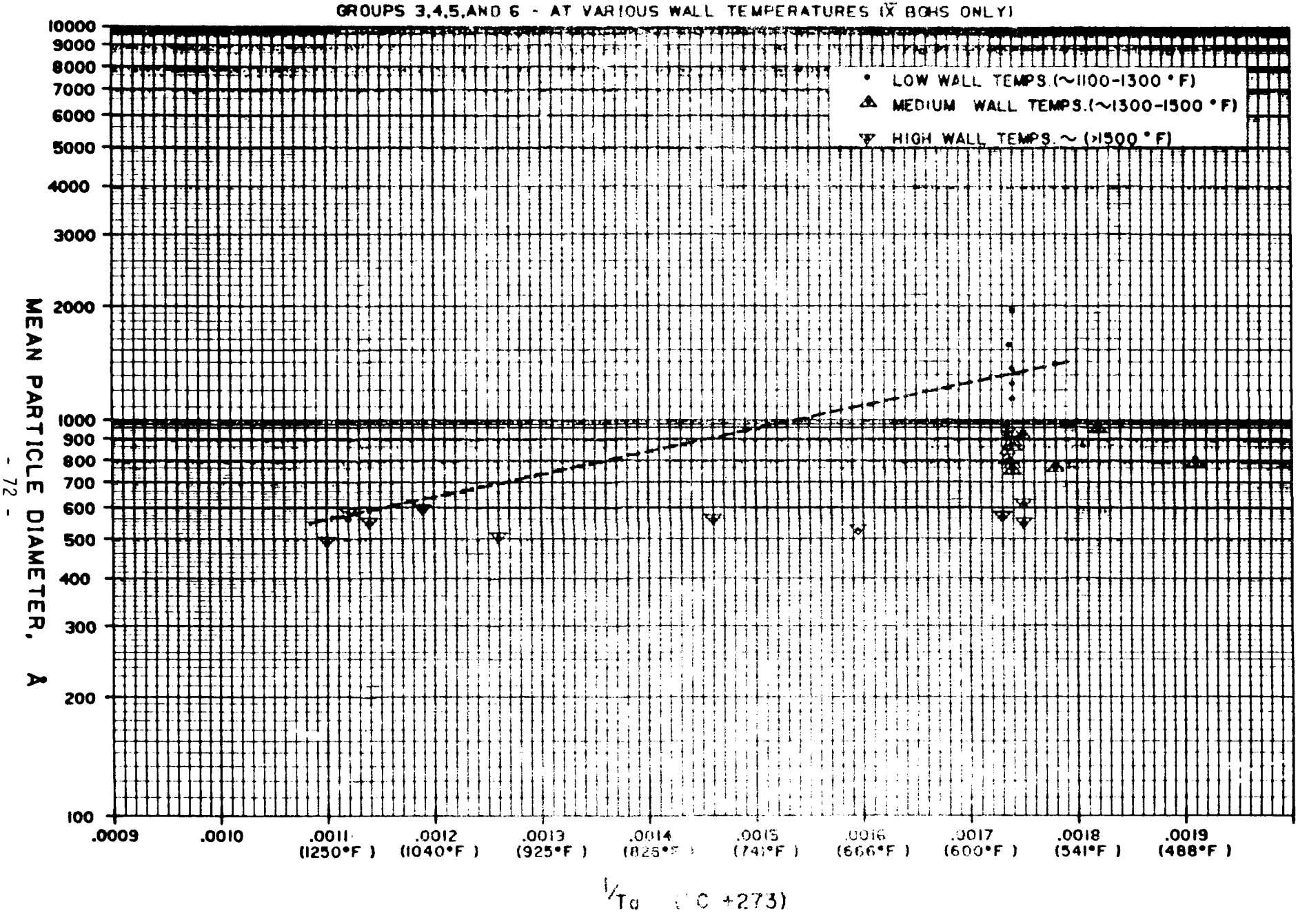

Figure 10. Particle Diameter [illegible]

mixing of the particle recycle and diborane feed streams was accomplished in a very short length in the feed jet region, yet the resulting particles were identical in size and distribution to those obtained when feeding only diborane under otherwise similar conditions. This is very significant because it means that the diborane has already: decomposed to form a vapor, undergone homogeneous nucleation to form particles, and those particles have solidified before any contact occurred with the recycled particles. Therefore, the decomposition/nucleation/solidification is extremely rapid; it is roughly estimated that this has occurred within 5 to 7 nozzle diameters of length in the reaction zone [11,13,14], or in other words solid particles have formed within about 0.035 ft (1 cm) from the end of the 13 gauge feed nozzle. Furthermore, since the recycled particle stream is between the diborane feed jet and the surrounding hot "heater nitrogen" stream, mixing with that hot nitrogen is <u>not</u> what causes the decomposition.

The actual driving force for reaction is the radiant heat transfer from the hot reactor wall. Looking at Figure 11, the obvious trend is increasing mean particle size with decreasing average wall temperature, although it is further required that T_a be sufficiently low. The conclusion drawn from this data is that most of the particle growth occurs through collisions; high wall temperatures and, to some extent, high T_a temperatures, "cook" already-formed particles so rapidly that collisions do not result in size growth.

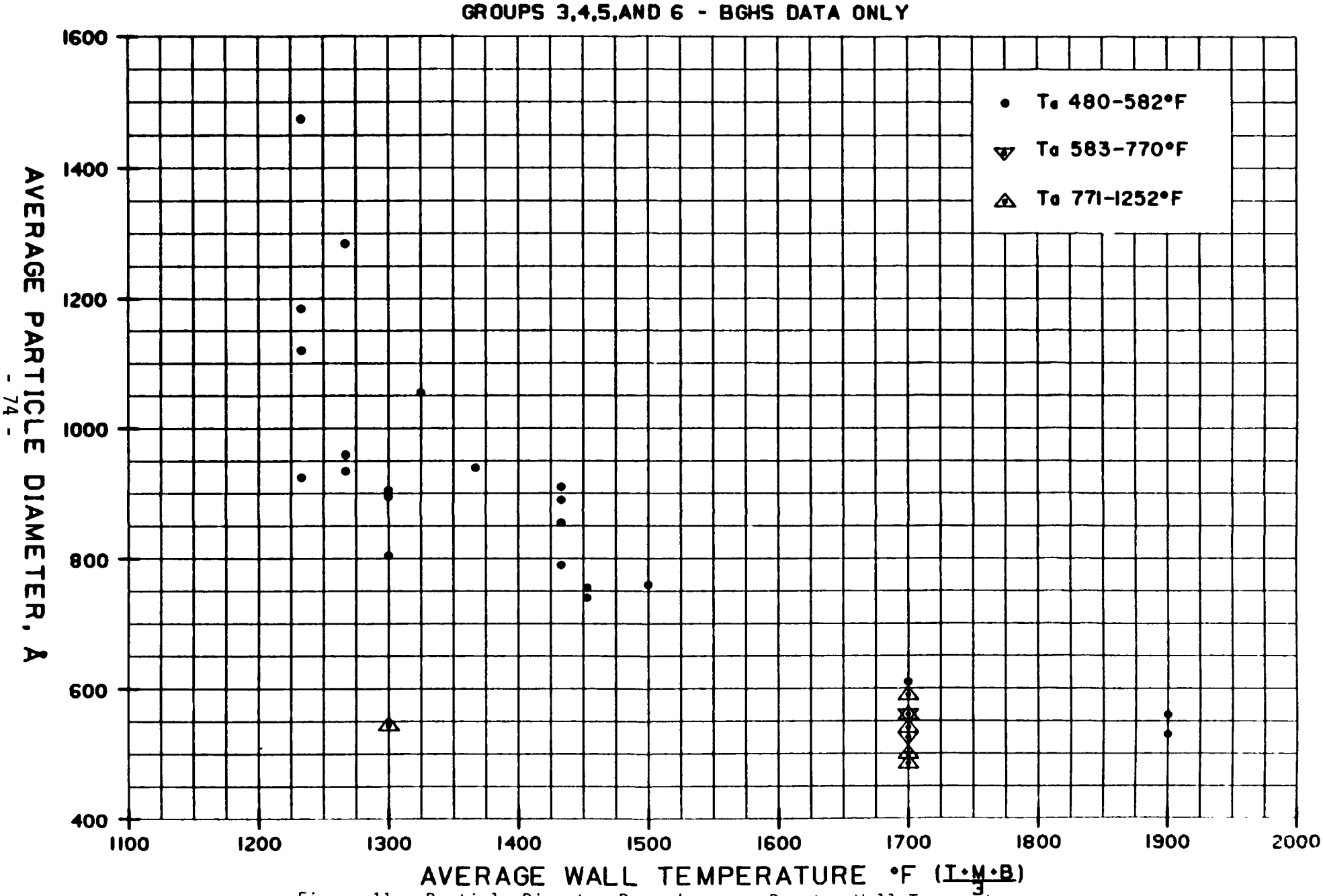

Figure 11. Particle Diameter Dependence on Reactor Wall Temperature

Wall temperatures have been demonstrated in Runs 3-6, 4-3, 4-4, 5-5, 6-4, 6-6, and 6-7 to have an overwhelming effect on resulting particle size; a top and middle reactor heater temperature of 1100°F results in the largest particles, 1300°F gives medium sizes, and any temperature above about 1350-1400°F prevents significant growth. Also demonstrated in those runs is that the final heater zone must be above about 1500°F to fully dehydrogenate the final particles; otherwise the overall decomposition is incomplete. Some approximate calculations of radiant heat flux show that at 1100°F the flux is 3662 Btu/Hr/ft of length (total spectrum, and assuming black-body radiator), at 1300°F flux is 5934 and at 1500°F flux is 9126. As a comparison, nitrogen at 10.15 lb/hr and 750°F has 1729 Btu/hr total enthalpy, and the energy delivered at 750°F-T_a or a Δ T of 168°F is only 442 Btu/hr. This, plus the fact that radiation is efficiently absorbed only by diborane and solid particles, explains the extreme sensitivity of the particle size to reactor wall temperature.

An interesting offshoot of the explanation above is that the plugging phenomenon is now believed to result from an imbalance between the rate of reaction and thermophoretic forces. At high wall temperatures (ca. 1700°F), the reaction is driven rapidly and considerable hydrogen evolution occurs in a very small volume of reaction, creating a rapid expansion - and therefore velocity - of the reaction products in all directions. However, the high heat flux from the hot reactor wall provides considerable thermal force in the direction away from the wall and prevents particles from actually impinging on the wall. At lower wall temperatures (ca. 1100°F) the reaction occurs more slowly although it is still rapid, but the heat flux away from the wall is only 1/4 as much, thereby allowing particles to impinge and stick to the wall. Of course, it is also possible that particles always impinge on the wall and only at the lower-wall-temperatures are

reaction particles liquid enough to stick to the wall. However, Runs 6-1 through 6-4 had considerable changes in heater nitrogen flow velocities but the plugging was always observed to be between 1 inch and 2 inch down from the end of the feed nozzle; the top reactor wall heater was at 1100°F for all these runs. Regardless of the cause, since lower wall temperatures are desirable for control of particle size, the best solution to plugging would be to use a larger reactor diameter. This would have two beneficial effects: the wall would be farther from the source of particles that cause plugging, and the heated surface area per unit of reactor volume would decrease. The suggested rule of thumb would be to double the reactor diameter when reducing top wall temperature from 1700°F to 1100°F, at constant diborane feedrate. This doubling of the existing diameter should effectively prevent plugging at feedrates up to about 8 lb/hr of diborane.

Returning to particle growth, even though lower wall temperatures allow collisions to result in growth (by delaying solidification of particles), there must still be particles being formed someplace that then undergo these collisions. Referring to the histograms of size distribution in the Appendix, it can be seen that the runs giving larger mean particle size still always have a significant percentage of sizes in the 300 Å to 500 Å range; this the source of the larger "standard deviation" in Figures 8 and 9 and reinforces the conclusion that the larger particles are formed by collisions among the population of 300 to 500 Å particles, rather than large particles being formed directly from nucleation or by vapor deposition onto small particles. The constant presence of the 300 Å to 500 Å size range, regardless of the major variations made in feedrate and feed jet mixing rate, means that the number of nuclei formed by homogeneous nucleation is changing with diborane feedrate, which in turn requires that the

nucleation rate J change with feedrate, which finally means that either the critical supersaturation, S_c, and/or the nucleation temperature (essentially, the condensing species' vapor pressure) is changing [4,5] with feedrate. It is probable that the nucleation temperature is what changes, because the decomposition reaction is exothermic and the flush N_2 stream adds low-enthalpy mass around the reaction zone. Since feed jet mixing now is known to have little effect on nucleation, and since runs made at constant T_a and varying feedrate all show similar populations of 300-500 Å particles, it is concluded that the T_a value is not the important temperature affecting the nucleation rate. This is why T_a variations showed only a mild influence on particle size.

To be strictly correct when discussing the homogeneous nucleation, it is impossible to determine from the data whether the "plane" of nucleation changes with feedrate and nucleation rate is constant, or whether nucleation rate changes and the volume in which it occurs is constant. It is believed, through the above explanation, that nucleation rate changes, but in either case the end result on the macroscopic scale is production of relatively constant-size particles which then may or may not experience growth via collisions. This "self-leveling" feature is quite handy for a production process, since particle size control is now reduced to controlling the collisions between "Base" particles. The particle formation mechanism should be viewed as consisting of primary, secondary, and tertiary particles: primary particles are formed directly from the vapor by homogeneous nucleation and are more or less constant in size at roughly 20 Å as described in Section II; secondary particles are formed extremely rapidly via collisions of about 6,000 to 10,000 primary particles in a distance controlled by the mean free path of the averaged size of particles (for 20 Å ——> 400 Å particles this distance is very roughly 10 to 100 $\times 10^{-6}$ meter)

[15]; then tertiary particles are formed via energetic collisions of secondary particles up to a size limited by the availability of fluid secondary and tertiary particles.

Since collision is seen to be the most important growth mechanism, a review of the results of changes in bulk flow turbulence must be made. Figure 12 shows the relationship of mean particle size with turbulence in the reactor, at various levels of T_a. No clear trend is visible from this plot; it is already known that reactor wall temperature is quite important for obtaining larger particle sizes, so Figure 13 has been assembled from the best constant conditions of T_a and reactor wall temperature. It can be seen that mean particle size increases substantially with higher turbulence up to about N_{Re} = 2,000. This is consistent with the expected trend. However, Runs 6-1 to 6-3 show a drop in size with further turbulence increases, and the question immediately arises: why would particle size decrease? Higher turbulence intensity should yield continued size growth, or at the very least, the curve should flatten out at higher turbulence if only a threshold of momentum were required for collisions to result in fusion. Part of the answer is that Runs 4-4, 6-1, 6-2, and 6-3 had respective diborane feedrates of 1.68, 3.0, 4.0, and 5.0 lb/hr. Looking at the histograms for those runs reveals that the "Base" secondary particles - the smallest-size fraction on the histogram - are respectively 500 Å, 460 Å, 400 Å, and 300 Å. Therefore, for an equal number of collisions due to the identical scale of turbulence in these four runs (ignoring the differing "Base" particle populations due to different feedrates), one would reasonably expect smaller tertiary particles to result. If Run 6-3 had "Base" secondary particles of 500 Å as did Run 4-4, equal collisions would have produced about 1600 Å final particle

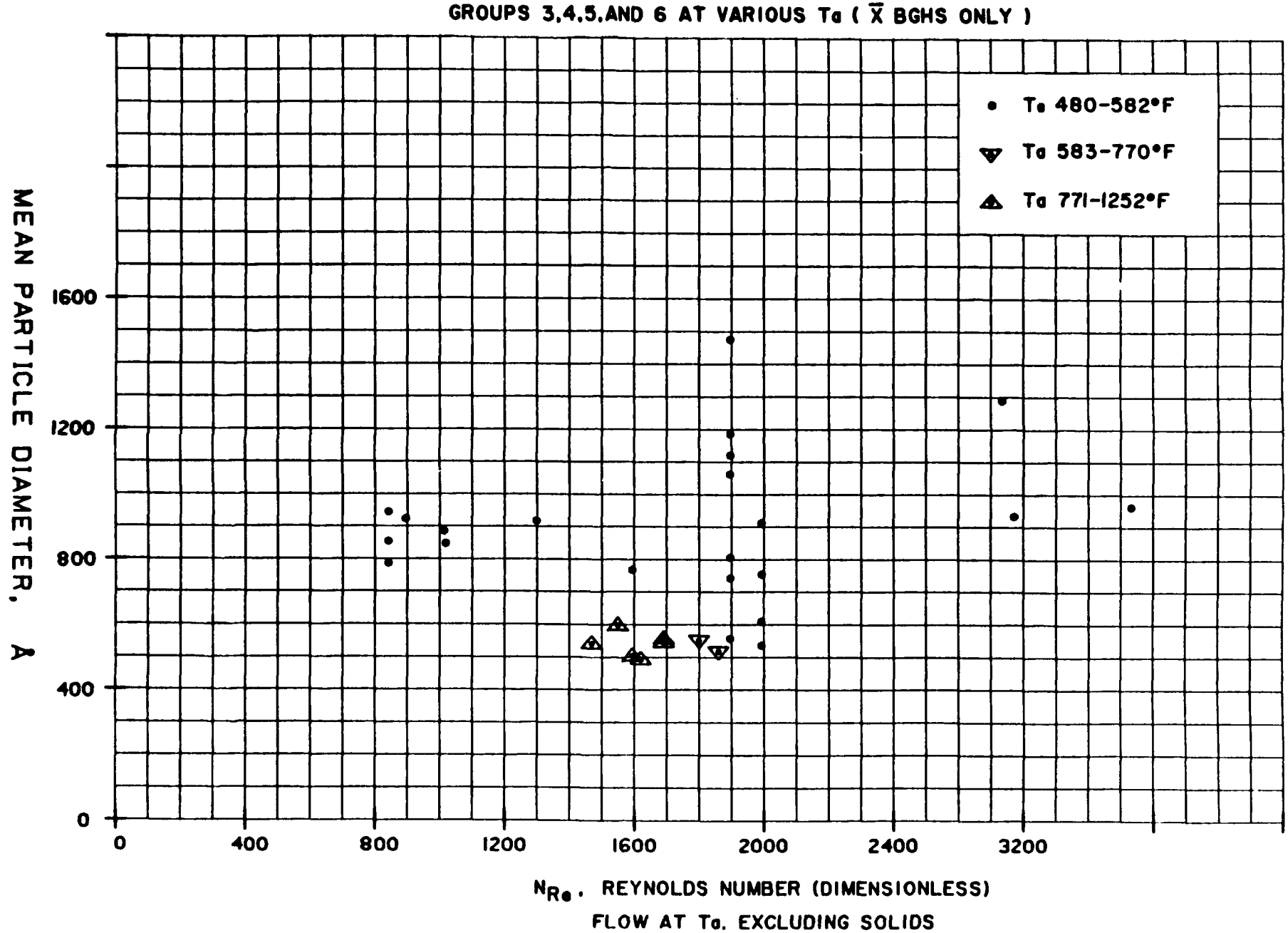

Figure 12. Particle Diameter Dependence on Reynolds Number

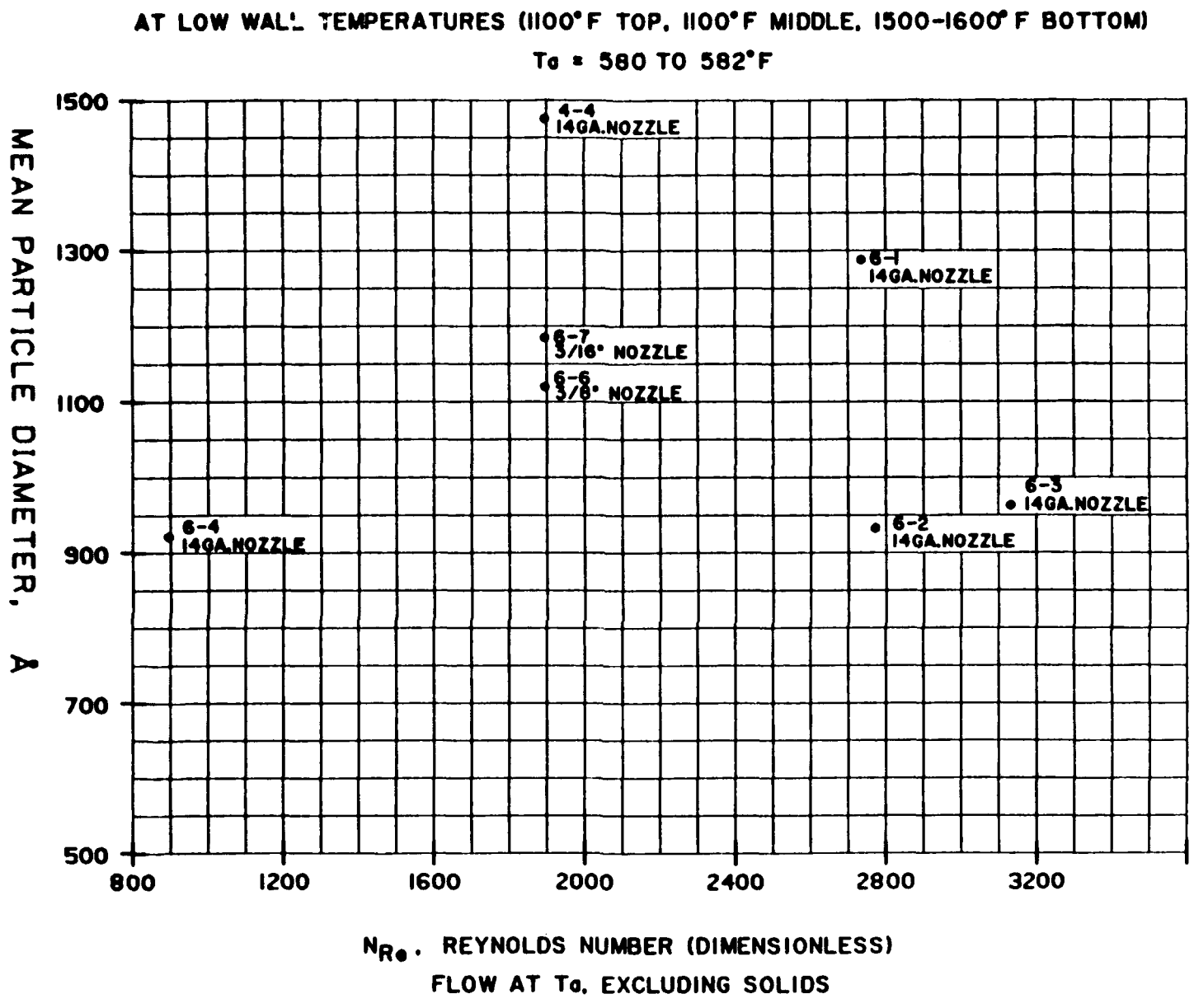

Figure 13. Particle Diameter Dependence on Reynolds Number

size, which would plot well on Figure 13 and would show the D_p vs. N_{Re} trend flattening out with increasing turbulence. Of course, the next question is why would the feedrate increase produce smaller secondary particles? Homogeneous nucleation theory [4,5] proposes the concept of a critical nucleus radius, which in our work is the so-called primary particle. The size of this nucleus is related to the nucleation temperature and decreases with higher temperature. Previously in this section, it had been suspected that the nucleation rate has been changing with diborane feedrate, and the results of Runs 6-1 to 6-3 appear to be another manifestation of this phenomenon.

The significant results of the work have been discussed, and as a concluding effort the hypothesized mechanism of particle formation needs to be reviewed in light of these results.

Part 1 - Thermal decomposition of the boron hydride, at a kinetic rate limited by rate of heat transfer: this event was found to be controlled in this study by the radiant heat transfer from the hot reactor wall, and by the heat of reaction of the specific boron hydride. It is totally intertwined with Part 2 of the original hypothesized mechanism. Efforts to modify the reaction rate and the resulting supersaturation have been essentially unsuccessful due to the extremely fast course of the reaction. Major variations of borane feedrate have a negligible effect on the reaction rate.

Part 2 - Nucleation and condensation of an intermediate species supersaturated vapor into a glassy or tarry fluid particle, at a temperature near T_a: the nucleation has been found to be so rapid that opportunities

for control of it are nonexistent. Particles produced by nucleation are on the order of a few tens of angstroms, and this size is slightly affected by borane feedrate. Feedrate increases appear to increase the nucleation rate; T_a is not a factor in Parts 1 or 2.

Part 3 - Continuing thermal decomposition of the particle while undergoing growth via collision and/or deposition: Growth immediately after nucleation may occur by deposition and does occur by collision, to form secondary particles. Vapor species are more or less completely depleted during formation of primary and secondary particles; tertiary particles are formed by collision only, under suitable radiant and convective heat conditions.

Part 4 - Escape from the "Reaction Zone" after being fully dehydrogenated: The original reaction zone concept considered only the turbulent feed jet. In actuality, only a very small portion of this feed jet is the true reaction zone; the remainder of it and the remaining reactor length only provide space for collisions to occur. Also, full dehydrogenation is a kinetic process requiring sufficient time and temperature; the reaction should be first-order, but higher solids loadings in the bulk flow and/or larger particle diameters would likely introduce homogeneity and thermal conduction requirements that may change the apparent kinetic rate towards zero-order.

The revised hypothesized mechanism of particle formation is therefore written as:

(1) Primary particle formation resulting from homogeneous nucleation of a supersaturated B_xH_y vapor. The vapor is produced by first-order irreversible thermal decomposition of boron hydride, driven primarily by absorption of thermal radiation. Particle size decreases and particle population increases with increasing boron hydride feedrate.

(2) Very rapid secondary particle formation resulting from multiple mean-free path collisions of primary particles and from remaining vapor condensing on primary particles. Particle size growth may be quenched by high temperatures of the radiation source or of the surrounding inert gas (T_a).

(3) Tertiary particle formation resulting from multiple collisions of secondary particles due to turbulence of the bulk reactor flow. Particle size growth may be quenched by high temperatures of the radiation source or of the bulk inert gas flow (T_a).

(4) Dehydrogenation of particles continues constantly at a rate affected by time and temperature.

E. Physical and Chemical Characterization

The boron particles produced by Callery were subjected to a variety of analyses to determine their physical and chemical properties. A determination of these properties is important for two reasons: first, provide Callery with the necessary information on the effects of reaction conditions on particle size and composition and second, the physical and chemical properties of the boron particles are important in their overall performance in slurry fuels. Due to the very large number of samples provided from the production runs, it was not possible to perform a thorough analysis on each. Particle size analyses were made on every sample since this was the key parameter in the program. The particle size analysis consisted of both SEM and light scattering techniques. Detailed analyses were made on four selected samples. These samples were chosen near the end of the program after the particle size information was available. We decided to analyze the baghouse samples from runs 2-4, 2-12, 4-4, and 7-4. Sample 2-4B was used as a reference material since it's size range was typical of material produced commercially by Callery. Sample 2-12B is very similar to 2-4B and was used as the seed nuclei in the Group 7 recycle runs. Comparing the analyses of this sample with those of 7-4B will allow us to determine the effects of particle recycle on overall purity and composition. Sample 4-4B was chosen since it had the largest average particle size.

1. Physical Characterization

Particle Size

The SEM particle size information has already been discussed in Section VI-D and will not be repeated here. However, we also subjected each sample to a second particle sizing analysis by light scattering. The boron/ethanol slurries used to prepare the SEM slides were also analyzed using light scattering. The lower size limit of the instrument is 0.1 micron, and therefore we were not able to measure the primary particles which are on the order of 0.05 to 0.15 micron. However, the light scattering data was able to provide complimentary information about the aggregate and agglomerate sizes of particles present in each sample.

A typical particle size distribution histogram is shown in Figure 14. The plot shows the volume percent of particles within the various size ranges listed along the x-axis. The size ranges listed on the figure are calculated in terms of an equivalent spherical diameter. The light scattering data were very consistent from sample to sample. For all but a couple of the baghouse samples, the particle distributions ranged between the lower size limit of 0.1 micron up to about 4 microns. The instrument is measuring agglomerates and aggregates of individual boron particles. These clusters of particles are strongly held together since they are not broken-up by the ultrasonic dispersion process. The SEM analysis, discussed in the previous section clearly shows the presence of these aggregates and agglomerates of boron particles. The SEM analysis was necessary to measure the diameters of the individual boron particles. Although the diameters of the primary boron particles are smaller than the target goal of

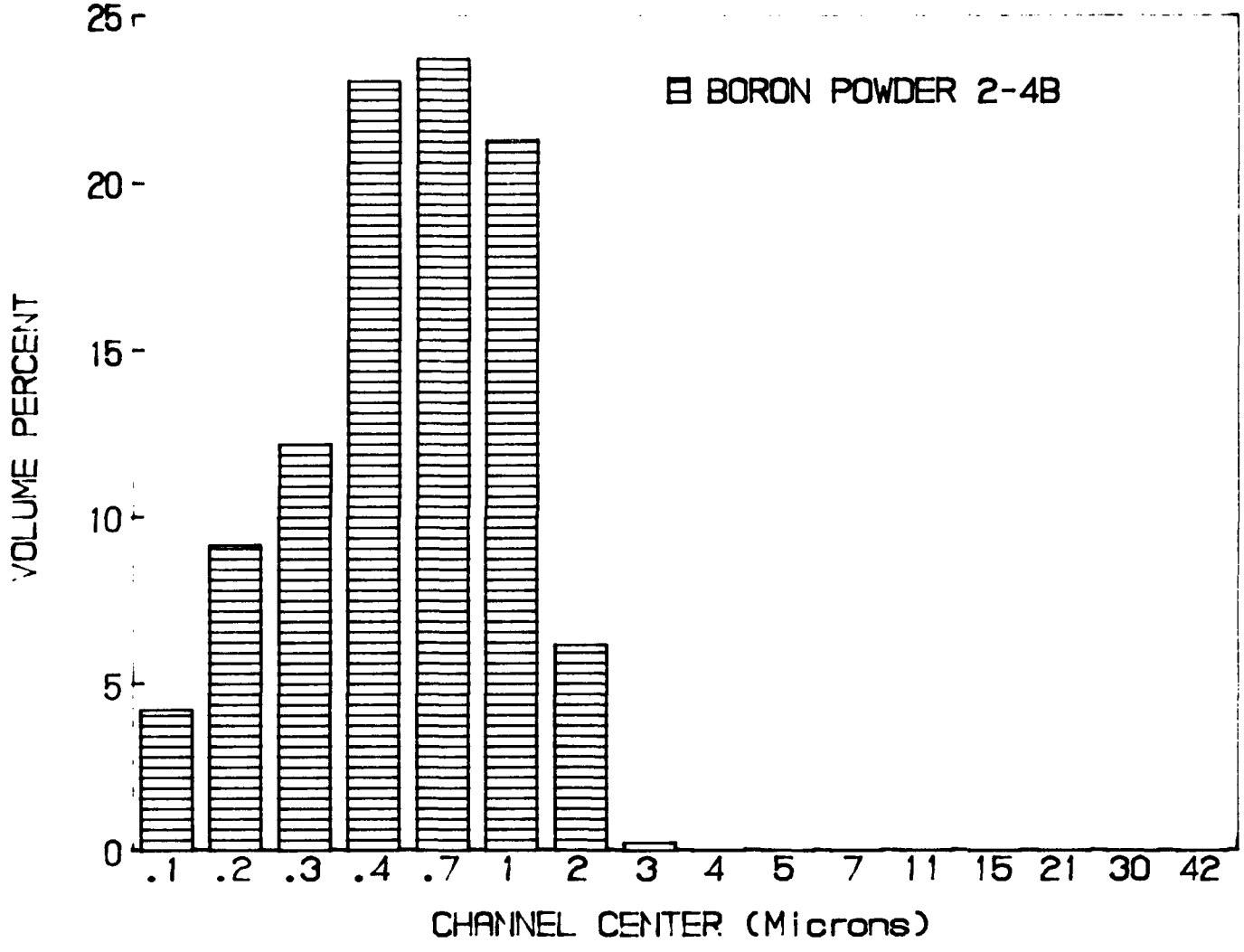

Figure 14. Particle Size Distribution

0.5 to 3 microns, the aggregate and agglomerate sizes are well within that range. As long as these aggregates and agglomerates are stable under shear, have a low surface area, and have sufficient purity, they may still be useful for the intended fuel applications.

Surface Area/Porosity

Surface area and porosity measurements using automated nitrogen adsorption techniques were made on 17 of the boron samples. This relatively large number of analyses was made to provide an independent comparison between calculated particle sizes from our SEM data and measured surface areas. This procedure serves two purposes. First, we can obtain a measure of the validity of our SEM sizing technique by comparing the measured surface areas with those calculated from the sample particle size distribution. Second, we can determine the extent of porosity of the particles from both the measured surface area and the pore size distribution calculated by the nitrogen adsorption instrument.

The BET surface areas for the selected boron samples are listed in Table 5. The surface areas range between 28 m^2/g for sample 4-4B to 66 m^2/g for sample 1-11B. The reproducibility for duplicate samples of this type is estimated to be about ±5%. These are relatively low surface areas for sub-micron particles and indicates that they are essentially solid spheres with very few pores. This is further confirmed by calculated pore volumes for these samples which range from 0.4-0.8 cc/g. The pore volume distribution shows that most of the pores are less than 4 nm in diameter. The micropore area is estimated to be about 10% of the total surface area of the samples. These conclusions about the relative

TABLE 5

B.E.T. Surface Areas for Boron Powders Samples

Sample ID*	Average Particle Diameter Calculated by SEM (Å)	B.E.T. Surface Area (m^2/g)
1-1P	631	46.2
1-1B	598	45.4
1-2B	598	47.2
1-4P	580	60.4
1-6B	621	39.7
1-8P	675	34.2
1-8B	656	36.9
1-11B	569	66.3
2-1P	629	49.3
2-4B	623	37.6
2-5B	637	37.8
2-7B	638	49.4
2-9B	546	37.2
2-12P	544	30.8
2-12BG	526	31.1
4-4B	1475	28.1
7-4B	532	34.1

* - B - Baghouse Samples; P - Primary Samples

non-porous nature of the boron particles are supported by the SEM photomicrographs which show smooth, spherical surfaces (see Appendix B).

If we compare the measured surface areas with those calculated from the measured particle size distributions by our SEM method, we find very good agreement. Figure 15 is a plot of calculated surface area versus particle diameter for hard, solid spheres with a density of 2.3 g/cc. For 75% of the samples, we find that the measured surface areas fall into the range of those calculated from the measured particle size distributions. This result indicates that our SEM sizing method is valid for the majority of the samples tested. Also, this result further supports the spherical, non-porous nature of the boron particles produced in this program.

Density

The true density of the selected boron samples were measured for comparison with literature values and most importantly, with each other. The densities are listed in Table 6. Samples 2-4B and 7-4B have densities of about 2 g/cc which compare well with the literature value of 2.3 g/cc [16]. The 4-4B sample has a significantly lower density of only 1.6 g/cc. This result suggests that there are other components with a lower density than elemental boron present in the 4-4B sample. Some of the possible components could be unreacted B-H species, boric acid, and boron oxides and nitrides. The presence of some of these species has been confirmed and is discussed in the next section on the chemical characterization of the samples.

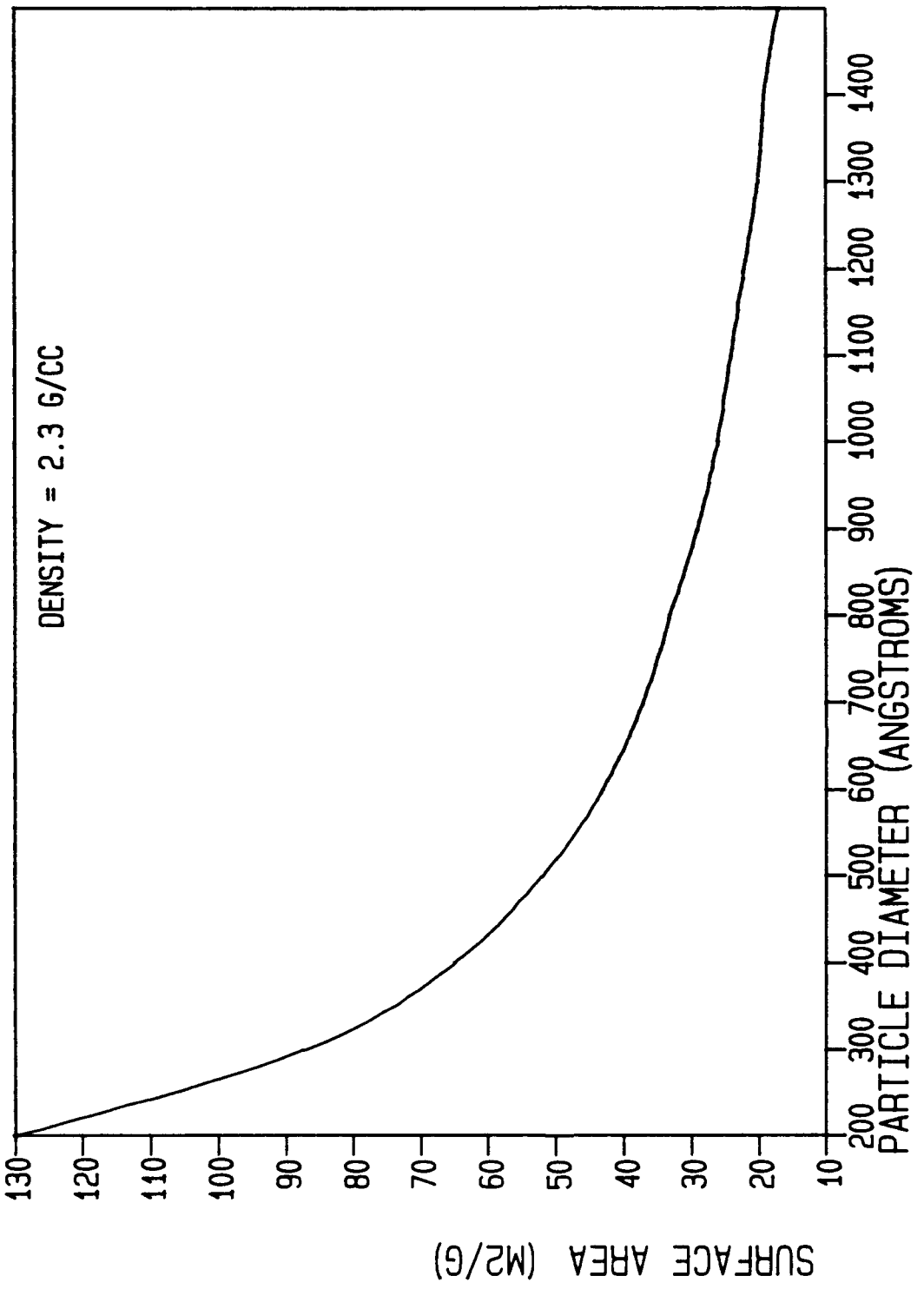

Figure 15. Calculated Surface Area for Spherical Particles

TABLE 6

Density of Boron Powder Samples

Sample ID	Helium Density (g/cm^3)
2-4B	2.06
4-4B	1.61
7-4B	1.93

2. Chemical Characterization

A thorough chemical characterization was made on the four selected samples to determine both their bulk and surface compositions.

Boron Assay/Bulk Purity

The total boron content in the samples was determined by an ICP-AES method. The results of these analyses are listed in Table 7. The measured boron content in all the analyzed samples was greater than 96 wt%. We feel that these samples are representative of those produced in this program and should accurately reflect the range of boron content within the other samples not analyzed. As expected from previous analyses on other boron powders produced commercially by Callery, the boron content is around 97-99 wt% for most of the samples. Only the 4-4B sample has a significantly lower boron content-96.39 ± 0.46 wt%. This coupled with the lower density of this sample further suggests the presence of a significant amount (~2.5 wt%) of lower density impurities. To determine what impurities are present, further analyses were made to determine both metallic and non-metallic components.

TABLE 7

Boron Content of Powder Samples by ICP-AES*

Sample ID	Boron Content (wt-%)+	Standard Deviation -1σ (wt-%)≠
2-4B	97.62	0.37
2-12B	98.83	0.46
4-4B	96.39	0.46
7-4B	99.34	0.38

* - emission wavelength - 249.773 nm
+ - referenced to NBS boric acid standard reference material
≠ - based on at least 15 determinations

Low-Level Impurities

The boron samples were also subjected to a semi-quantitative ICP-AES analysis for 66 other elements and micro-elemental analysis for carbon, nitrogen, oxygen, hydrogen, and sulfur. The results of the semi-quantitative ICP-AES analyses are listed in Table 8. Only samples 2-4B, 4-4B, and 7-4B were analyzed by this procedure. A total impurity level of about 500 μg/g or 0.05 wt.% was found for these 66 elements. Boron, of course, is the major component and scandium was used as the internal standard. Iron was by far the major metallic impurity in all of the samples. Other significant impurities included chromium, silicon, aluminium, and calcium. The iron and chromium are probably due to the steel reactor tubes in which the boron is made. The silicon could come from the glass sample bottles in which the samples were stored and shipped. These low levels of metallic impurities were expected from previous experience at Callery. The remaining 1-2 wt% of impurities is probably due to non-metallic, ubiquitous elements such as carbon, nitrogen, hydrogen, and oxygen.

TABLE 8

Semi-Quantitative Multi-Elemental Analysis by ICP-AES

Element	Concentration (µg/g) 2-4B	4-4B	7-4B
Mo	<6.1	<6.1	<6.1
Cr	63	32	12
Zn	3.4	7.8	8.7
Bi	<19	<19	<19
Cu	1.6	3.4	3.6
Ni	39	<8.0	<9.3
Zr	<2.0	<2.0	<2.0
Fe	356	313	114
Ca	27	54	17
Al	71	61	23
Ba	4.1	<7.1	<1.0
Si	38	115	36
Mn	7.9	3.6	2.2
Na	13	<2.6	<3.2
Mg	5.9	5.4	3.0
Ti	2.2	1.4	1.6

Qualititative Scan, (not detected)*

Ag	Hg	Ge	Eu	Co
Th	Yb	Tb	Ir	Cs
V	Se	P	Os	Ru
Ga	Re	Dy	Pr	Au
Nb	Er	Sm	Tq	Li
Ae	Pd	Te	Ce	K
Be	Gd	Cd	In	Rb
Sn	Sb	Y	Rh	Lu
Tm	W	Pb	Nd	Pt
Tl	Ho	La	Sr	He

* - Signal level at or below that of matrix solution; B - major component, Sc - internal standard.

Elemental Analysis

The boron powder samples were shown by ICP-AES to contain very low levels (<0.05 wt%) metallic impurities. We also analyzed these samples for carbon, hydrogen, nitrogen, and sulfur since these elements are not easily determined by emission analysis. The results of these elemental analyses are listed in Table 9. Carbon and sulfur were below the instrument detection limits for all 3 samples. Nitrogen and hydrogen were found at varying levels in the samples. The hydrogen concentration in the 2-4B and 7-4B samples was about 0.5 wt% and was much higher, 2.2 wt%, in the 4-4B sample. This hydrogen is probably in the form of incompletely reacted boron-hydrogen species in the particles. The remaining material in the samples is expected to be adsorbed oxygen or oxygen-containing compounds such as boric oxide or boric acid. We did not analyze these samples specifically for elemental oxygen.

The nitrogen levels are well below 1 wt% for the 2-4B and 4-4B samples. The 1.1 wt% nitrogen found in the 7-4B sample is not consistent with the other analyses, particularly the boron assay which is >99 wt% boron. This discrepancy may be the result of an instrumental error due to the non-specific method used to determine the nitrogen concentration by the LECO instrument. Another problem with these analyses is that the particular LECO instrument we used is not the best one for these very low concentrations. The instrument was designed for the analysis of hydrocarbons which contain much higher levels of carbon, hydrogen, and nitrogen. The instruments made specifically for low level C, H, N analyses were not available at the time of this work. Even though this data does not provide us with more precise concentrations for carobn, hydrogen, nitrogen, and sulfur, they do give us an upper limit for these elements in the boron samples.

TABLE 9

Elemental Analysis (C, H, N, S) of Boron Powder Samples

Sample ID	wt% C	wt% H	wt% N	wt% S
2-4B	<0.4	0.35	0.55	<0.01
4-4B	<0.4	2.15	0.30	<0.01
7-4B	<0.4	0.60	1.1	<0.01

Infrared and X-ray Diffraction

The elemental analyses confirm that there is oxygen and hydrogen present in the boron samples. However, the analysis does not provide any information about the types of compounds present. Both infrared (IR) and X-ray diffraction (XRD) can be used to detect the presence of boron compounds in the samples. The IR spectra allow us to identify specific functional groups present in the samples by their characteristic absorption frequencies. IR spectra of both the 2-4B and 4-4B samples were obtained for comparison. These are shown in Figures 16 and 17. The 4-4B spectrum has many strong absorption bands whereas the 2-4B spectrum has only a few weakly absorbing bands. Some of the band assignments have been made and are listed in Table 10 [17]. The IR clearly shows the presence of B-OH, B-H, and B-O bonds present in the 4-4B sample. These absorption features are consistant with the presence of boric acid and some boron-hydrogen species. These bands are very weak or non-existent in the 2-4B spectrum. The IR data is therefore consistant with the elemental analysis in which the 4-4B sample has a lower boron content and higher concentrations of hydrogen and oxygen. There are also two absorption bands around 3440 and 1625 cm^{-1} which indicate the presence of water on both samples. This is water that has probably adsorbed to the powders while they were exposed to the atmosphere during preparation for analysis.

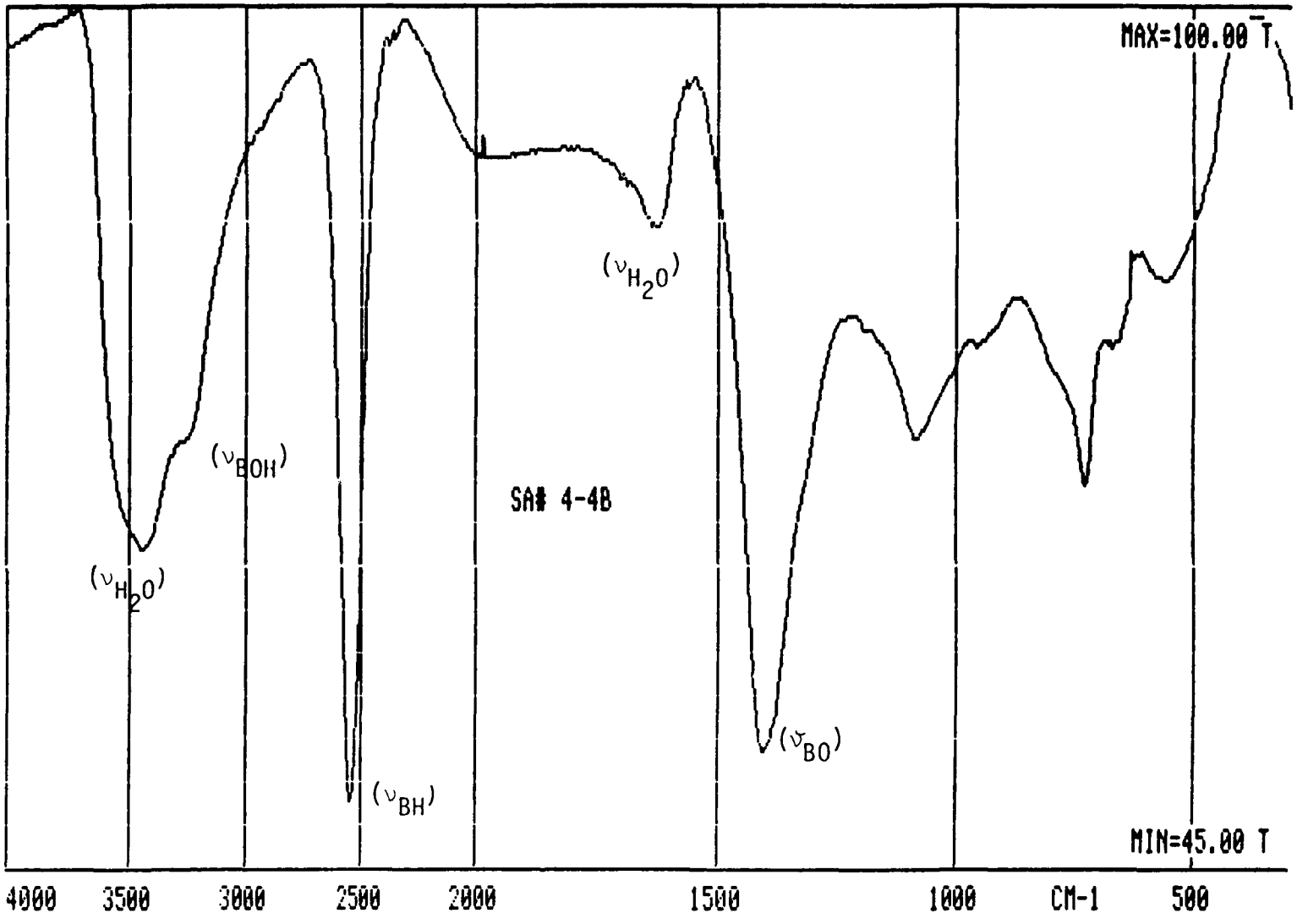

Figure 16. Infrared Spectrum of Sample 4-4B

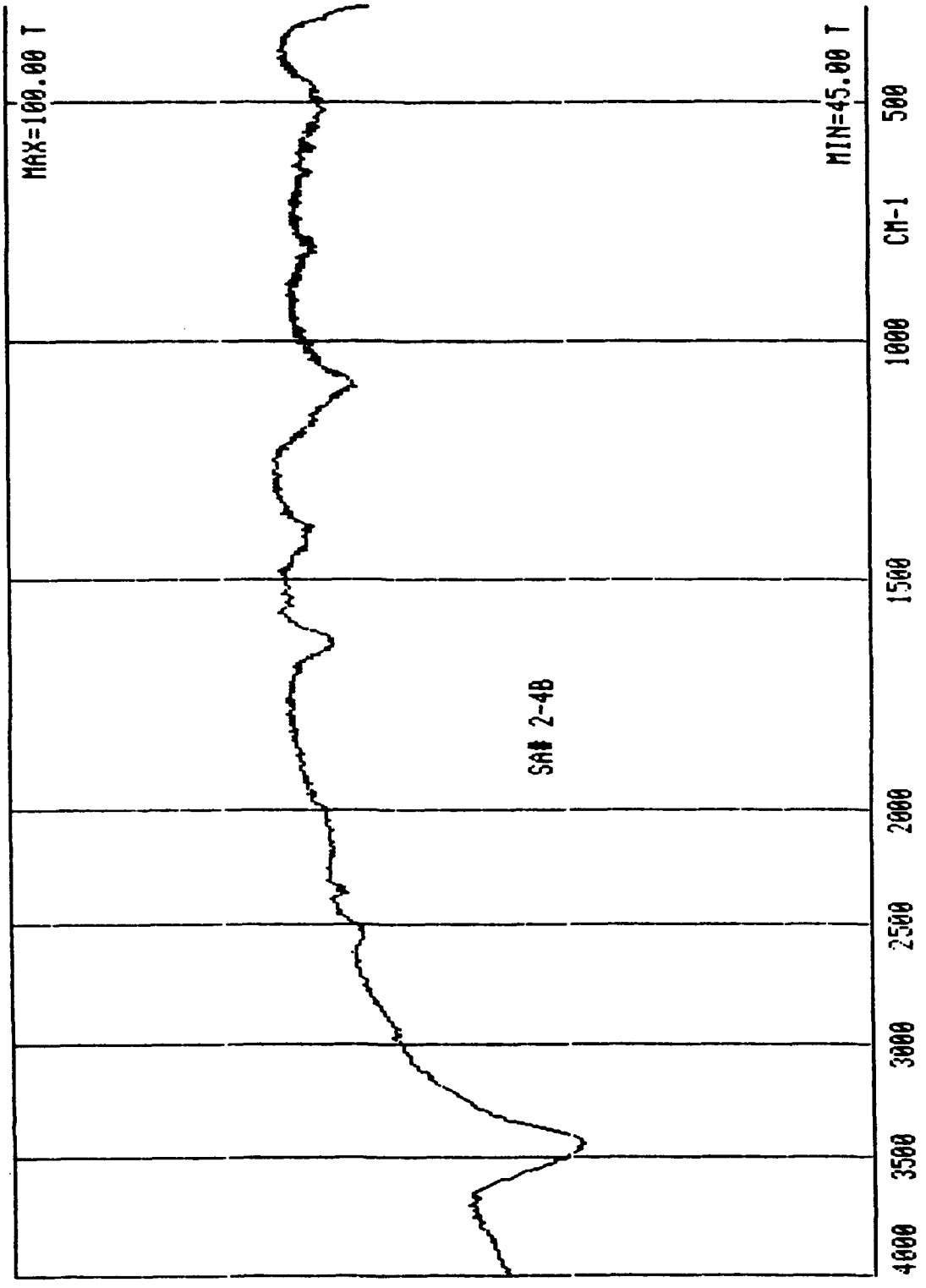

Figure 17. Infrared Spectrum of Sample 2-4B

TABLE 10

Infrared Absorption Based Assignments for Boron Powder Samples

Bond Type	Characteristic Absorption Frequency* (cm^{-1})	Absorption Maximum for 4-4B Sample (cm^{-1})
B-OH (ν_{OH})	3200-3300 (Broad)	3250
Boranes (ν_{BH})	2350-2640 (strong)	2545
B-O (ν_{BO})	1335-1430	1407

* - From reference [17]

XRD spectra were also obtained for samples 2-4B, 4-4B, and 7-4B and are shown in Figures 18-20. From the positions of the peak maxima in the spectra, we can identify any crystalline phases that may be present in the material. The 2-4B and 7-4B XRD patterns are essentially identical with the maximum intensities occurring at the same Bragg angles. This pattern indicates that there is some short range ordering, but the material does not contain well-defined crystalline boron [18]. Therefore, from the XRD analysis on these samples, it appears that the boron particles are not truly amorphous, but they also do not contain 3-dimensional crystallites. They are best described as having some short range ordering. Both samples appear to contain very small amounts of crystalline B_2O_3 with the 2-4B sample having the higher amount.

The pattern for the 4-4B sample appears to be a sum of the pattern similar to those of the other two samples and a pattern exhibiting intense low angle scattering. This low angle scattering could be indicative of another boron

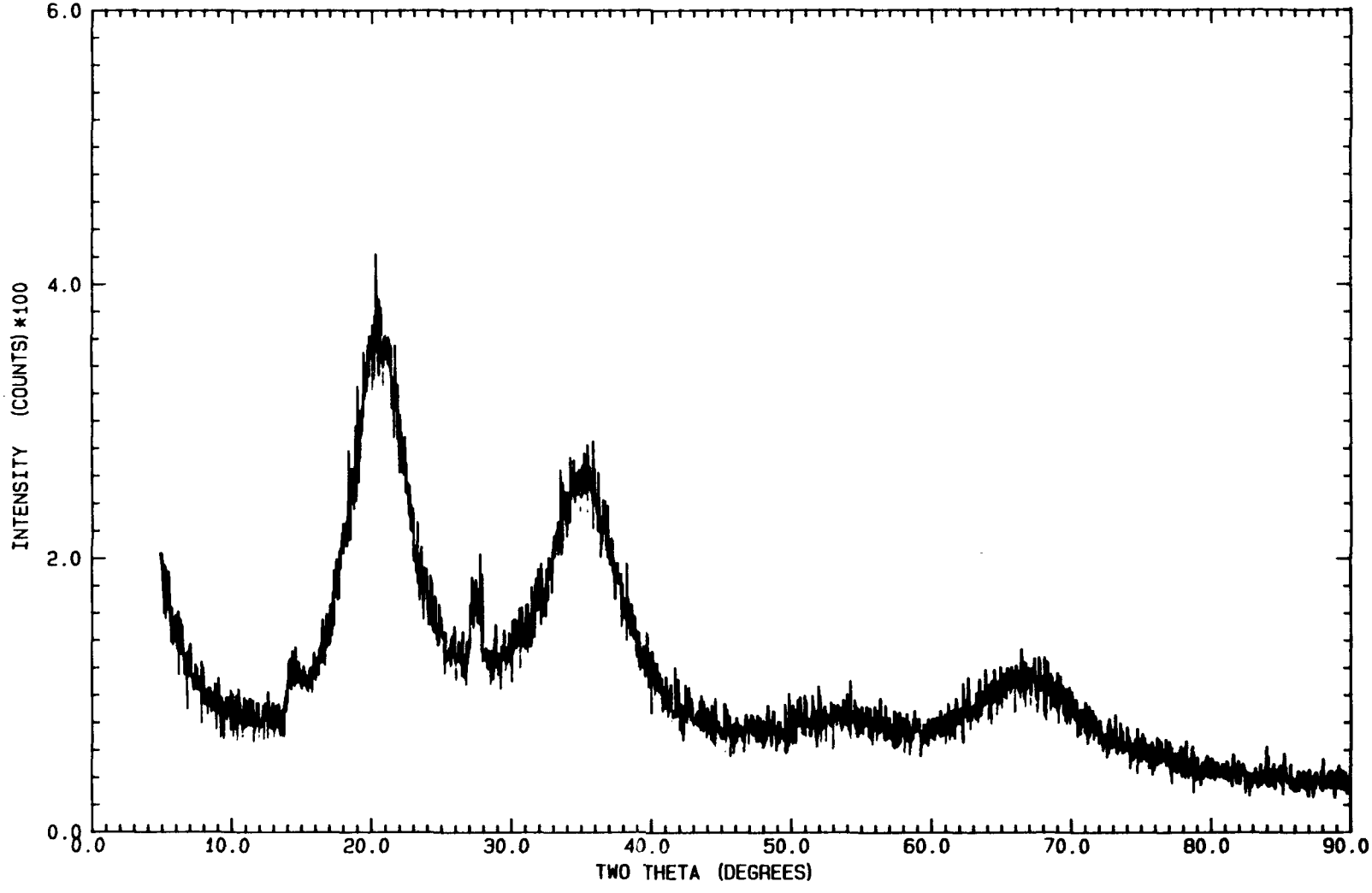

Figure 18. XRD Pattern for Sample 2-4B

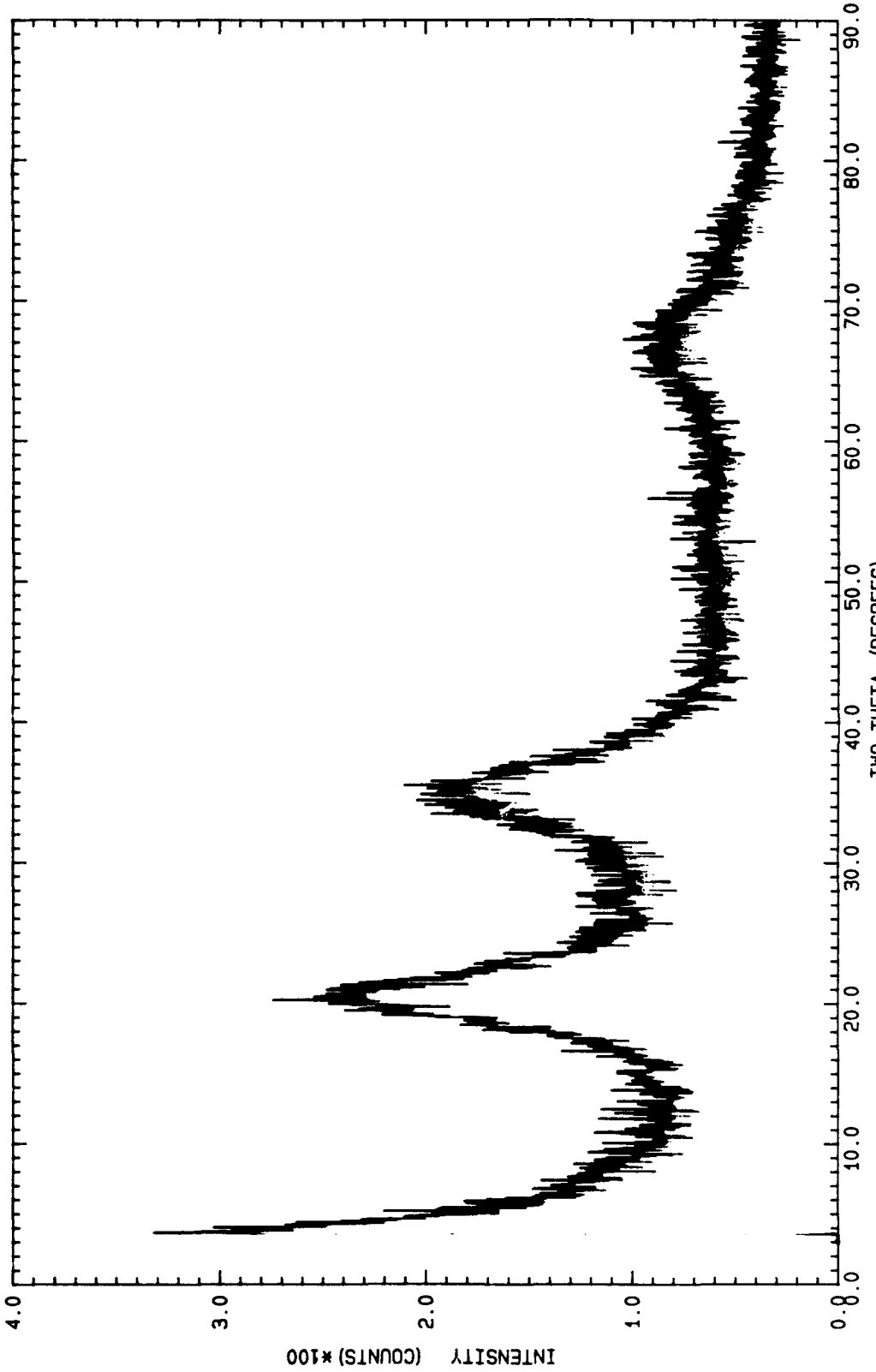

Figure 19. XRD Pattern for Sample 7-4B

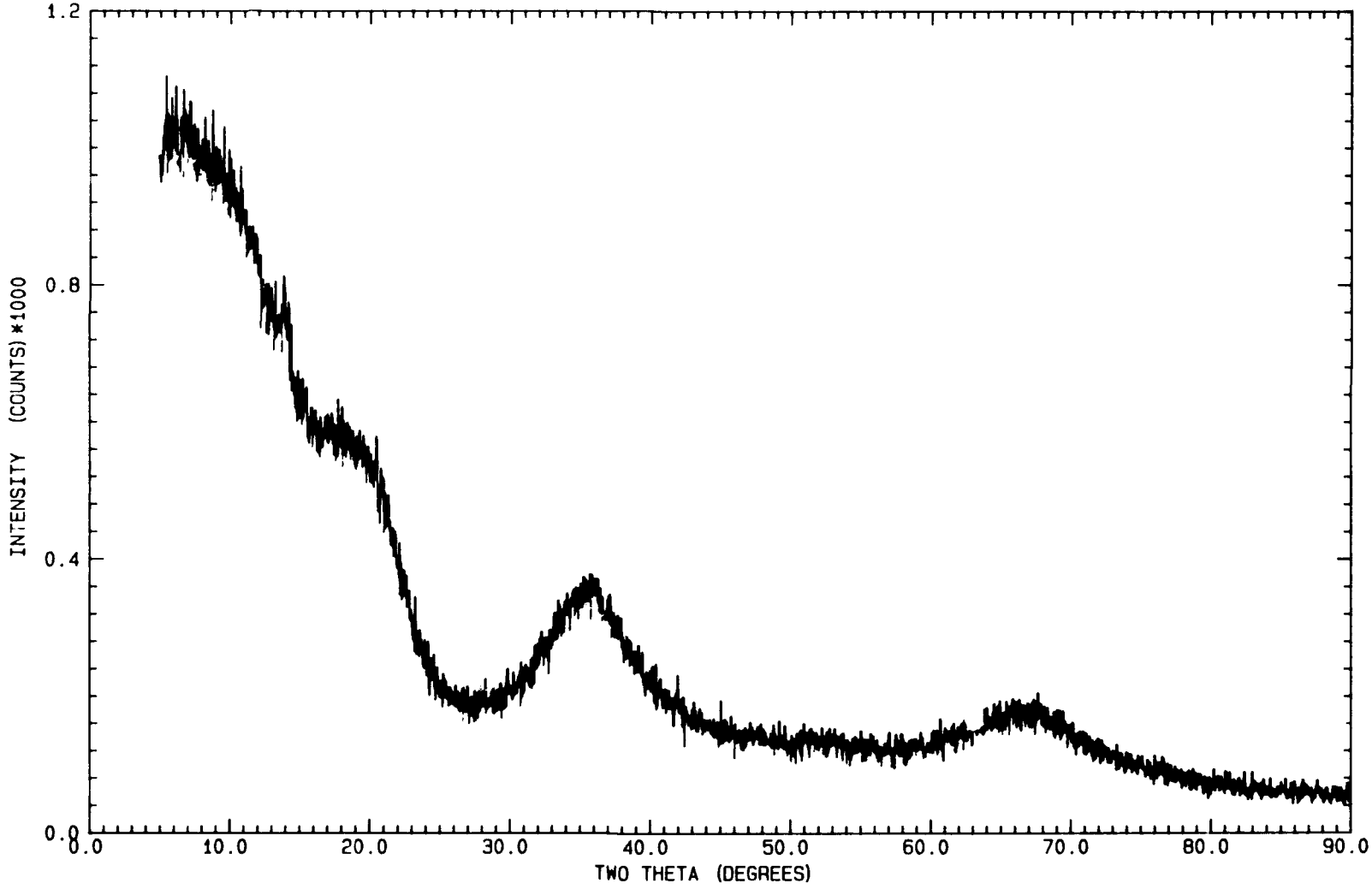

Figure 20. XRD Pattern for Sample 4-4B

phase being present (such as a B-H species), but we currently do not have the capability to rigorously interpret the diffuse scattering. Interestingly, no evidence for B_2O_3 was found in the spectrum. This appears to contradict the IR data. However, since the XRD analysis identifies crystalline phases, amorphous B_2O_3 or H_3BO_3 could be present and would not be observed in the XRD pattern.

X-Ray Photoelectron Analysis (XPS)

The chemical analyses described above measure the bulk composition of the boron powders. The bulk boron content is important in determining the overall volumetric heating value of the boron in a fuel. Very high (>99 wt%) purity is required to obtain optimum heating values. However, the surface compostion, which can be very different from that of the bulk, determines the kinetics of the burning process. The presence of a glassy oxide coating on the particle surface can delay the ignition of the boron and slow it's burning rate. Therefore, the composition at the surface of the particles should be known to determine the suitability of the boron for use in solid fuel applications.

We used an XPS analysis to determine the chemical composition at the particle surface [19,20]. Due to the surface sensitivity of the XPS process, we can measure the elemental composition of the surface by analyzing the energy of the ejected photoelectrons. In addition, shifts in the binding energies of the photoelectrons provide information about the chemical environments of the elements. This allows us to distinguish between elemental boron and boron compounds such as oxides, hydrides, nitrides, etc.

Qualitative survey scans on the boron samples detected only boron, oxygen, carbon, and nitrogen. Hydrogen is not detectable by XPS. By scanning smaller energy windows around the 1s electron regions for each of the elements found, we can measure the characteristic binding energies of the ejected electrons. The boron 1s region for sample 2-4B is shown in Figure 21. The XPS spectra for the other samples were very similar. Shifts towards higher binding energies indicate that an element is in a higher oxidation state. The measured binding energies and the atomic percents of each element are listed in Table 11. The low concentrations of carbon and nitrogen are expected and these ubiquitous elements are seen on most samples unless they have been very carefully cleaned before analysis.

Looking at the boron 1s binding energies, we find there are actually two convoluted peaks present around 187-188 eV for all 3 samples. The lower binding energy peak is attributable to elemental boron and the higher energy peak is due to an "oxidized" species, but not B_2O_3. The boron corresponding to the higher binding energy peak may be due to boron-hydrogen species or could be a result of chemisorbed oxygen which is tightly bound to the particle surface but is not in the form of an oxide. Boron(III) in boric oxide or boric acid has a binding energy around 193 eV which is not observed [21]. The oxygen concentrations vary between 3.2 atom% for the 4-4B sample to 5.0 atom% for the 2-4B sample. The majority of the oxygen present on these samples, particularly the 2-4B and 7-4B samples may be from exposure to the atmosphere since no effort was made to exclude air once the sample bottles were opened for analysis. The total boron concentration at the particle surface is over 90 atom% for all 3 samples. The B 1s binding energies are slightly higher for the 4-4B sample than the other two. This shift would be consistent with more B-H character present in this sample. However, this evidence is far from conclusive.

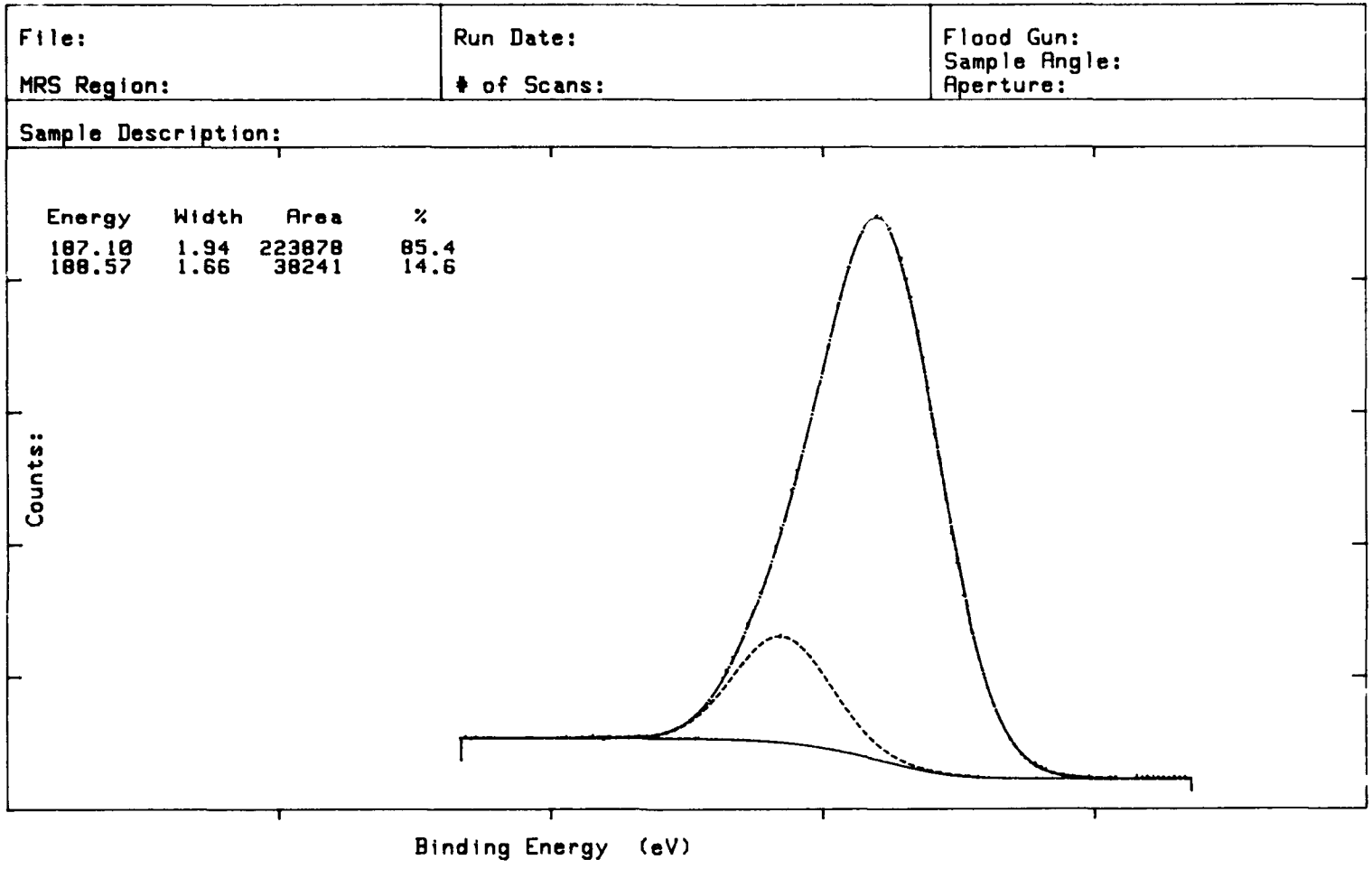

Figure 21. XPS Spectrum of B 1s Region for Sample 2-4B

TABLE 11

XPS Data for Boron Powder Samples

Photoelectron Core Level	Sample 2-4B Binding Energy (eV)	Sample 2-4B Atomic %	Sample 4-4B Binding Energy (eV)	Sample 4-4B Atomic %	Sample 7-4B Binding Energy (eV)	Sample 7-4B Atomic %
B 1s	178.10	78.54	188.26	80.81	187.32	71.57
B 1s	188.57	13.42	189.67	13.76	188.59	22.88
C 1s	281.75	0.18	-	-	-	-
C 1s	283.72	1.33	283.98	1.21	283.89	1.01
C 1s	285.65	0.99	286.69	0.72	286.03	0.46
N 1s	398.99	0.19	399.12	0.06	399.39	0.49
N 1s	401.33	0.35	402.32	0.24	401.98	0.98
O 1s	531.94	4.65	532.41	2.66	532.30	3.48
O 1s	534.20	0.36	534.22	0.54	-	-

* - Binding energies are as recorded on the instrument. An electron floodgun was used to minimize or eliminate sample charging.

An important point to re-emphasize is that XPS is looking primarily at the surface of the boron particles. The composition of the surface can be very different from that of the bulk. As a result, discrepances between the compositions calculated from each technique are not surprising and do not necessarily contradict one another. Although the boron content of the surface is somewhat lower than that in the bulk (compare Tables 7 and 11), no boric oxide was detected on the surfaces of the sampled particles.

The results of the analyses for samples 2-4B, 4-4B, and 7-4B are summarized in Table 12.

TABLE 12

Summary of Analytical Results on Boron Powder Samples

Analysis	2-4B	4-4B	7-4B
Boron (wt %)	97.62	96.39	99.34
Other Metals (wt %)	<0.06	<0.06	<0.04
Carbon (wt %)	<0.4	<0.4	<0.4
Hydrogen (wt %)	0.35	2.15	0.60
Nitrogen (wt %)	0.55	0.30	1.10
Sulfur (wt %)	<0.01	<0.01	<0.01
Total Composition (wt %)			
Surface Area (m^2/g)	37.7	28.1	34.1
Pore Volume (cc/g)	0.066	0.040	0.067
Density (g/cc)	2.063	1.610	1.927
Mean Particle Size (Å)	522	1128	532

VII. CONCLUSIONS

A. Summary

1. The boron particle size at high reactor wall temperatures is proportional to (Diborane Feedrate)$^{1/3}$.

2. Significant particle size enlargement in this type of process can only be obtained through conditions of moderate reactor wall temperature ($\leq$ 1100°F), moderate adiabatic combustion temperature ($\leq$ 600°F), and sufficient bulk flow turbulence (N_{Re} >~2000).

3. From our results, no particular limit to maximum particle size appears to exist for sizes up to roughly 1 μ, if the process is operated at optimum conditions and reactor length is sufficient. The rate of particle size increase will drop off as [particle population/volume] decreases, due to decreased probability of collision.

4. Complete dehydrogenation of the particles can only be achieved by exposing them to radiant heat at temperatures above 1500-1600°F for at least 0.1 second.

5. The hypothesized mechanism of particle formation is substantially correct, after certain modifications. However, opportunity for significant control of particle size is possible only in Part 3, and only by collisions of particles.

6. The plugging tendency can be reduced or eliminated by an increase of reactor diameter to a 3 inch I.P.S. schedule 40 size. This size should be capable of handling up to about 8 lb/hr diborane feedrate without significant plugging.

7. Feed nozzles should be kept at as small a diameter as practical, within available feed pressure drop constraints.

8. Particle recycle is not effective for size enlargement in the manner utilized. Recycle particles would need to be mixed with the diborane feed stream for growth to be achieved.

9. Any scaling of the reactor should be done using constant Reynolds number, constant diameter, and constant temperatures.

10. Reactor length required, at otherwise optimum conditions, to form larger particles would be proportional to $L(D_{p_2}/D_{p_1})^3$ where D_{p_1} is approximately 0.2 μ and L = 39 inch. Due to the extreme length required to form large particles, particle recycle is considered to be the most viable method for producing large particles.

11. Larger particle sizes are likely to maintain the wide size distribution already observed, which is characteristic of the statistical nature of the collisions that produce the size increase.

12. The boron particles with average diameters between 500 and 700 Å have very high purities, containing greater than 98 wt% boron. Total metallic impurities are less than 0.05 wt% and the major contaminant is oxygen. This oxygen is confined primarily to the particle surfaces and appears to be chemisorbed rather than in the form of an oxide. Futhermore, this oxygen is probably from exposure of the particles to the atmosphere during sampling and analysis. More rigorous exclusion of oxygen after production should reduce the surface contamination to much lower levels. Even with exposure to the atmosphere, the boron particle surfaces are still greater than 90 atom % boron.

13. The larger particles (1000-1500 Å average diameter) produced in this program contain appreciable amounts of hydrogen. Infrared data indicates that this hydrogen is in the form of B-H species from incomplete decomposition of diborane. These particles are relatively unstable and show evidence of oxide and hydroxide formation with time after exposure to atmospheric oxygen and water.

14. High boron purity, safe operation, and high system reliability have all been demonstrated.

15. The particle sizing method developed during this program is adequate for the intended purpose, and avoids some of the drawbacks of indirect methods.

B. Recommended Follow-On Work

1. A longer reactor should be operated to test the effectiveness of further particle size enlargement via collision.

2. Operation at even lower T_a and reactor wall temperatures should be conducted to determine if secondary particle growth can be enhanced.

3. Particle recycle using a mixed borane/particle feed stream in appropriate equipment has a high probability of success, and should be investigated.

4. Application of the methods for enlarging particle size found useful in this work may have utility for production of other high-purity powders such as Ti or GaAs, and should be investigated.

5. Study of the boron particle fine structure (to 10 - 20 Å) could be quite revealing.

C. Economic Projection

Task 1.4 of the original scope of work, "Scale-up Demonstration", had been eliminated and replaced with the recycle effort. For this reason, and the fact that the present system has been operated in a research mode (short run times, etc.), an economic projection based on current costs would be of limited reliability.

ACKNOWLEDGMENTS

Callery Chemical Division of Mine Safety Applicances Company and the Allied-Signal Engineered Materials Research Center wish to thank the U.S. Air Force for support this work. The authors acknowledge the following people for their help in the completion of this work.

Callery Chemical Co.

Dr. William J. Cooper

Allied-Signal EMRC

Caryl Fabian - Infrared work

Gregory Peterson - ICP-AES work

John Souza, Jeff Donner - XPS work

Andrzej Ringwelski - XRD work

Dawn Bloomquist - Particle Size Preparation

EMRC Analytical Department

REFERENCES

1. Lewis and Von Elbe, "Combustion, Flames, and Explosions of Gases," p. 527-557.

2. Bond, A. C., and G. Hairston, "The Pyrolysis of Pentaborane (9)," J. Organic Chemistry, 9 No. 11, pp. 2610-11, 1970.

3. Private Communication, W. J. Cooper, 1984.

4. Lothe, Jens and G. M. Pound, "Reconsiderations of Nucleation Theory," J. of Chem. Physics, 36, No. 8, p. 2080-2085, 1962.

5. Vergnon, Pierre and H. B. Landoulsi, "Formation of Ultrafine Fe_2O_3 Aerosols," I. & E.C. Process R&D, 19, p. 147-151, 1980.

6. Russell, K. C., "Nucleation of Gaseous Ions," J. of Chemical Physics, 50, No. 4., p 1809, 1969.

7. Hesketh, H. E., "Fine Particles in Gaseous Media," Ann Arbor Science Publishers, 1979.

8. Savilonis, B. J. and J. S: Lee, "Particle Deposition in a Charged Aerosol Flowing Through a Conducting Tube," J. of Fluids Engr., 100, p. 449-452, 1978.

9. Singh, Bhuminder and R. Lee Byers, "Particle Deposition Due to Thermal Force in Transition and Near-Continuum Regimes," I. & E.C. Fundamentals, 11, No. 1, p. 127-133, 1972.

10. Gillespie, G. R., and H. F. Johnstone, "Particle-Size Distribution in some Hygroscopic Aerosols," Chem. Engr. Progress, 51, No. 2, p. 74F - 80F, 1955.

11. Perry and Chilton, "Chemical Engineer' Handbook," McGraw-Hill, 5th Edition, 1973, and 6th Edition, 1986.

12. Levenspiel, O., "Chemical Reaction Engineering," Wiley & Sons, 2nd Edition, 1972.

13. Hern, R. B, and R. G. Sidall, M. W. Thring, "Flow Patterns in a Phase Change Rocket Combustion Model," Second British Rocket Symposium, Cranfield, April 27, 1962.

14. Owen, F. K., "Measurements and Observations of Turbulent Recirculating Jet Flows," AIAA Journal, 14, No. 11, pp. 1556-1562, 1976.

15. Reynolds, W. C., "Thermodynamics," McGraw-Hill, Second Edition, 1968.

16. Weist, R. C., ed. Handbook of Chemistry and Physics, 52nd ed., The Chemical Rubber Co., Cleveland, OH, 1971.

17. Smith, A. L., Applied Infrared Spectroscopy, John Wiley and Sons, New York, 1979.

18. Allied-Signal Memorandum, A. Z. Ringwelski to T. M. Mezza, "Qualitative XRD Analysis of Amorphous Boron Preparations," February 23, 1988.

19. Allied-Signal Memorandum, J. T. Donner to T. M. Mezza, "XPS Analysis of High Purity Boron Powders: II," November 18, 1987.

20. Alied-Signal Memorandum, J. T. Donner to T. M. Mezza, "XPS Analysis of High Purity Boron Powders: III," January 11, 1988.

21. Mullenberg, G. E., et al., ed. Handbook of X-Ray Photoelectron Spectroscopy, Perkin-Elmer Corp., Eden Prairie, MN, 1979.

General References

Walker, K.L., Gevling and Nagel, "Thermophoretic Deposition of Small Particles in Modified CVD Process," J. of American Ceramic Society, 63, No. 9-10, p. 552-558, 1980.

IYA, S. K., R. N. Flagella, F. S. DiPaolo, "Heterogeneous Decomposition of Silane in Fixed Bed Reactor," J. Electro-Chemical Society, 129, No. 7, p. 1531-5, 1982.

Byers, R. Lee and S. Calvert, "Particle Deposition from Turbulent Streams by Means of Thermal Force," I. & E. C. Fundamentals, 8, No. 4, p. 646-655, 1969.

El-Shobokshy, M. S., "A Method for Reducing Deposition of Small Particles...By Thermal Gradient," Canadian J. of Chem. Engr., 59, pp. 155-157, 1981.

"Diborane Handling Bulletin," Callery Chemical Company, 1982.

APPENDIX A

HISTOGRAMS AND STATISTICAL ANALYSES

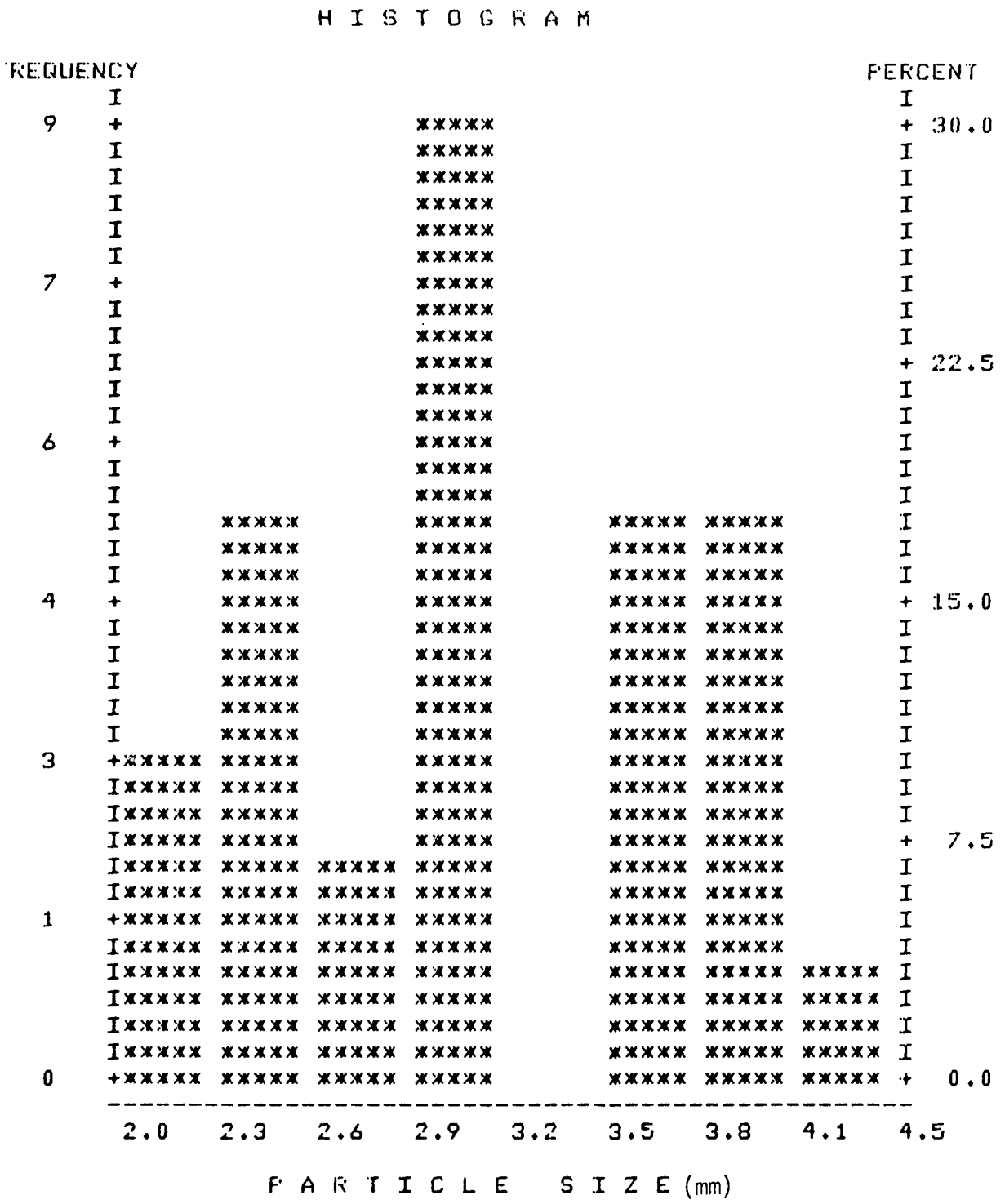

1-6 BHGHS

(particle size x 200 = size in Å)

H I S T O G R A M

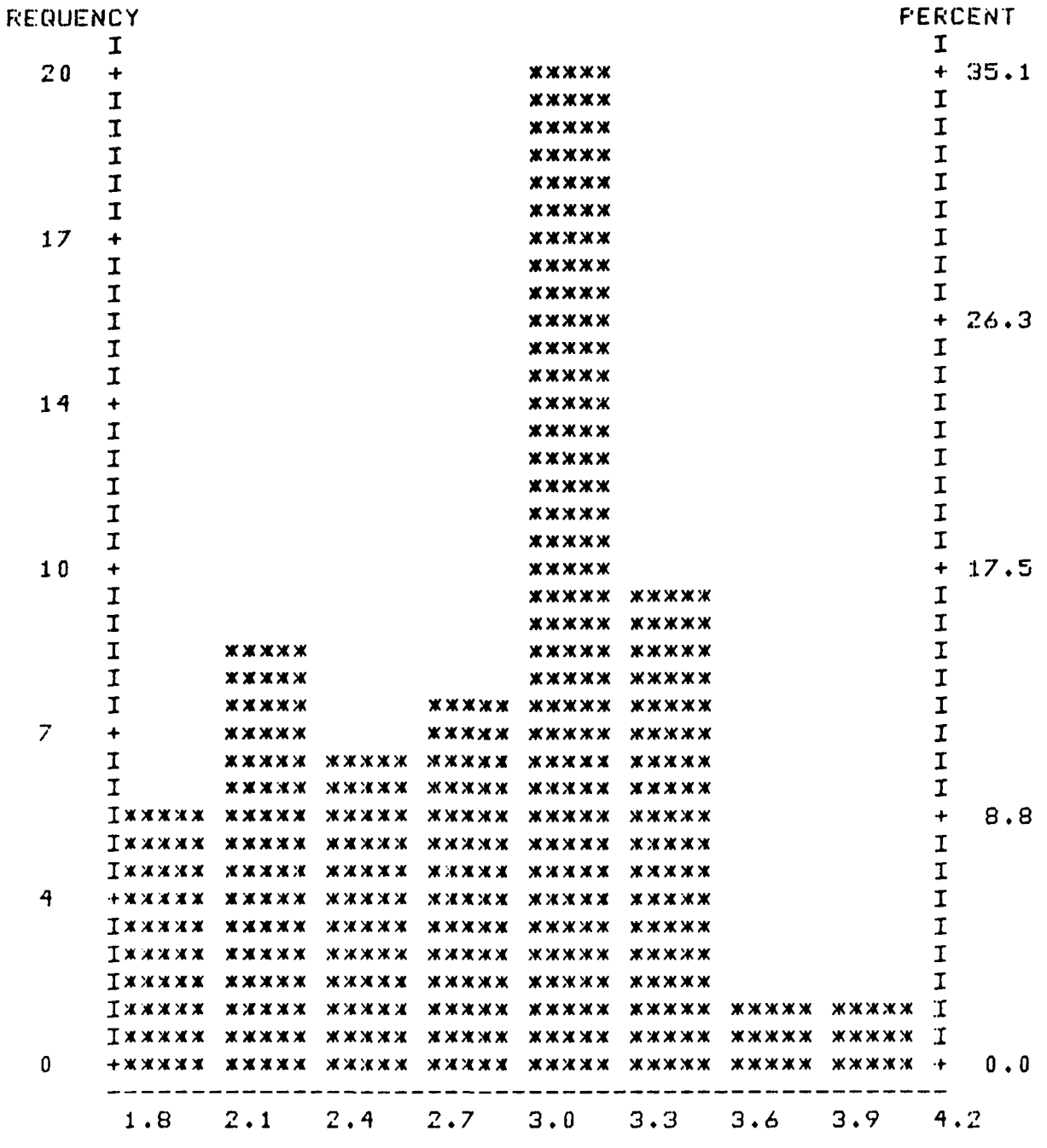

P A R T I C L E S I Z E

1-11 BGHS

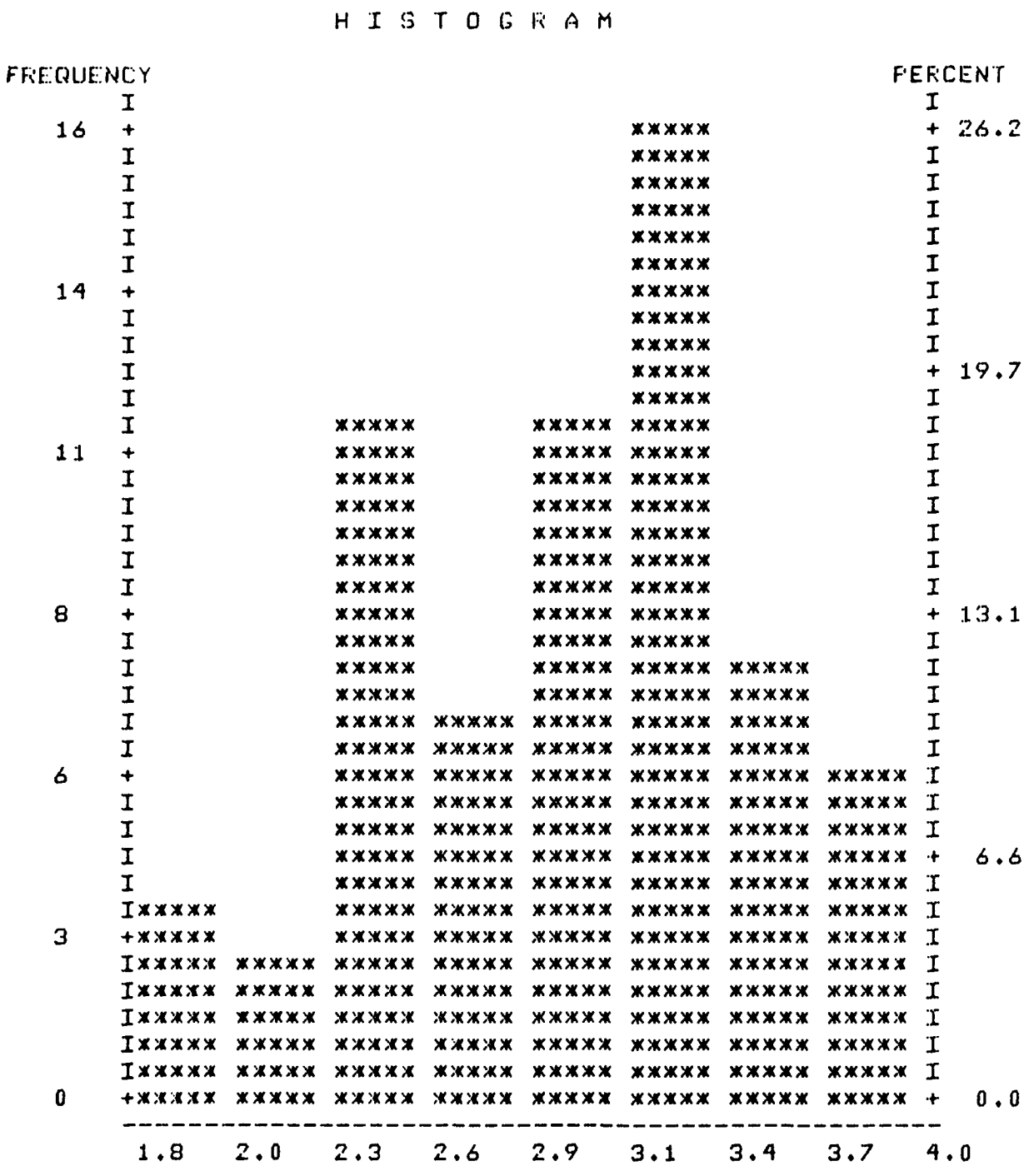
H I S T O G R A M
FREQUENCY
PERCENT
16
14
11
8
6
3
0
26.2
19.7
13.1
6.6
0.0
1.8
2.0
2.3
2.6
2.9
3.1
3.4
3.7
4.0
P A R T I C L E S I Z E

2-4 BGHS

H I S T O G R A M

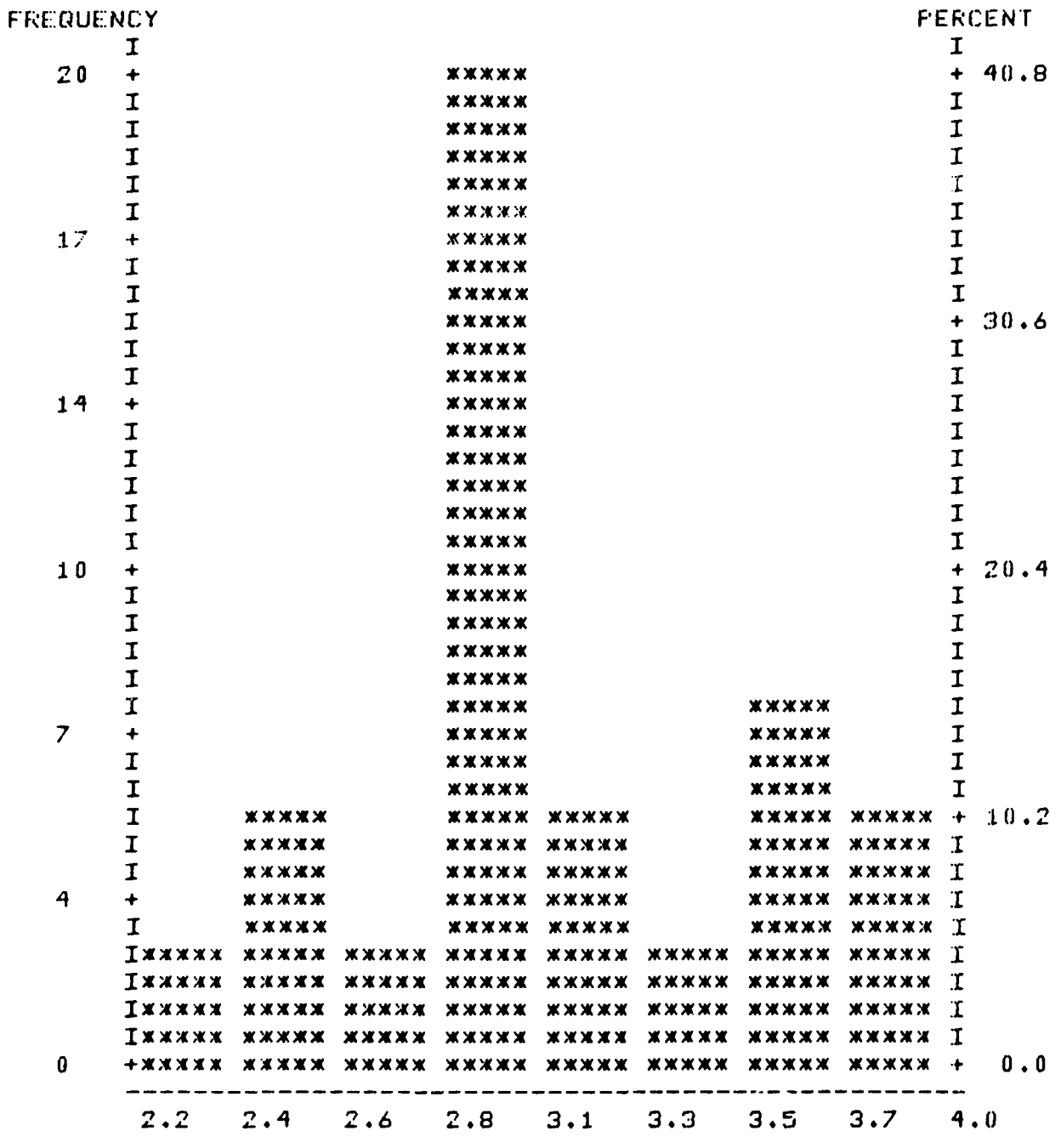

P A R T I C L E S I Z E

Composite

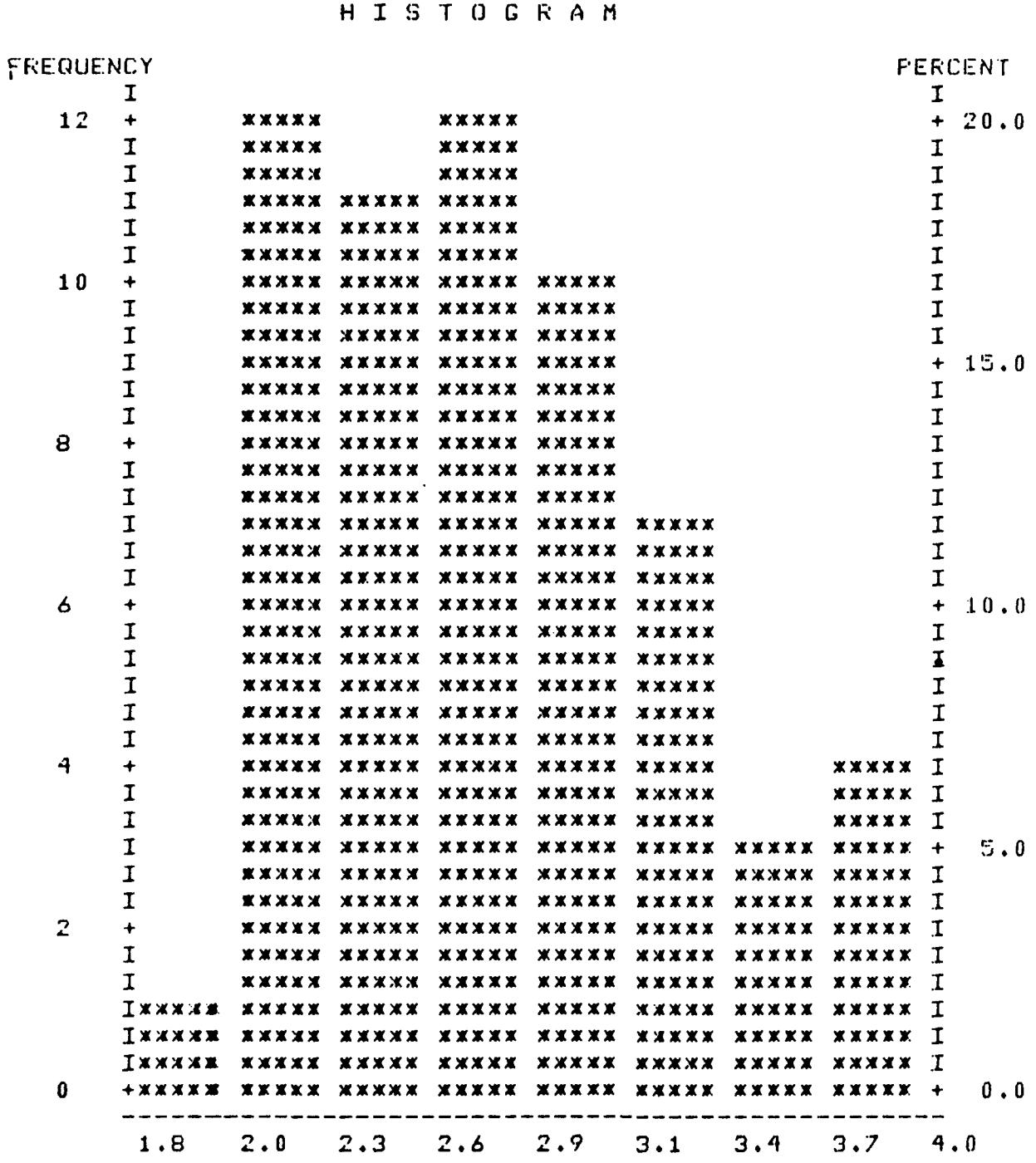
HISTOGRAM
FREQUENCY
PERCENT
12
10
8
6
4
2
0
20.0
15.0
10.0
5.0
0.0
1.8
2.0
2.3
2.6
2.9
3.1
3.4
3.7
4.0
PARTICLE SIZE

3-1 BGHS

H I S T O G R A M

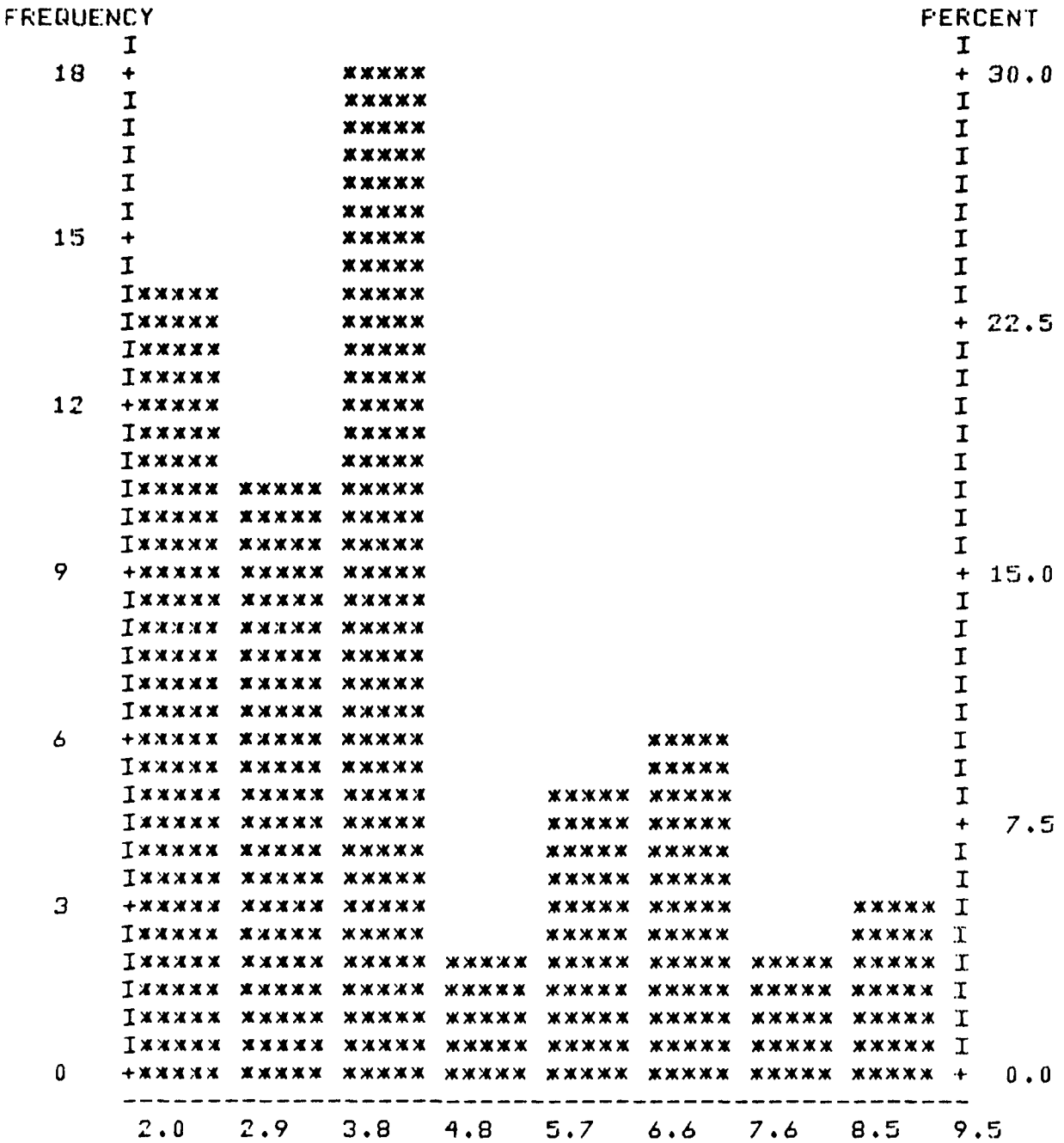

P A R T I C L E S I Z E

3-6 BGHS

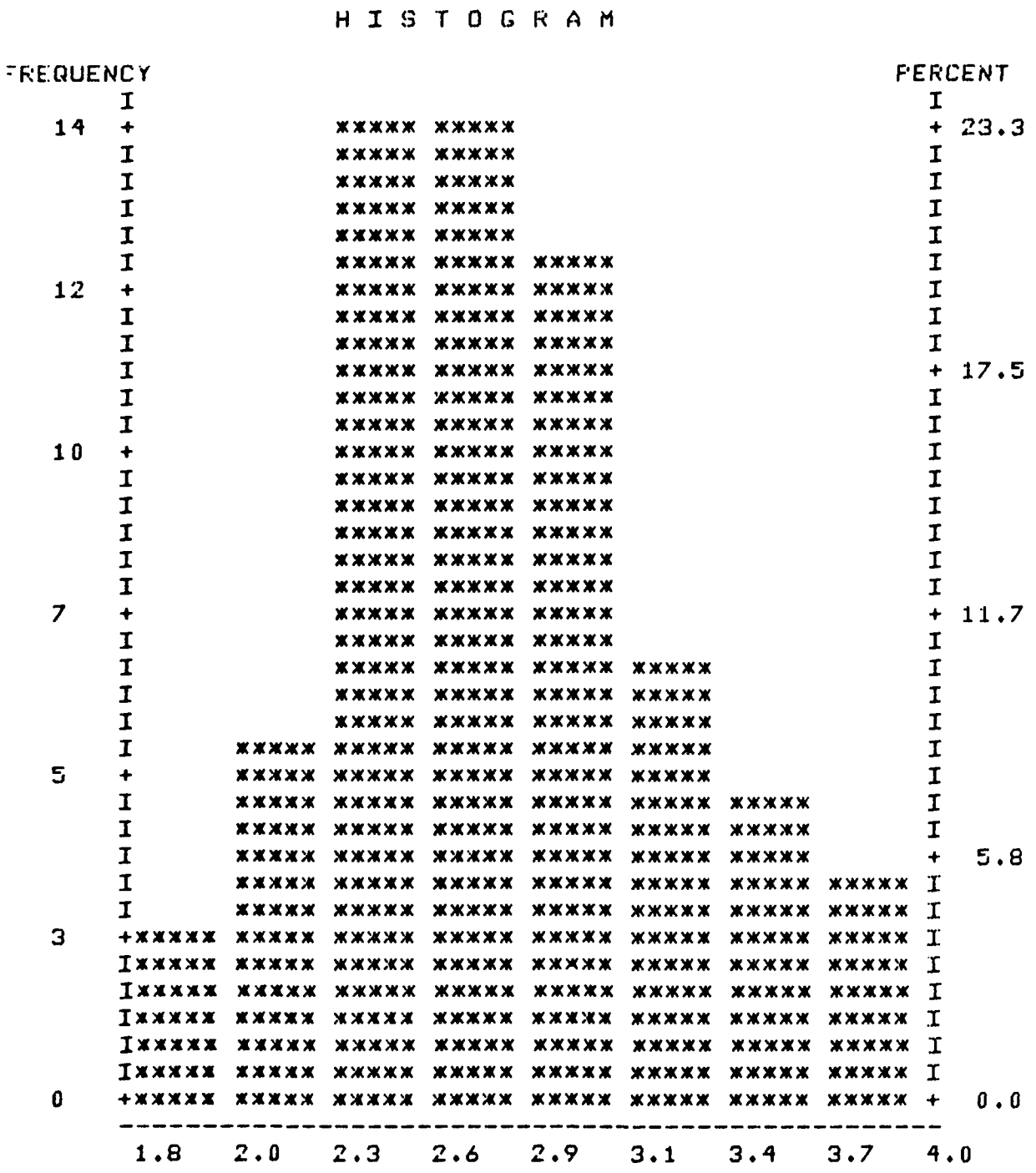
H I S T O G R A M
FREQUENCY
PERCENT
14
12
10
7
5
3
0
23.3
17.5
11.7
5.8
0.0
1.8
2.0
2.3
2.6
2.9
3.1
3.4
3.7
4.0
P A R T I C L E S I Z E

3-12 BGHS

H I S T O G R A M

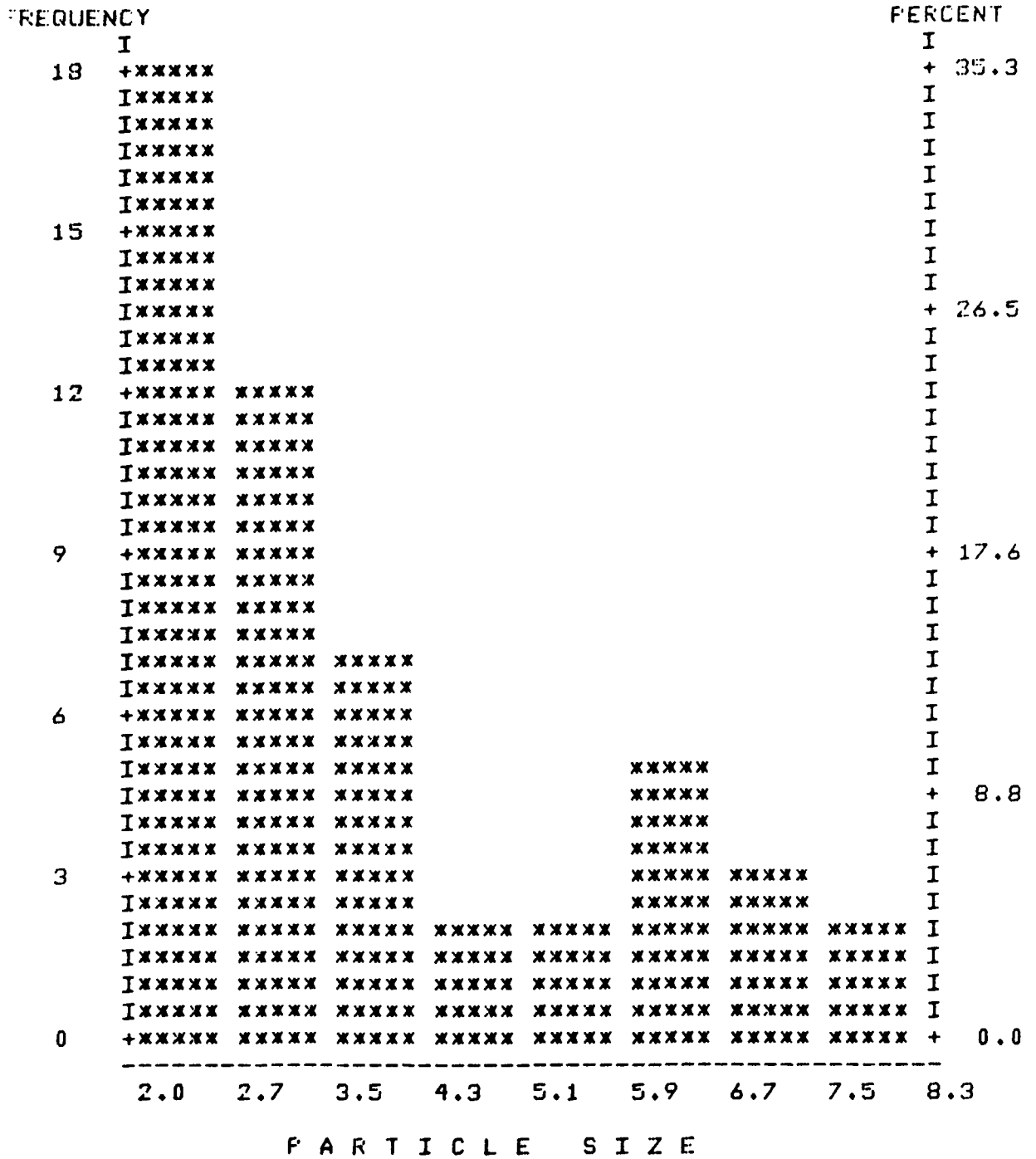

P A R T I C L E S I Z E

D E S C R I P T I V E S T A T I S T I C S

VARIABLE: PARTICLE SIZE SAMPLE SIZE (N) = 51

SAMPLE STATISTICS:

MEAN	= 3.76863	RANGE	= 6.3
VARIANCE	= 3.04883	MINIMUM	= 2
STD. DEV.	= 1.74609	MAXIMUM	= 8.3

UNBIASED ESTIMATES OF POPULATION PARAMETERS:

VARIANCE	= 3.10981	STD. DEV.	= 1.76346

DATA DISTRIBUTION COEFFICIENTS:

SKEWNESS	= 1.02673	KURTOSIS	= -.147304

4-1 BGHS

HISTOGRAM

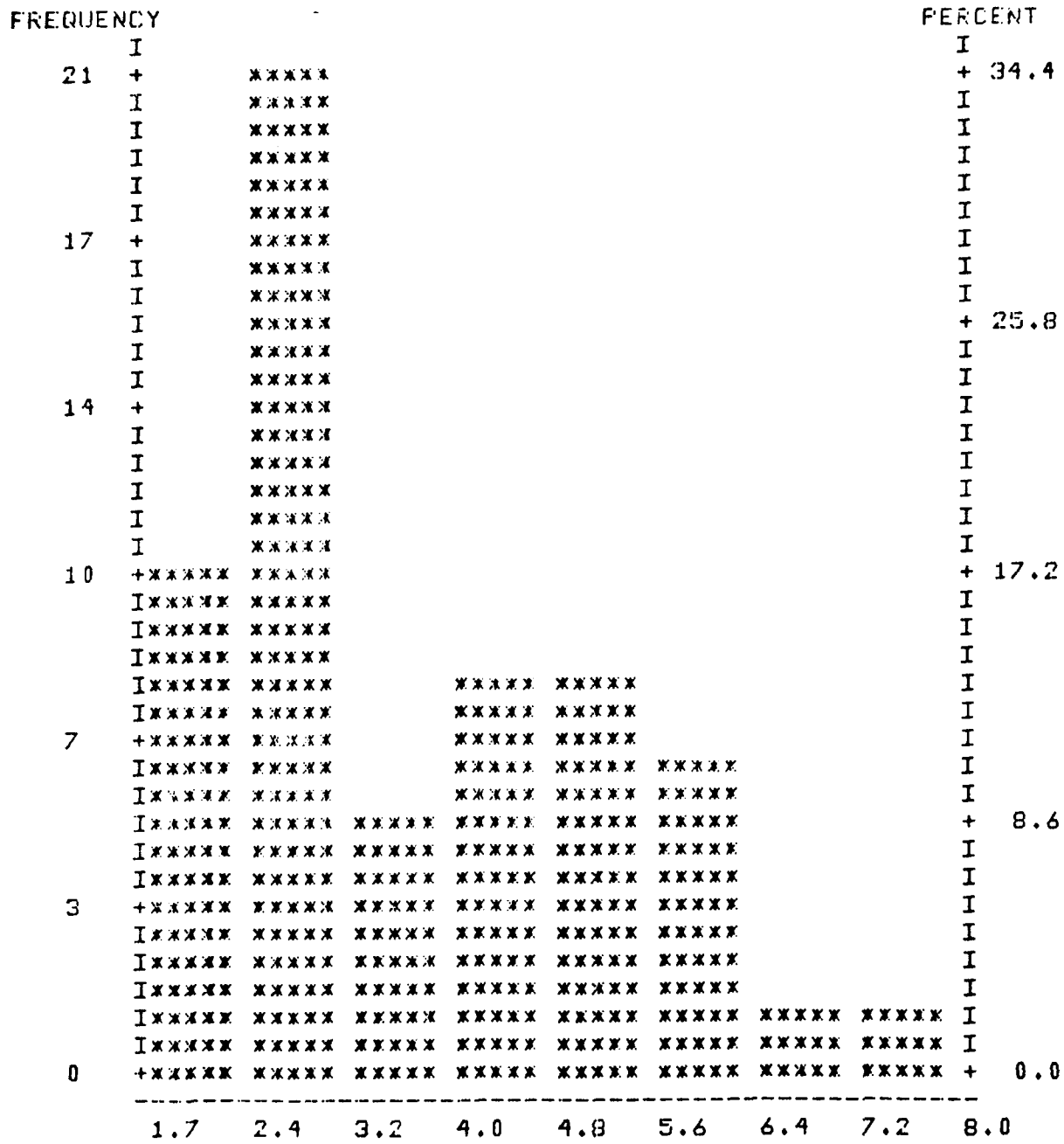

PARTICLE SIZE

4-2 BAGHOUSE

D E S C R I P T I V E S T A T I S T I C S

VARIABLE: PARTICLE SIZE SAMPLE SIZE (N) = 61

SAMPLE STATISTICS:

MEAN	= 3.71312	RANGE	= 6.3
VARIANCE	= 2.09425	MINIMUM	= 1.7
STD. DEV.	= 1.44715	MAXIMUM	= 8

UNBIASED ESTIMATES OF POPULATION PARAMETERS:

VARIANCE	= 2.12915	STD. DEV.	= 1.45916

DATA DISTRIBUTION COEFFICIENTS:

SKEWNESS	= .752484	KURTOSIS	= -.25228

4-2 BGHS

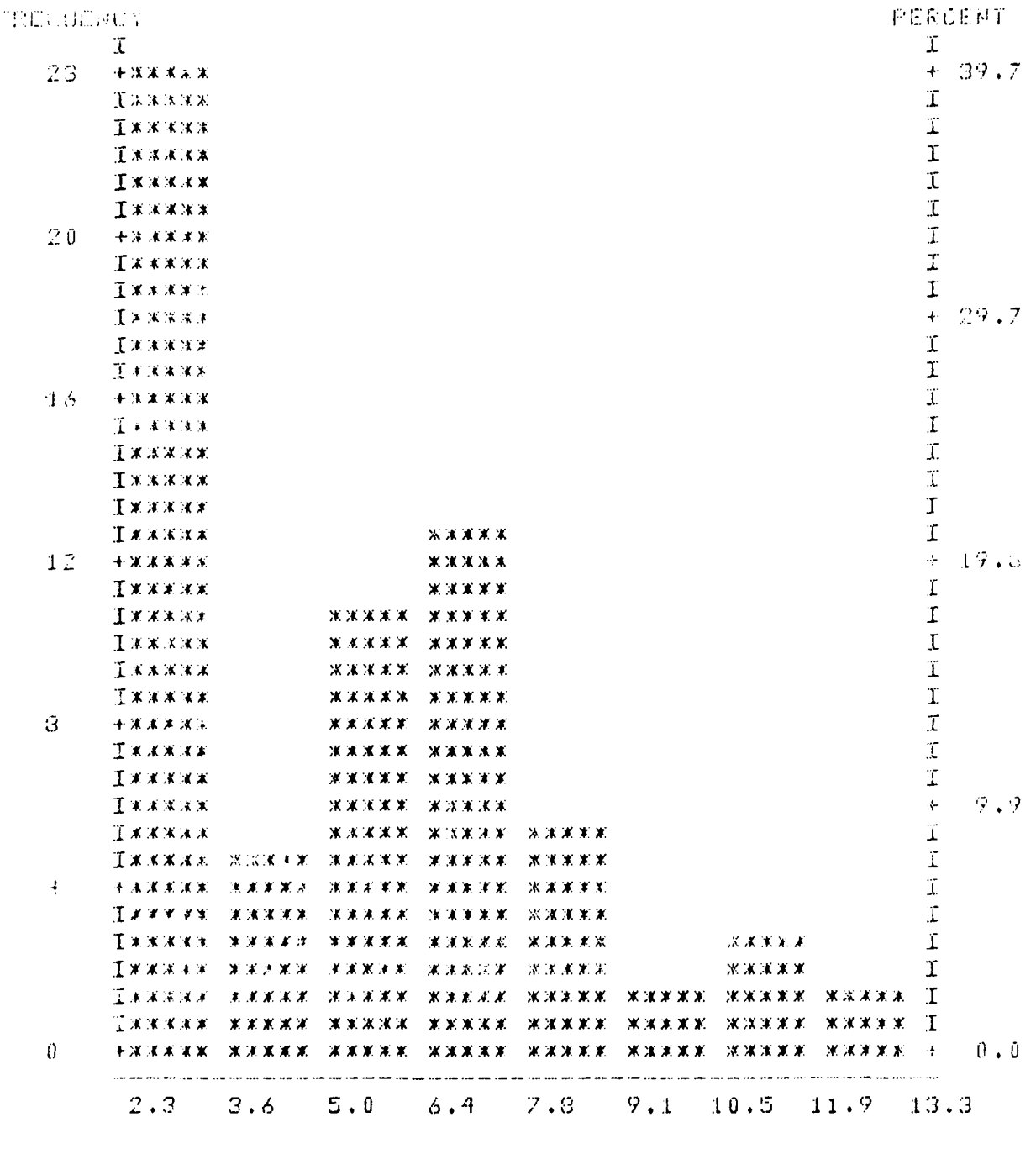
HISTOGRAM
FREQUENCY
PERCENT
23
20
16
12
8
4
0
39.7
29.7
19.8
9.9
0.0
2.3
3.6
5.0
6.4
7.8
9.1
10.5
11.9
13.3
PARTICLE SIZE

4-3 BGHS

D E S C R I P T I V E S T A T I S T I C S

VARIABLE: PARTICLE SIZE SAMPLE SIZE (N) = 58

SAMPLE STATISTICS:

MEAN	= 5.30862	RANGE	= 11
VARIANCE	= 6.59217	MINIMUM	= 2.3
STD. DEV.	= 2.56752	MAXIMUM	= 13.3

UNBIASED ESTIMATES OF POPULATION PARAMETERS:

VARIANCE	= 6.70782	STD. DEV.	= 2.58995

DATA DISTRIBUTION COEFFICIENTS:

SKEWNESS	= .881454	KURTOSIS	= .368849

4-3 BGHS

H I S T O G R A M

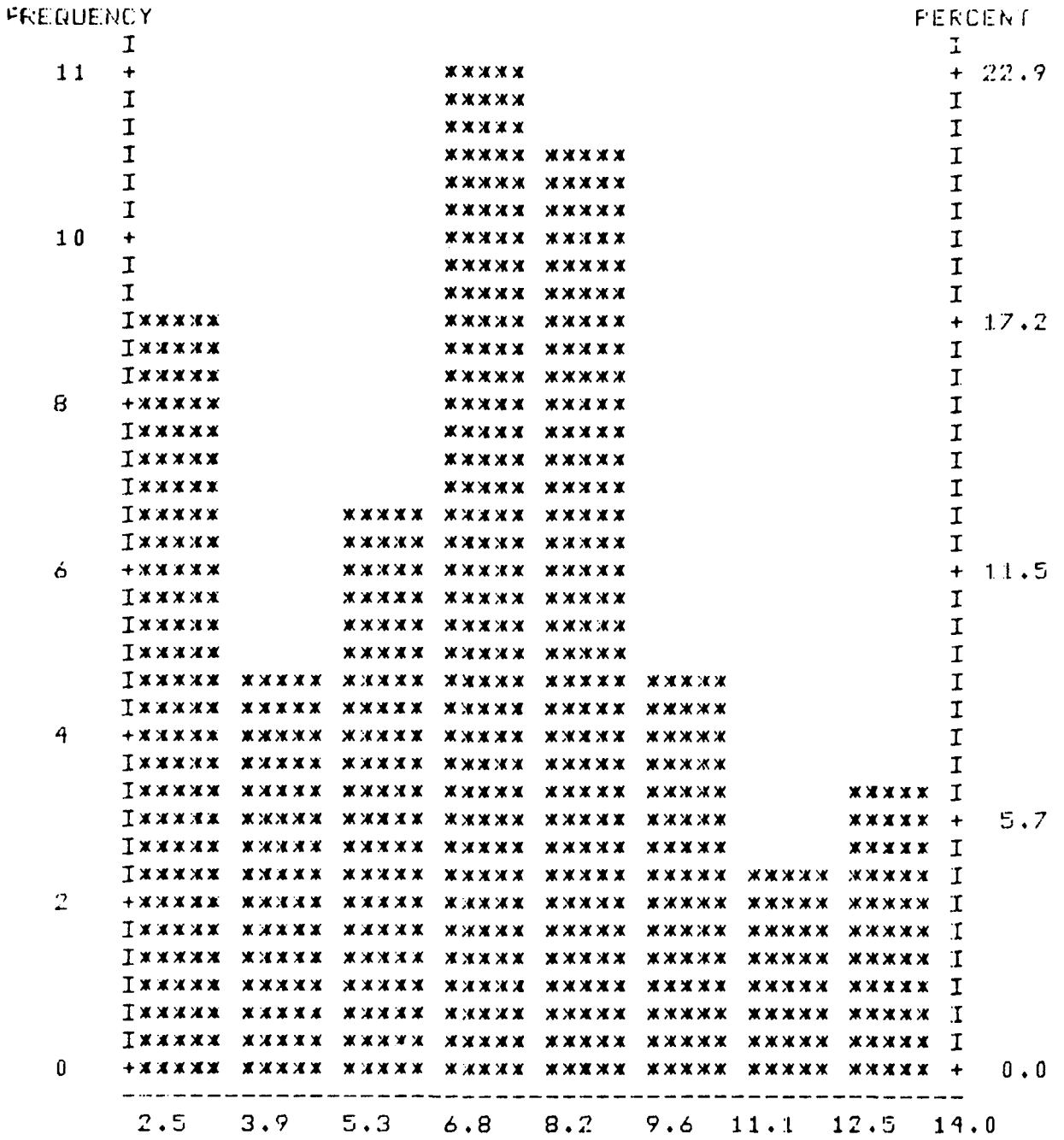

P A R T I C L E S I Z E

4-4 BGHS

D E S C R I P T I V E S T A T I S T I C S

VARIABLE: PARTICLE SIZE SAMPLE SIZE (N) = 48

SAMPLE STATISTICS:

MEAN	= 7.37292	RANGE	= 11.5
VARIANCE	= 8.13448	MINIMUM	= 2.5
STD. DEV.	= 2.8521	MAXIMUM	= 14

UNBIASED ESTIMATES OF POPULATION PARAMETERS:

VARIANCE	= 8.30755	STD. DEV.	= 2.88228

DATA DISTRIBUTION COEFFICIENTS:

SKEWNESS	= .227467	KURTOSIS	= -.369882

H I S T O G R A M

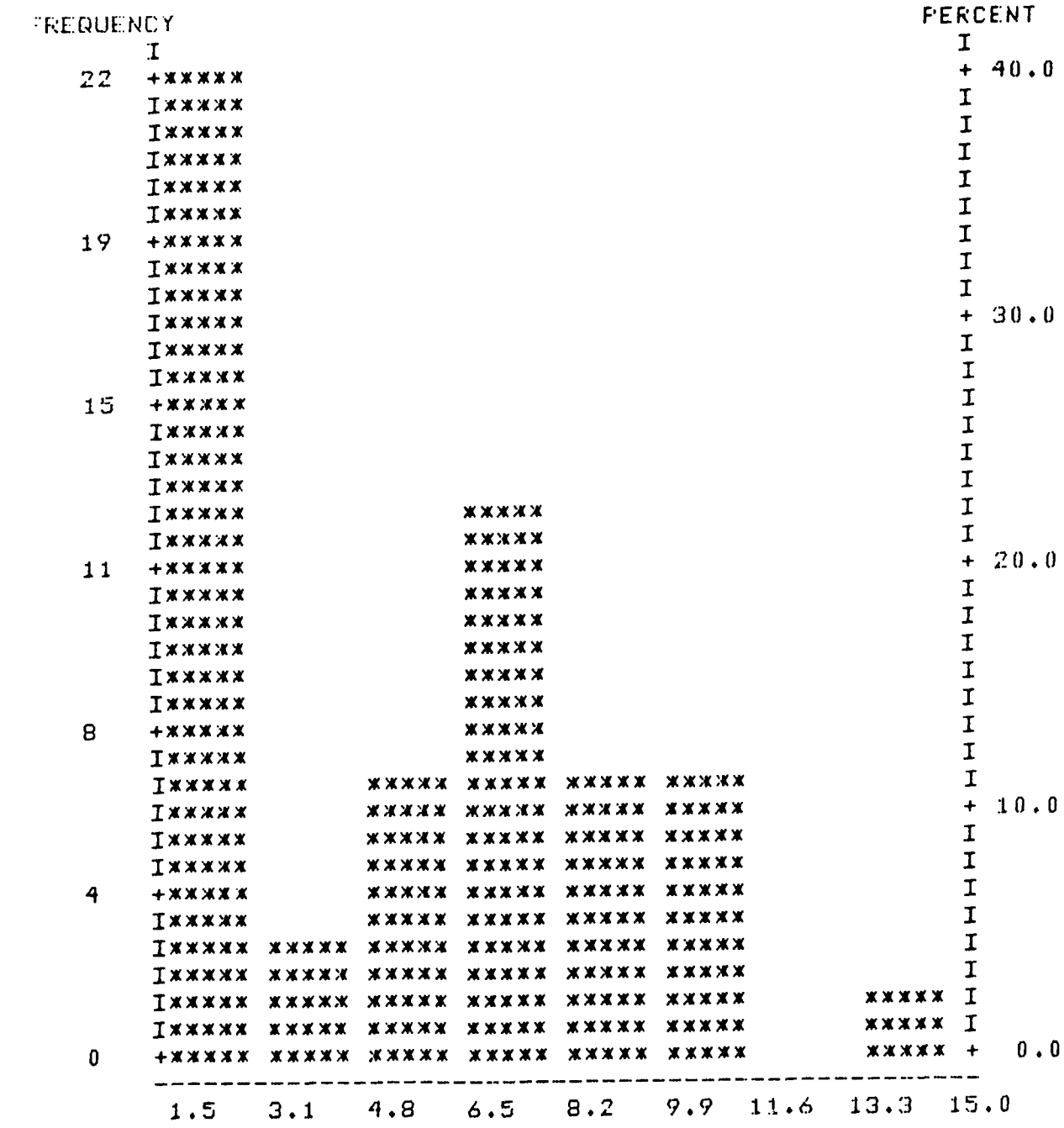

P A R T I C L E S I Z E

4-4 BGHS (Retake)

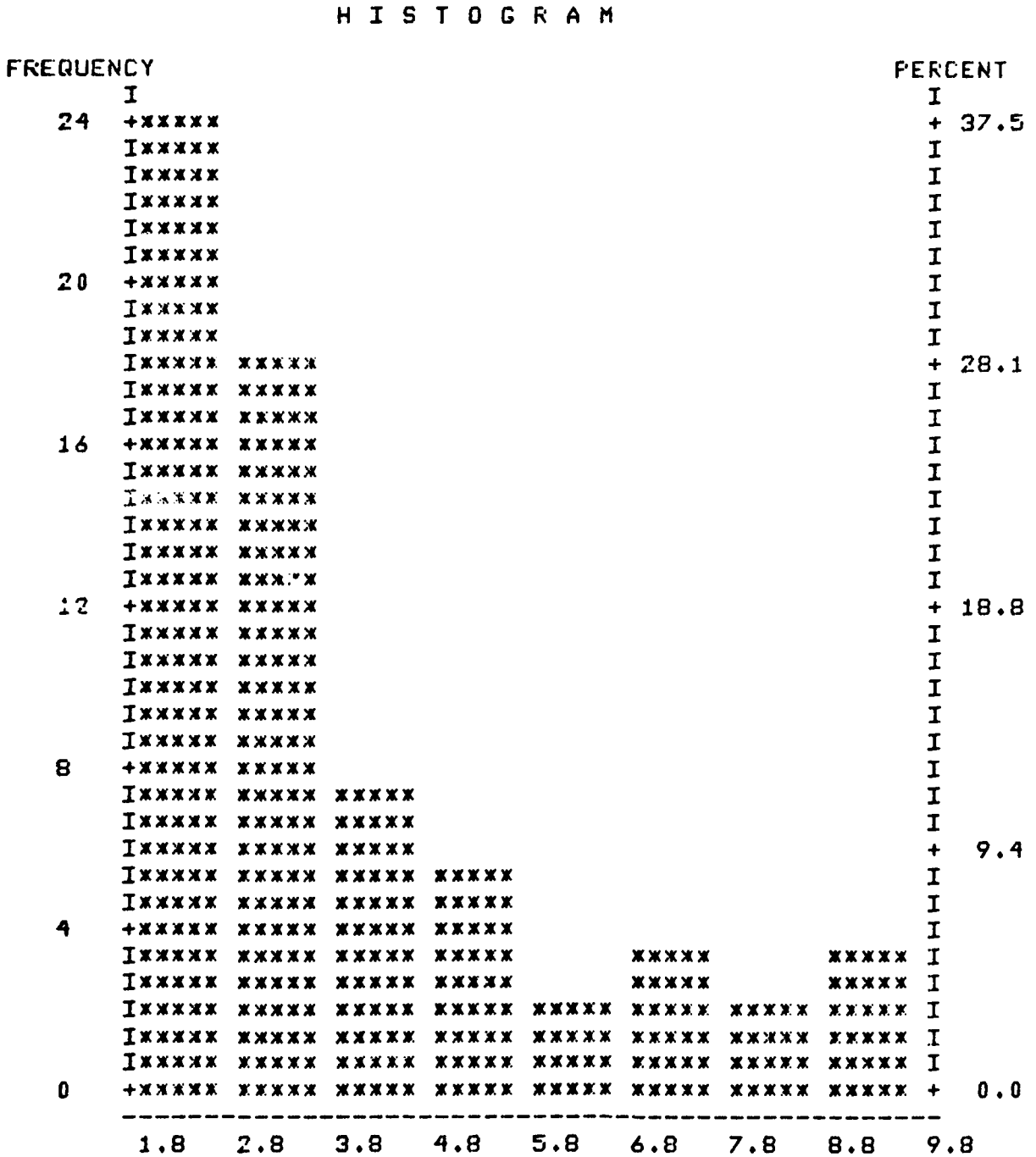
H I S T O G R A M
FREQUENCY
PERCENT
24
20
16
12
8
4
0
37.5
28.1
18.8
9.4
0.0
1.8
2.8
3.8
4.8
5.8
6.8
7.8
8.8
9.8
P A R T I C L E S I Z E

5-1 BAGHOUSE

D E S C R I P T I V E S T A T I S T I C S

VARIABLE: PARTICLE SIZE SAMPLE SIZE (N) = 64

SAMPLE STATISTICS:

MEAN	= 3.84688	RANGE	= 8
VARIANCE	= 4.28531	MINIMUM	= 1.8
STD. DEV.	= 2.0701	MAXIMUM	= 9.8

UNBIASED ESTIMATES OF POPULATION PARAMETERS:

VARIANCE	= 4.35333	STD. DEV.	= 2.08646

DATA DISTRIBUTION COEFFICIENTS:

SKEWNESS	= 1.38174	KURTOSIS	= 1.00122

5-1 BGHS

H I S T O G R A M

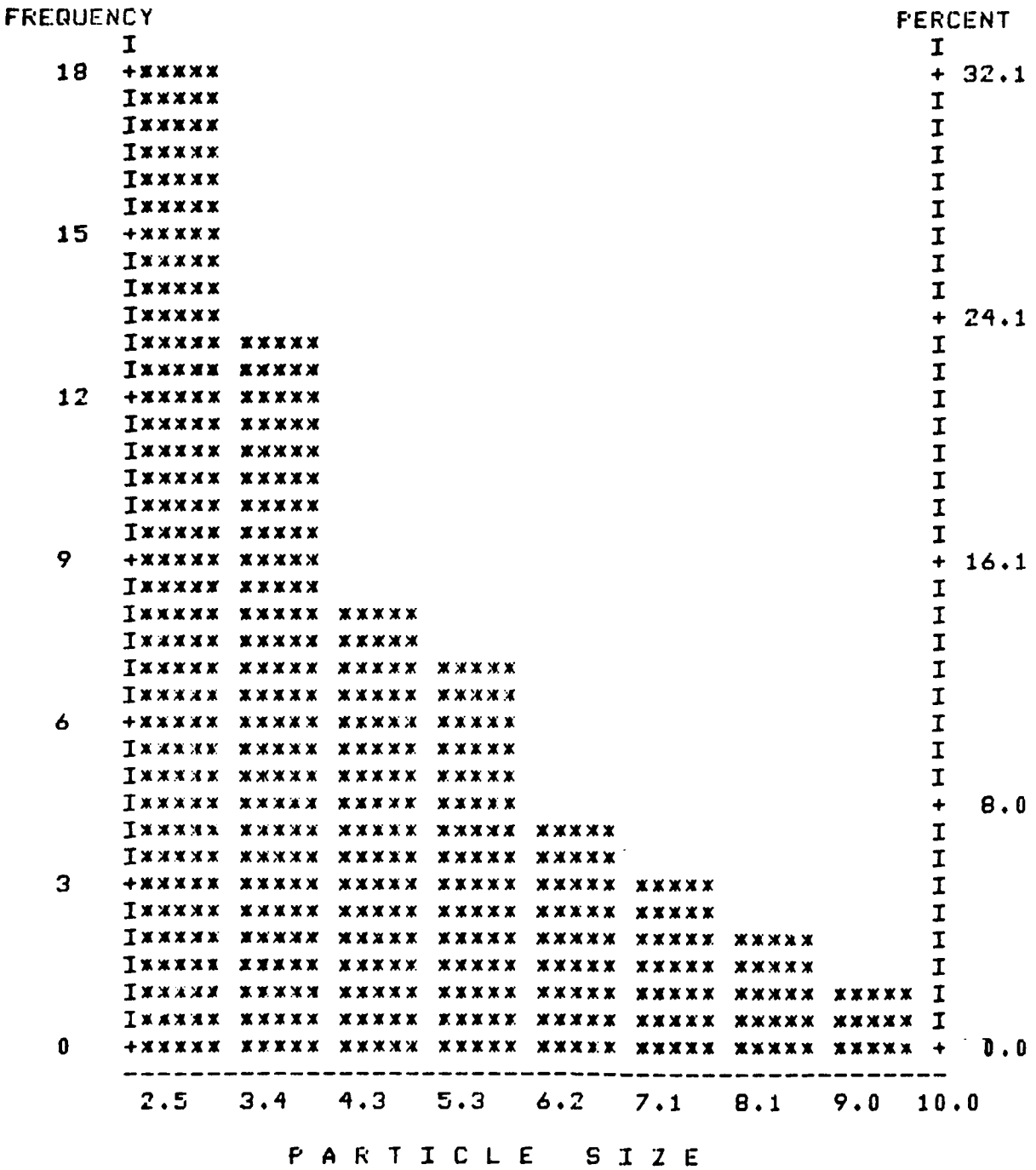

5-2 BAGHOUSE

D E S C R I P T I V E S T A T I S T I C S

VARIABLE: PARTICLE SIZE SAMPLE SIZE (N) = 56

SAMPLE STATISTICS:

MEAN	= 4.58036	RANGE	= 7.5
VARIANCE	= 3.07445	MINIMUM	= 2.5
STD. DEV.	= 1.75341	MAXIMUM	= 10

UNBIASED ESTIMATES OF POPULATION PARAMETERS:

VARIANCE	= 3.13035	STD. DEV.	= 1.76928

DATA DISTRIBUTION COEFFICIENTS:

SKEWNESS	= .912375	KURTOSIS	= .249621

5-2 BGHS

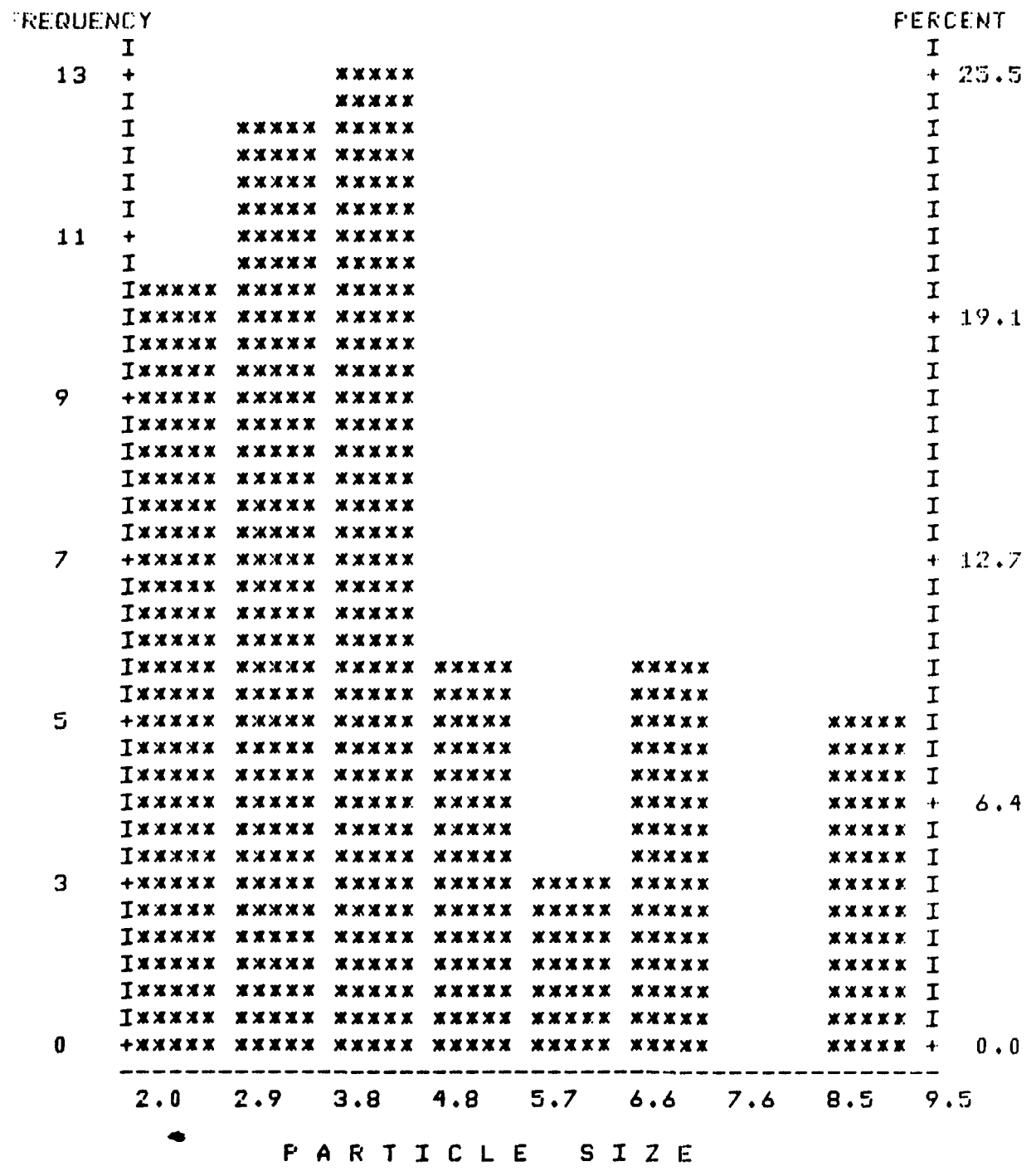
H I S T O G R A M
FREQUENCY
PERCENT
13
11
9
7
5
3
0
25.5
19.1
12.7
6.4
0.0
2.0 2.9 3.8 4.8 5.7 6.6 7.6 8.5 9.5
P A R T I C L E S I Z E

5-3 BGHS

D E S C R I P T I V E S T A T I S T I C S

VARIABLE: PARTICLE SIZE SAMPLE SIZE (N) = 51

SAMPLE STATISTICS:

MEAN	= 4.41961	RANGE	= 7.5
VARIANCE	= 3.86432	MINIMUM	= 2
STD. DEV.	= 1.96579	MAXIMUM	= 9.5

UNBIASED ESTIMATES OF POPULATION PARAMETERS:

VARIANCE	= 3.94161	STD. DEV.	= 1.98535

DATA DISTRIBUTION COEFFICIENTS:

SKEWNESS	= 1.1113	KURTOSIS	= .296463

5-3 BGHS

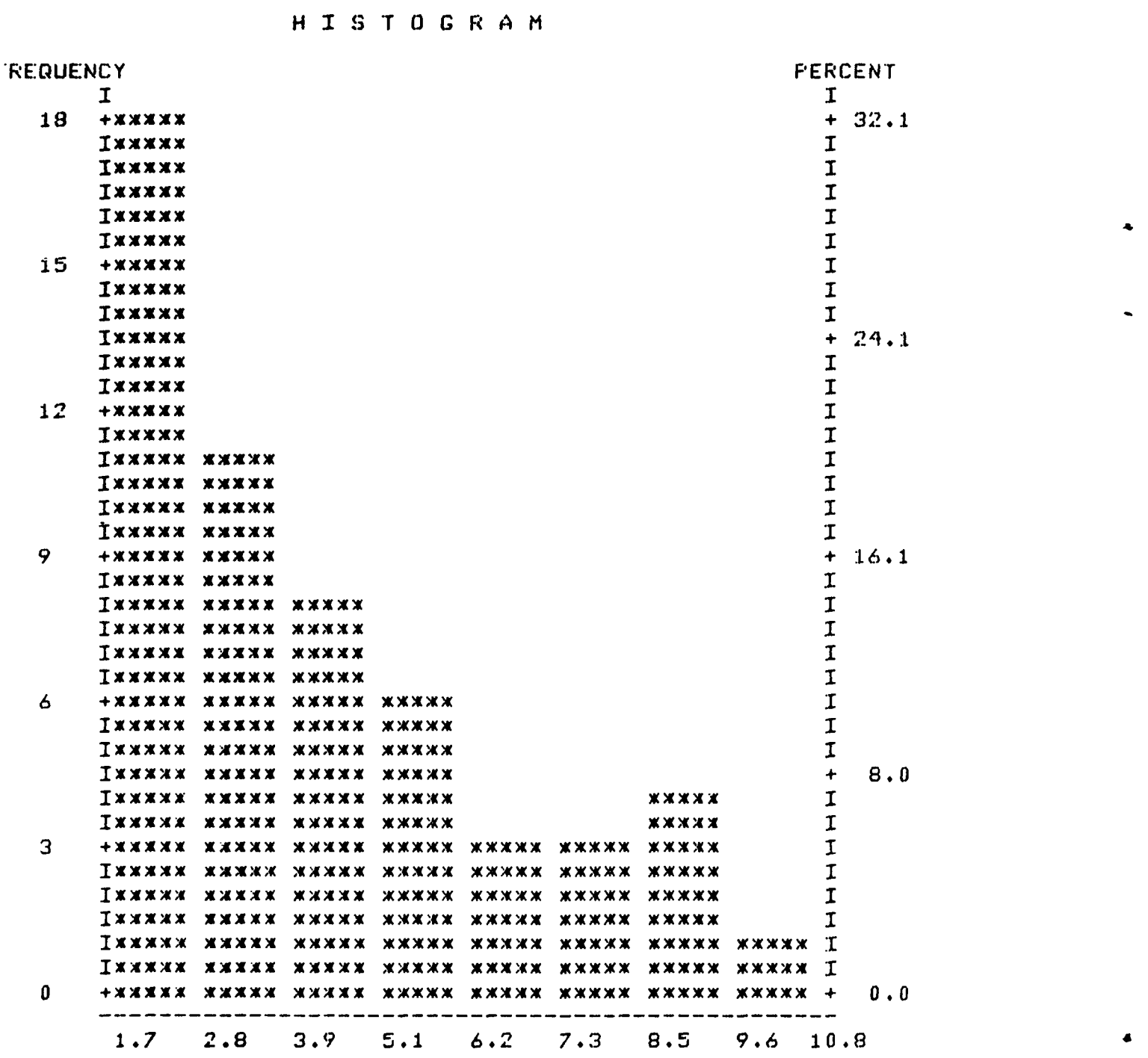
H I S T O G R A M
FREQUENCY
PERCENT
18
15
12
9
6
3
0
32.1
24.1
16.1
8.0
0.0
1.7
2.8
3.9
5.1
6.2
7.3
8.5
9.6
10.8
P A R T I C L E S I Z E

VARIABLE: PARTICLE SIZE SAMPLE SIZE (N) = 56

SAMPLE STATISTICS:

MEAN	= 4.26607	RANGE	= 9.1
VARIANCE	= 5.50831	MINIMUM	= 1.7
STD. DEV.	= 2.34698	MAXIMUM	= 10.8

UNBIASED ESTIMATES OF POPULATION PARAMETERS:

VARIANCE	= 5.60847	STD. DEV.	= 2.36822

DATA DISTRIBUTION COEFFICIENTS:

SKEWNESS	= .97496	KURTOSIS	= 1.51071E-03

5-4 BGHS

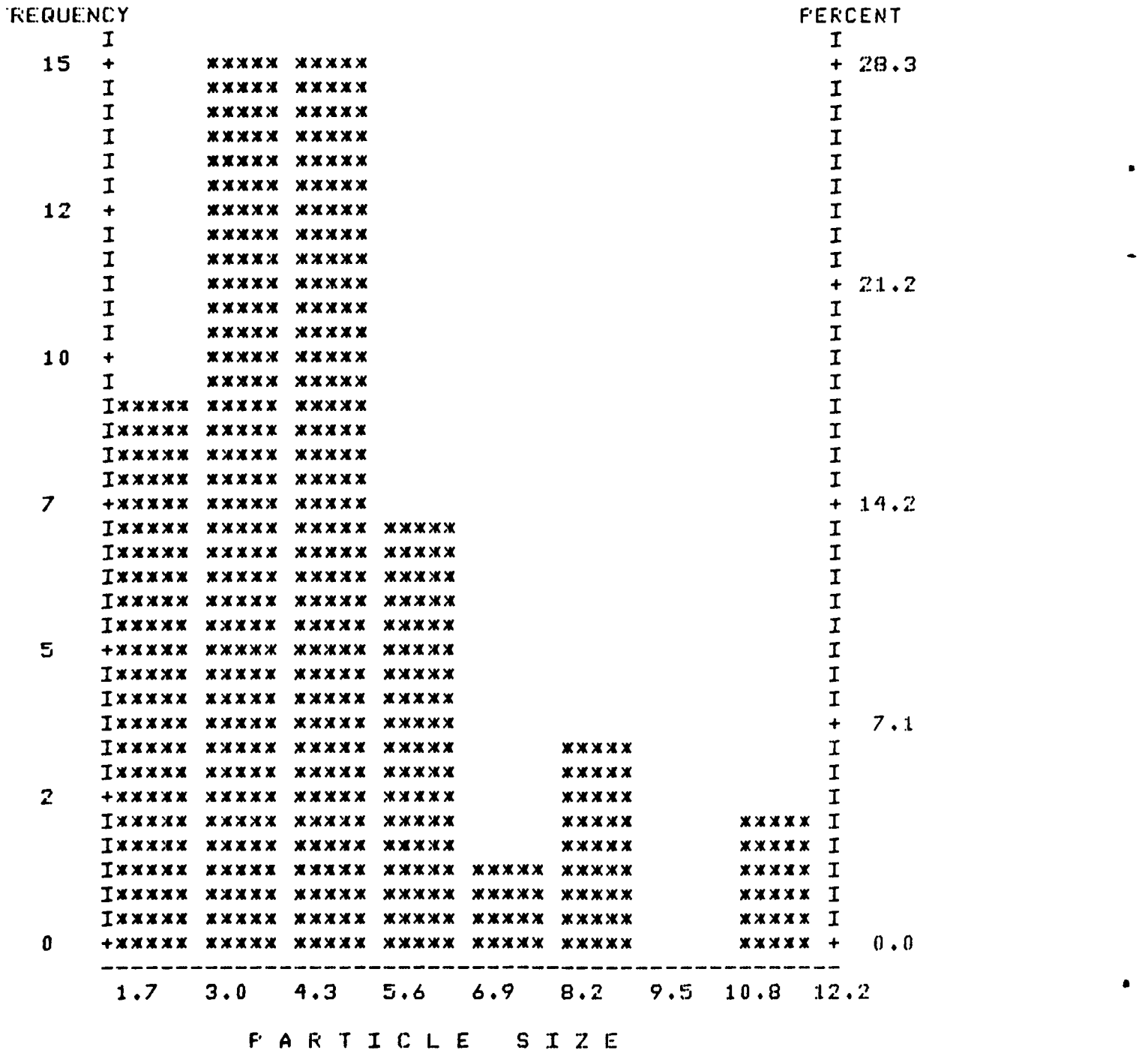
HISTOGRAM
FREQUENCY
PERCENT
15
12
10
7
5
2
0
28.3
21.2
14.2
7.1
0.0
1.7
3.0
4.3
5.6
6.9
8.2
9.5
10.8
12.2
PARTICLE SIZE

5-5 BGHS

D E S C R I P T I V E S T A T I S T I C S

VARIABLE: PARTICLE SIZE SAMPLE SIZE (N) = 53

SAMPLE STATISTICS:

MEAN	= 4.71887	RANGE	= 10.5
VARIANCE	= 4.76794	MINIMUM	= 1.7
STD. DEV.	= 2.18356	MAXIMUM	= 12.2

UNBIASED ESTIMATES OF POPULATION PARAMETERS:

VARIANCE	= 4.85963	STD. DEV.	= 2.20446

DATA DISTRIBUTION COEFFICIENTS:

SKEWNESS	= 1.34286	KURTOSIS	= 2.34636

5-5 BGHS

H I S T O G R A M

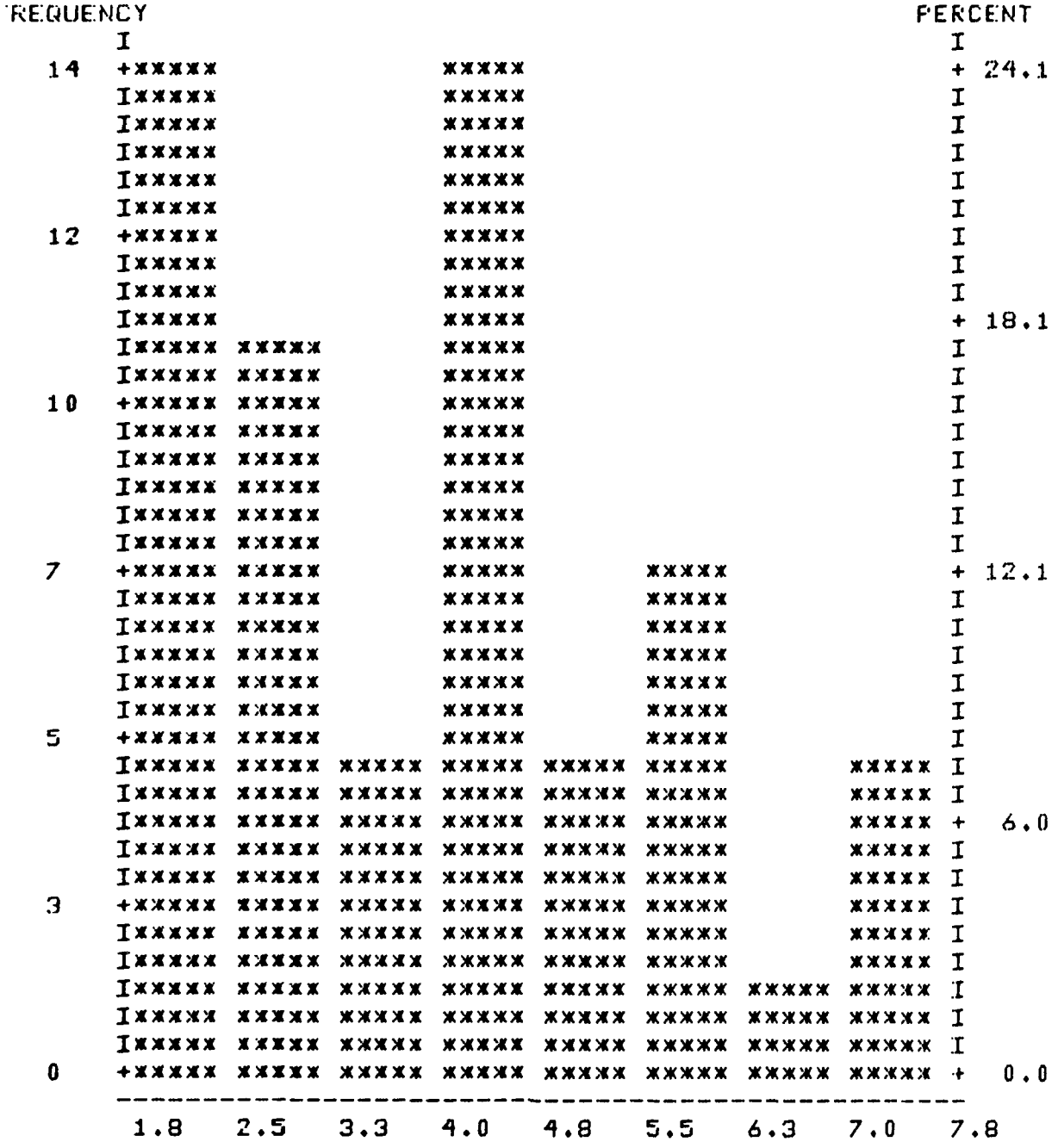

5-6 BGHS

D E S C R I P T I V E S T A T I S T I C S

VARIABLE: PARTICLE SIZE SAMPLE SIZE (N) = 58

SAMPLE STATISTICS:

MEAN	= 3.93103	RANGE	= 6
VARIANCE	= 2.57834	MINIMUM	= 1.8
STD. DEV.	= 1.60572	MAXIMUM	= 7.8

UNBIASED ESTIMATES OF POPULATION PARAMETERS:

VARIANCE	= 2.62357	STD. DEV.	= 1.61975

DATA DISTRIBUTION COEFFICIENTS:

SKEWNESS	= .523307	KURTOSIS	= -.673673

5-6 BGHS

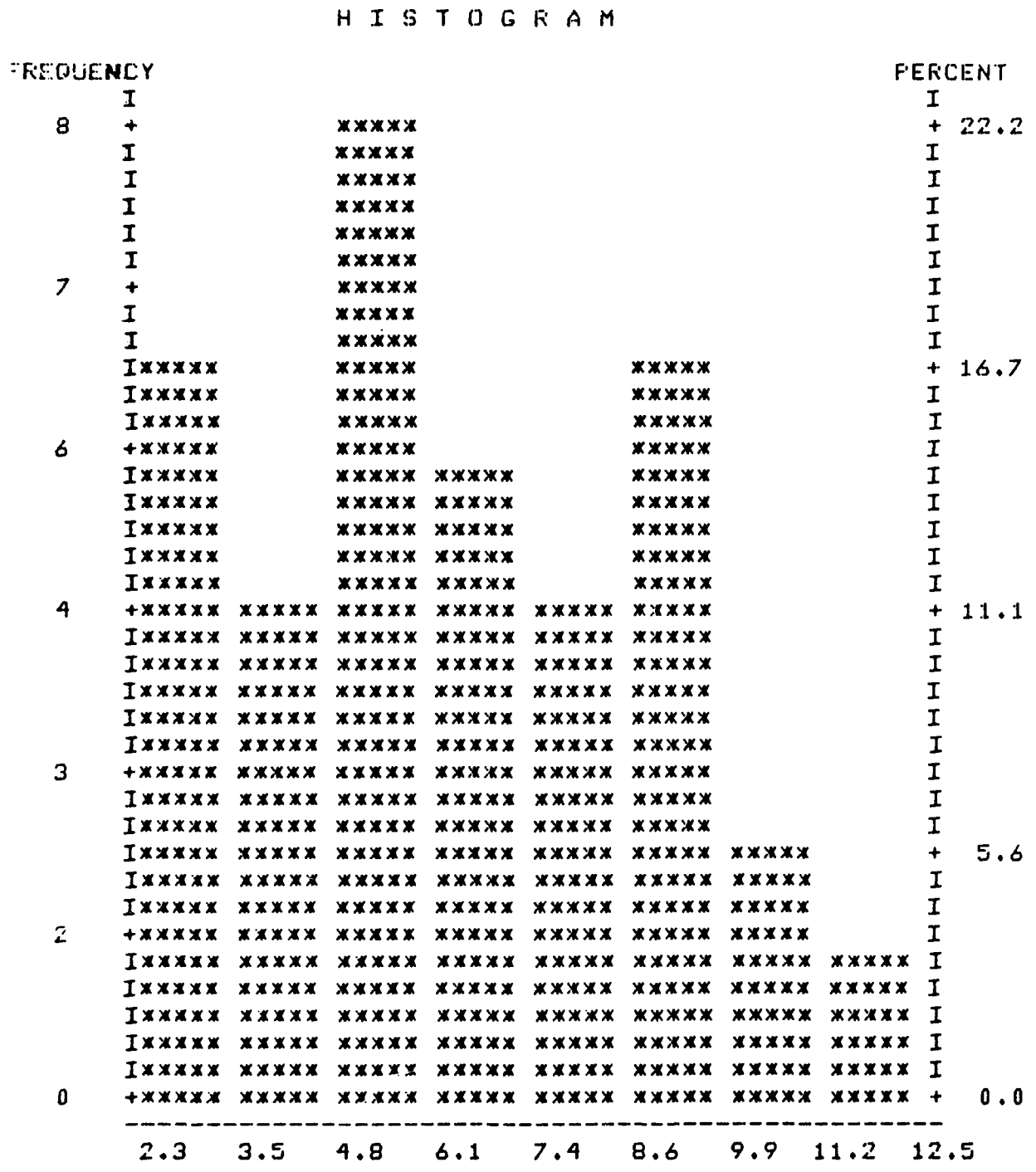
HISTOGRAM
FREQUENCY
PERCENT
8
7
6
4
3
2
0
22.2
16.7
11.1
5.6
0.0
2.3
3.5
4.8
6.1
7.4
8.6
9.9
11.2
12.5
PARTICLE SIZE

6-1 BGHS

D E S C R I P T I V E S T A T I S T I C S

VARIABLE: PARTICLE SIZE SAMPLE SIZE (N) = 36

SAMPLE STATISTICS:

MEAN	= 6.43889	RANGE	= 10.2
VARIANCE	= 6.62515	MINIMUM	= 2.3
STD. DEV.	= 2.57394	MAXIMUM	= 12.5

UNBIASED ESTIMATES OF POPULATION PARAMETERS:

VARIANCE	= 6.81444	STD. DEV.	= 2.61045

DATA DISTRIBUTION COEFFICIENTS:

SKEWNESS	= .217701	KURTOSIS	= -.687156

6-1 BGHS

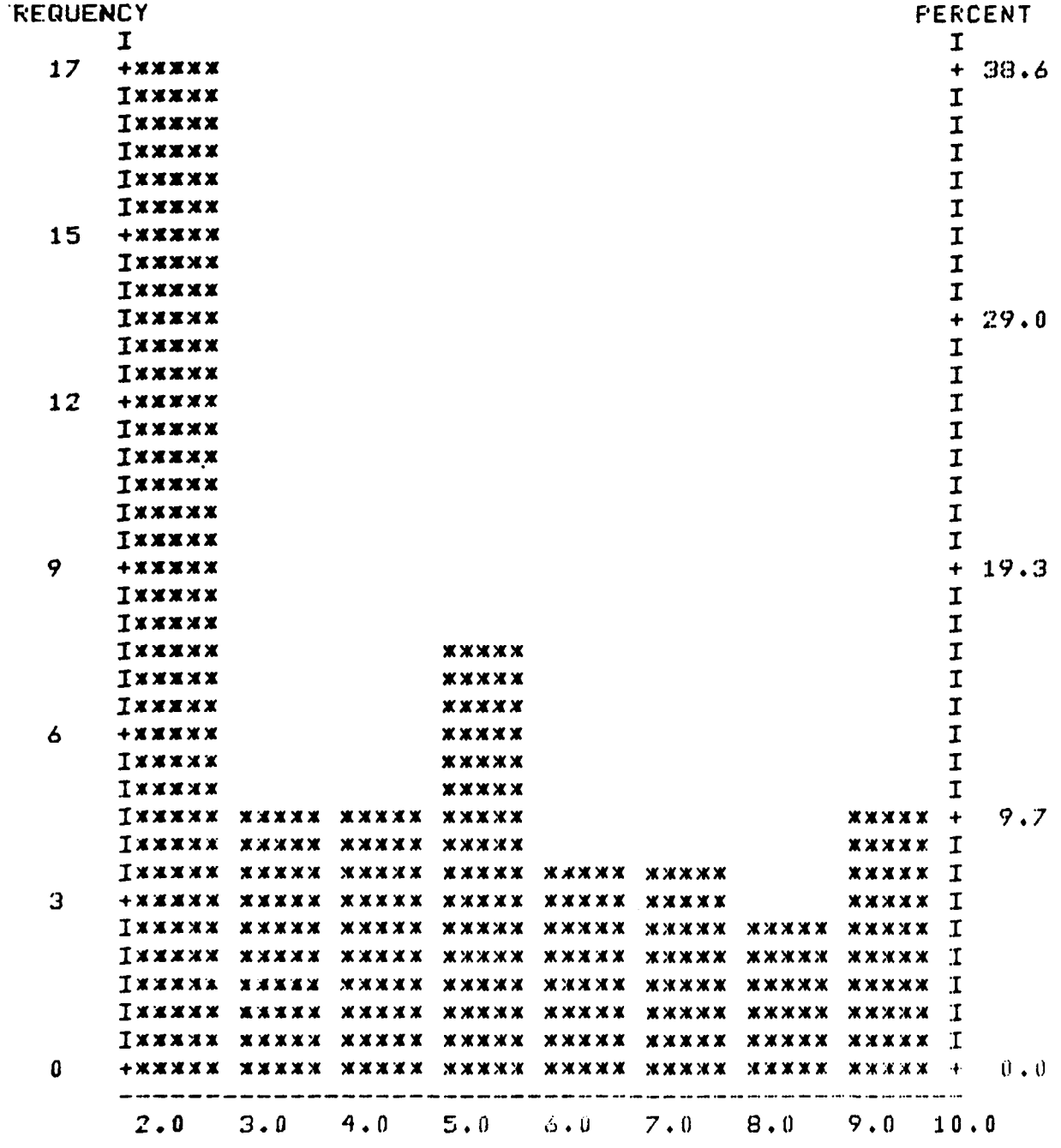
HISTOGRAM
FREQUENCY
PERCENT
17
15
12
9
6
3
0
38.6
29.0
19.3
9.7
0.0
2.0 3.0 4.0 5.0 6.0 7.0 8.0 9.0 10.0
PARTICLE SIZE

6-2 BGHS

D E S C R I P T I V E S T A T I S T I C S

VARIABLE: PARTICLE SIZE SAMPLE SIZE (N) = 44

SAMPLE STATISTICS:

MEAN	= 4.66364	RANGE	= 8
VARIANCE	= 5.62414	MINIMUM	= 2
STD. DEV.	= 2.37153	MAXIMUM	= 10

UNBIASED ESTIMATES OF POPULATION PARAMETERS:

VARIANCE	= 5.75493	STD. DEV.	= 2.39894

DATA DISTRIBUTION COEFFICIENTS:

SKEWNESS	= .689742	KURTOSIS	= -.735063

6-2 BGHS

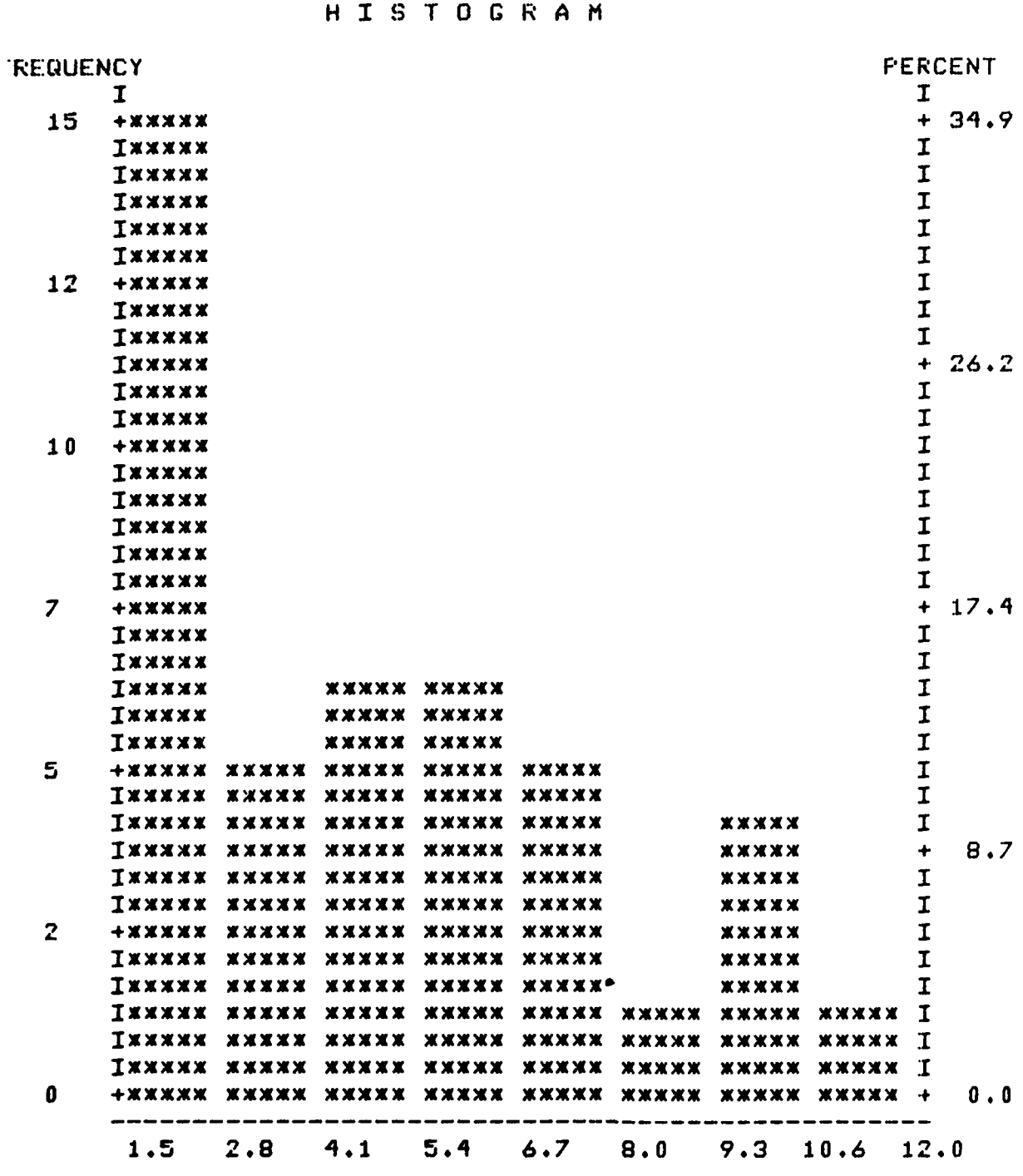
HISTOGRAM
FREQUENCY
PERCENT
15
12
10
7
5
2
0
34.9
26.2
17.4
8.7
0.0
1.5
2.8
4.1
5.4
6.7
8.0
9.3
10.6
12.0
PARTICLE SIZE

6-3 BGHS

D E S C R I P T I V E S T A T I S T I C S

VARIABLE: PARTICLE SIZE SAMPLE SIZE (N) = 43

SAMPLE STATISTICS:

MEAN	= 4.81628	RANGE	= 10.5
VARIANCE	= 7.27064	MINIMUM	= 1.5
STD. DEV.	= 2.69641	MAXIMUM	= 12

UNBIASED ESTIMATES OF POPULATION PARAMETERS:

VARIANCE	= 7.44376	STD. DEV.	= 2.72832

DATA DISTRIBUTION COEFFICIENTS:

SKEWNESS	= .861483	KURTOSIS	= -.152145

6-3 BGHS

H I S T O G R A M

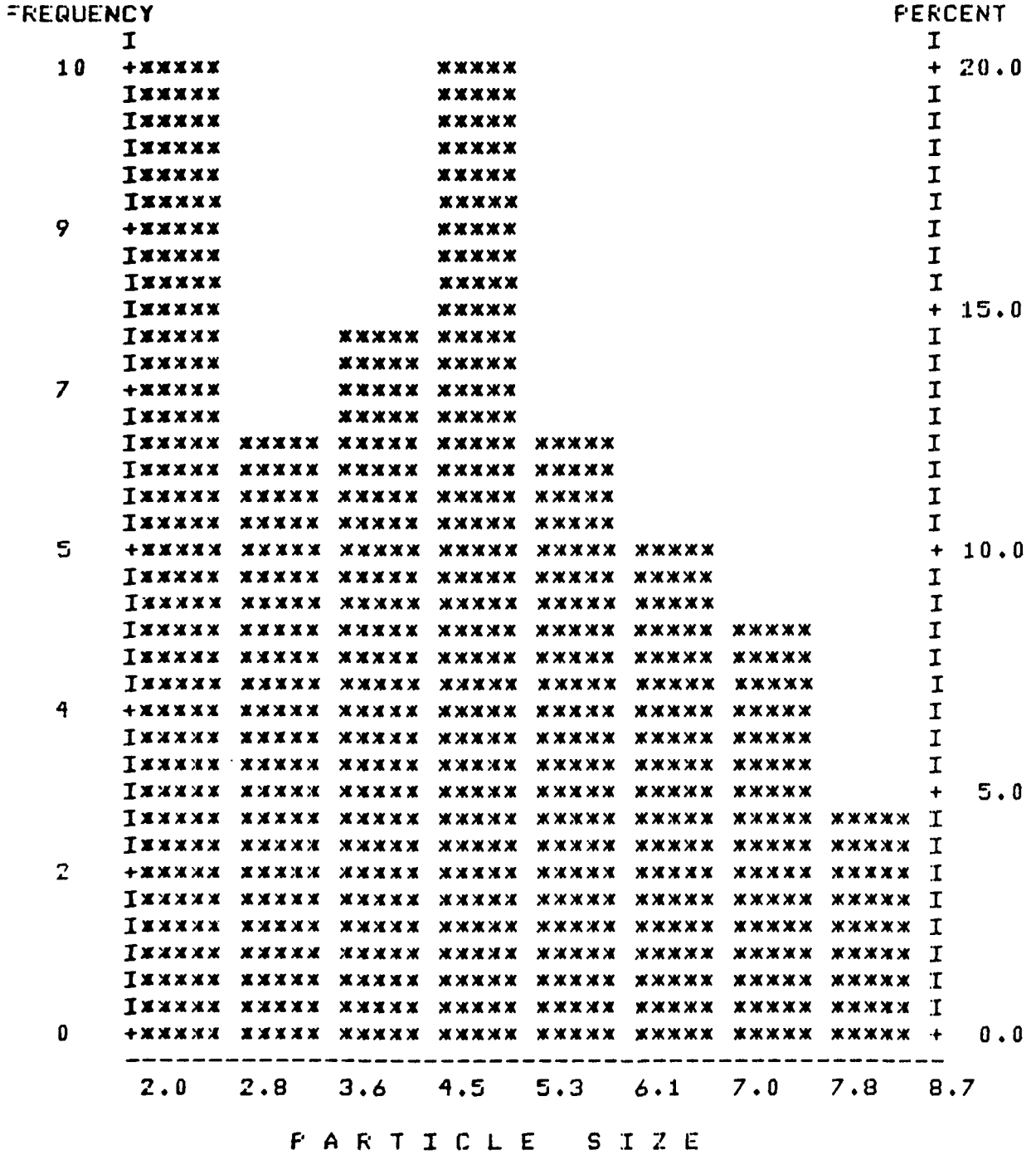

6-4 BGHS

D E S C R I P T I V E S T A T I S T I C S

VARIABLE: PARTICLE SIZE SAMPLE SIZE (N) = 50

SAMPLE STATISTICS:

MEAN	= 4.61	RANGE	= 6.7
VARIANCE	= 2.98491	MINIMUM	= 2
STD. DEV.	= 1.72769	MAXIMUM	= 8.7

UNBIASED ESTIMATES OF POPULATION PARAMETERS:

VARIANCE	= 3.04582	STD. DEV.	= 1.74523

DATA DISTRIBUTION COEFFICIENTS:

SKEWNESS	= .369043	KURTOSIS	= -.744985

6-4 BGHS

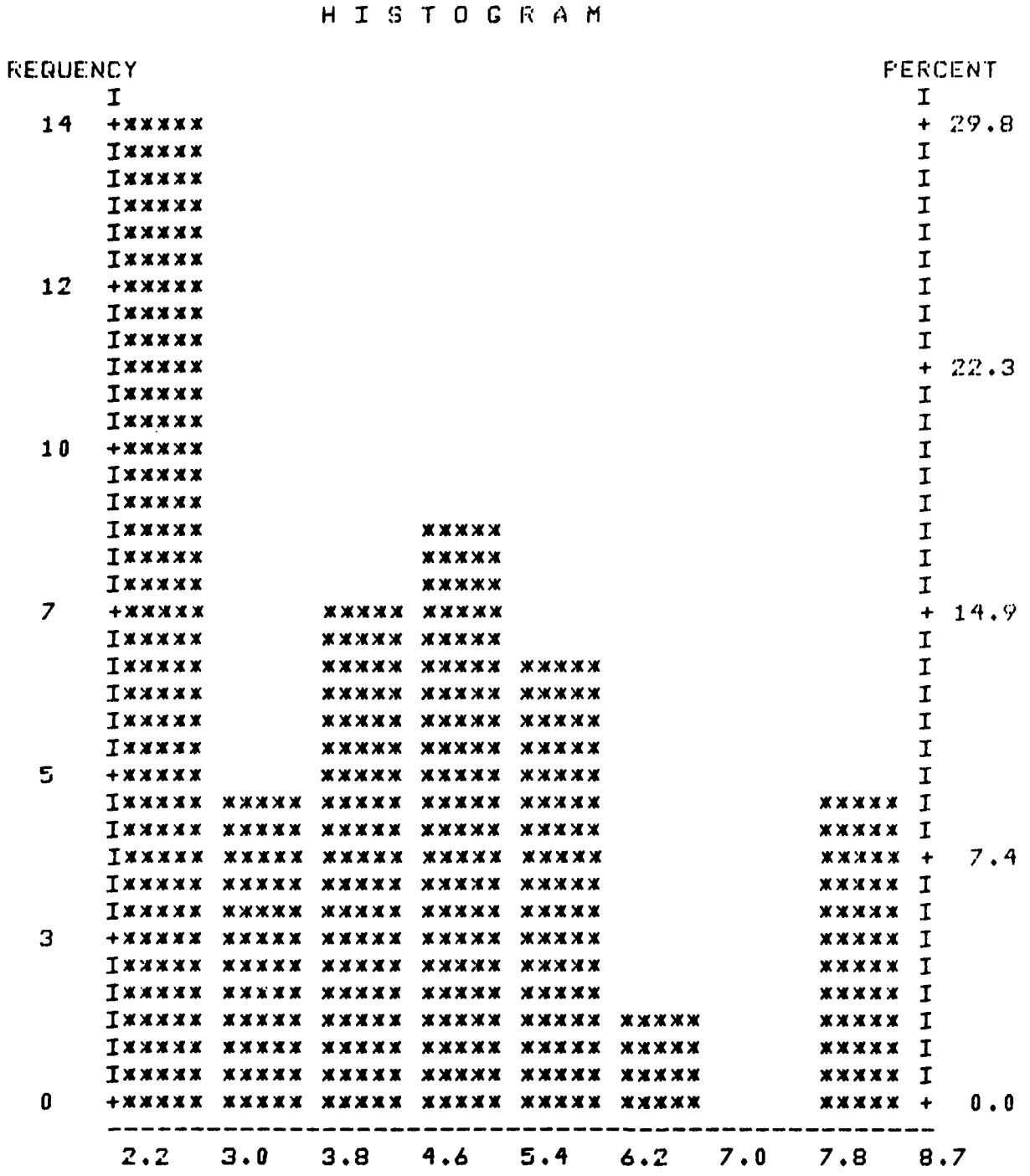
H I S T O G R A M
REQUENCY
PERCENT
14
12
10
7
5
3
0
29.8
22.3
14.9
7.4
0.0
2.2
3.0
3.8
4.6
5.4
6.2
7.0
7.8
8.7
P A R T I C L E S I Z E

6-5 BGHS

D E S C R I P T I V E S T A T I S T I C S

VARIABLE: PARTICLE SIZE SAMPLE SIZE (N) = 47

SAMPLE STATISTICS:

MEAN	= 4.22979	RANGE	= 6.5
VARIANCE	= 3.17484	MINIMUM	= 2.2
STD. DEV.	= 1.78181	MAXIMUM	= 8.7

UNBIASED ESTIMATES OF POPULATION PARAMETERS:

VARIANCE	= 3.24386	STD. DEV.	= 1.80107

DATA DISTRIBUTION COEFFICIENTS:

SKEWNESS	= .802989	KURTOSIS	= -.0633651

6-5 BGHS

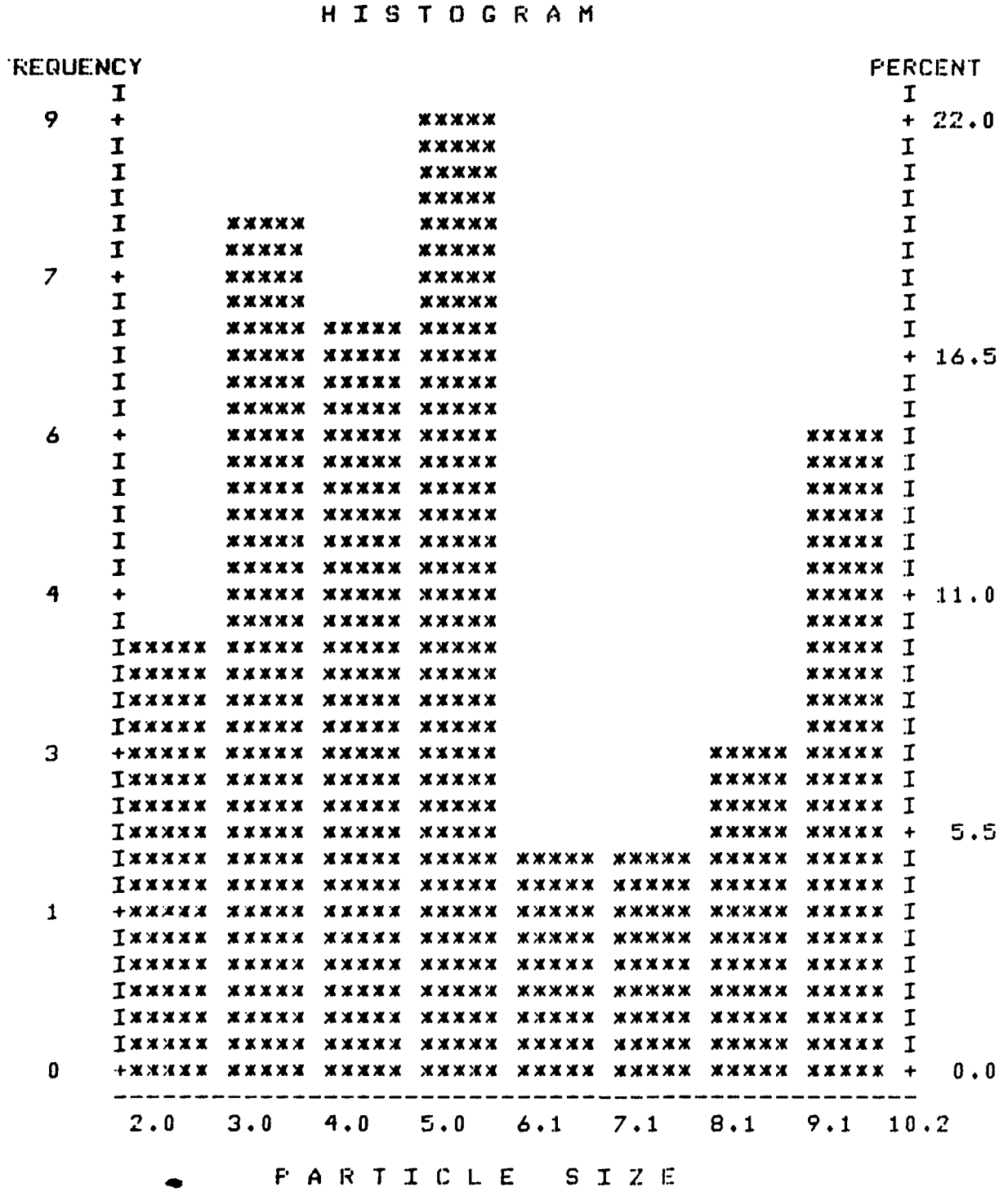
HISTOGRAM
FREQUENCY
PERCENT
9
7
6
4
3
1
0
22.0
16.5
11.0
5.5
0.0
2.0
3.0
4.0
5.0
6.1
7.1
8.1
9.1
10.2
PARTICLE SIZE

6-6 BGHS

D E S C R I P T I V E S T A T I S T I C S

VARIABLE: PARTICLE SIZE SAMPLE SIZE (N) = 41

SAMPLE STATISTICS:

MEAN	= 5.59756	RANGE	= 8.2
VARIANCE	= 5.58316	MINIMUM	= 2
STD. DEV.	= 2.36287	MAXIMUM	= 10.2

UNBIASED ESTIMATES OF POPULATION PARAMETERS:

VARIANCE	= 5.72274	STD. DEV.	= 2.39223

DATA DISTRIBUTION COEFFICIENTS:

SKEWNESS	= .585752	KURTOSIS	= -.810199

6-6 BGHS

H I S T O G R A M

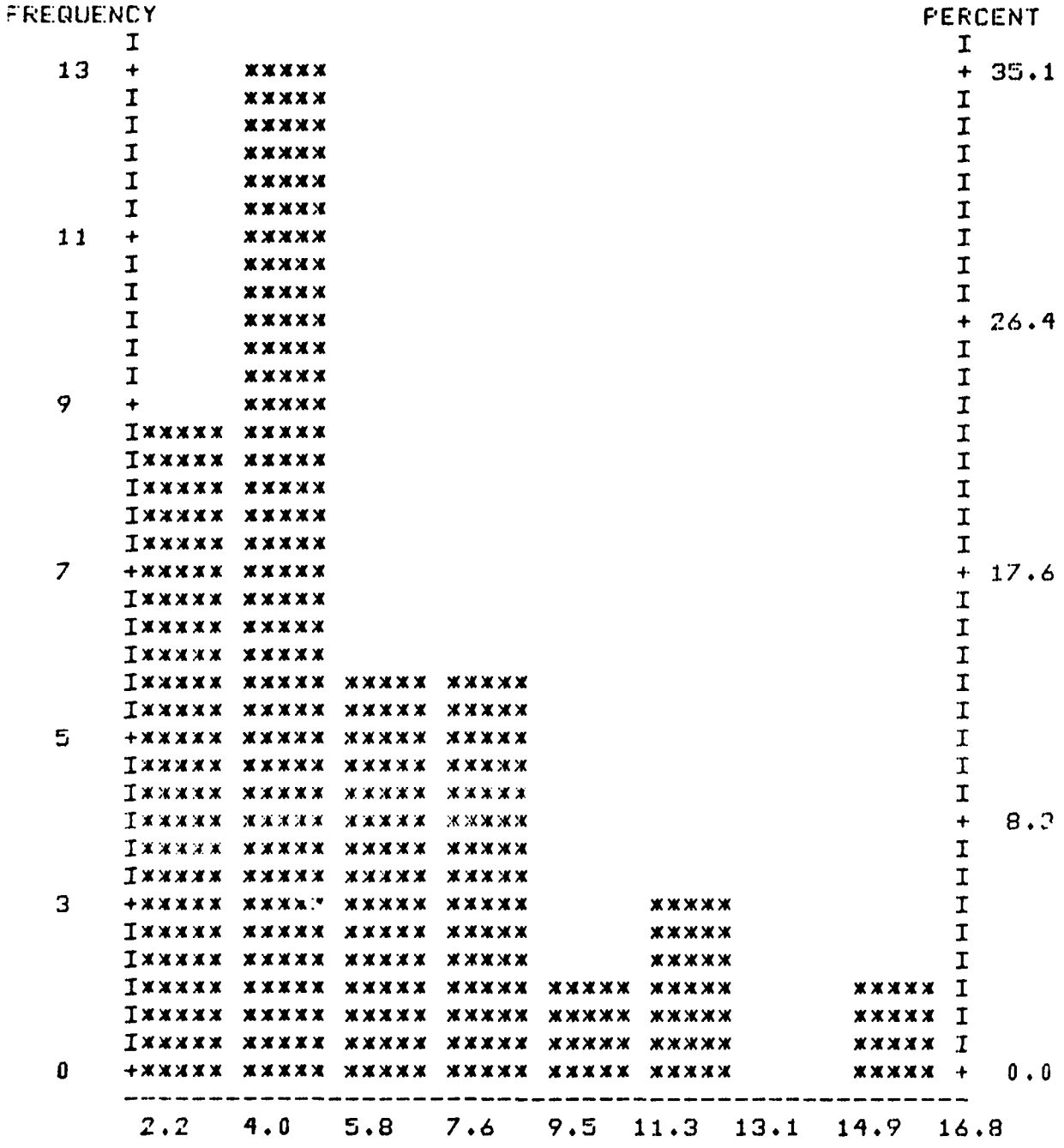

6-7 BGHS

D E S C R I P T I V E S T A T I S T I C S

VARIABLE: PARTICLE SIZE SAMPLE SIZE (N) = 37

SAMPLE STATISTICS:

MEAN	= 5.92432	RANGE	= 14.6
VARIANCE	= 9.6386	MINIMUM	= 2.2
STD. DEV.	= 3.10461	MAXIMUM	= 16.8

UNBIASED ESTIMATES OF POPULATION PARAMETERS:

VARIANCE	= 9.90634	STD. DEV.	= 3.14743

DATA DISTRIBUTION COEFFICIENTS:

SKEWNESS	= 1.37804	KURTOSIS	= 2.28149

6-7 BGHS

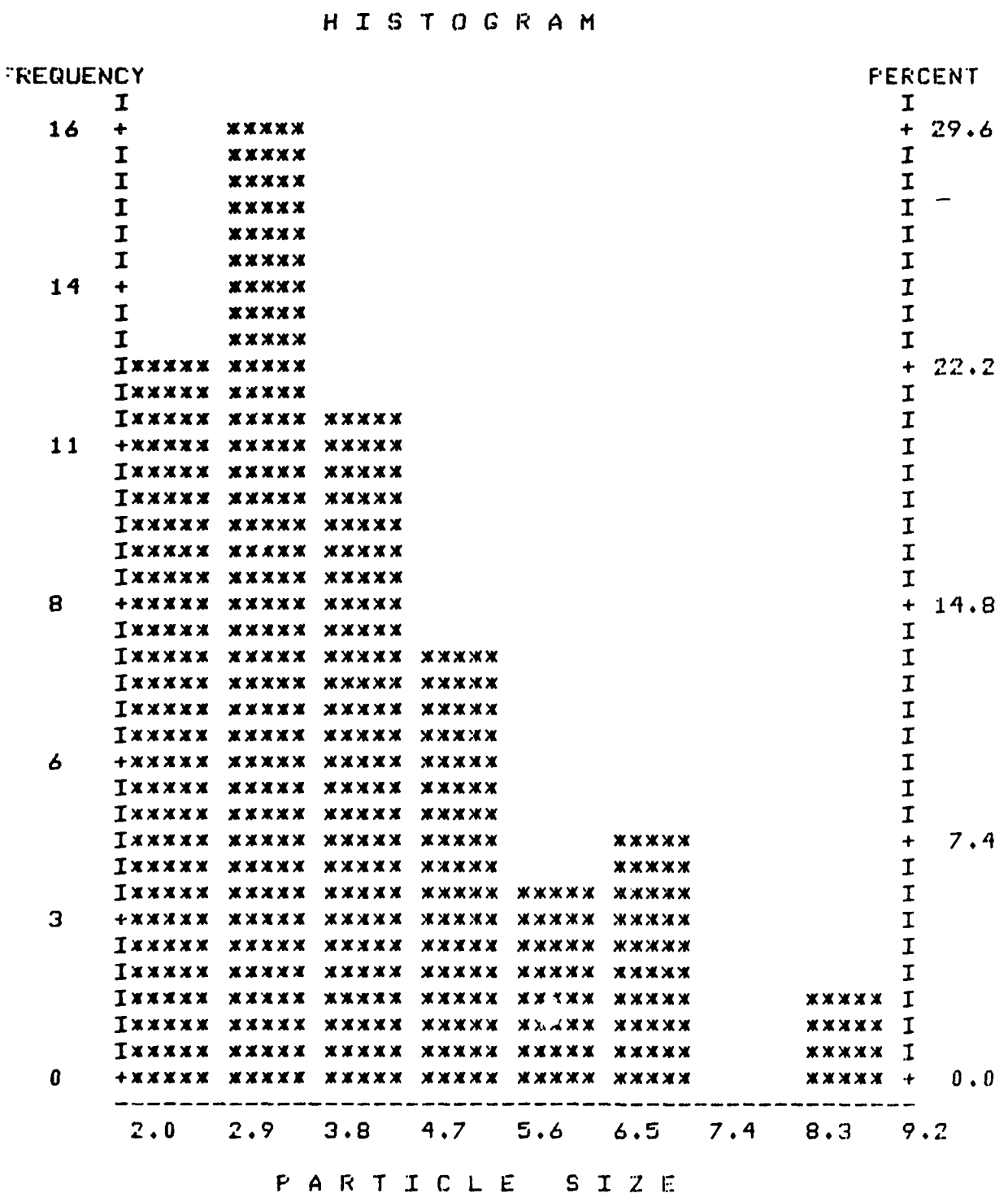
H I S T O G R A M
FREQUENCY
PERCENT
16
14
11
8
6
3
0
29.6
22.2
14.8
7.4
0.0
2.0 2.9 3.8 4.7 5.6 6.5 7.4 8.3 9.2
P A R T I C L E S I Z E

6-8 BGHS

D E S C R I P T I V E S T A T I S T I C S

VARIABLE: PARTICLE SIZE SAMPLE SIZE (N) = 54

SAMPLE STATISTICS:

MEAN	= 4.02963	RANGE	= 7.2
VARIANCE	= 2.14876	MINIMUM	= 2
STD. DEV.	= 1.46586	MAXIMUM	= 9.2

UNBIASED ESTIMATES OF POPULATION PARAMETERS:

VARIANCE	= 2.1893	STD. DEV.	= 1.47963

DATA DISTRIBUTION COEFFICIENTS:

SKEWNESS	= 1.14916	KURTOSIS	= 1.3323

6-8 BGHS

APPENDIX B

SEM PHOTOMICROGRAPHS

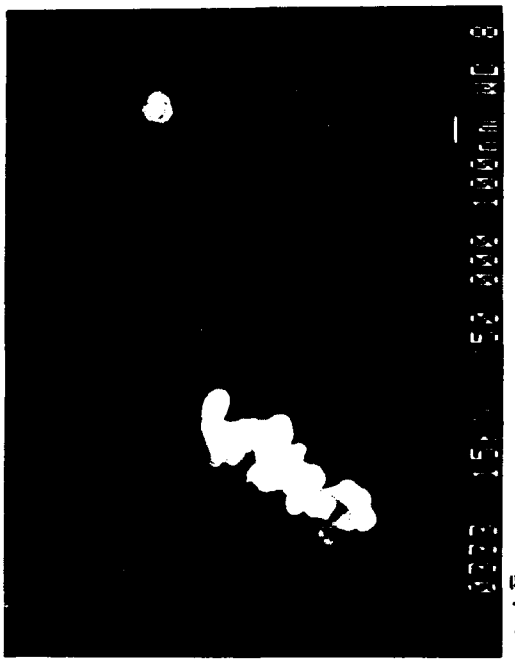

1-1B

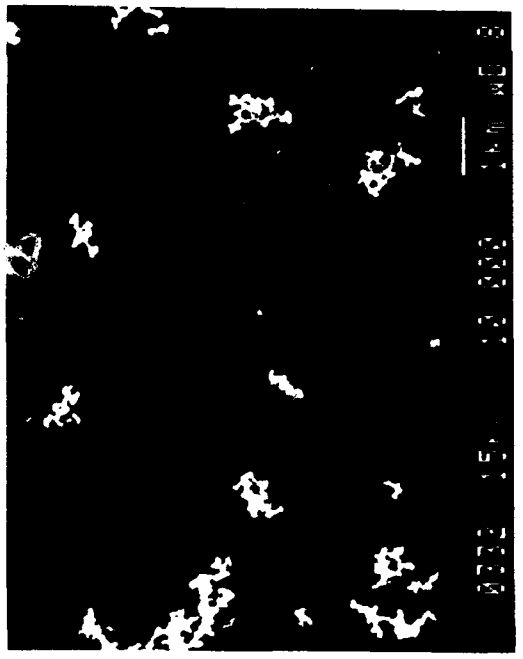

1-1B

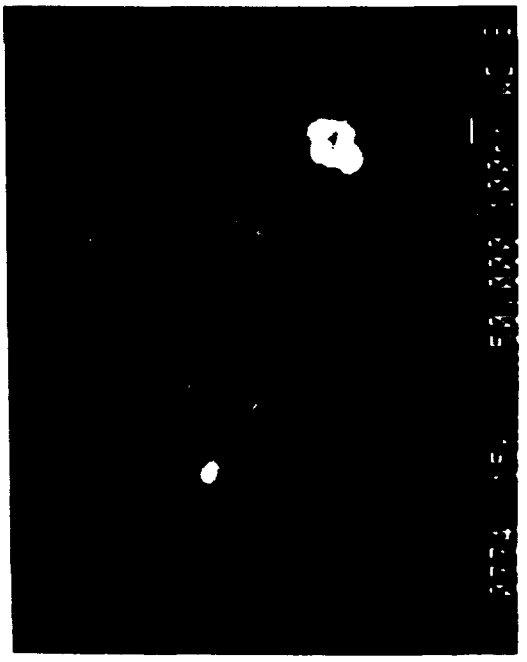

1-1B

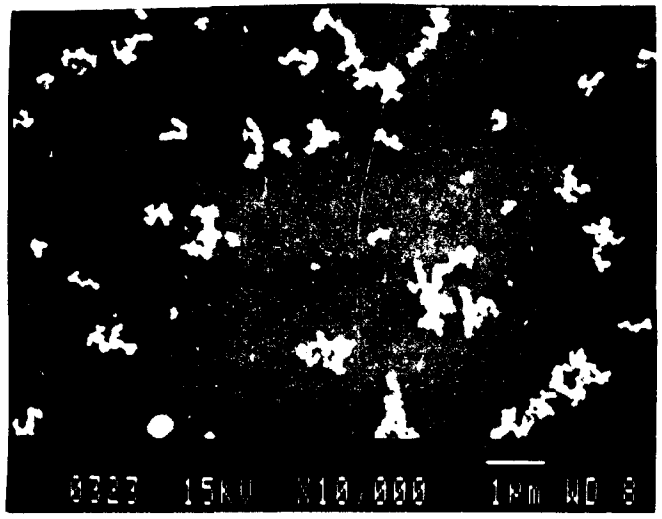
0323 15kV X10,000 1μm WD 8

I-IP

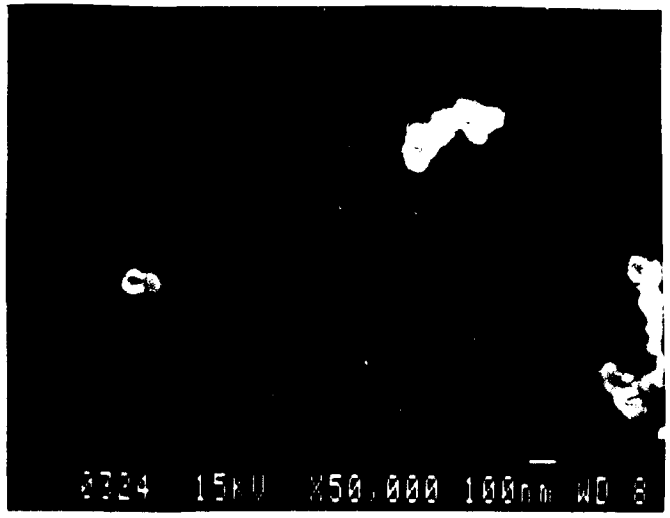
0324 15kV X50,000 100nm WD 8

I-IP

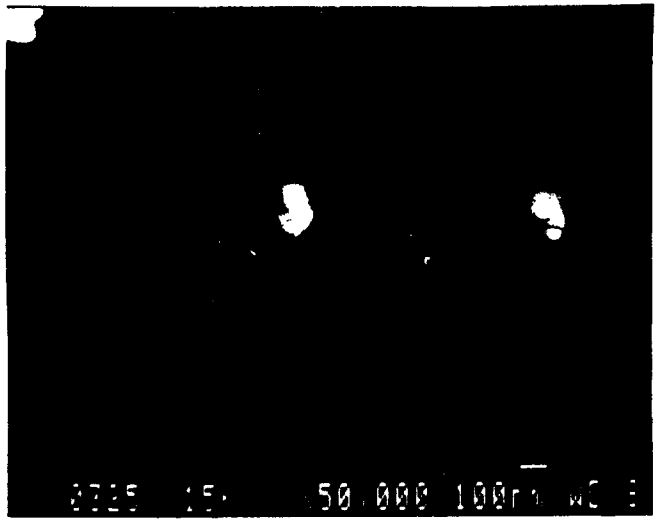
0325 15. 50,000 100n WD 8

I-IP

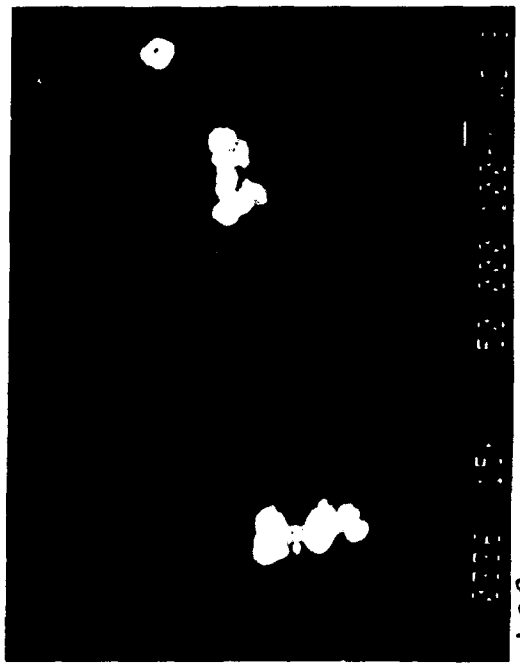
1-28

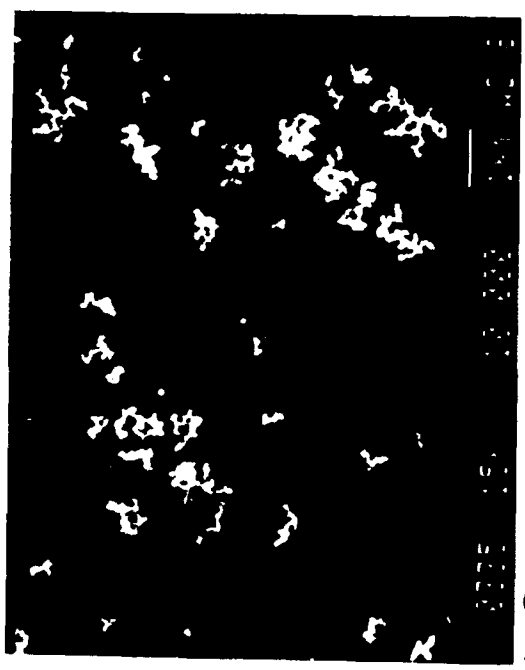
1-28

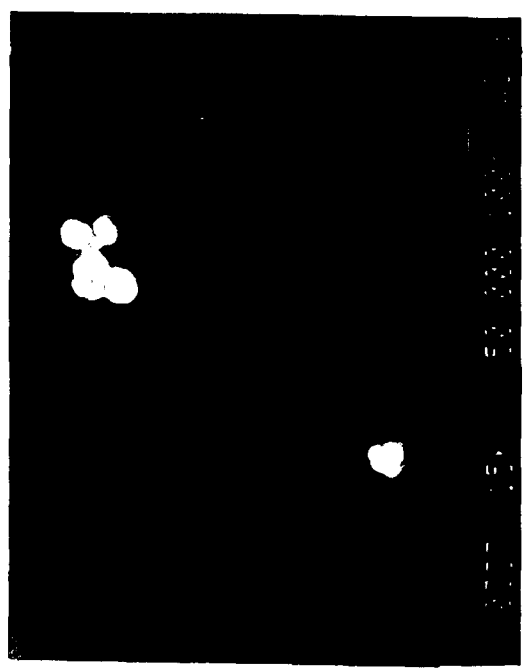
1-28

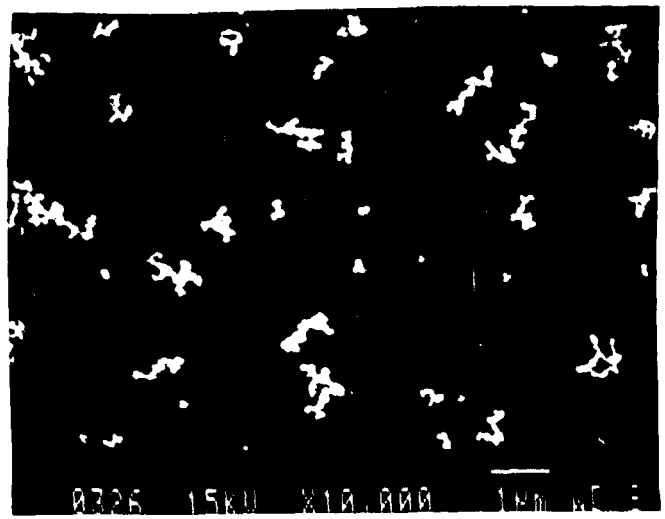

1-2P

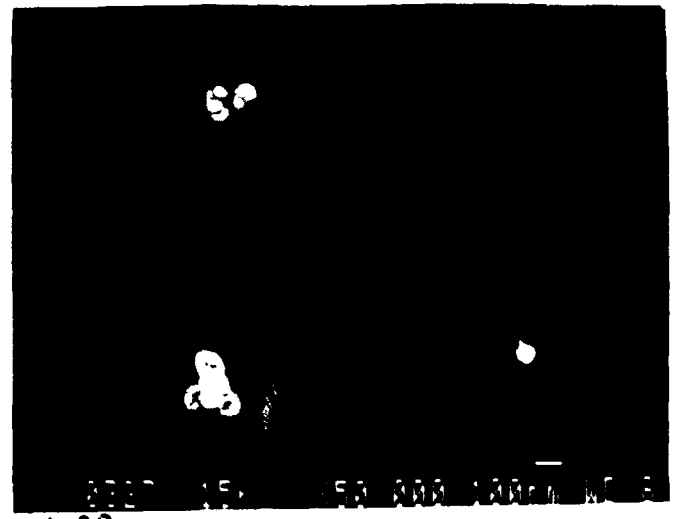

1-2P

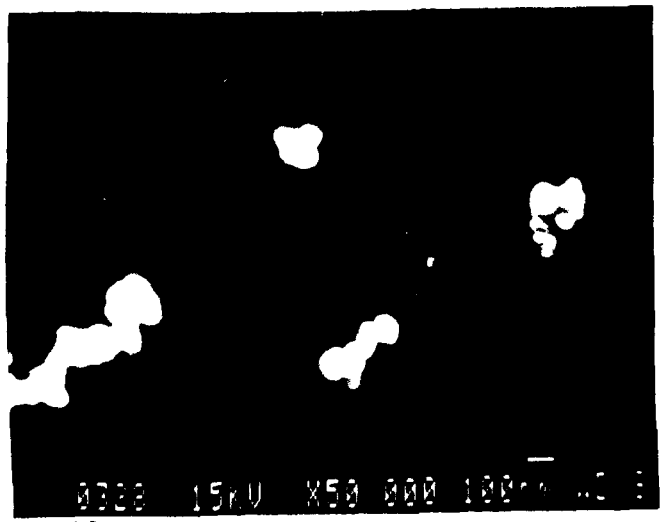

1-2P

891

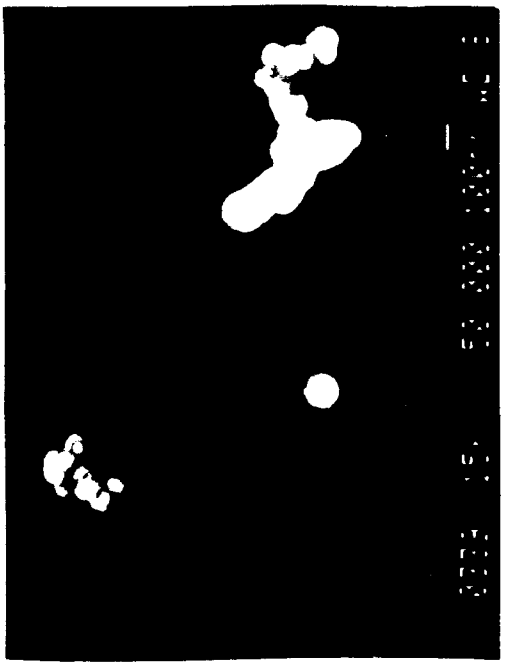

1-3B

1-3B

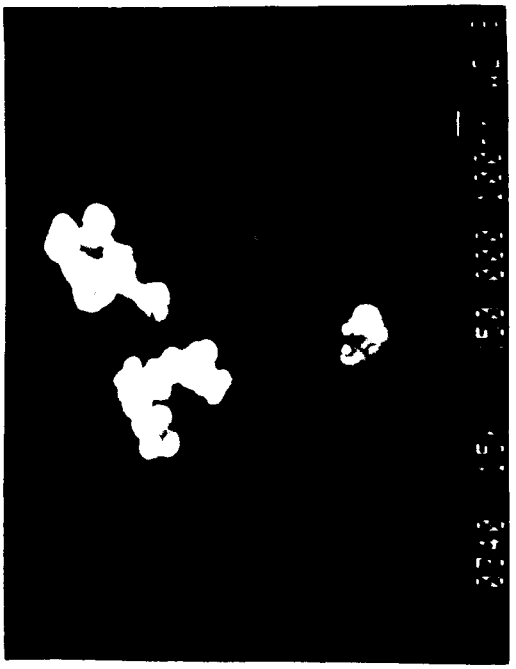

1-3B

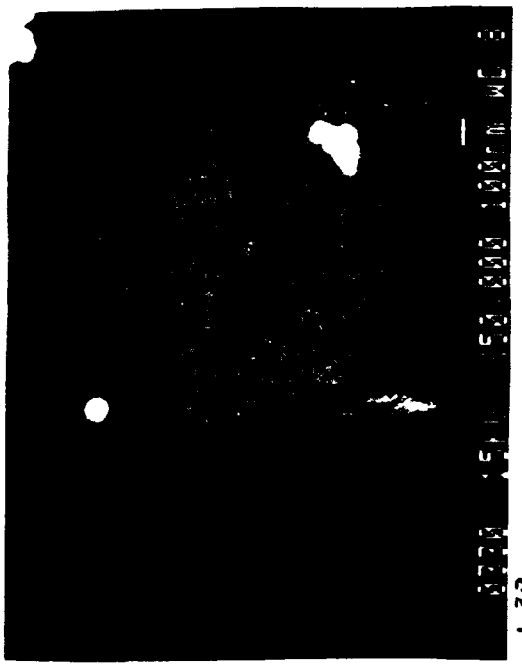

1-3P

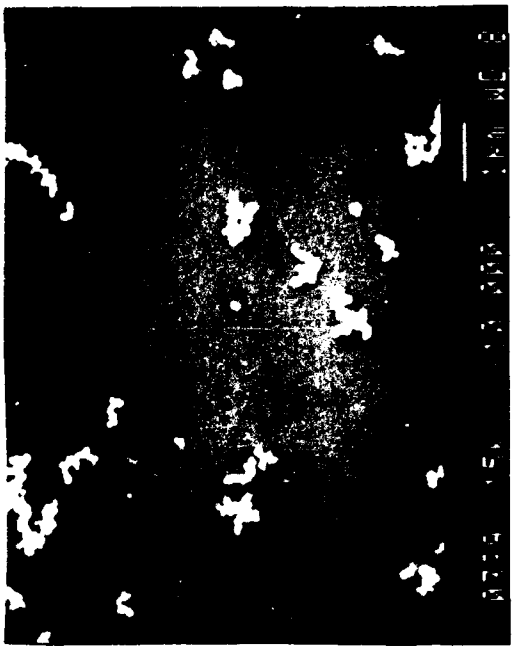

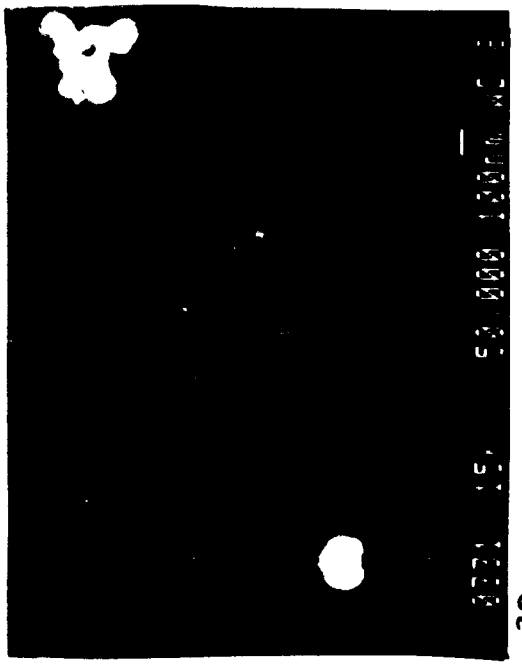

-3P

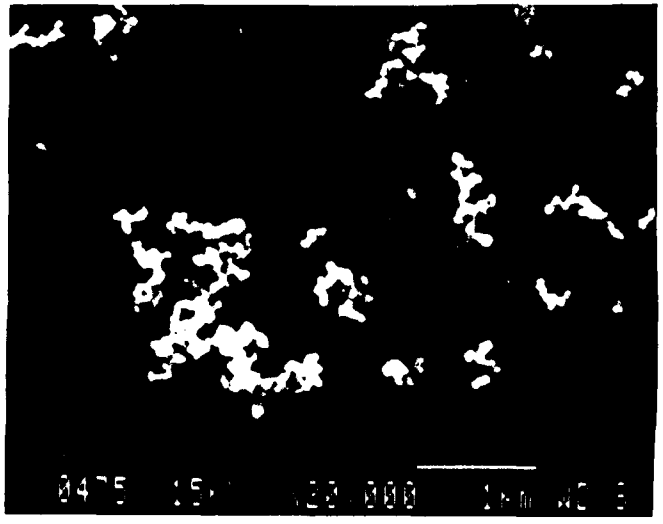

1-4B

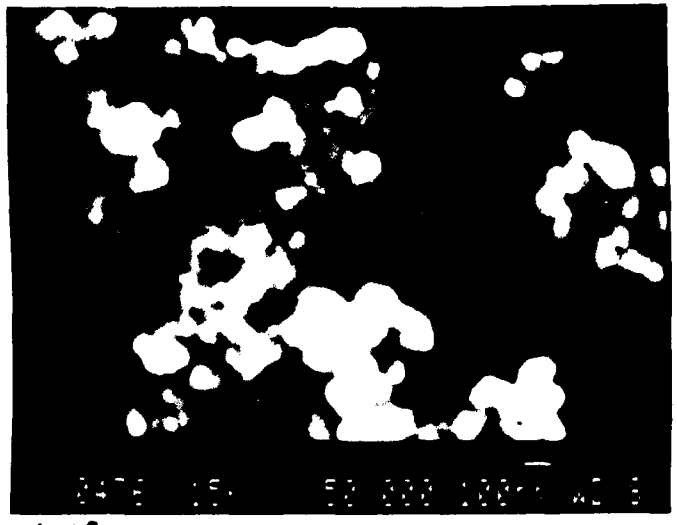

1-4B

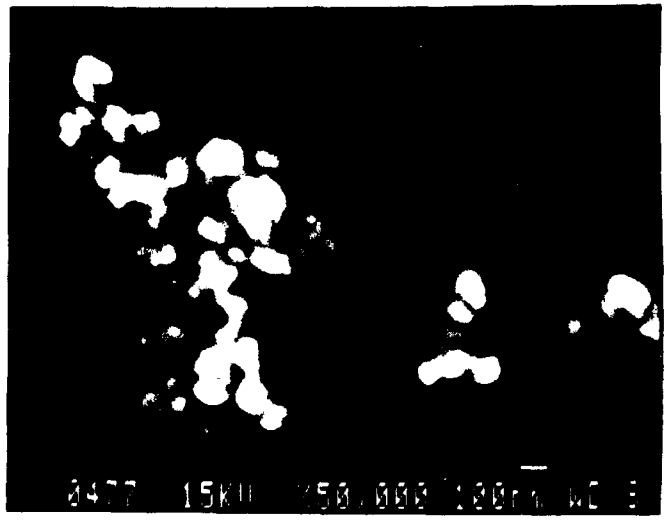

1-4B

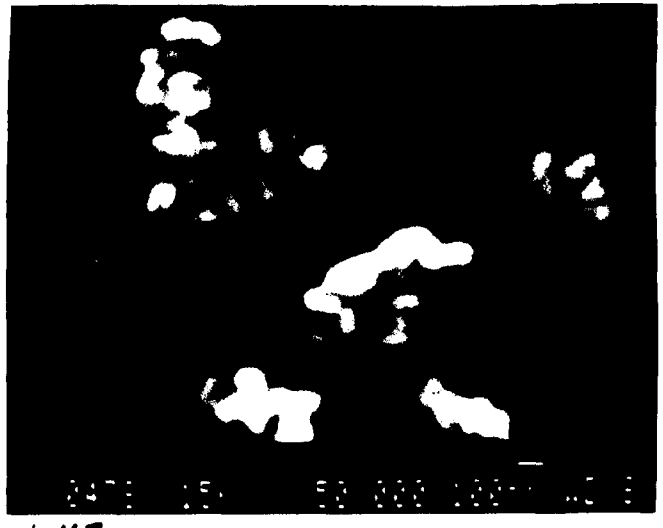

1-4B

1-4P

1-4P

1-4P

1-4P

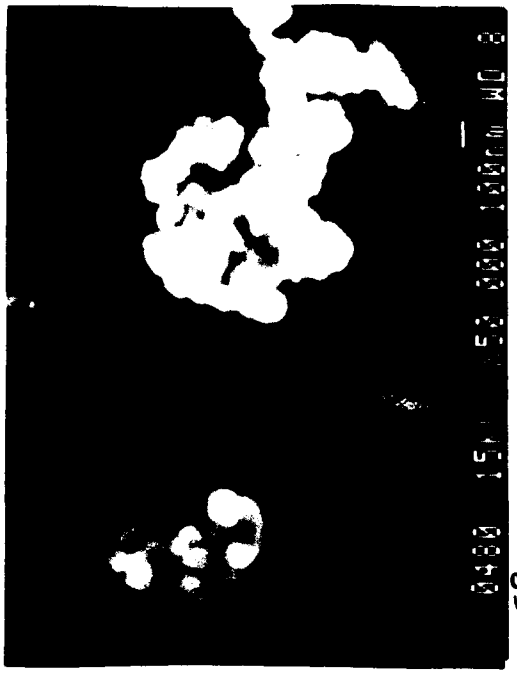

1-5B

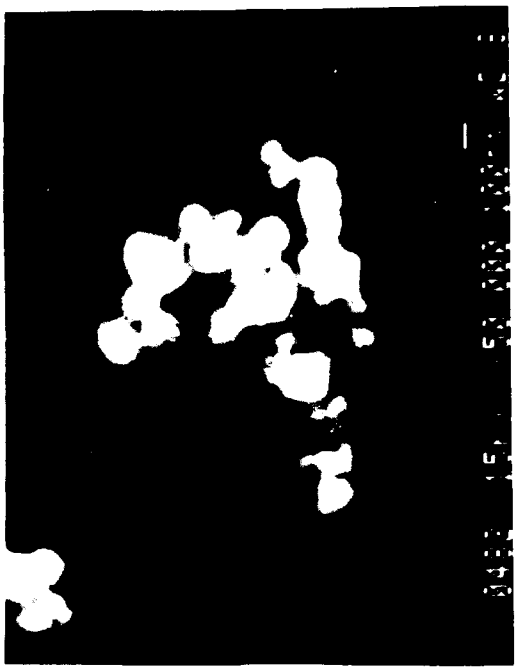

1-5B

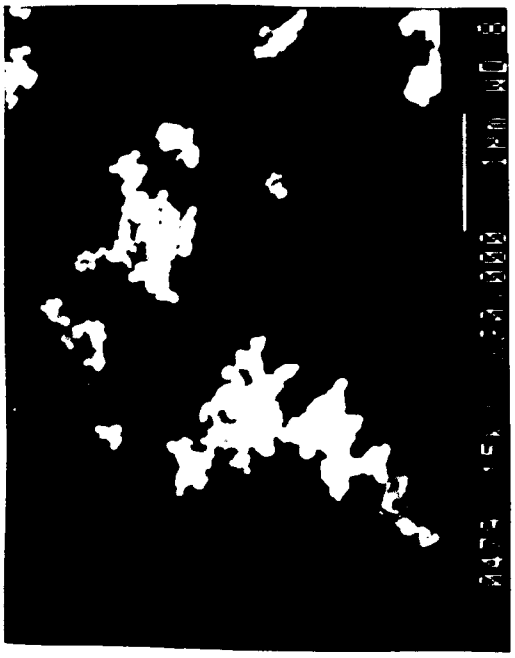

1-5B

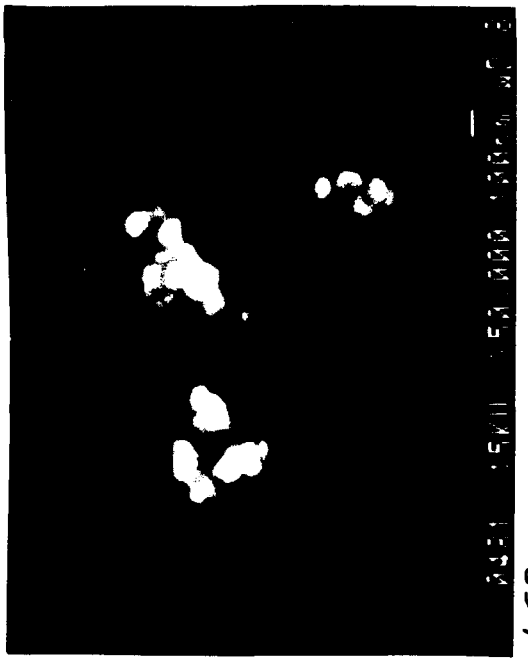

1-5B

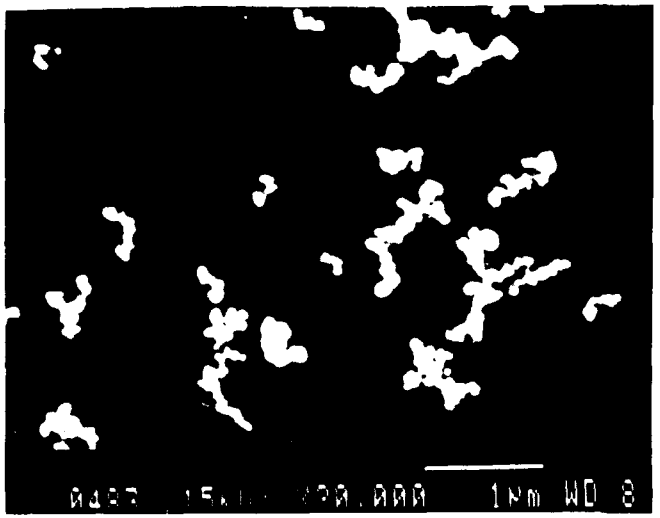

1-6B

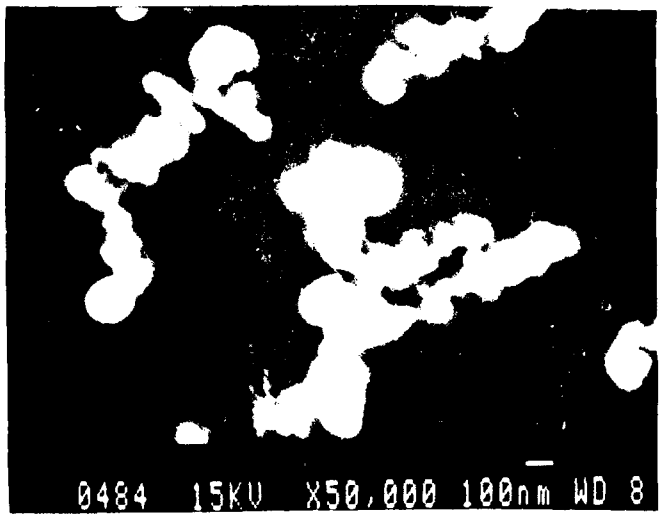

1-6B

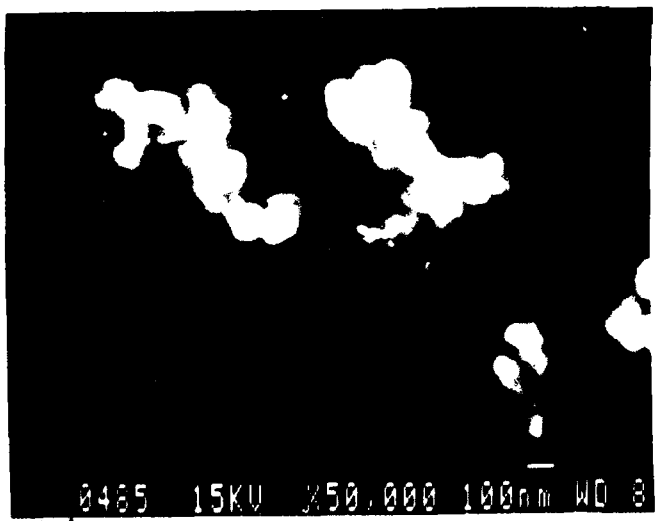

1-6B

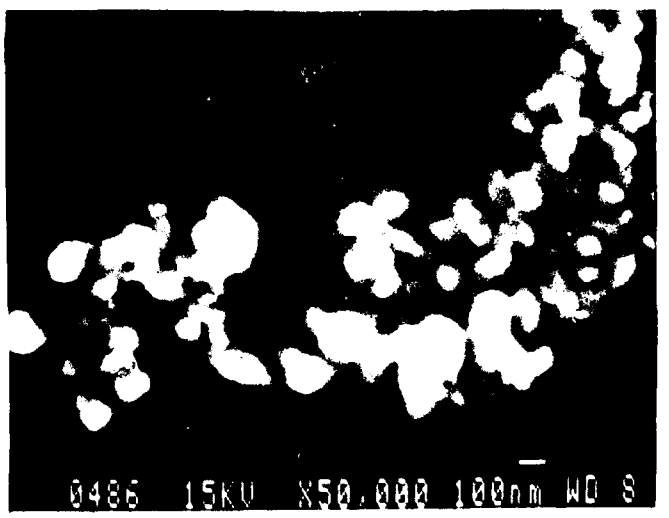

1-6B

74

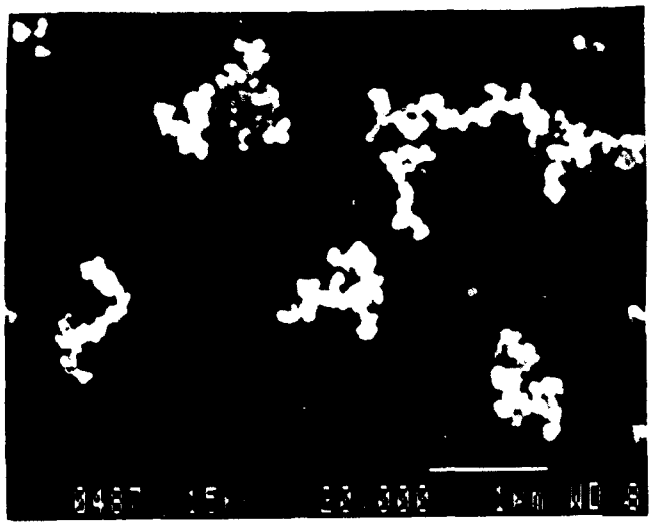

1-7B

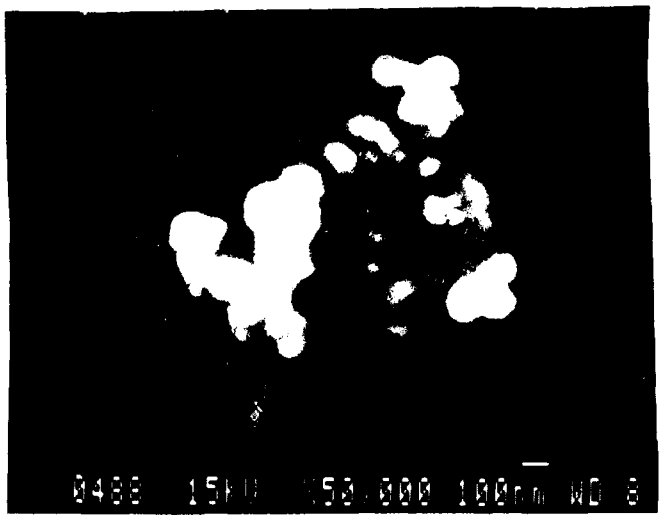

1-7B

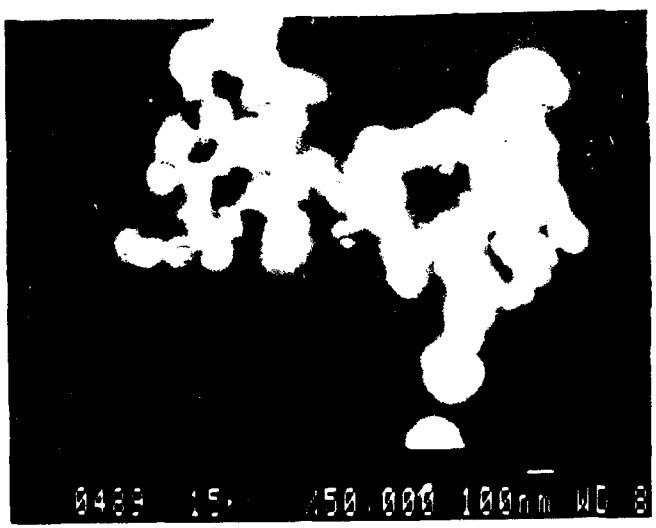

1-7B

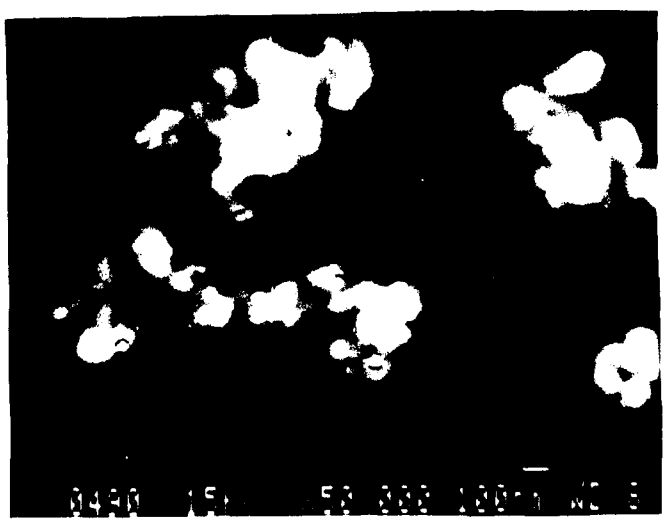

1-7B

175

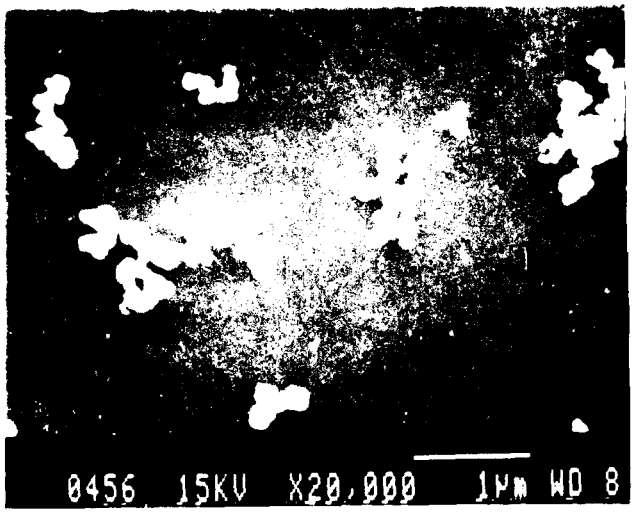

1-8B

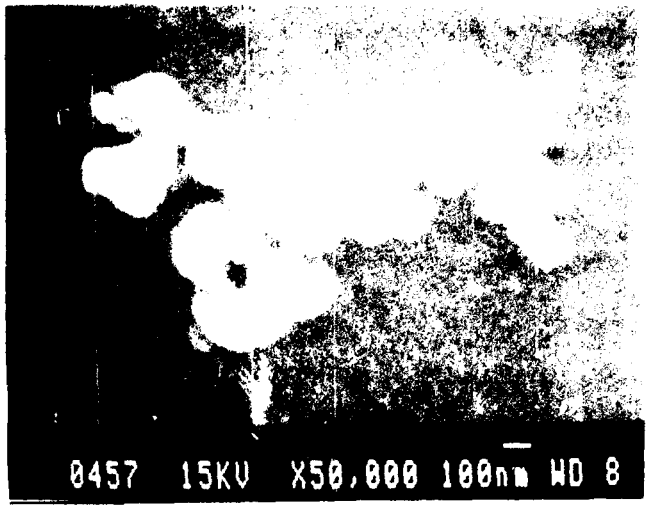

1-8B

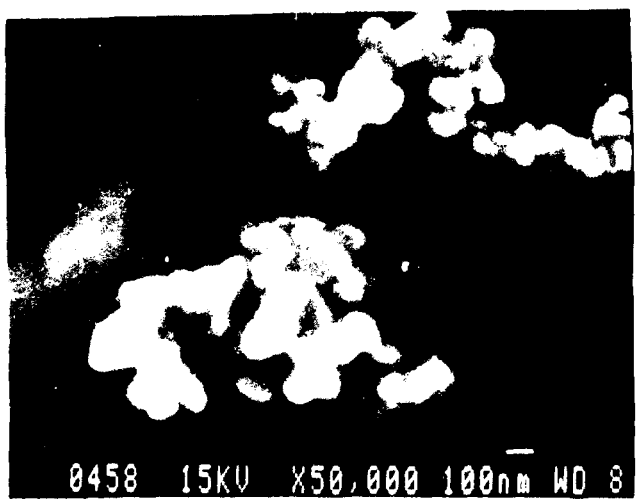

1-8B

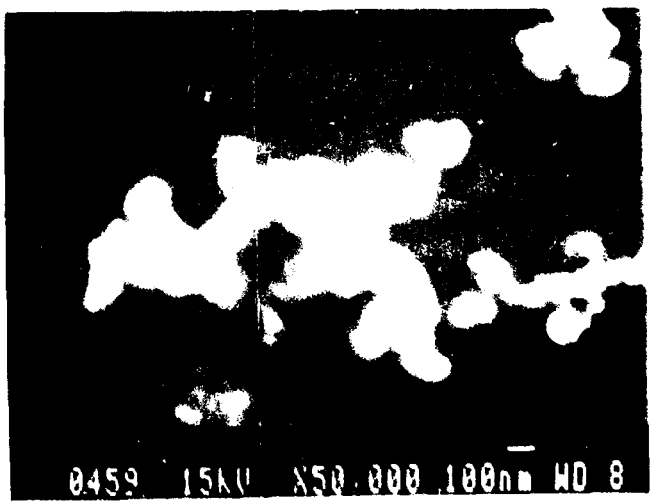

1-8B

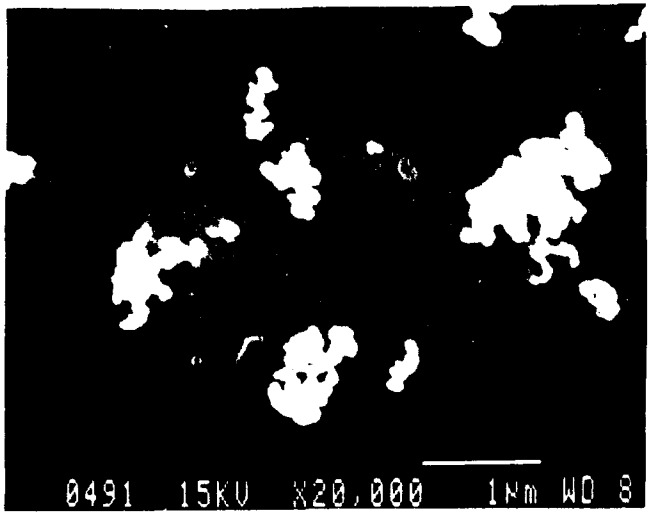

1-8B

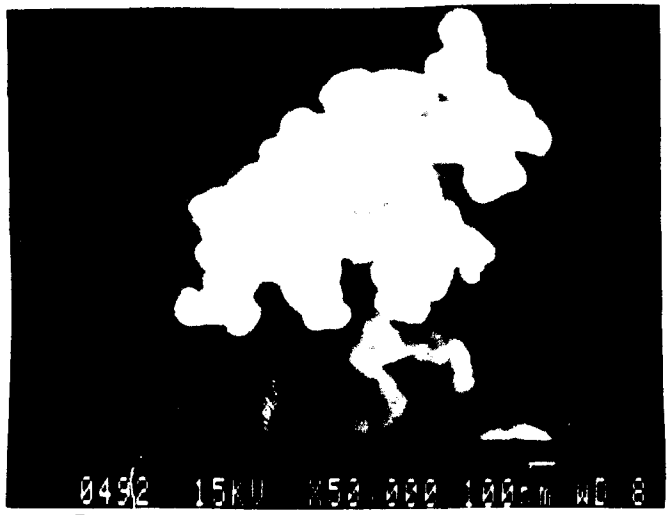

1-8B

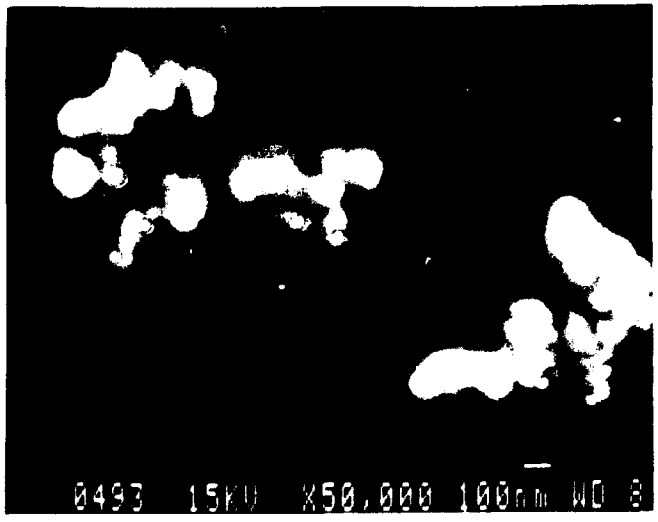

1-8B

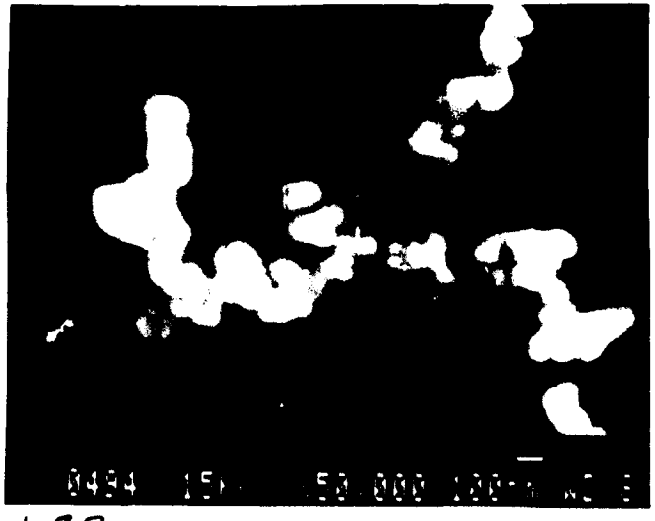

1-8B

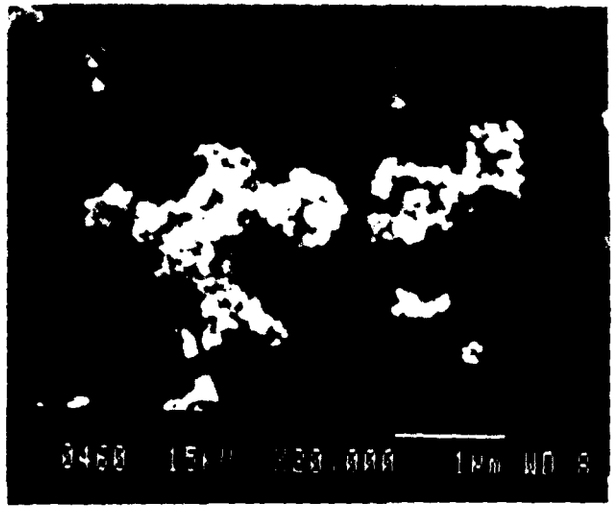

1-8P

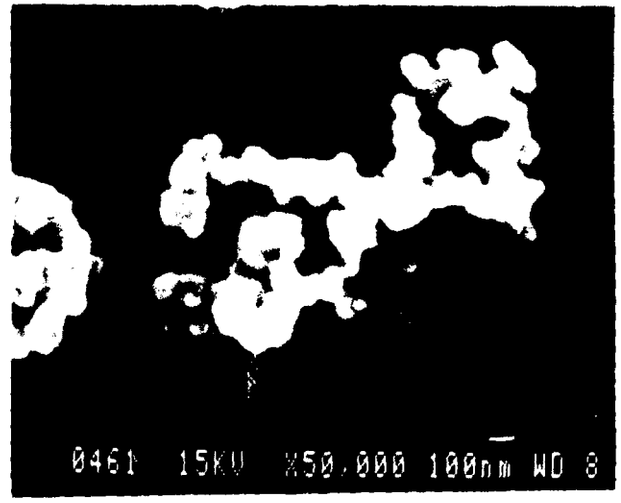

1-8P

841

1-8P

1-8P

1-8P

1-8P

1-8P

1-8P

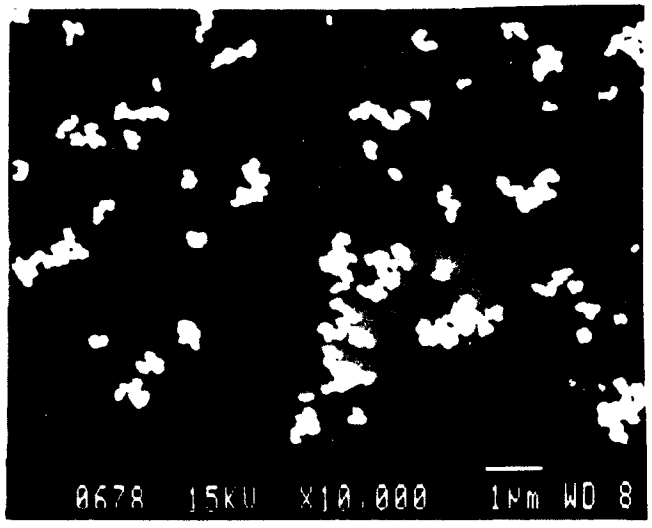

1-78

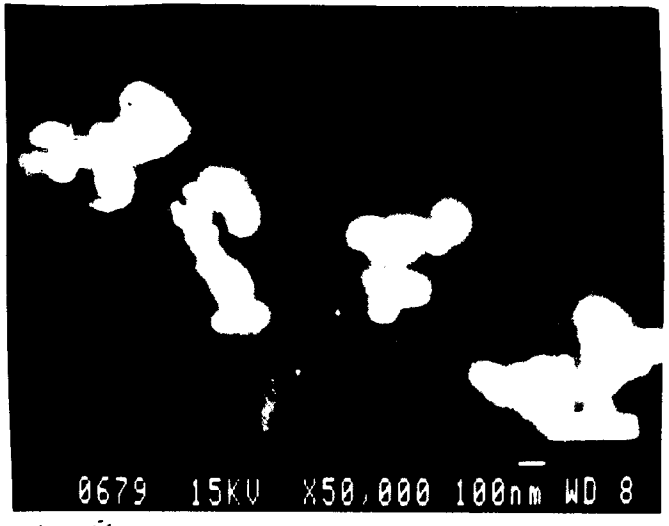

1-78

081

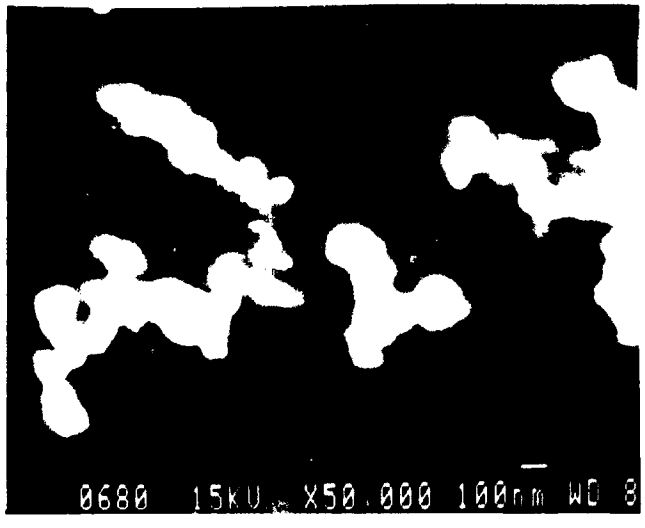

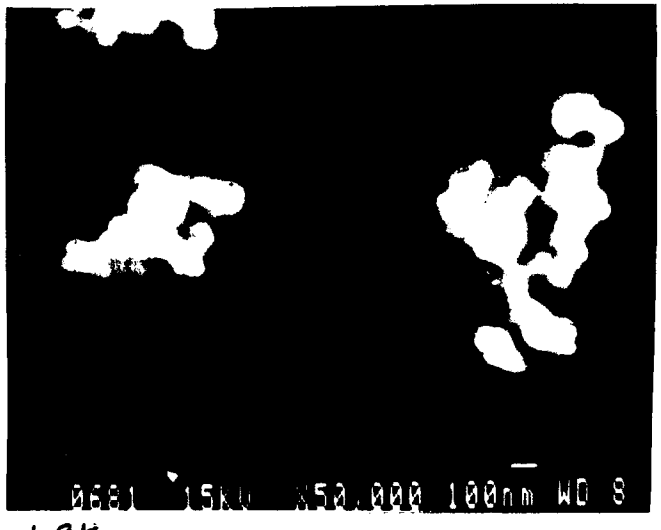

1-96

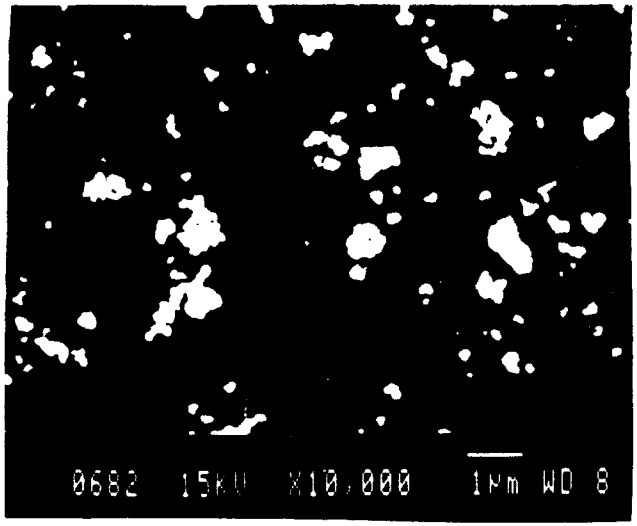

1-10B

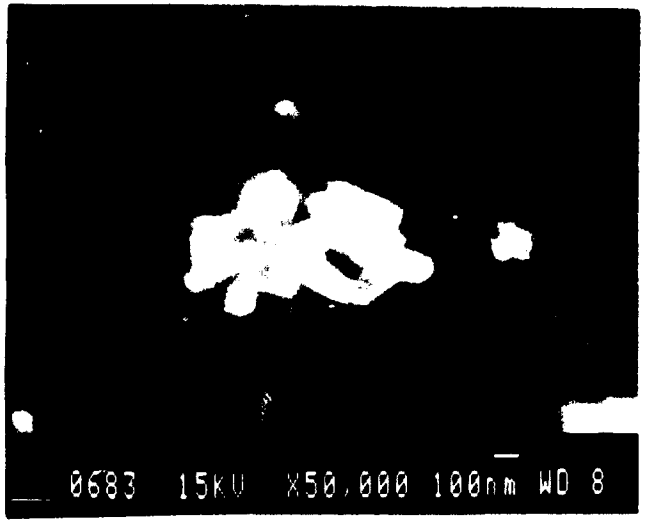

1-10B

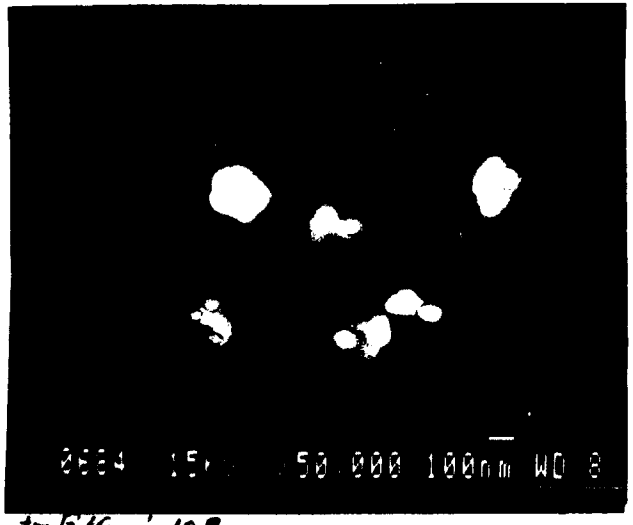

1-10C 1-10B

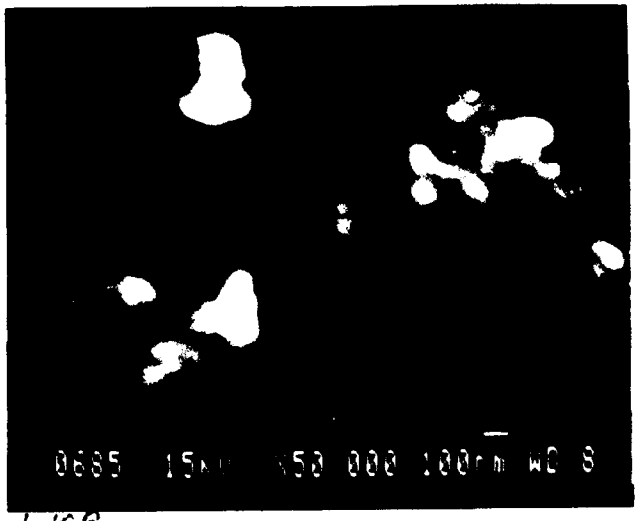

1-10B

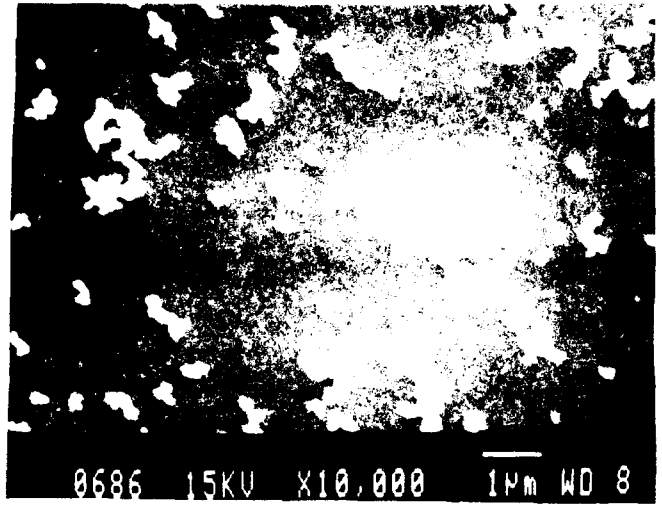

I-11B

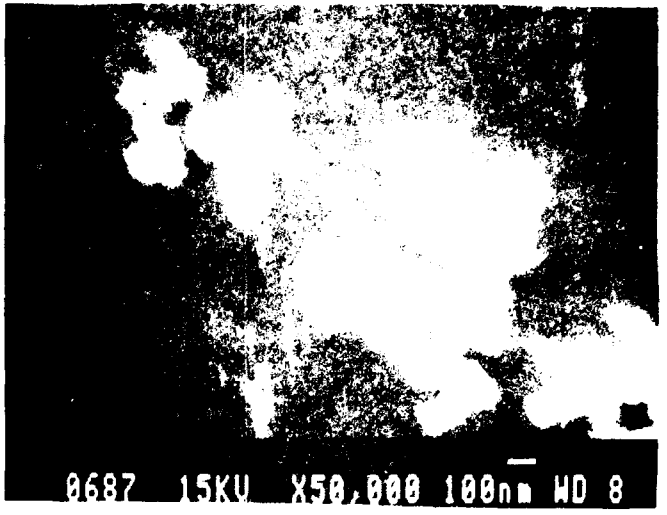

I-11 B

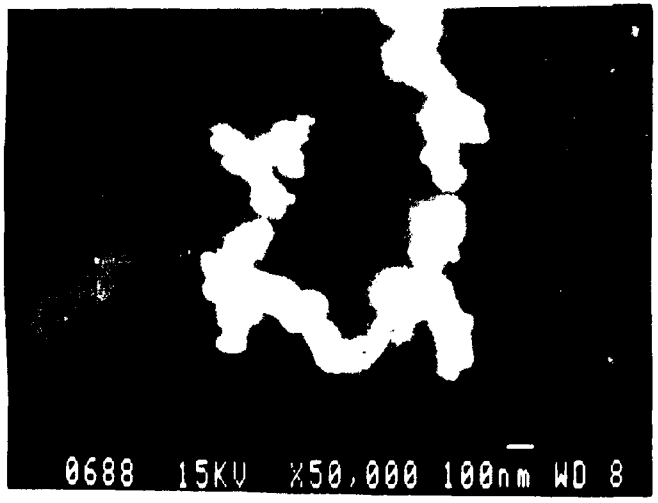

I-11 B

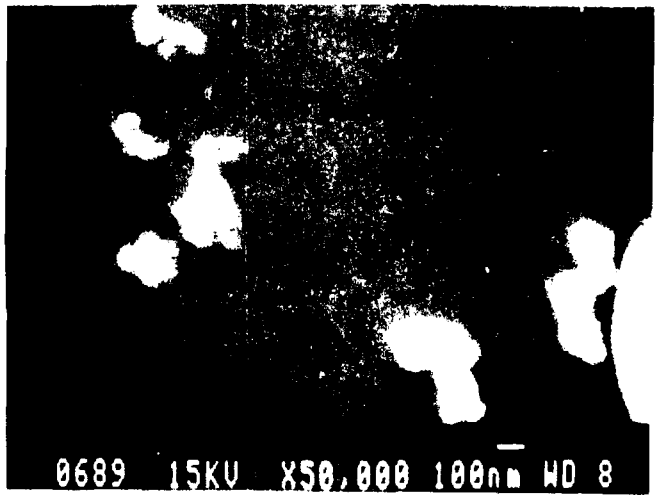

I-11 B

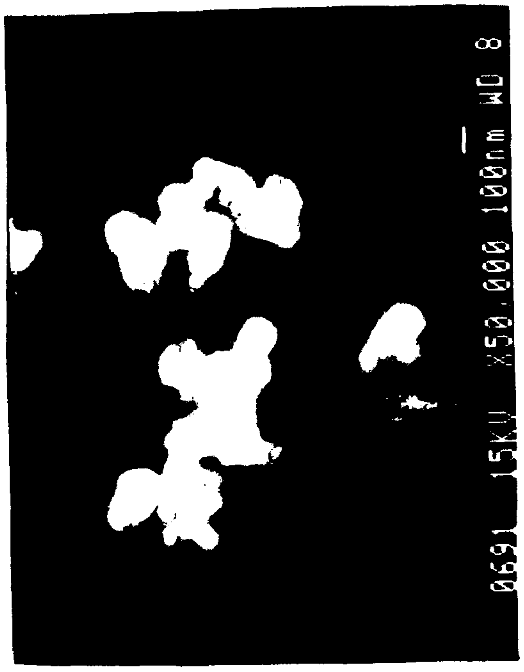
0691 15KV X50,000 100nm WD 8
2-1B

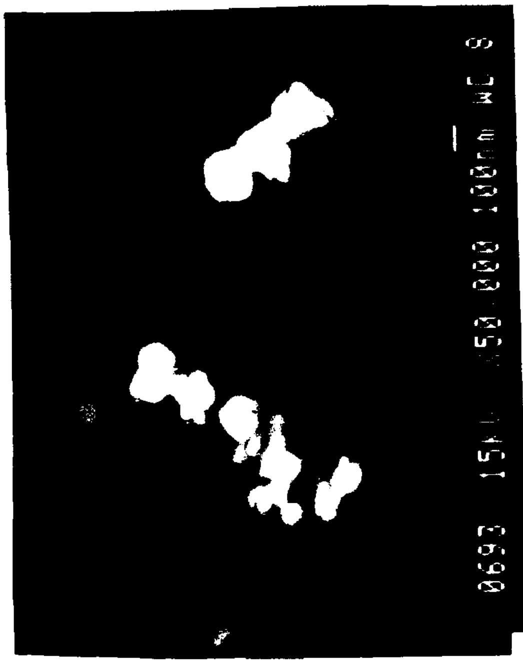
0693 100nm WD 8

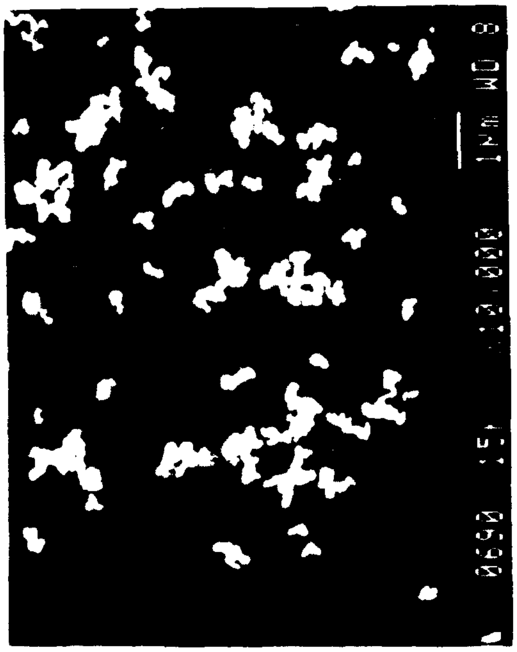
0690 1µm WD 8

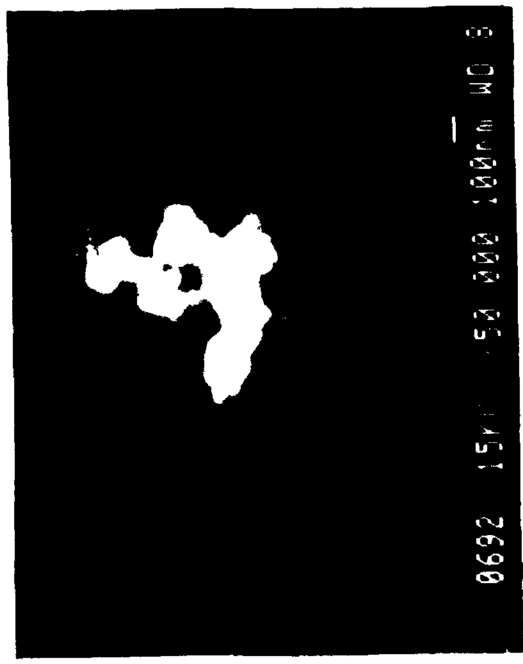
0692 100nm WD 8

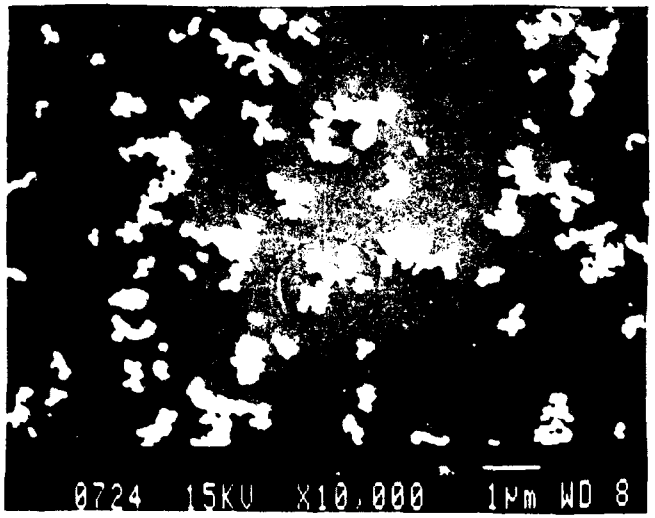

2-1P

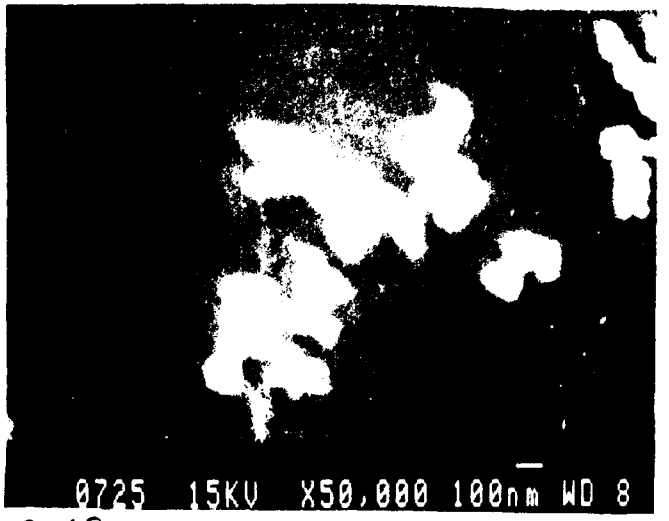

2-1P

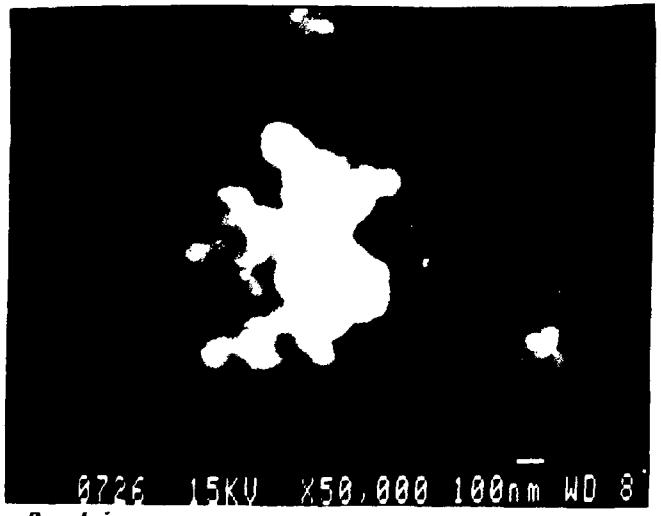

2-1P

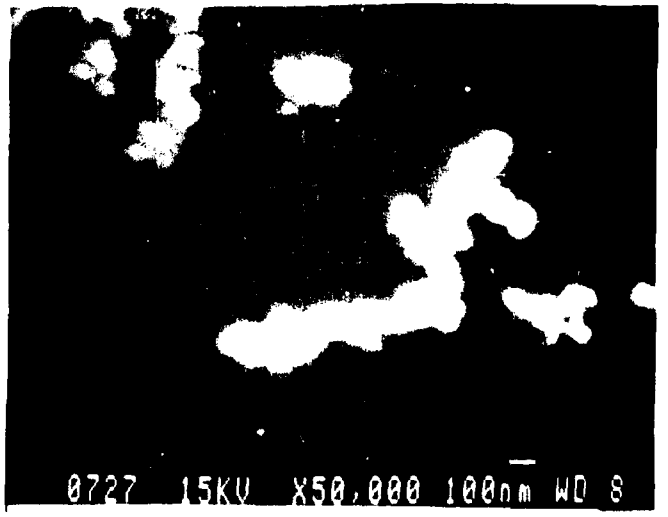

2-1P

481

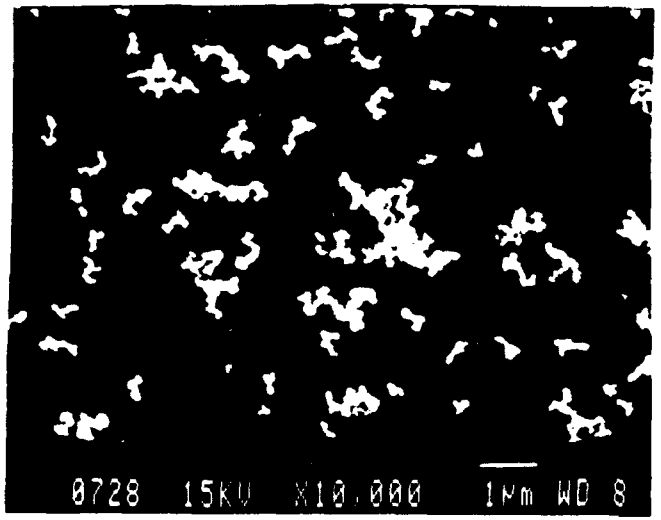

2-26

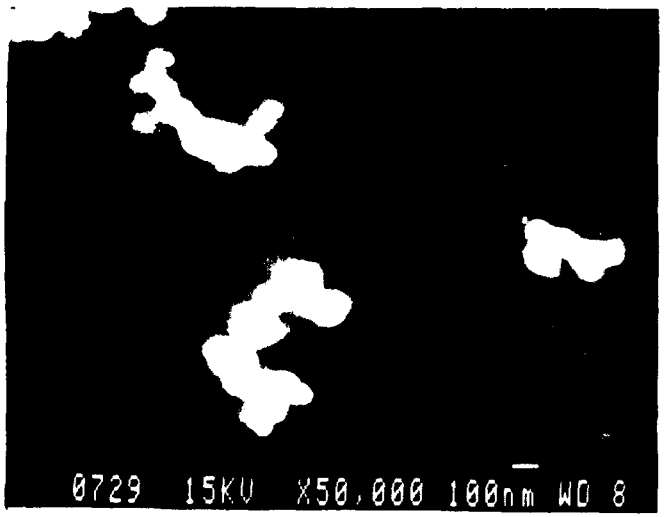

2-26

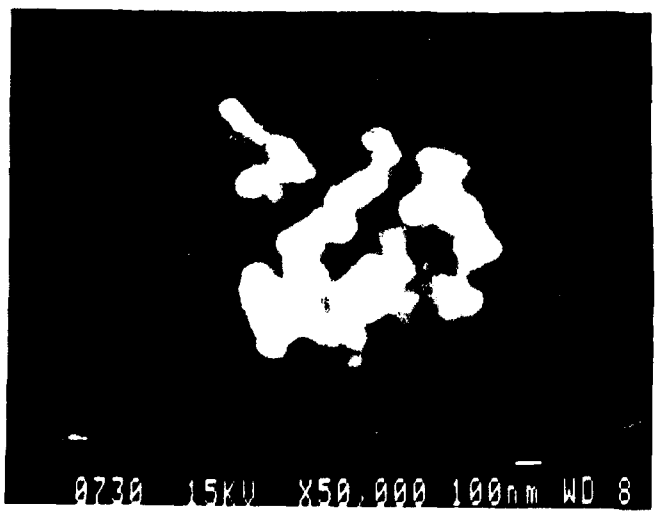

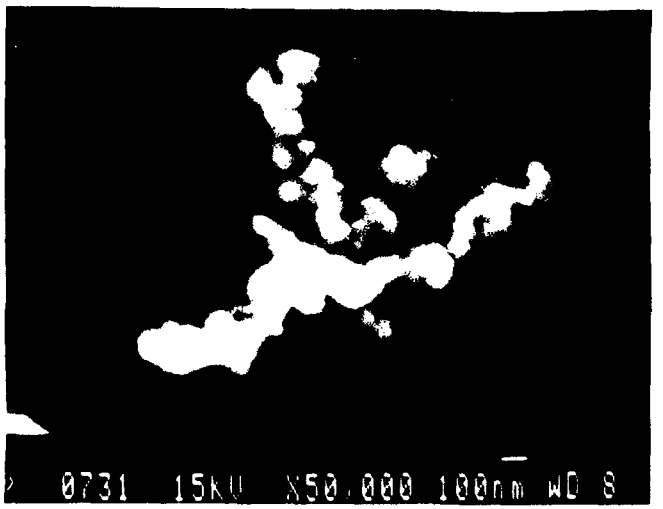

2-28

581

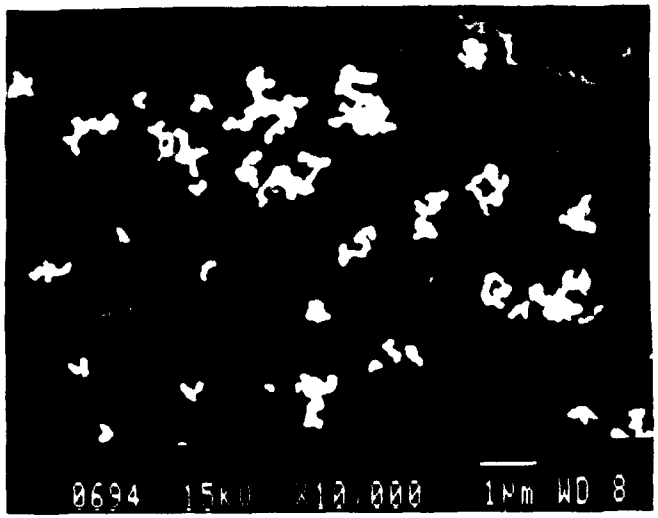

2-2B

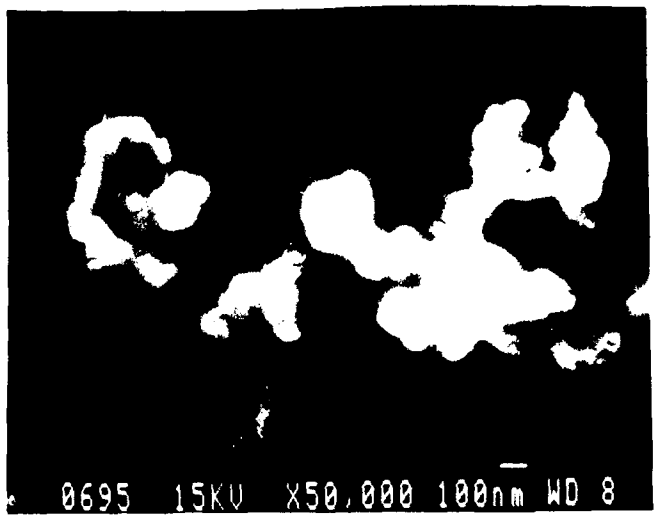

2-3B

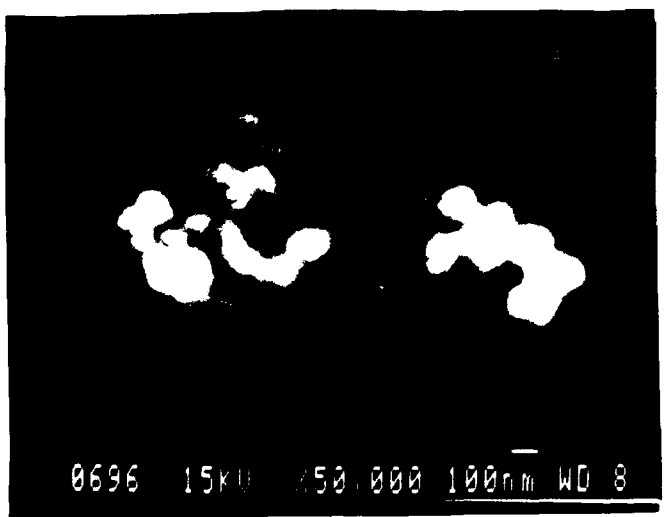

2-3B

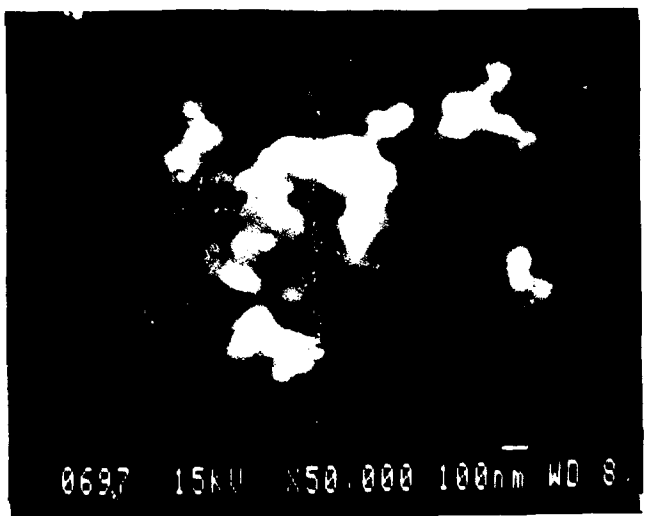

2-3B

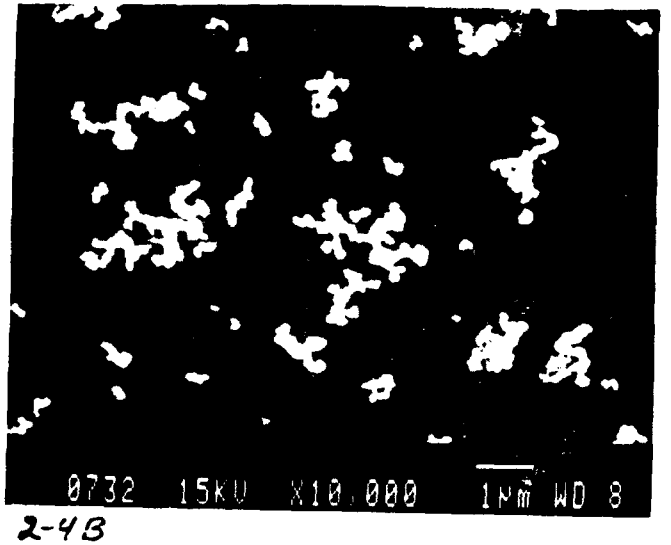

2-4B

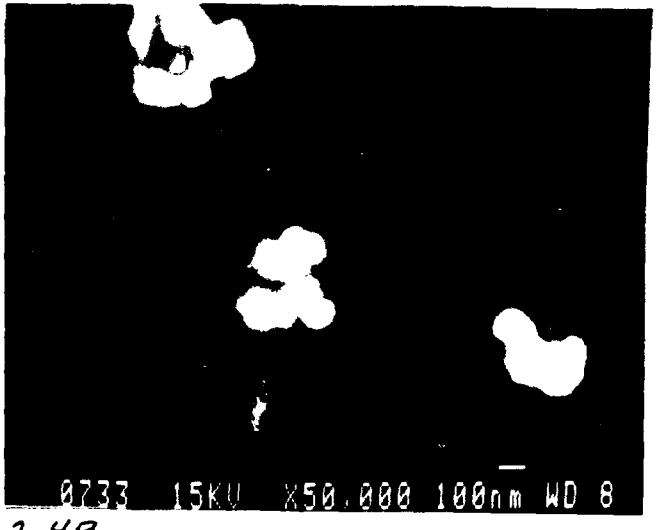

2-4B

481

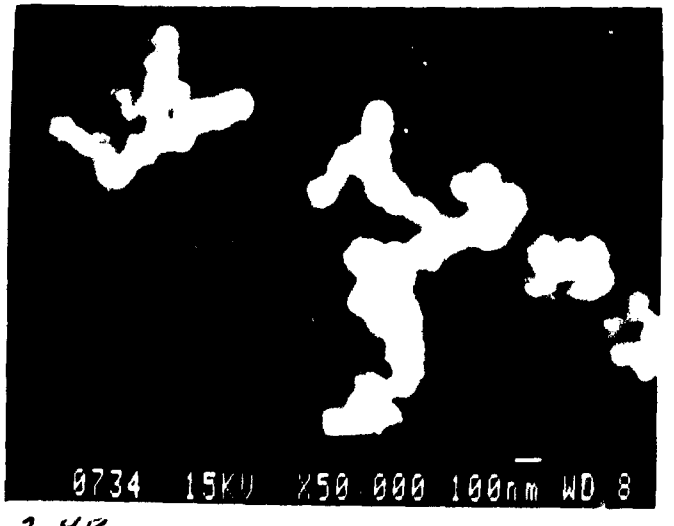

2-4B

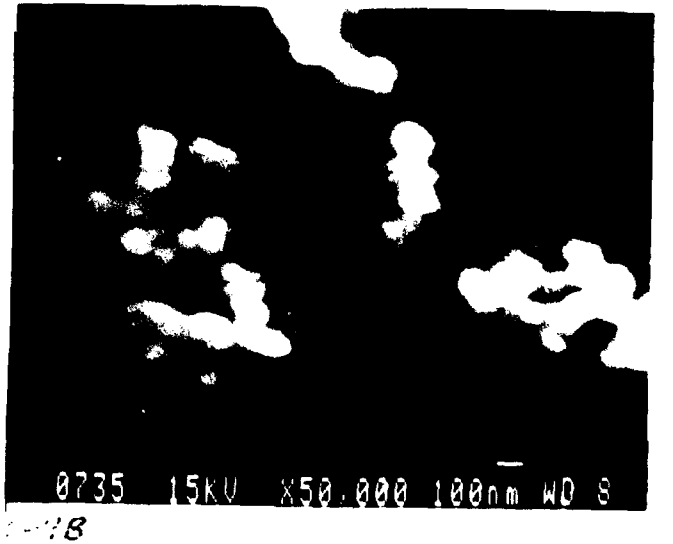

2-4B

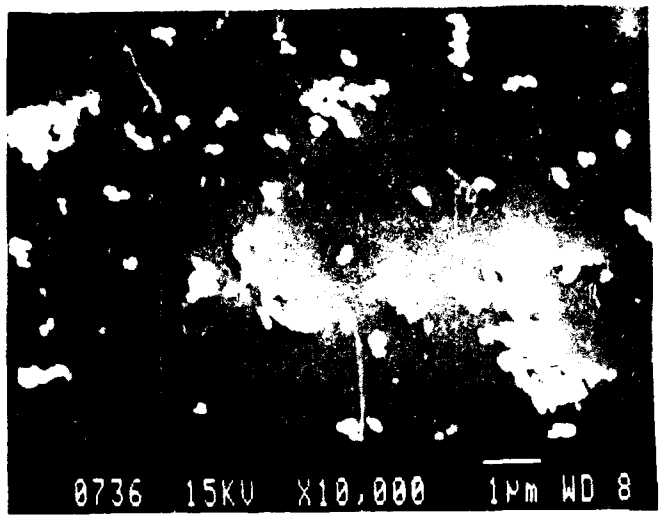
0736 15KV X10,000 1µm WD 8

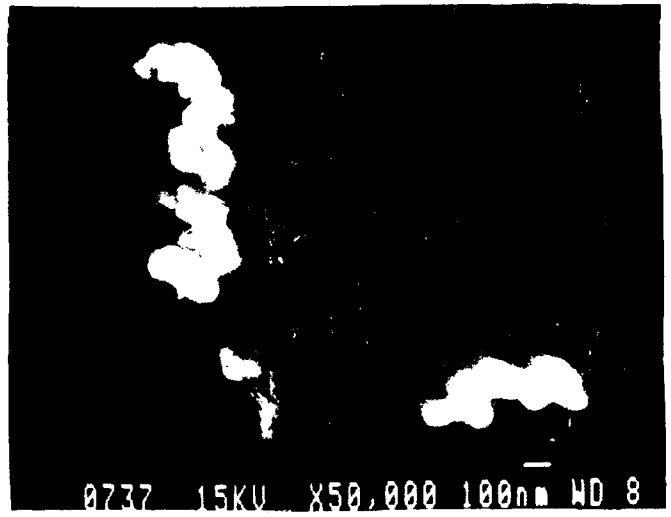
0737 15KV X50,000 100nm WD 8

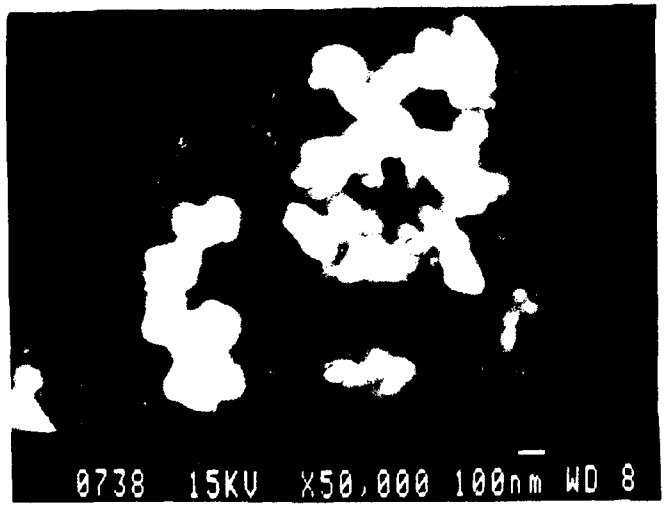
0738 15KV X50,000 100nm WD 8

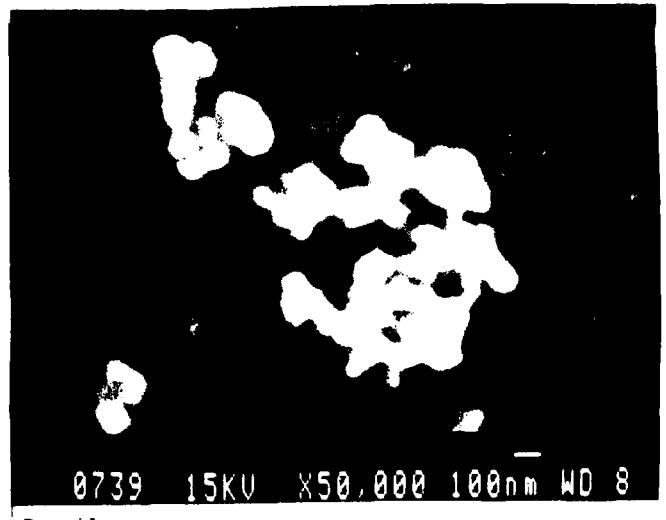
0739 15KV X50,000 100nm WD 8

881

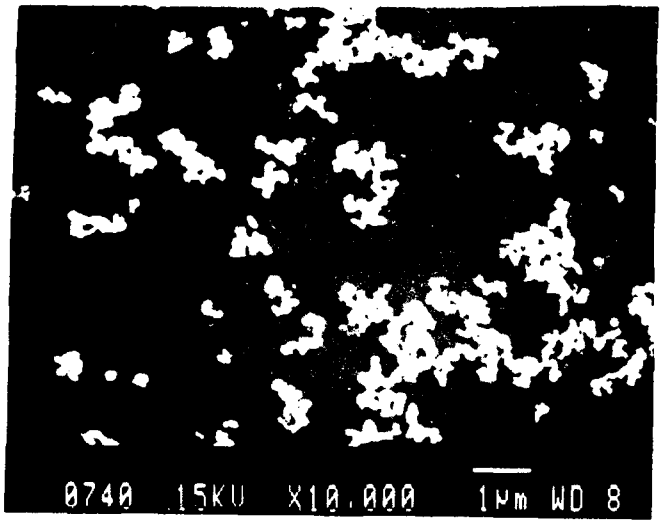

2-5P

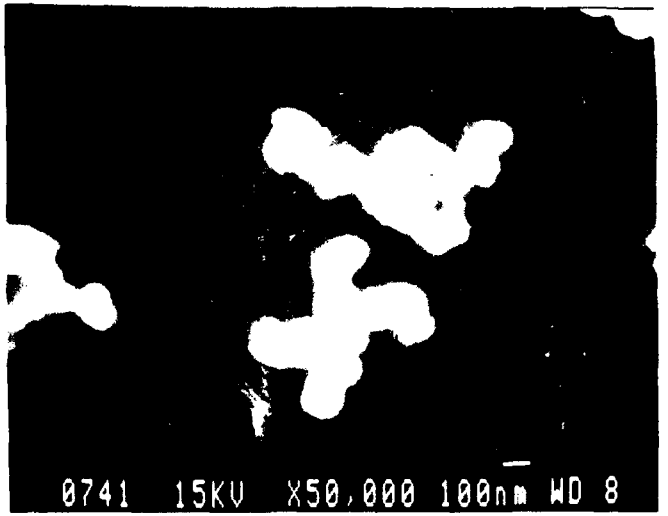

2-5P

681

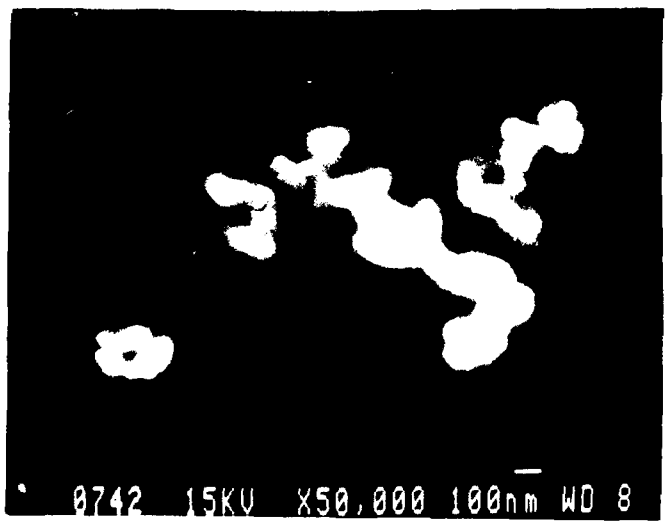

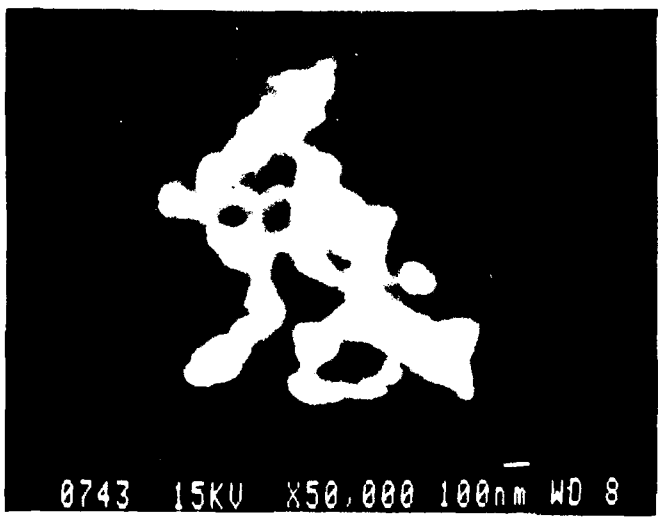

2-5P

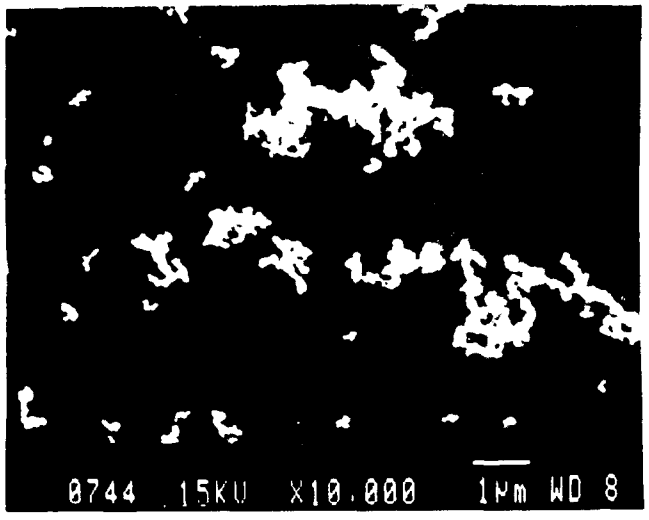

2-6B

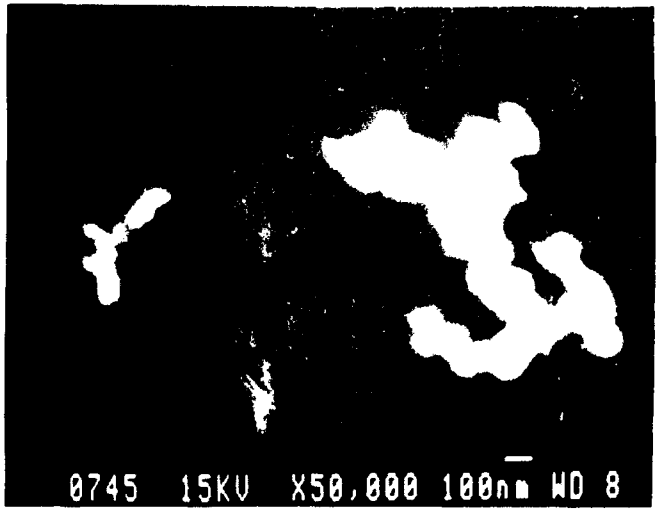

2-6B

061

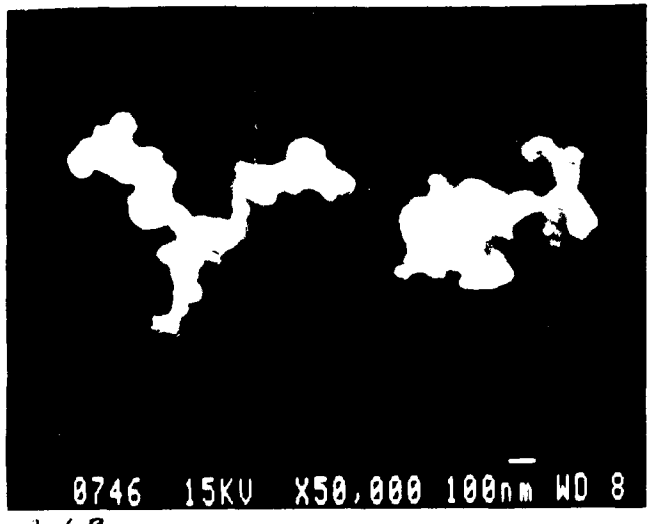

2-6B

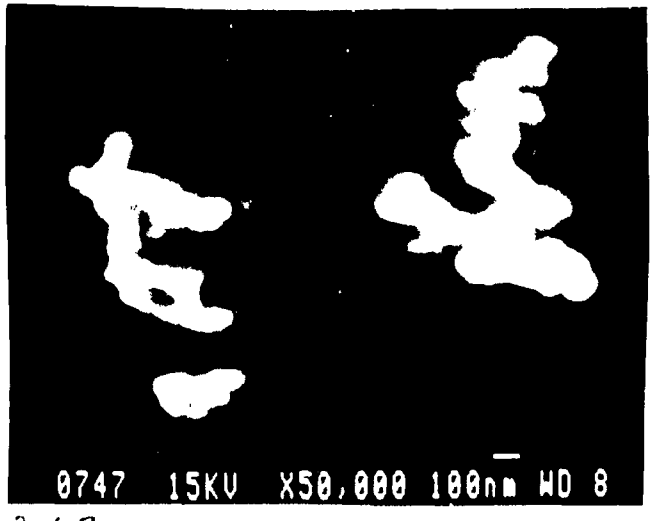

2-6B

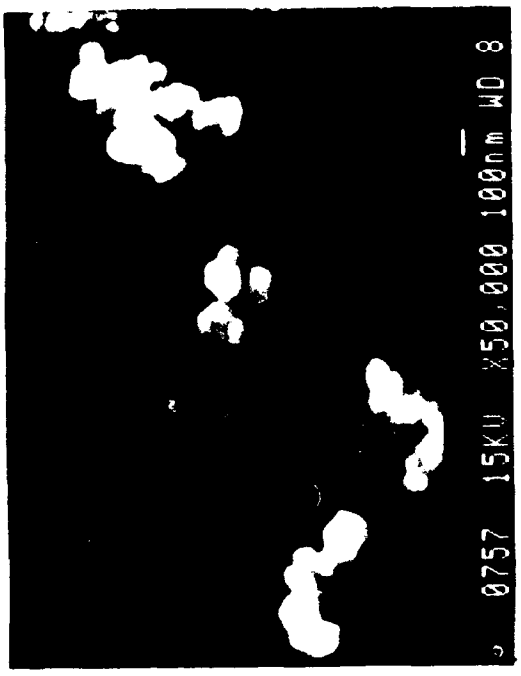
0757 15KV X50,000 100nm WD 8

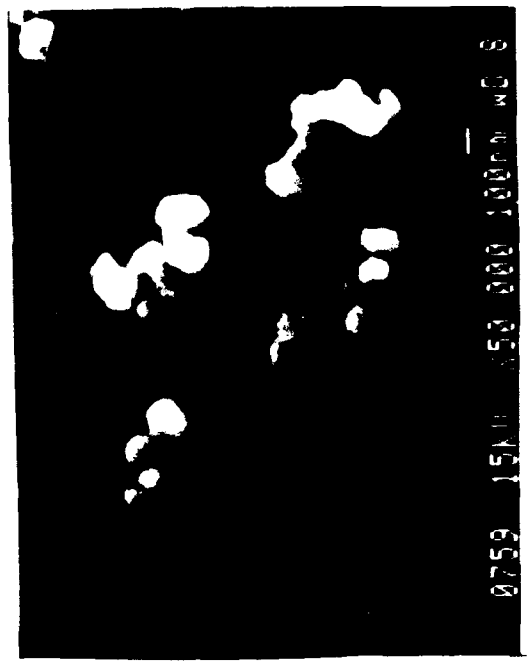
0759 15KV X50,000 100nm WD 8

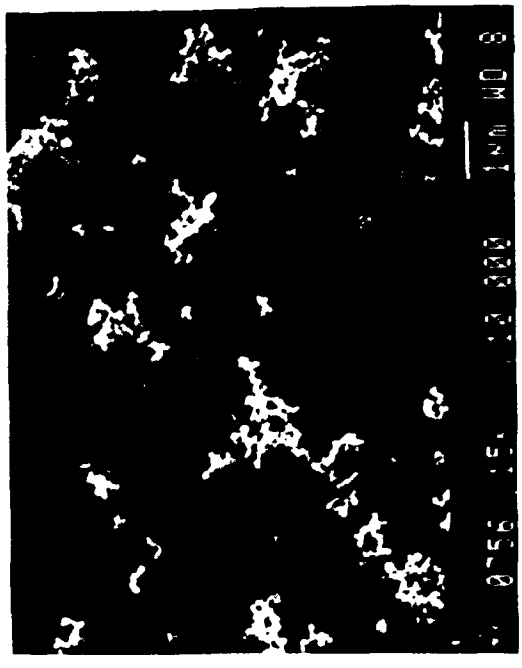
0756 15KV X50,000 100nm WD 8

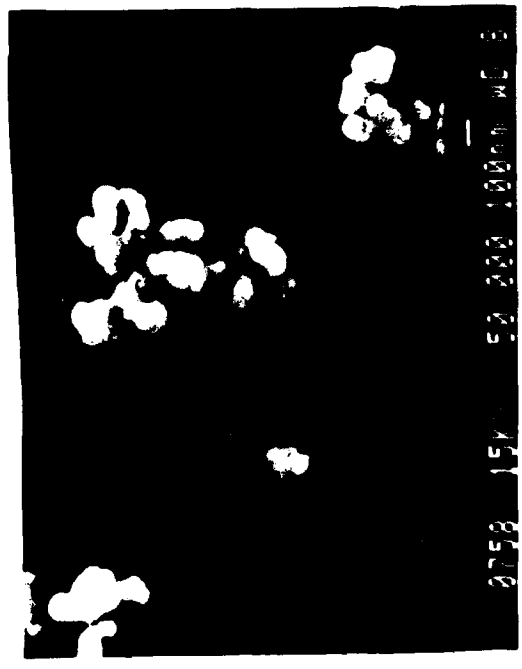
0758 15KV X50,000 100nm WD 8

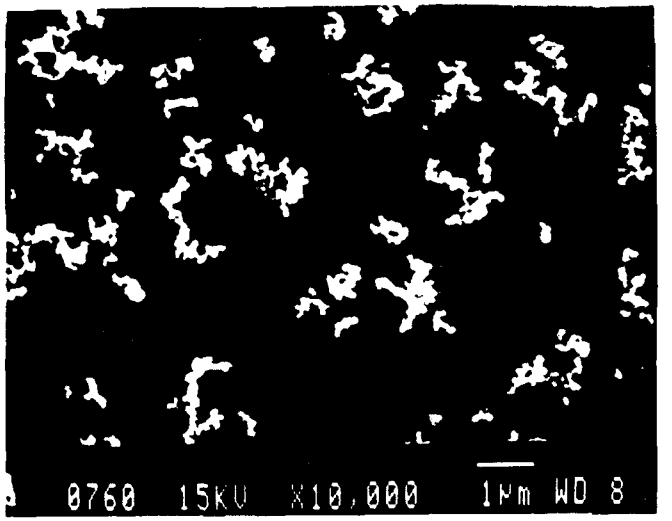

2-8A

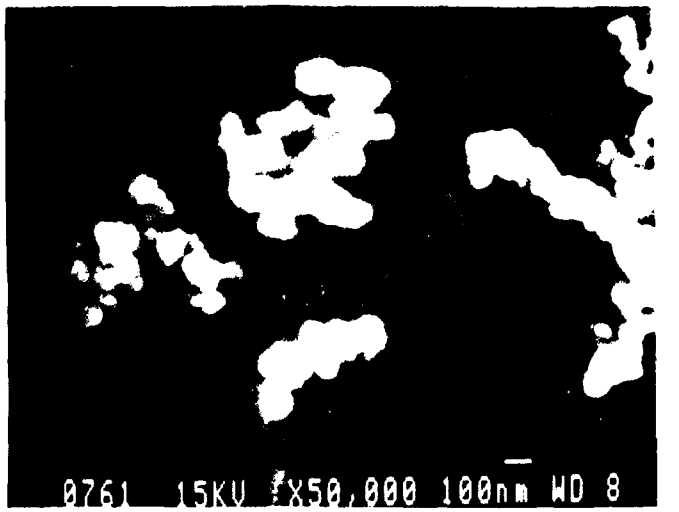

2-8B

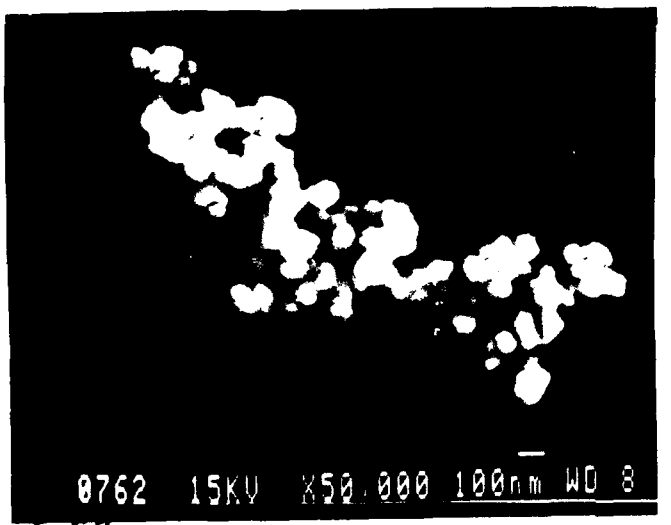

2-8B

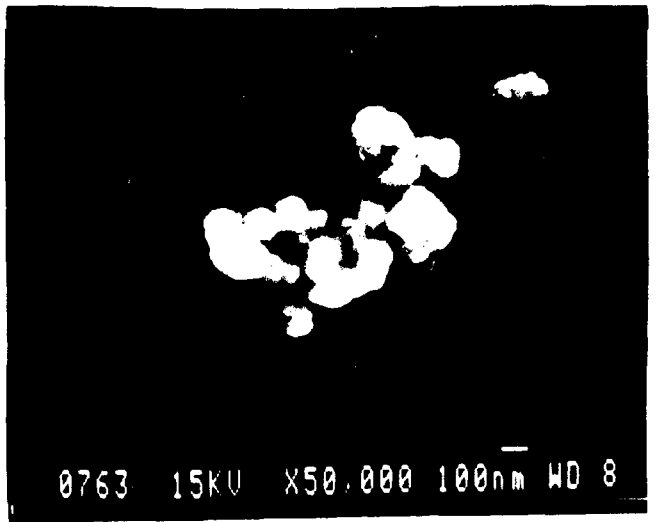

2-8B

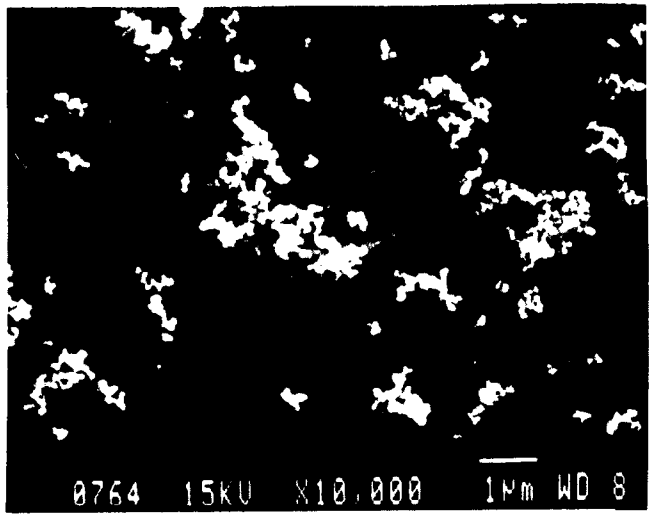

2-98

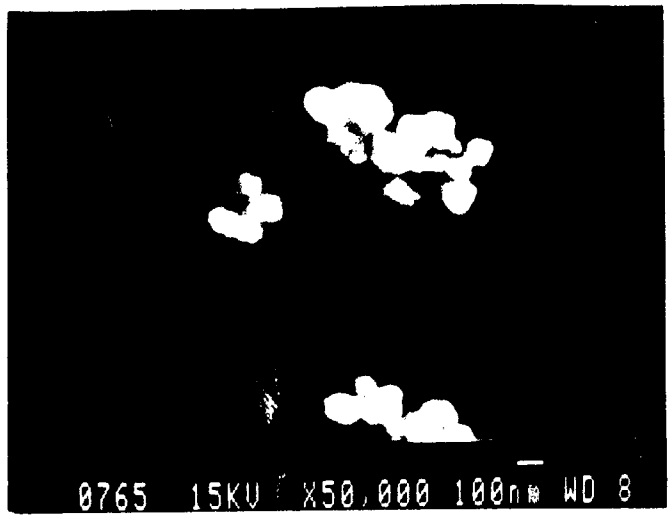

2-98

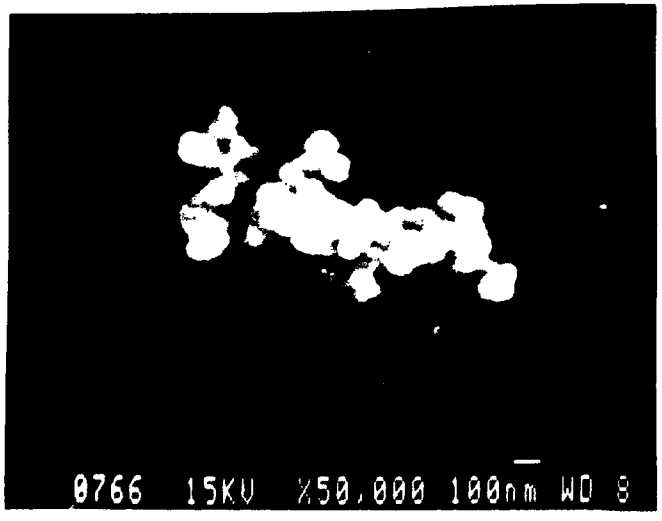

2-98

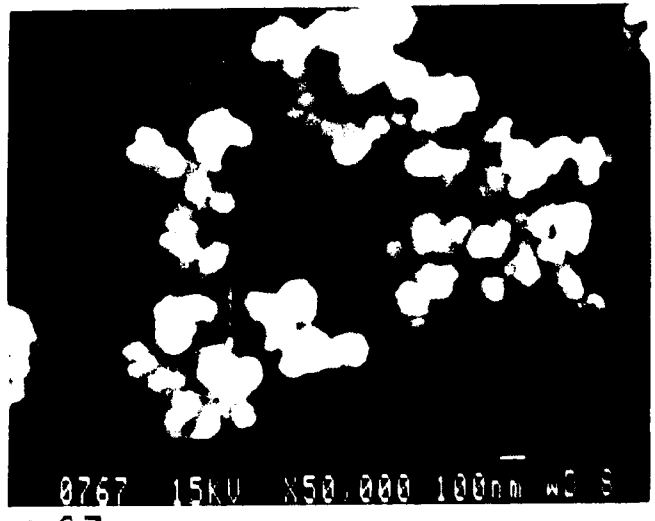

2-98

193

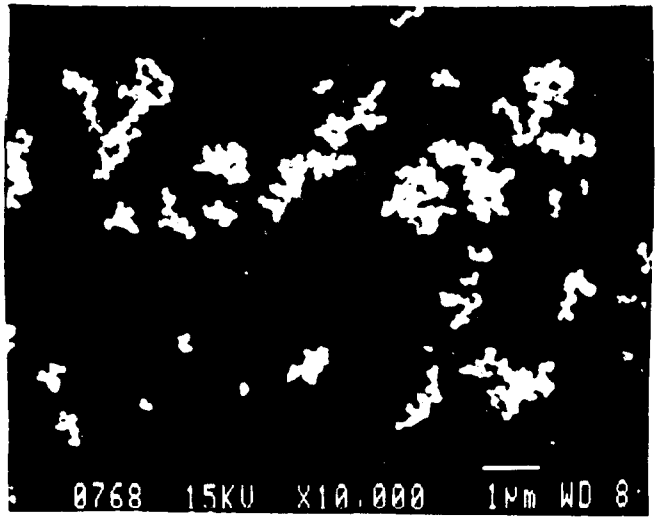

2-9P

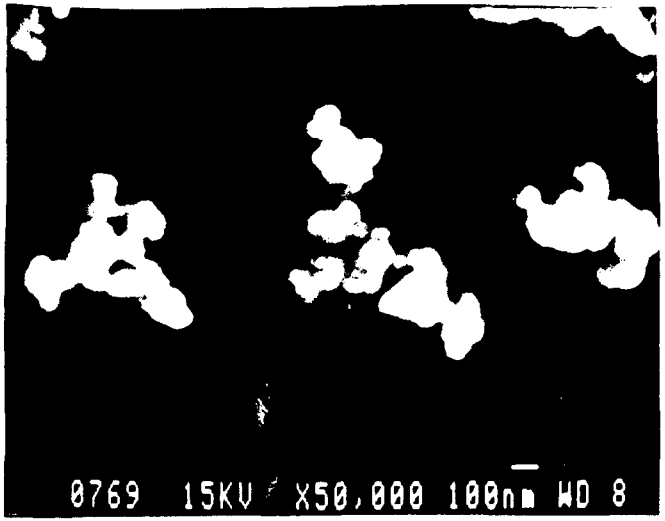

2-9P

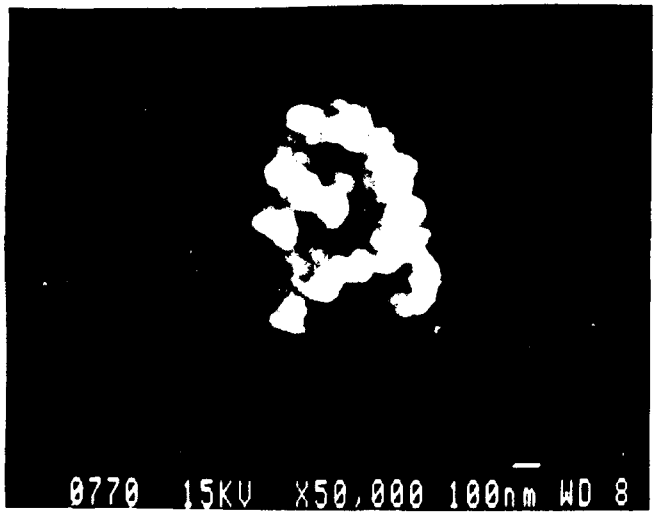

2-9P

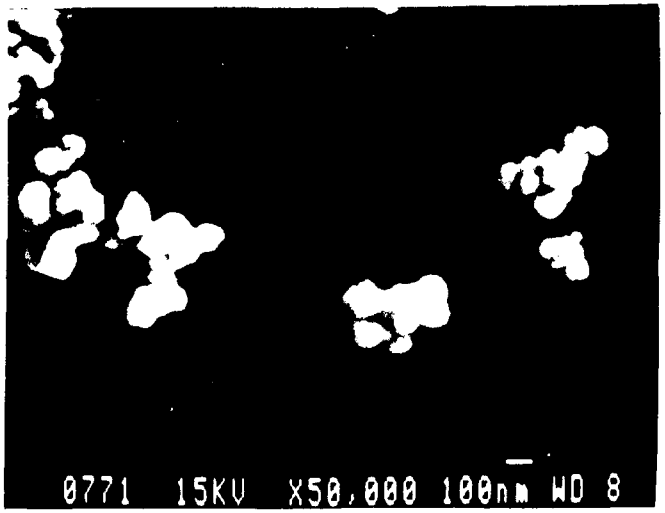

2-9P

461

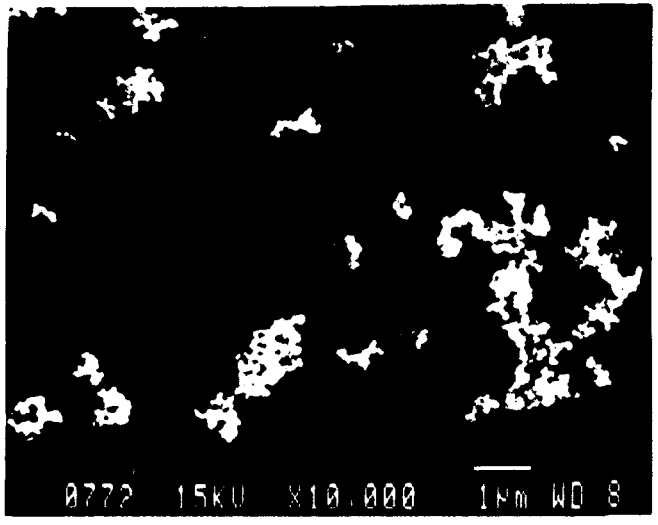

2-19B

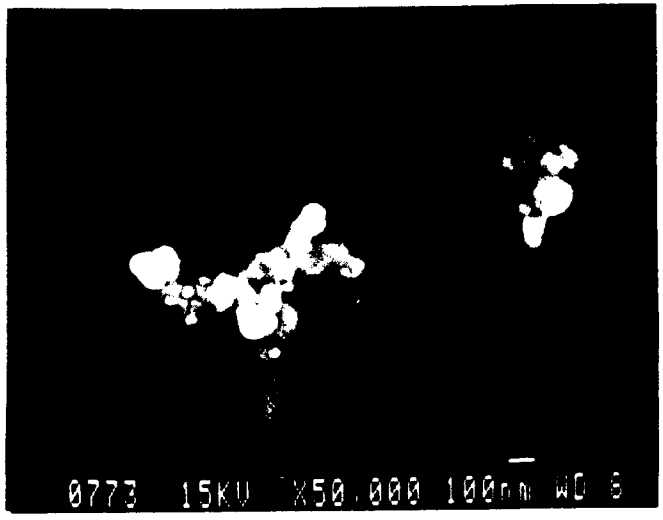

2-20B

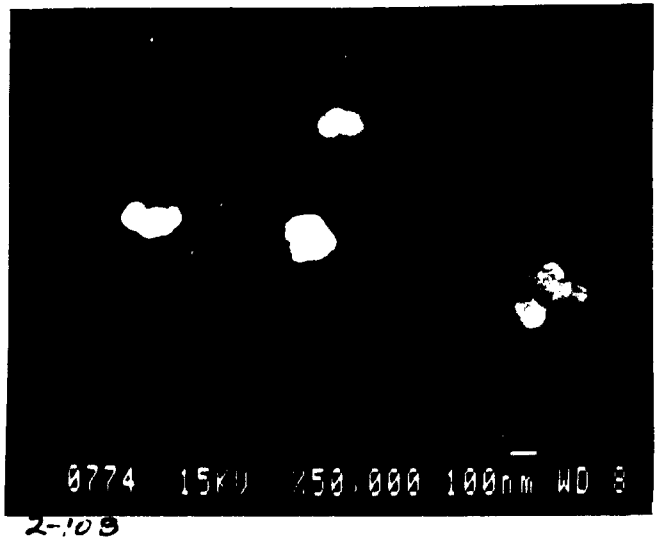

2-10B

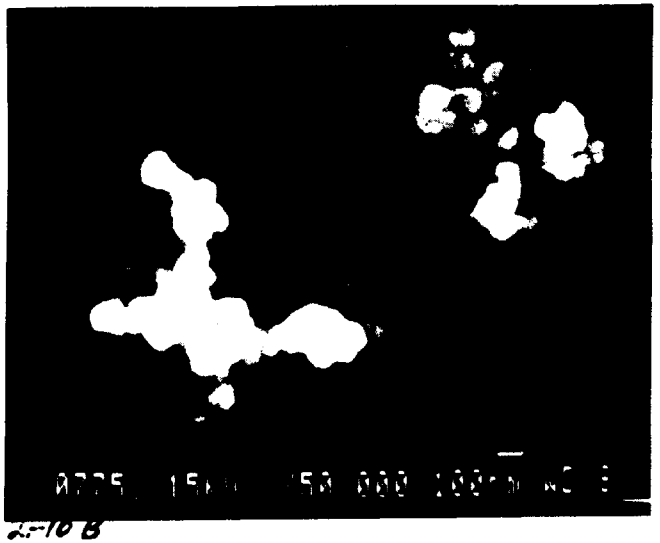

2-16B

561

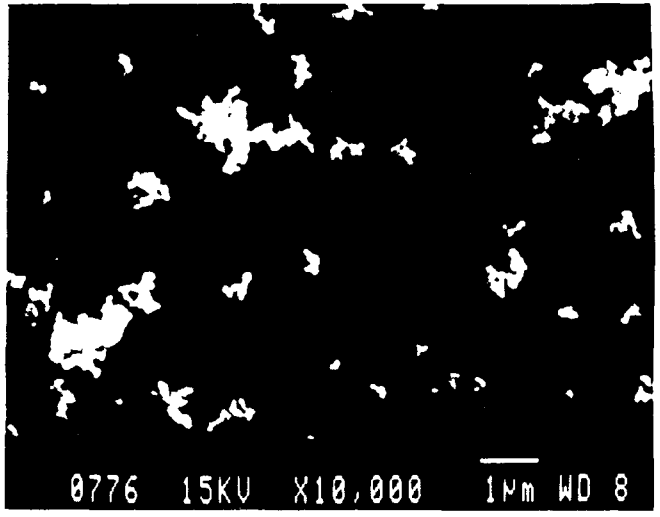

2-11B

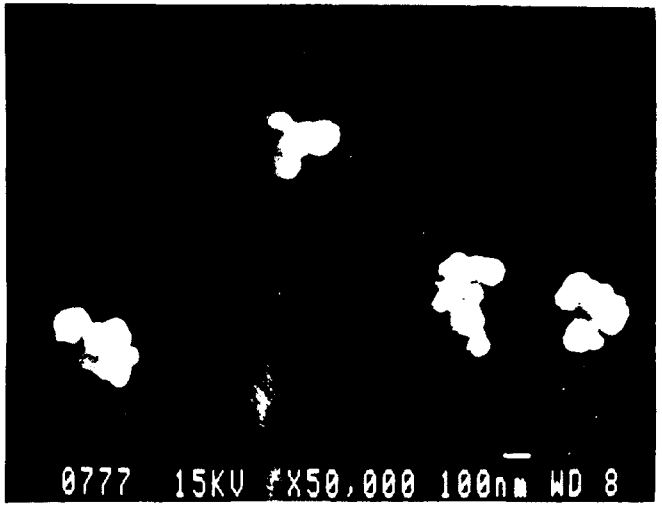

2-11B

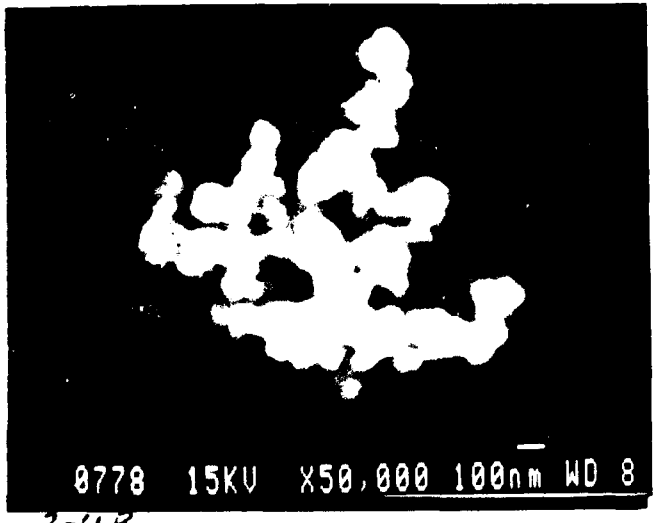

2-11B

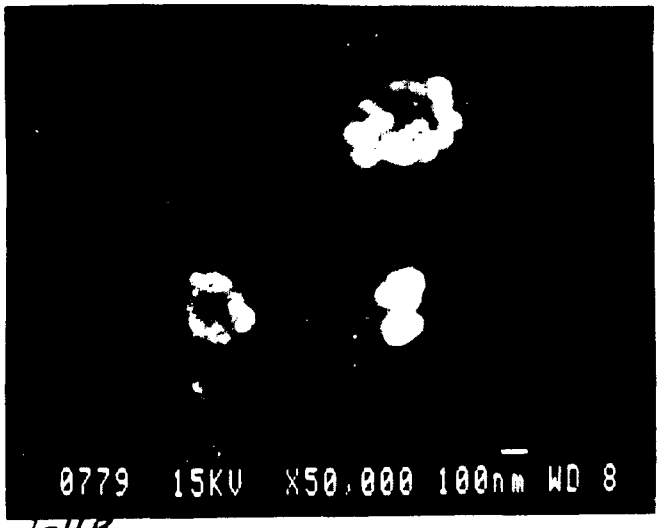

2-11B

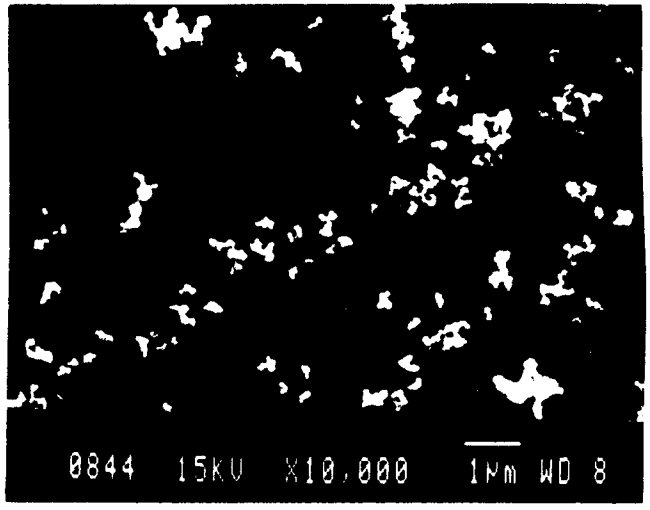

2-12B

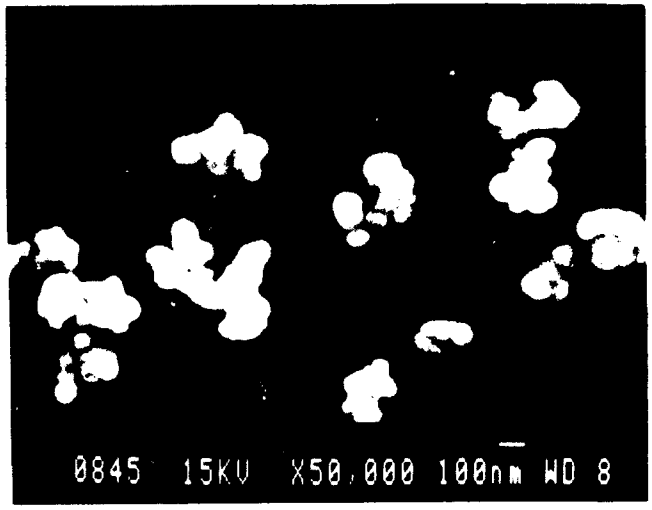

2-12B

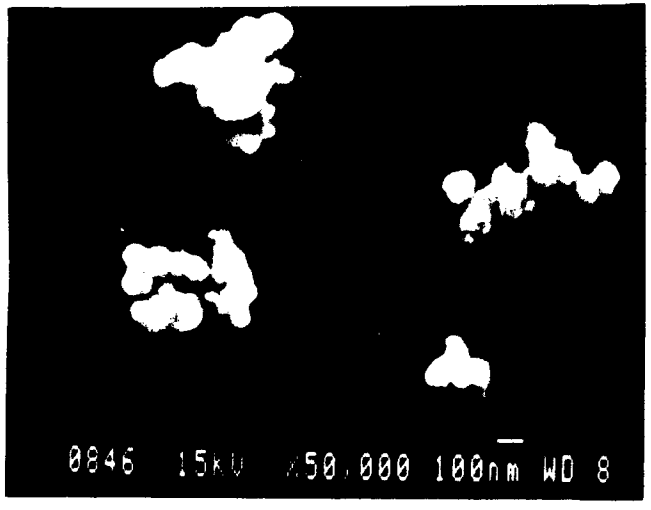

2-12B

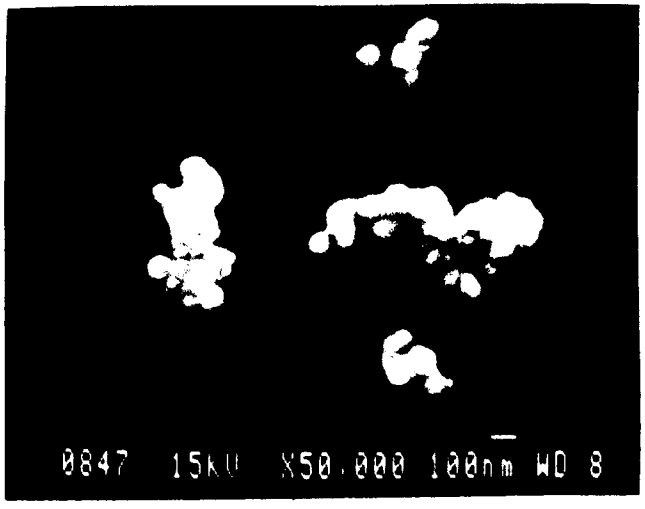

2-12B

861

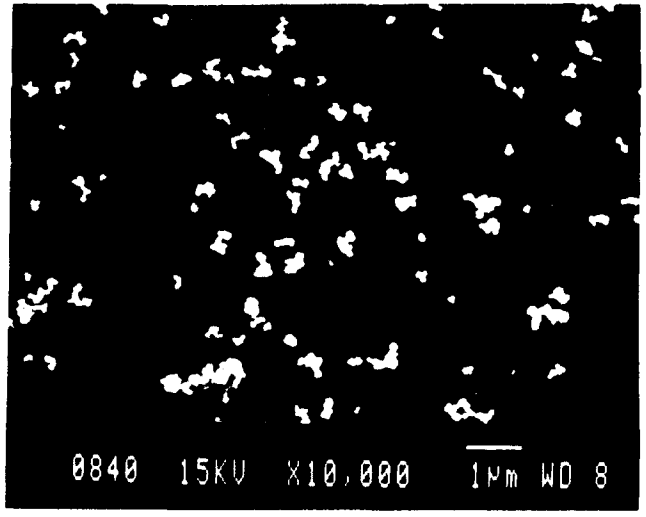

2-12P

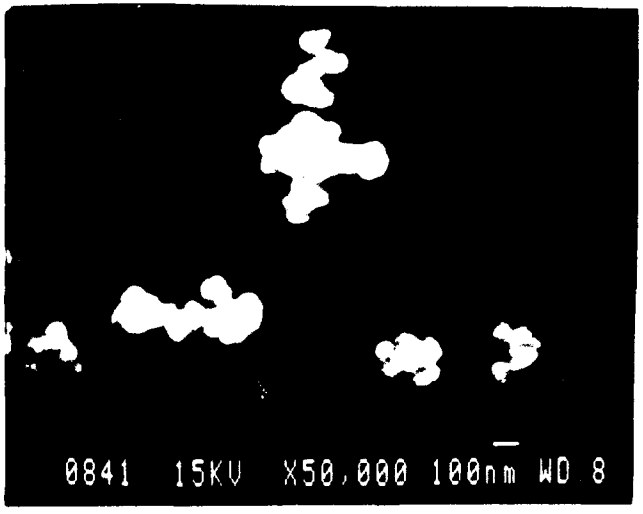

2-12P

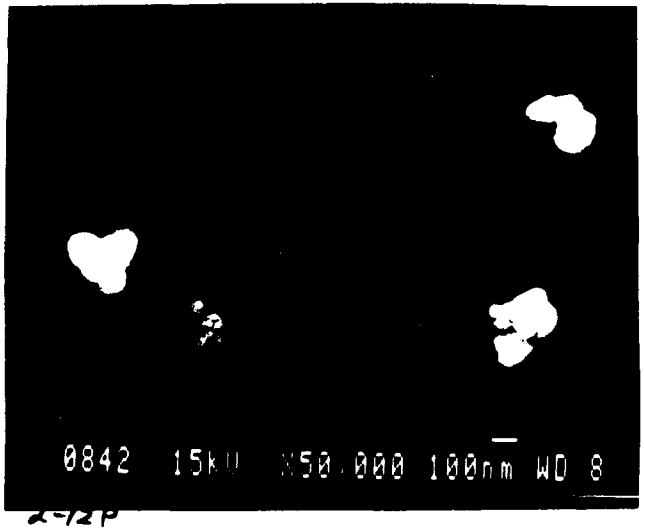

2-12P

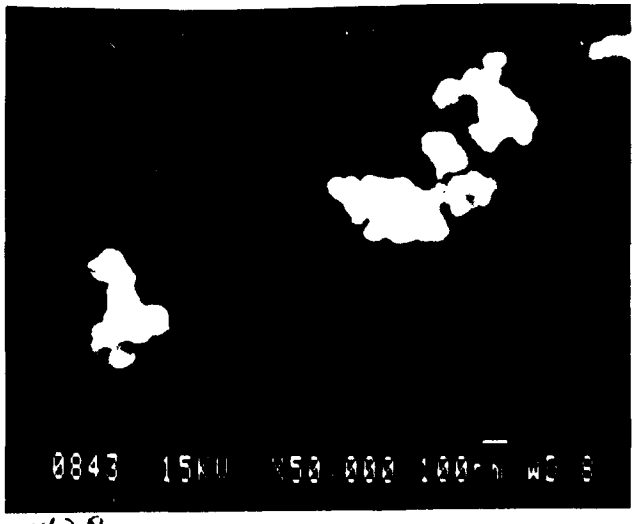

2-12P

0699 15KV X50,000 100nm WD 8

0701 15KV X50,000 100nm WD 8

0698 15KV X10,000 1μm WD 8

0700 15KV X50,000 100nm WD 8

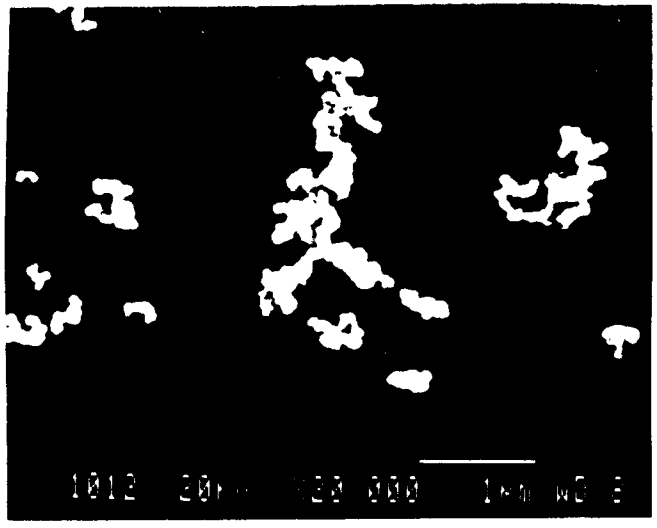

3-1B

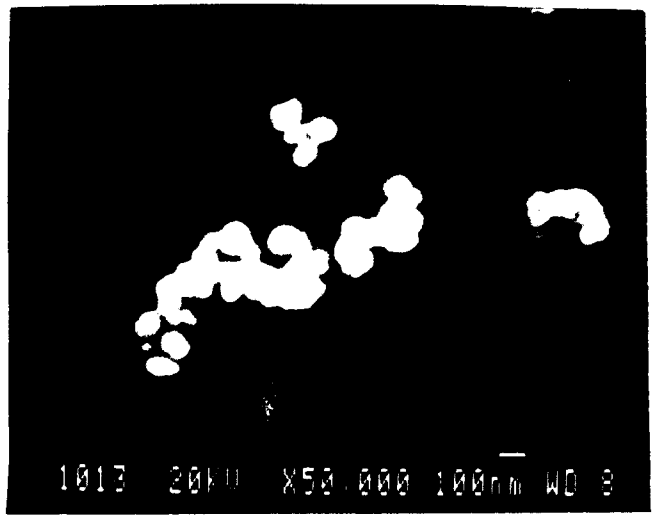

3-1B

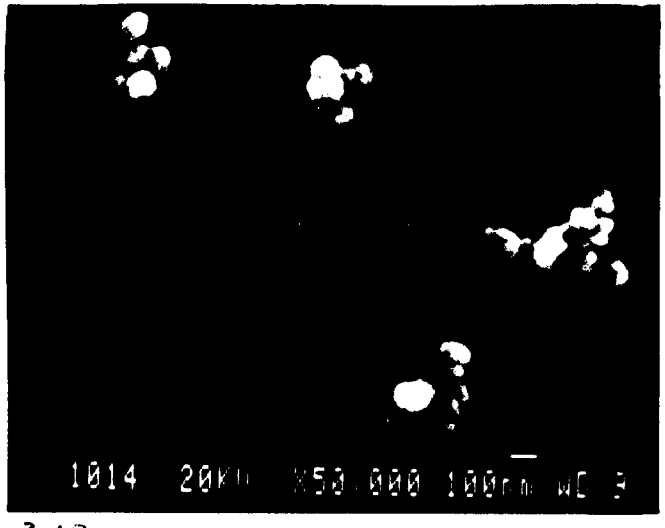

3-1B

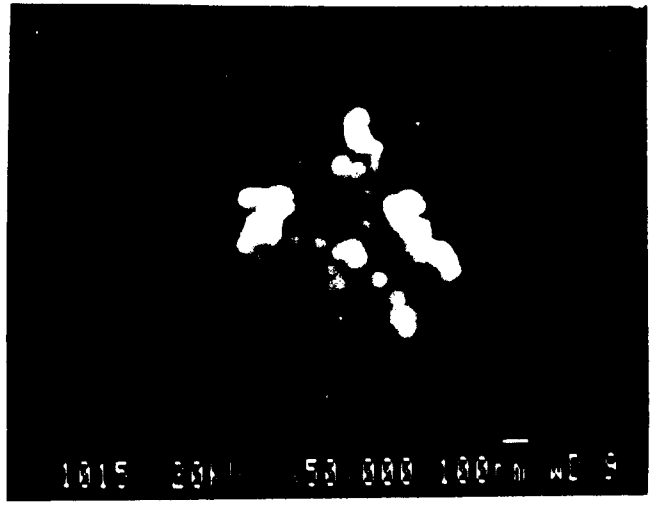

3-1B

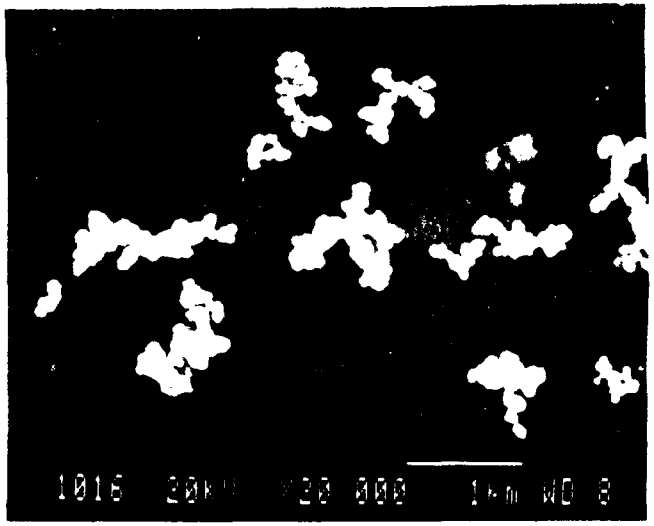

3-2B

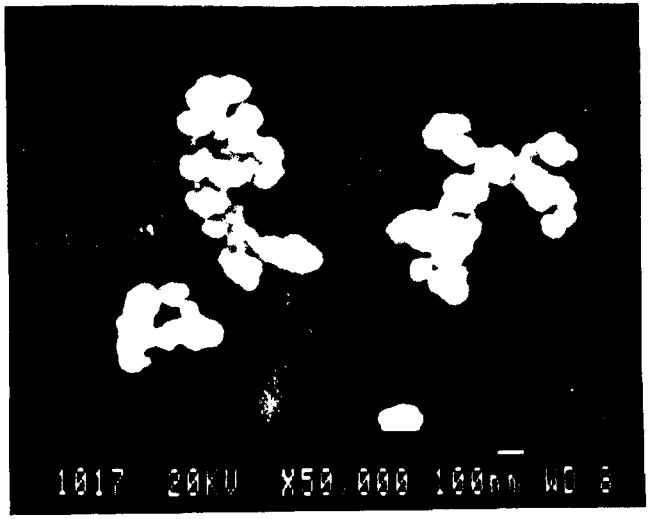

3-2B

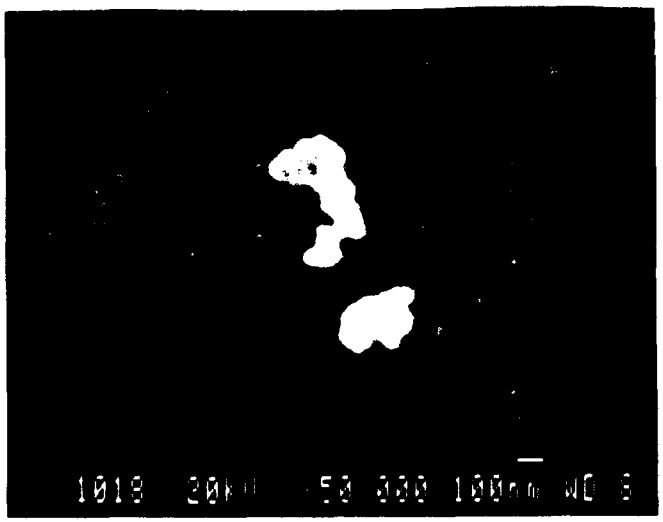

3-2B

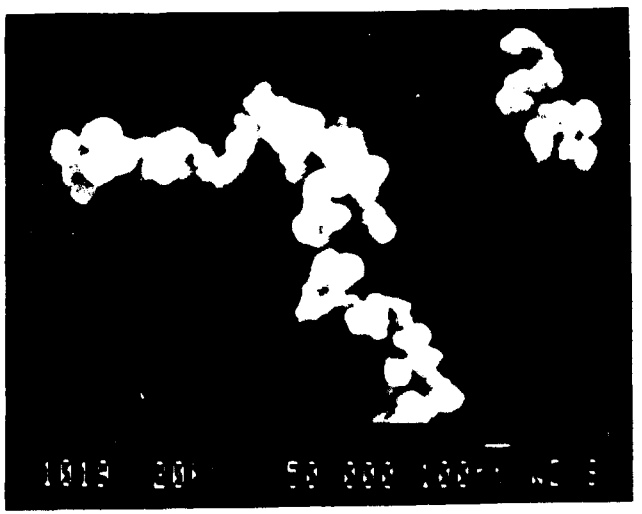

3-2B

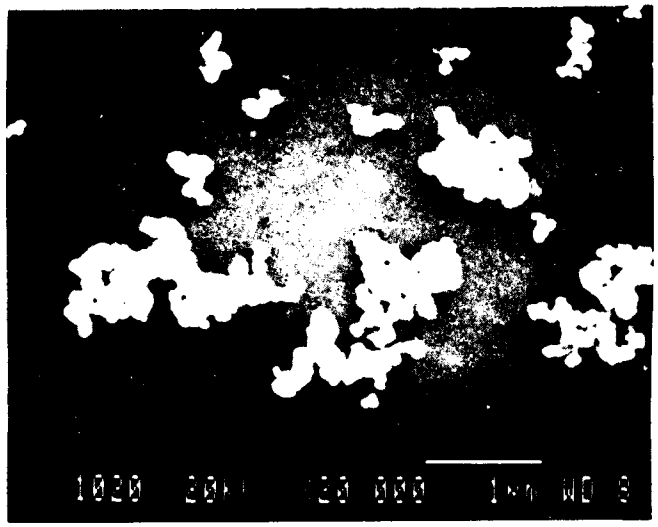

3-3B

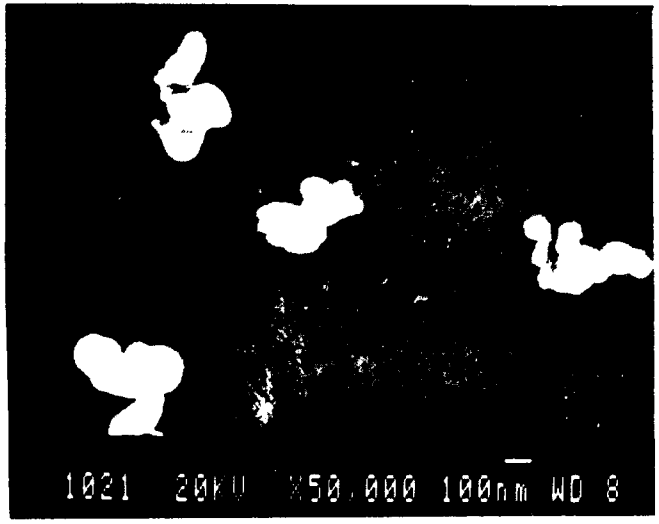

3-3B

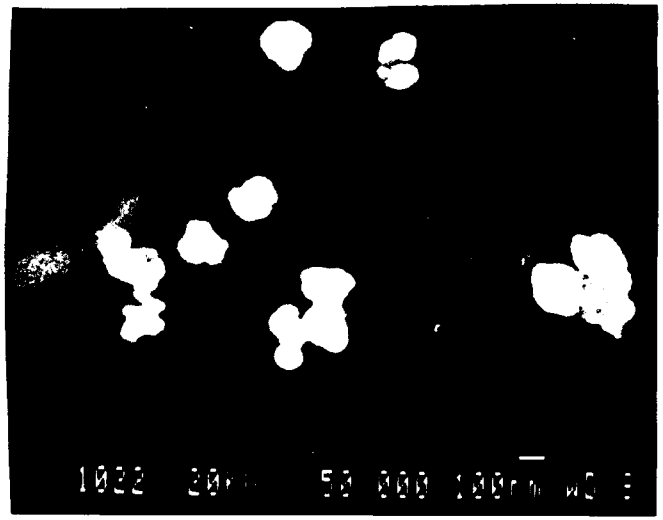

3-3B

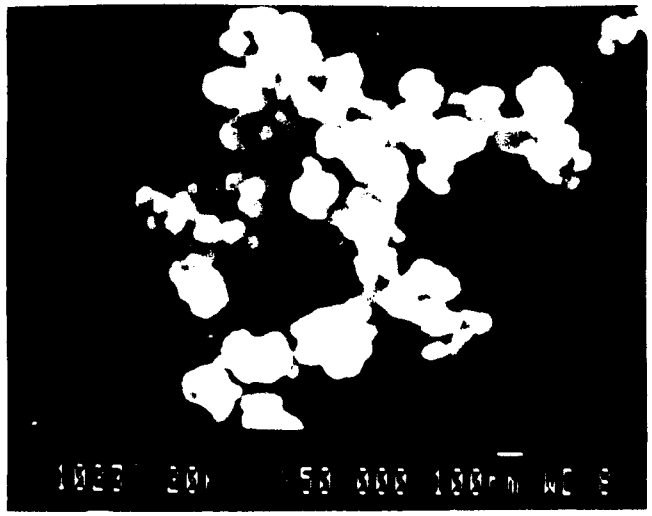

3-3B

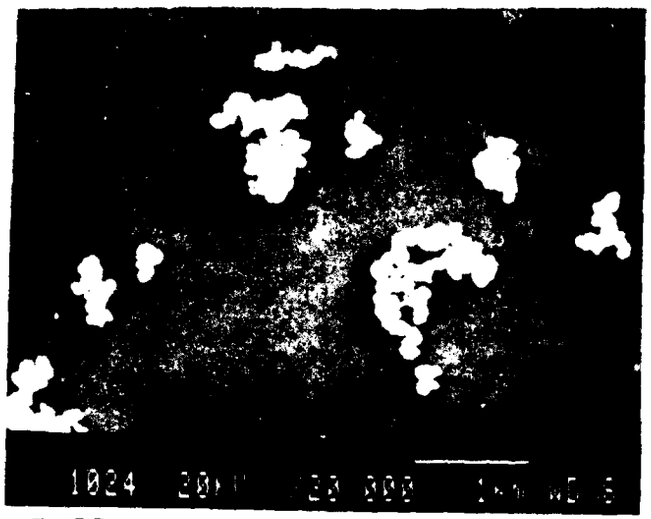

3-3P

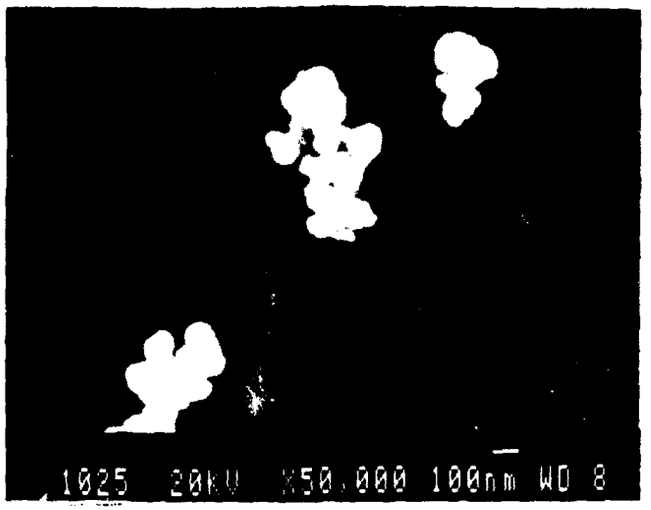

3-3P

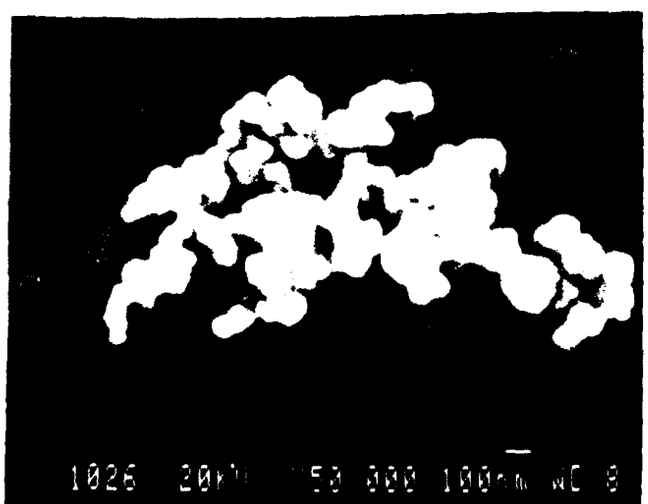

3-3P

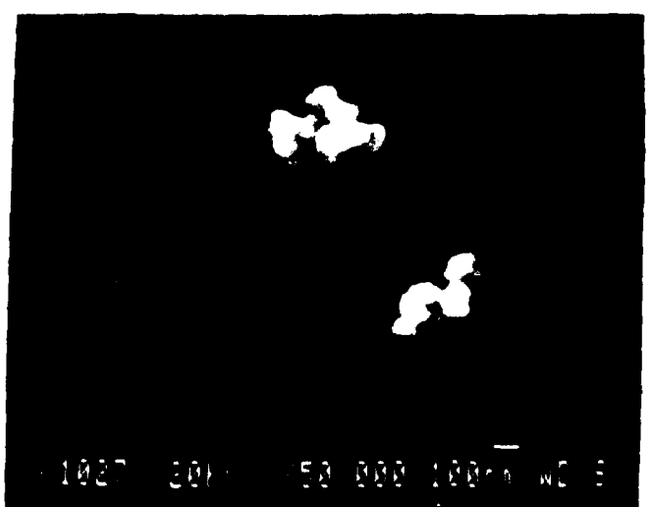

3-3P

2013

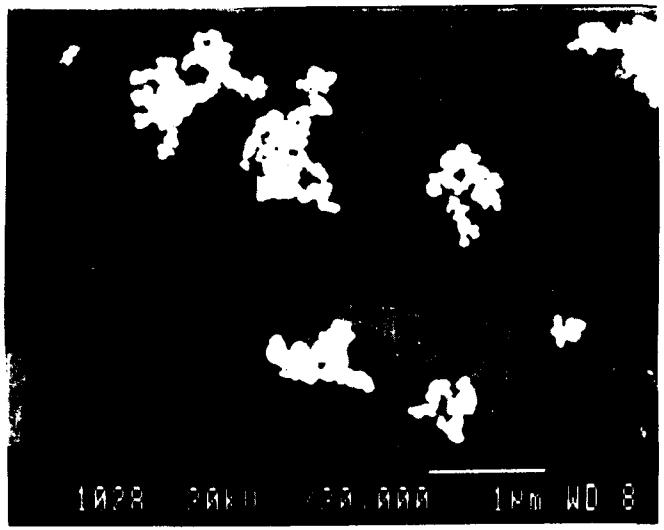

3-4B

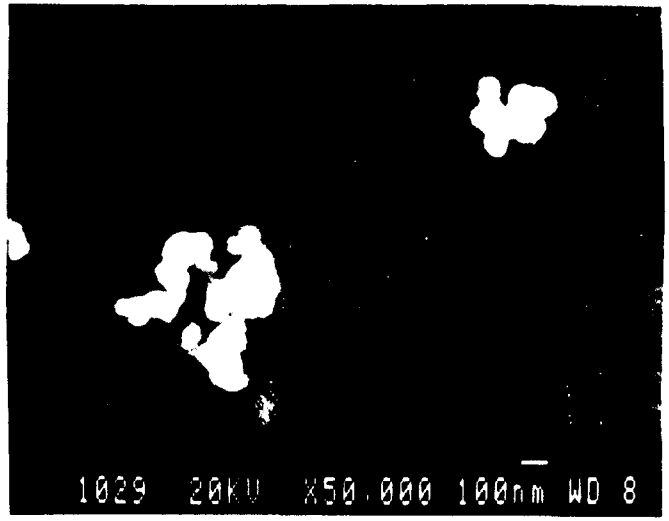

3-4B

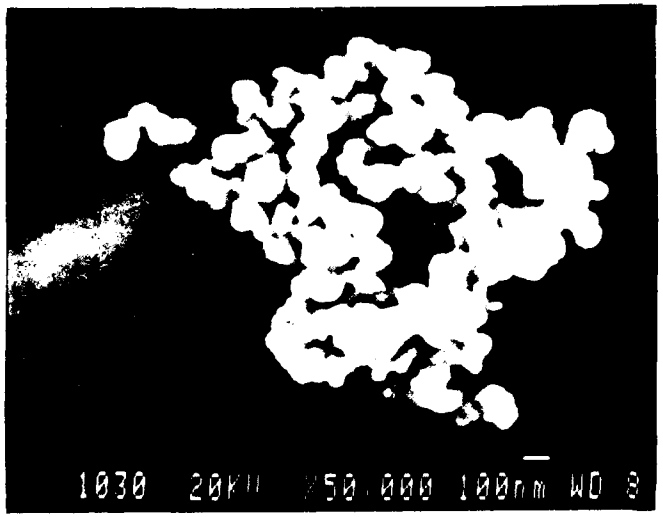

3-4B

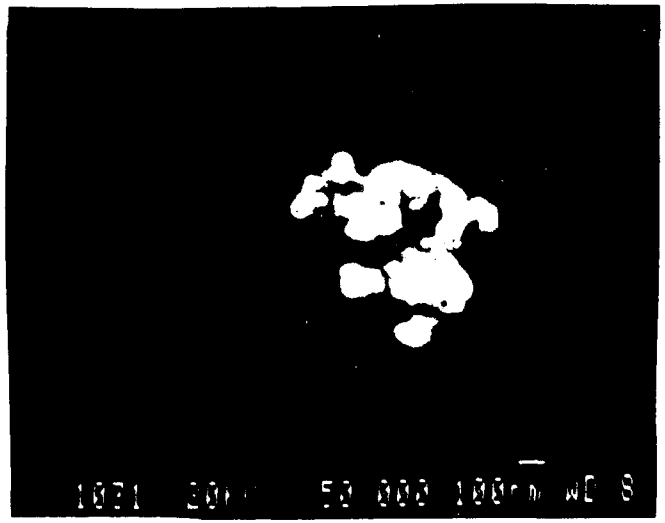

3-4B

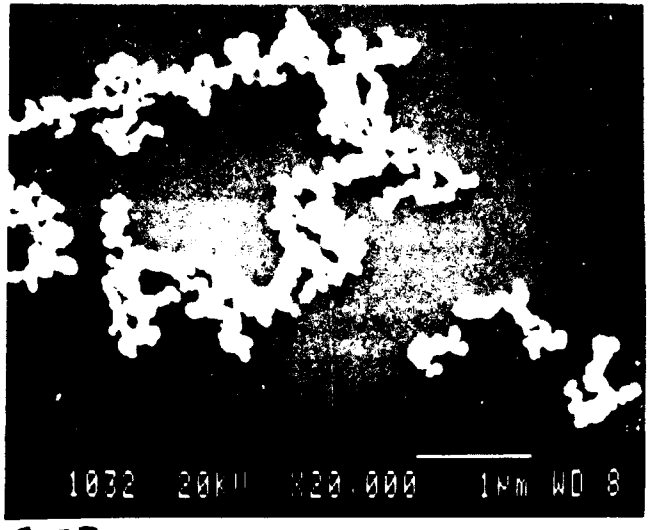

3-5B

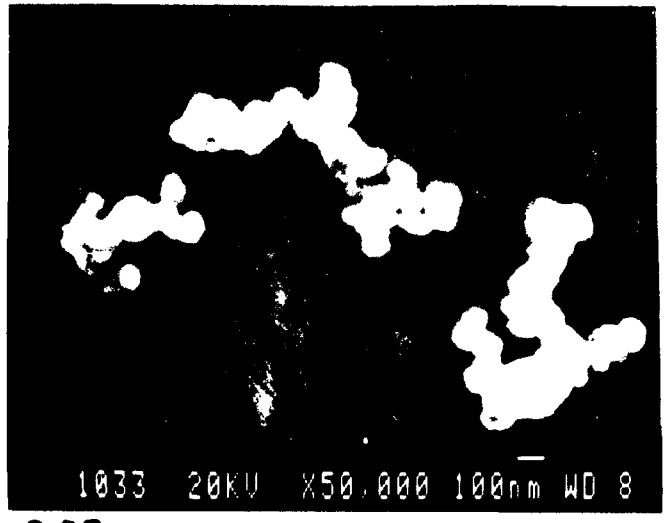

3-5B

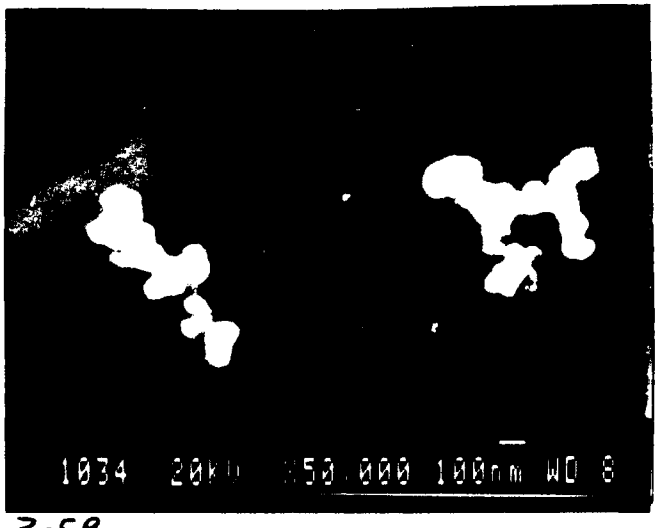

3-5B

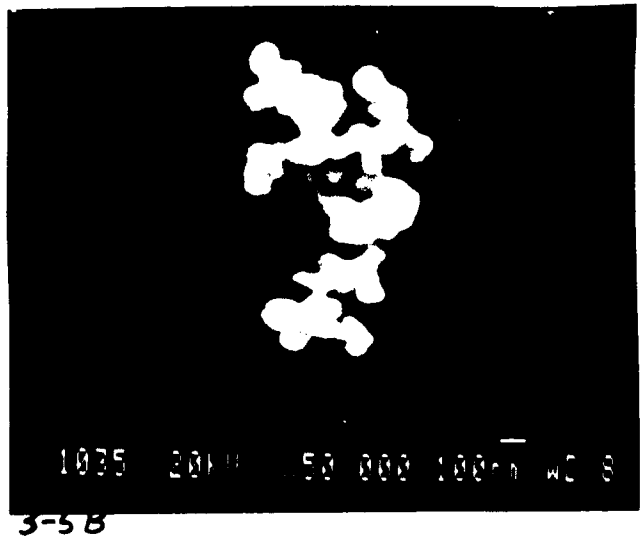

3-5B

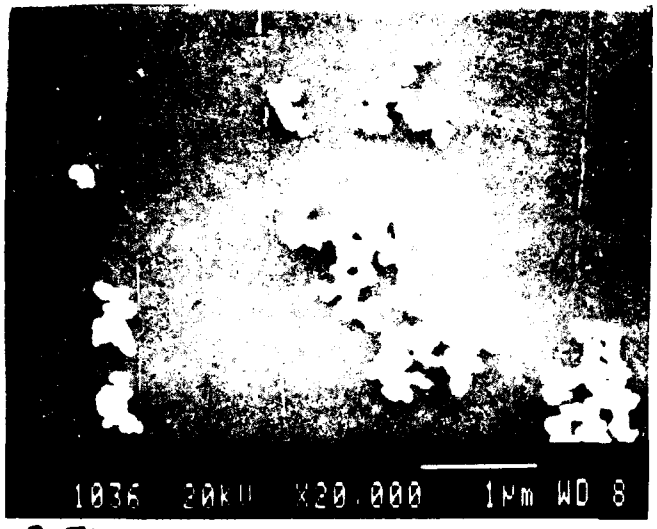

3-5P

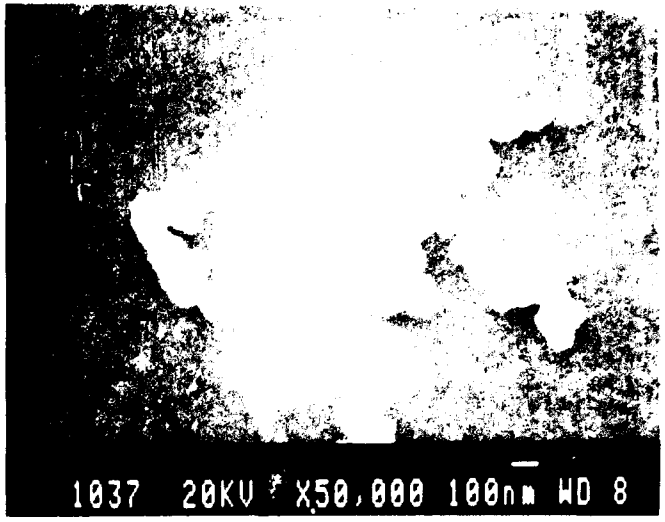

3-5P

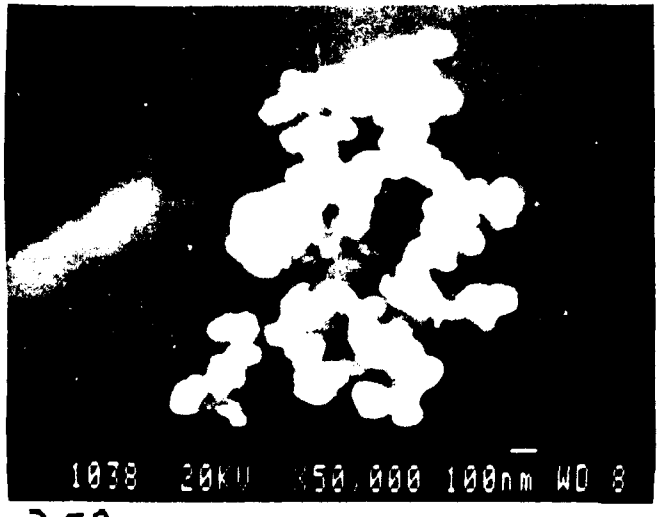

3-5P

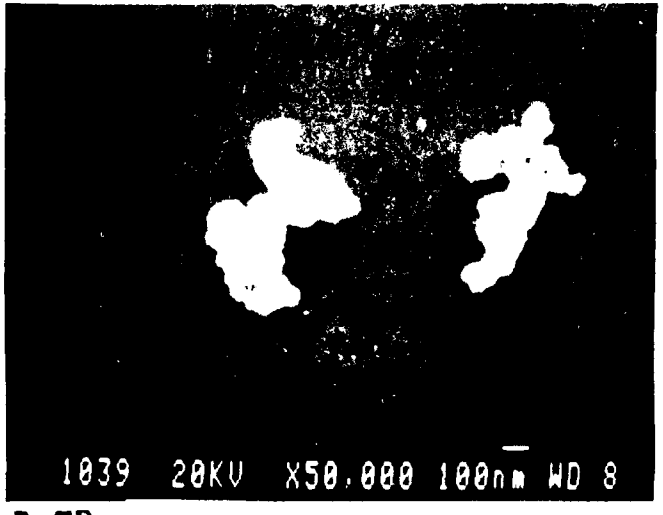

3-5P

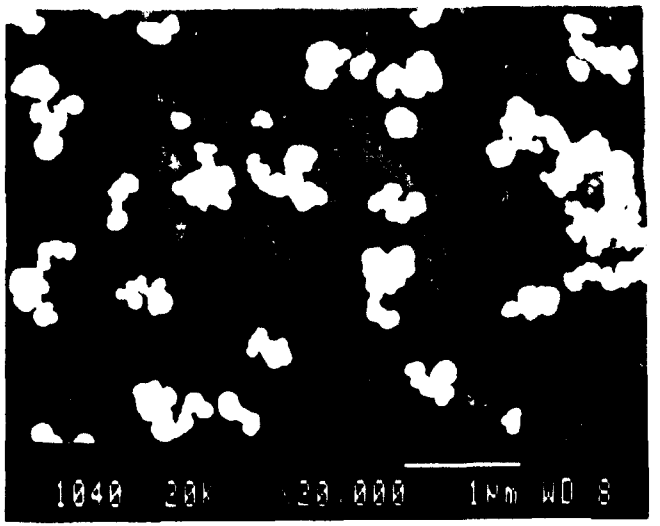

3-6B

3-6B

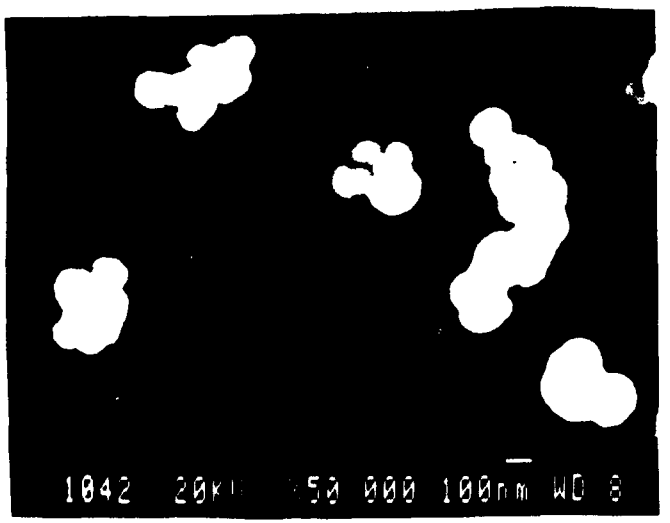

3-6B

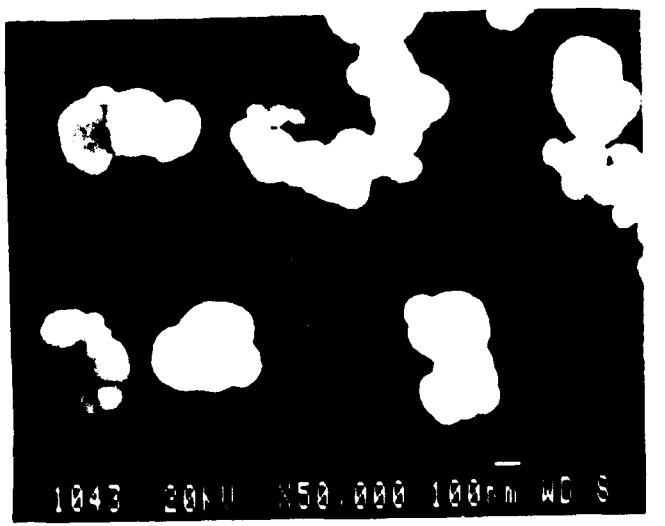

3-6B

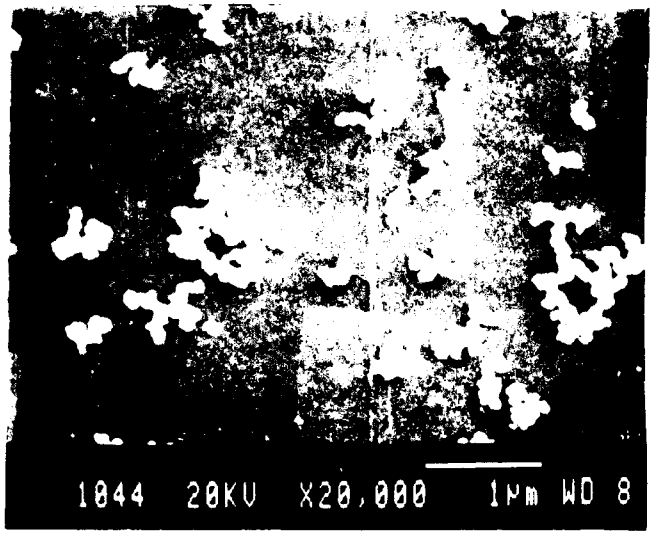
1044 20KV X20,000 1µm WD 8

3-7B

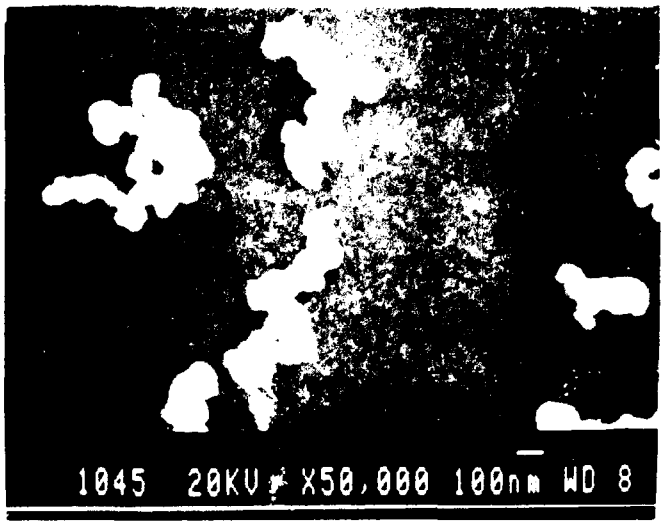
1045 20KV X50,000 100nm WD 8

3-7B

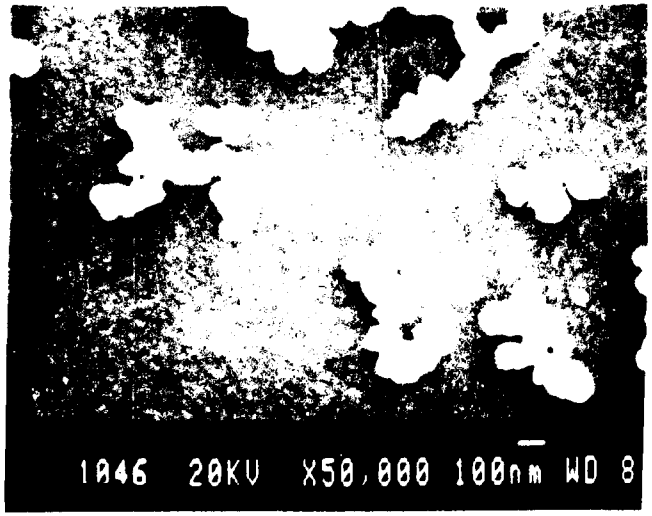
1046 20KV X50,000 100nm WD 8

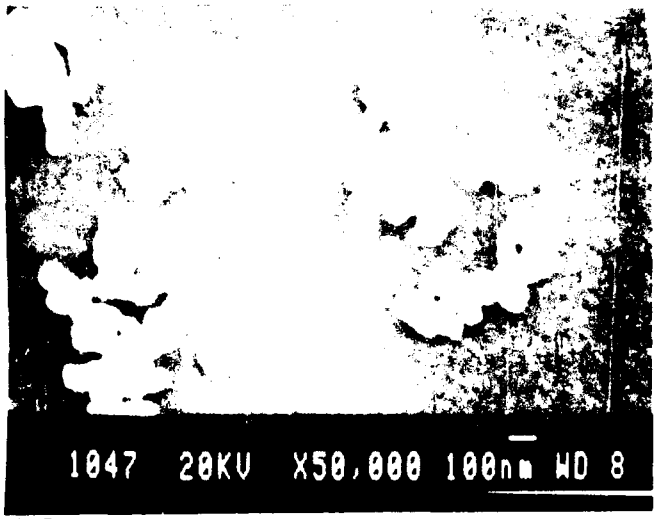
1047 20KV X50,000 100nm WD 8

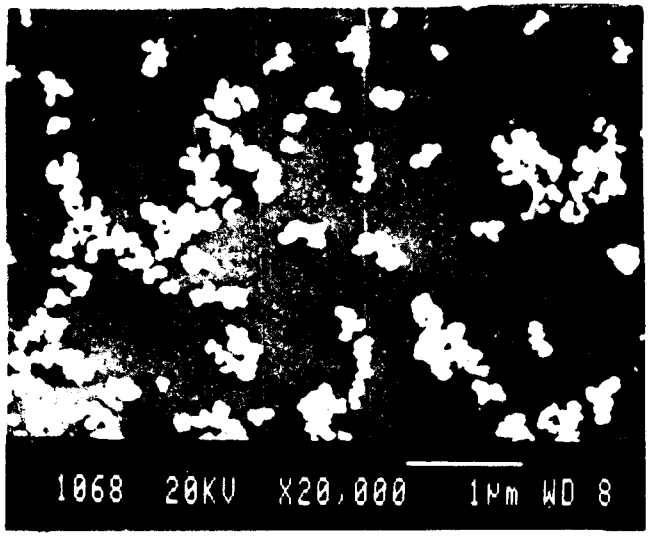

5-9P

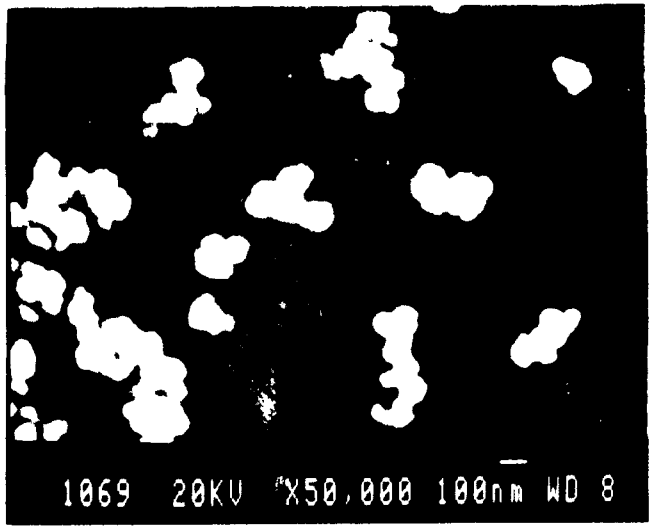

B-9P

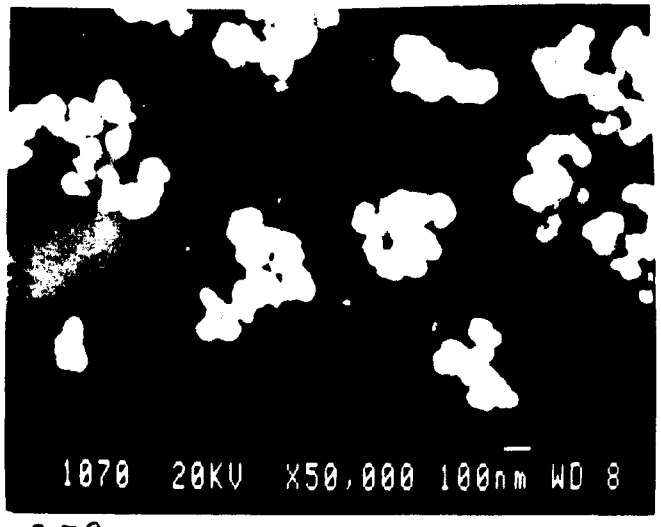

3-9P

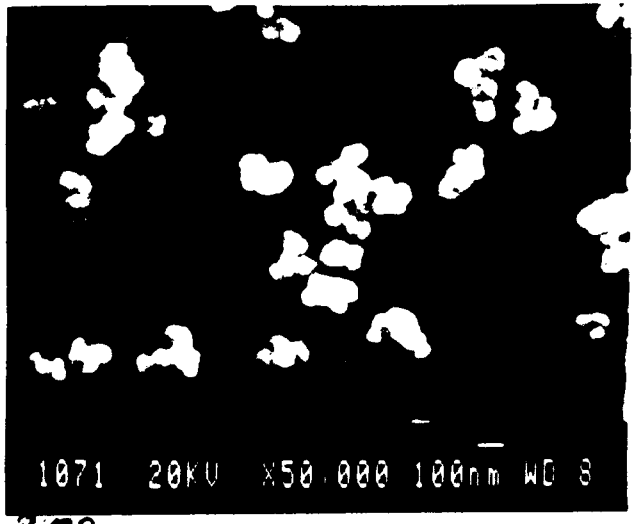

8-9P

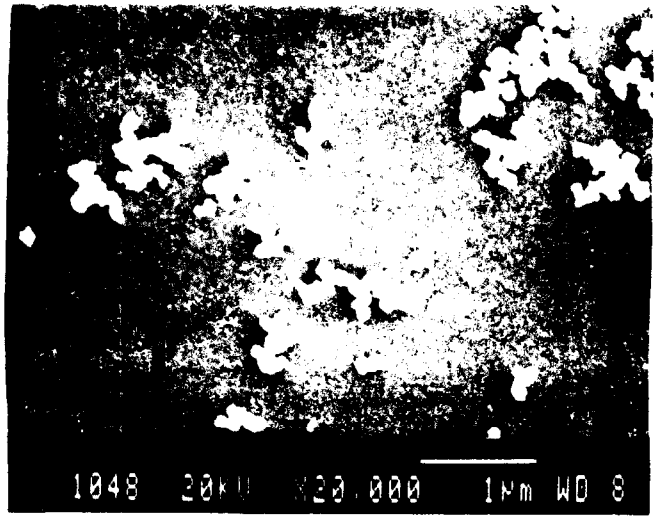

3-8B

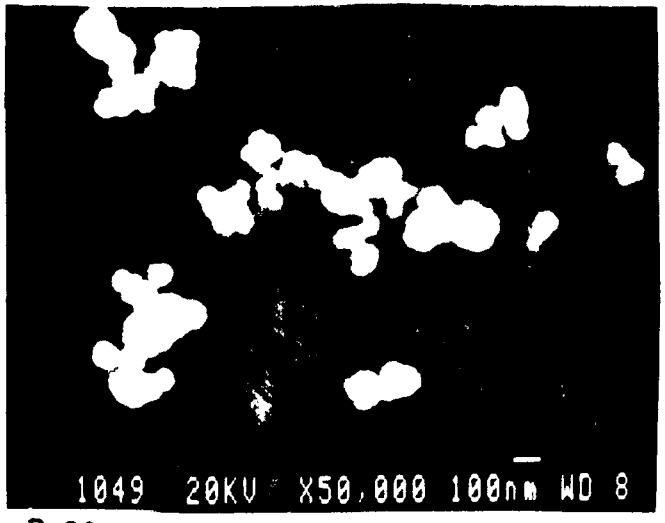

3-8B

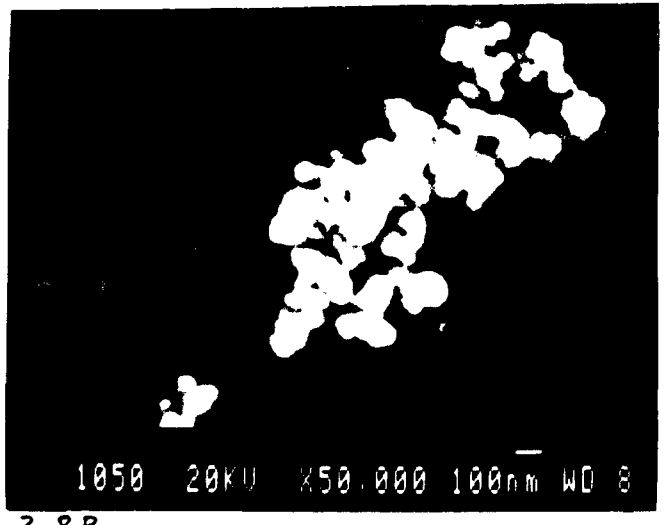

3-8B

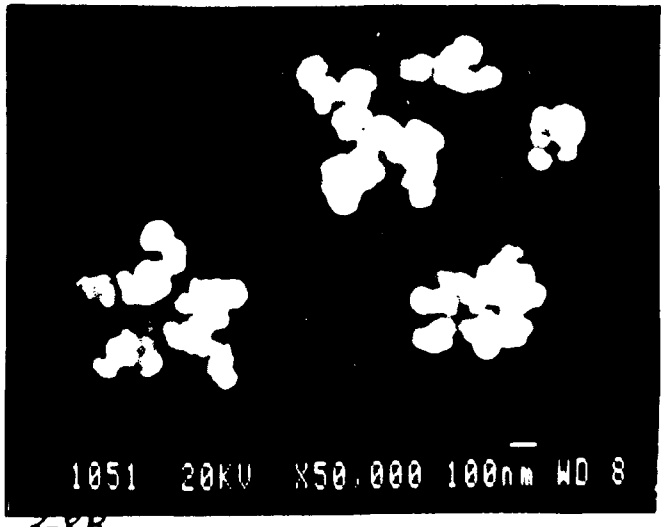

3-8B

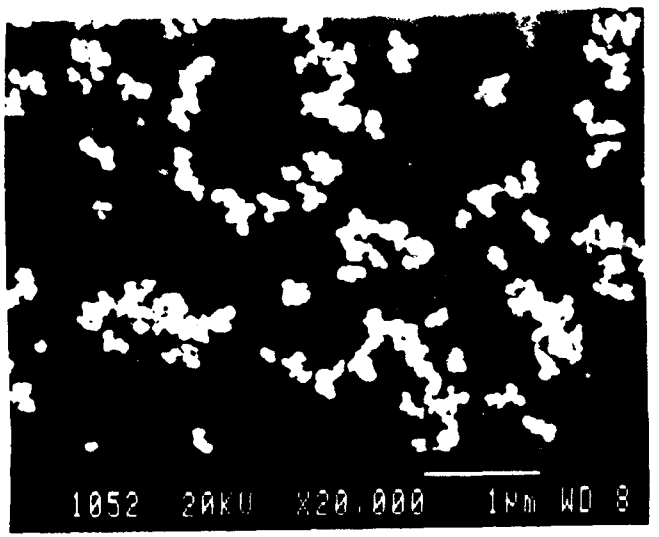

3-9B

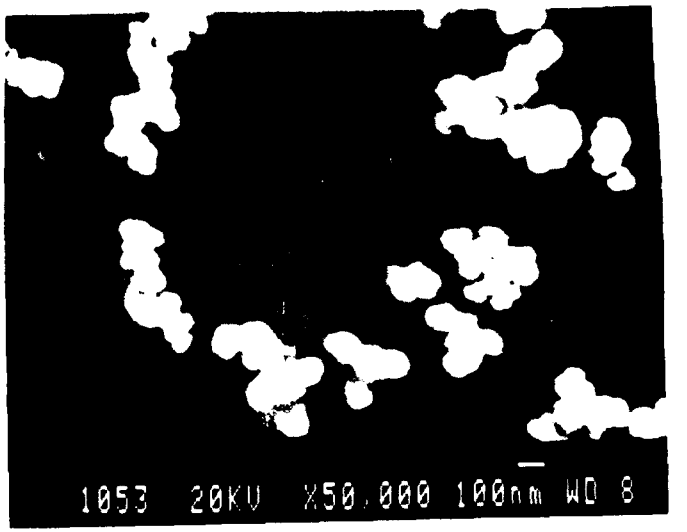

3-9B

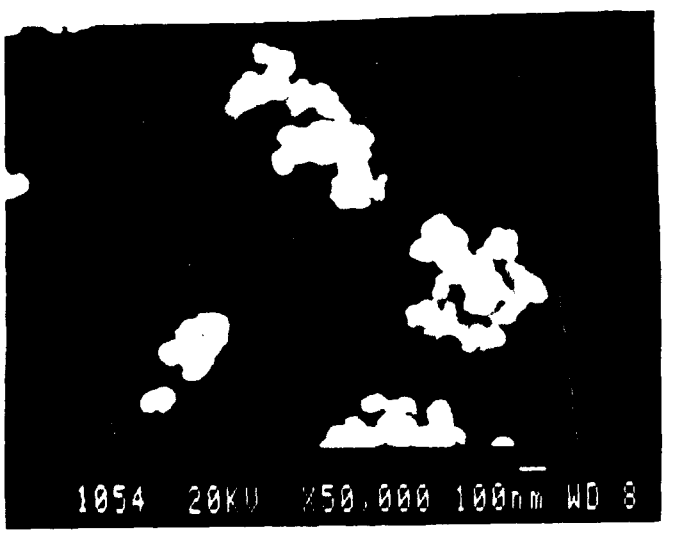

3-9B

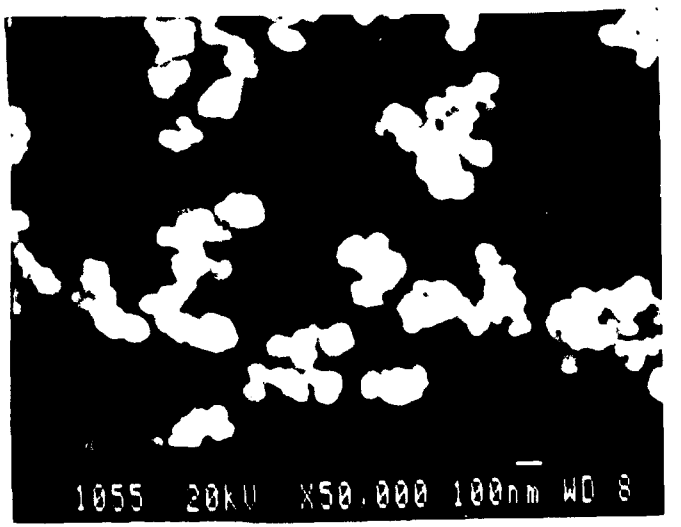

3-9B

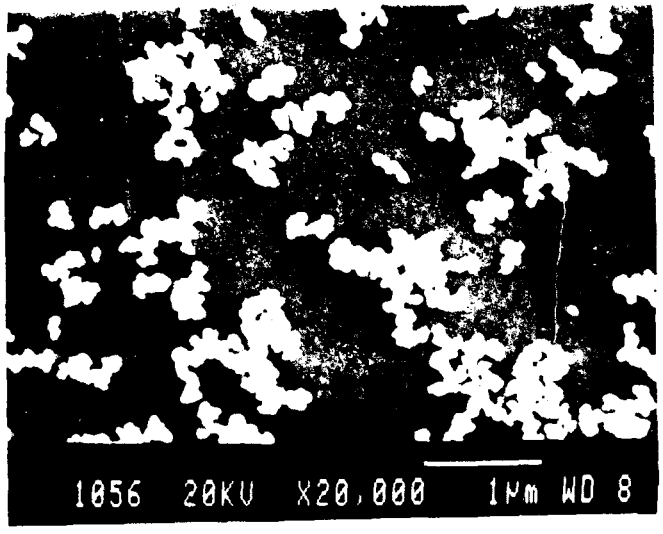

3-10 B

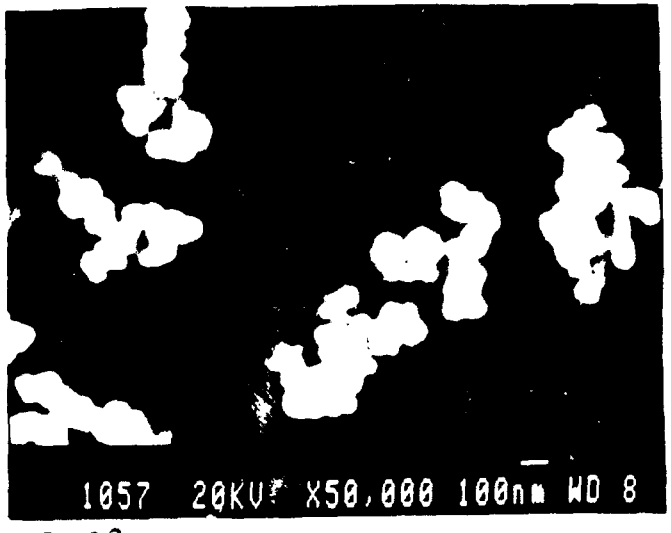

3-10B

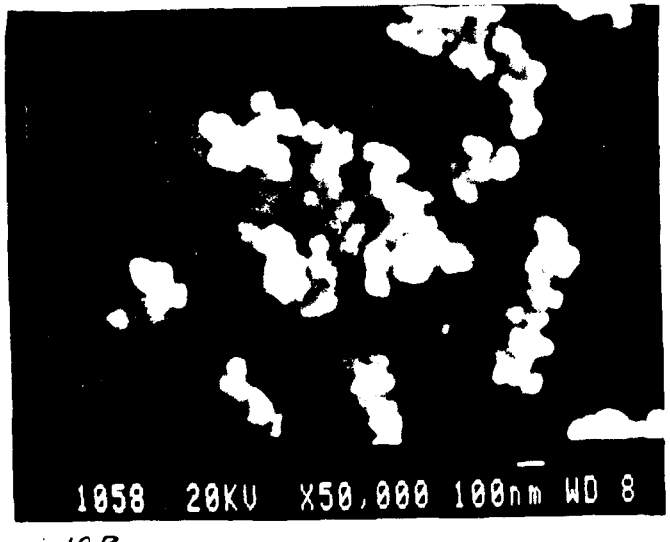

3-10 B

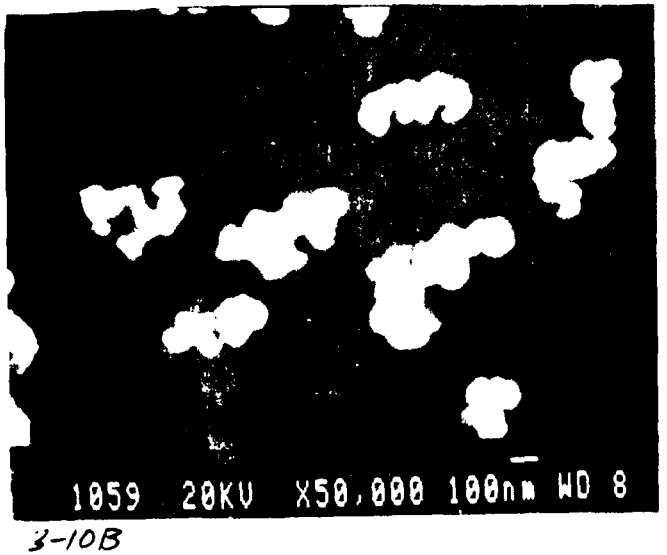

3-10B

2/2

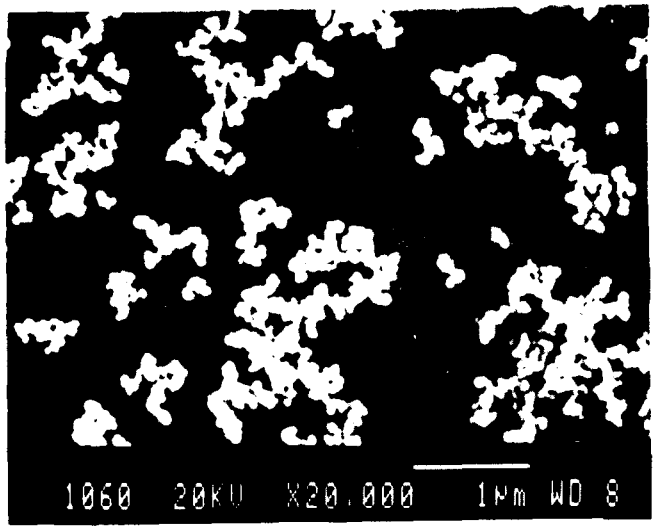

3-11B

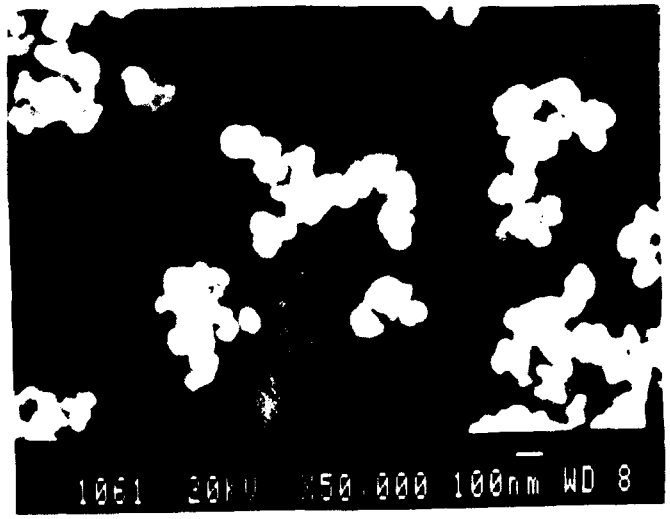

3-11B

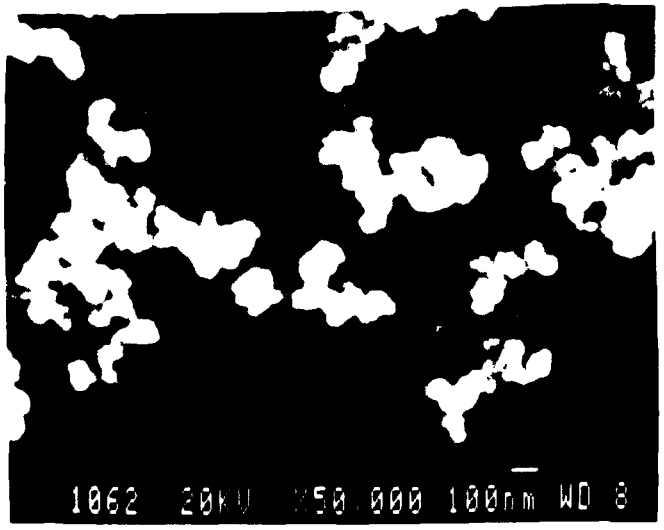

3-11B

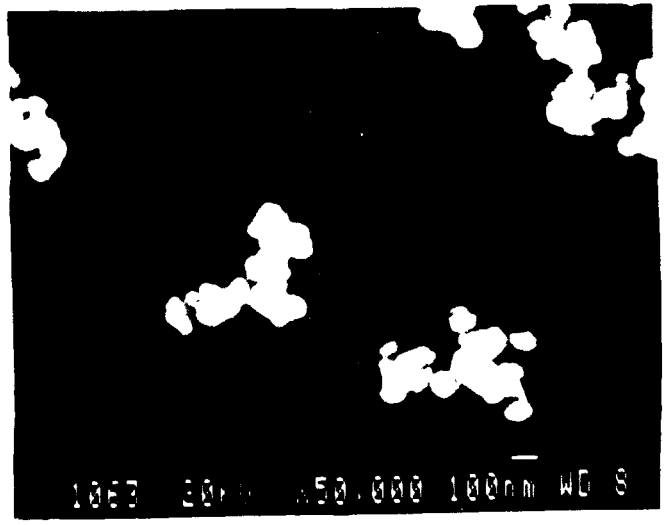

3-11B

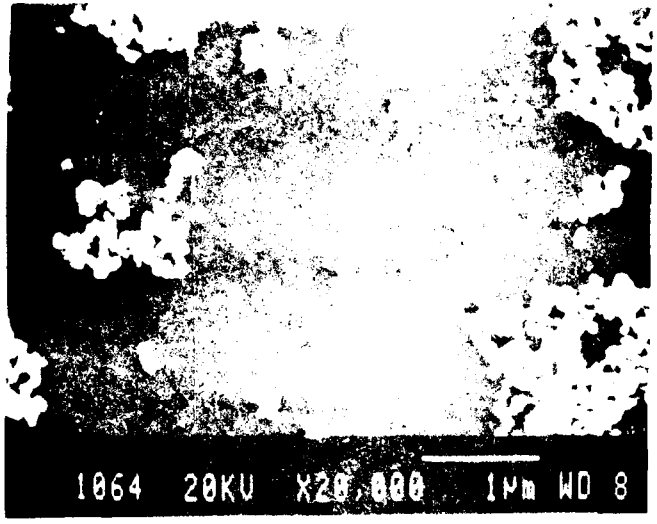

3-12B

3-12

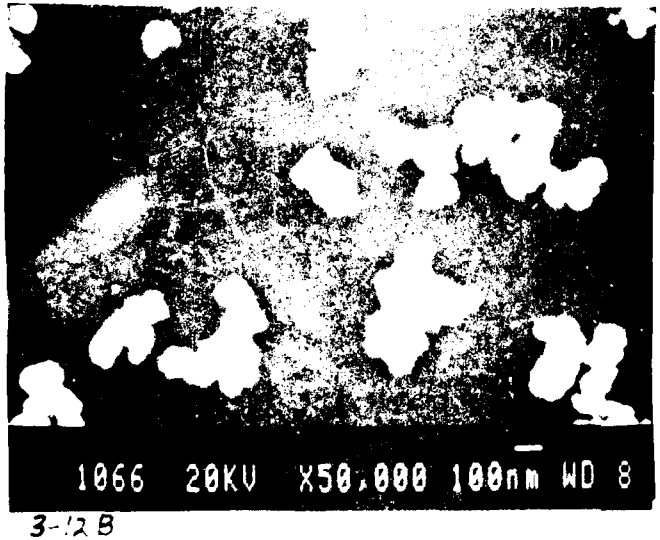

3-12B

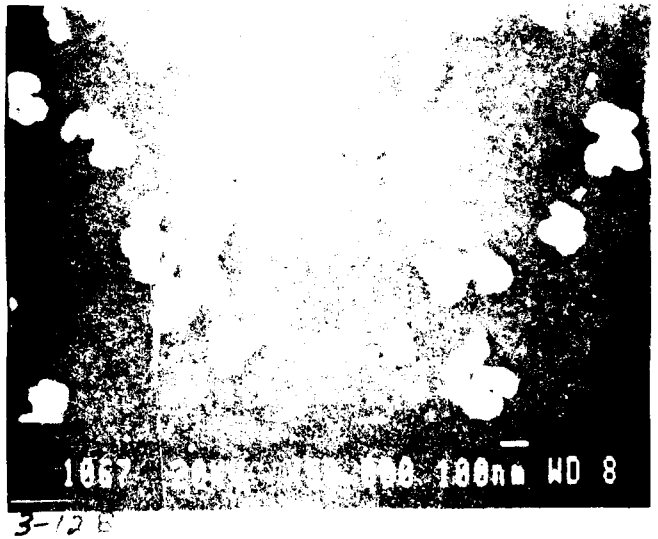

3-12

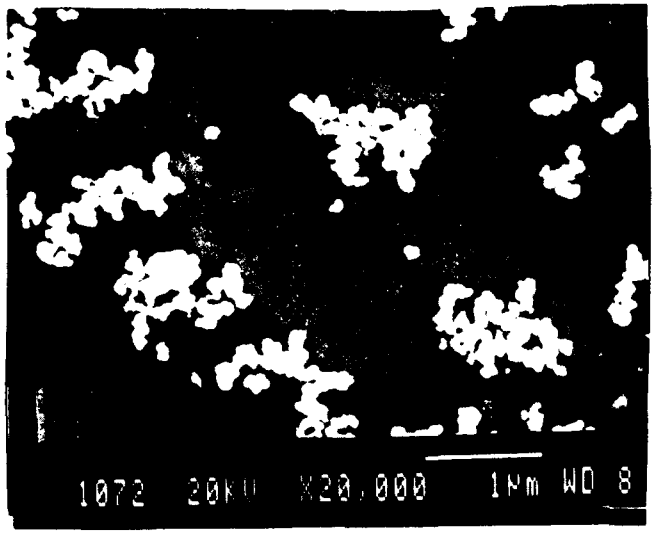

3-12P

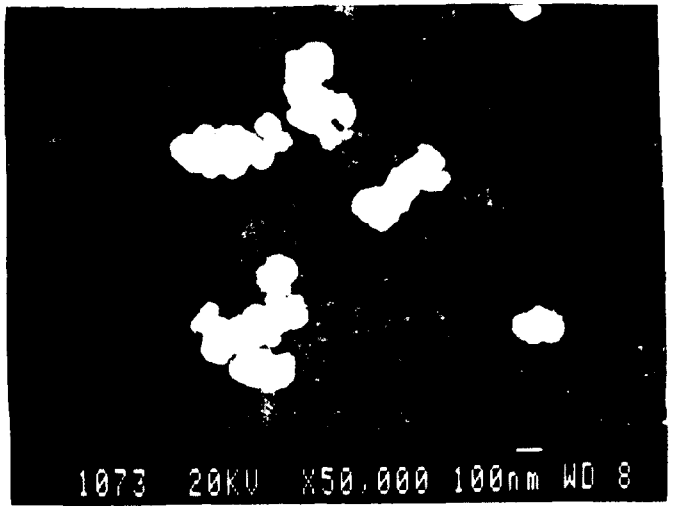

3-12P

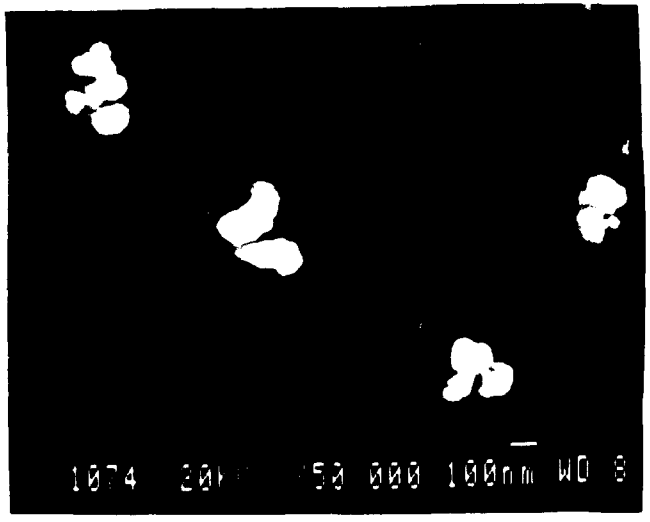

3-12P

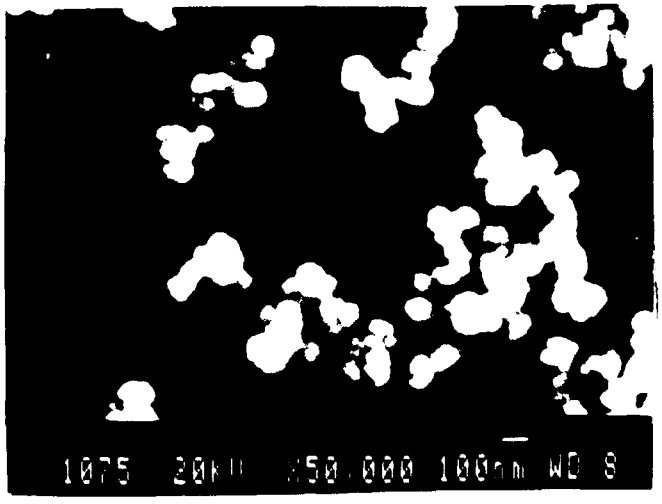

3-12P

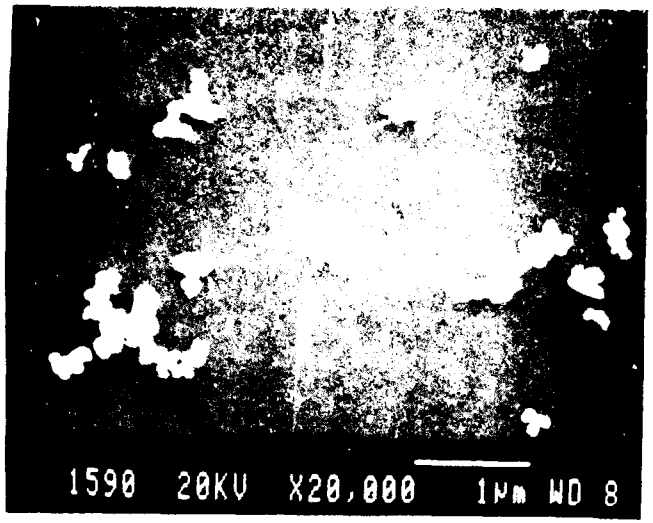

4-1B

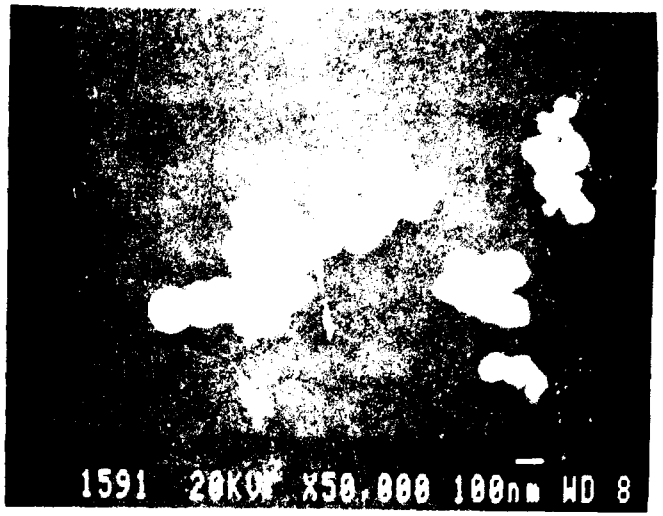

4-1B

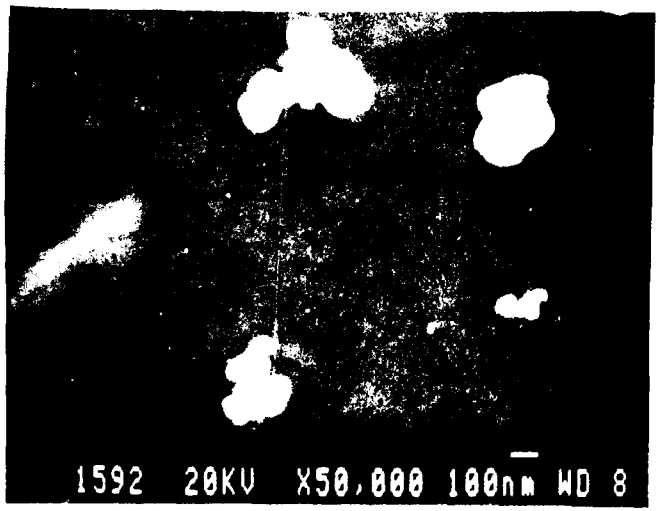

4-1B

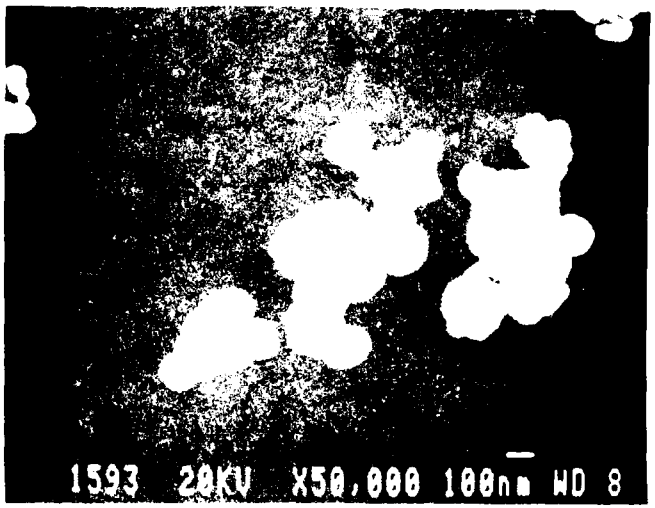

4-1B

216

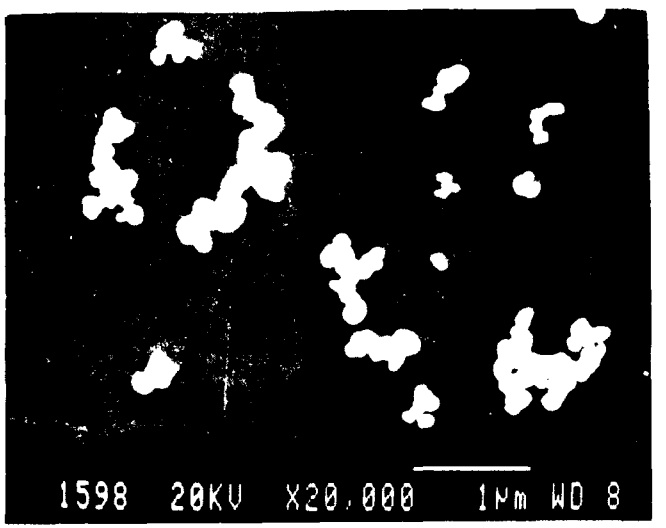

4-2B

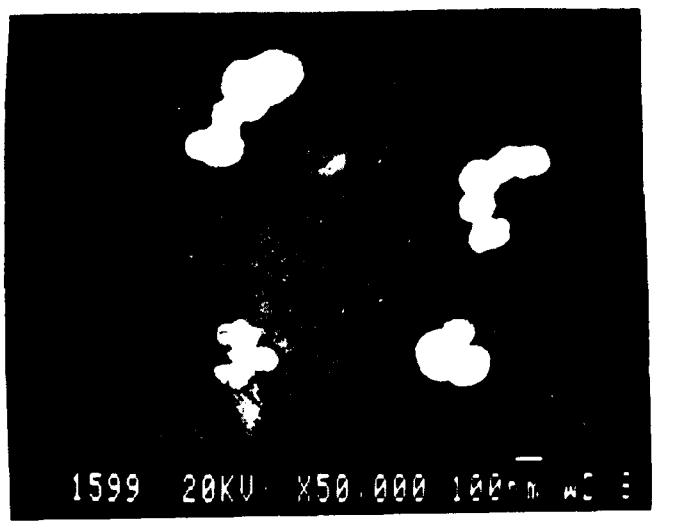

4-2B

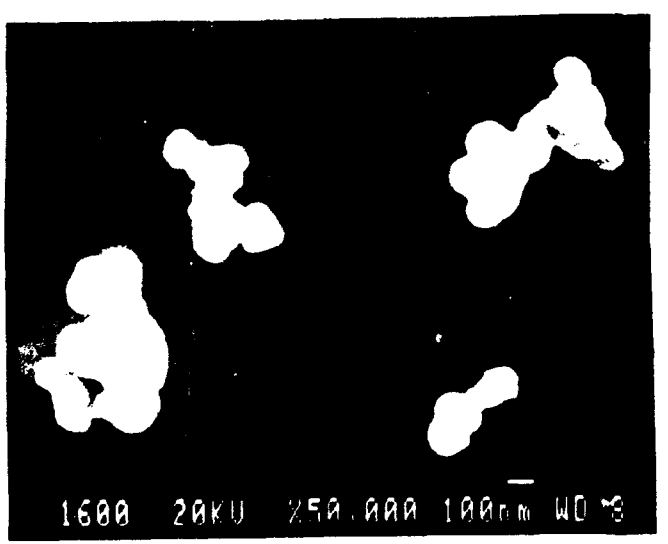

4-2B

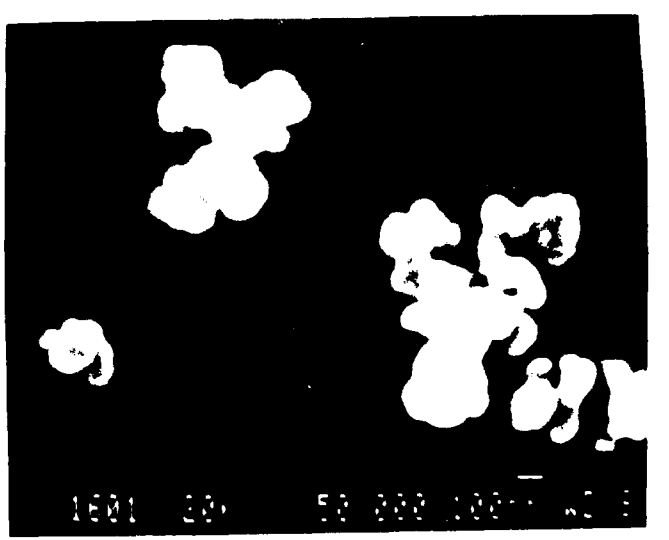

4-2B

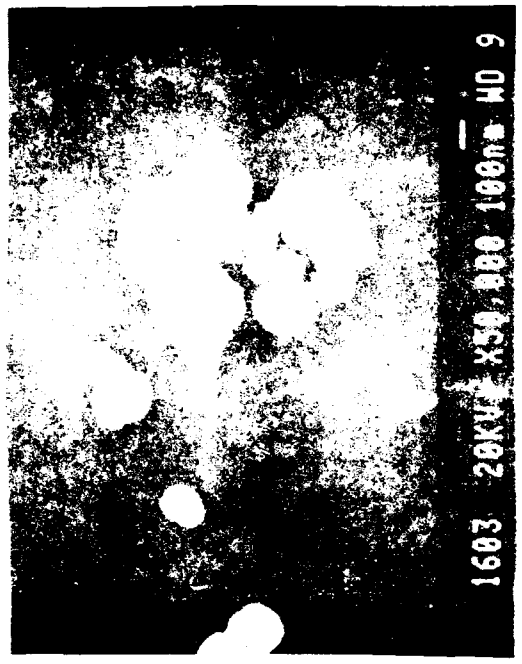

4-3B

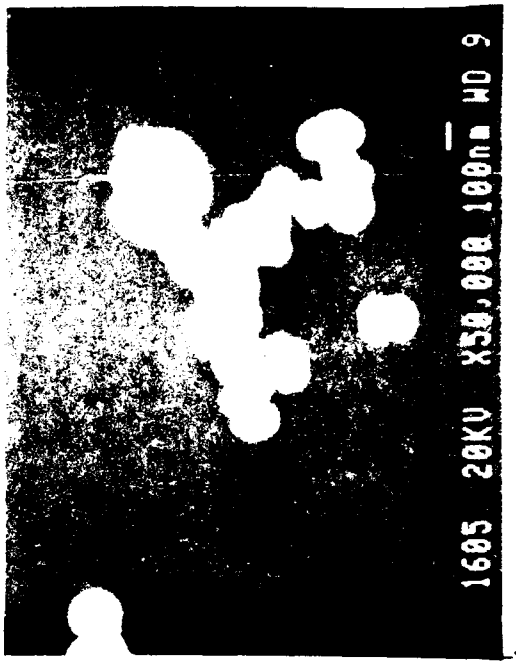

4-3B

4-3B

4-3B

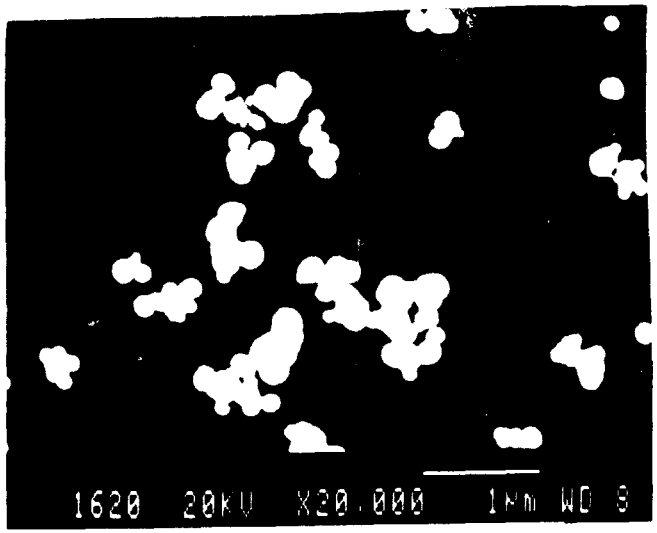

4-4B

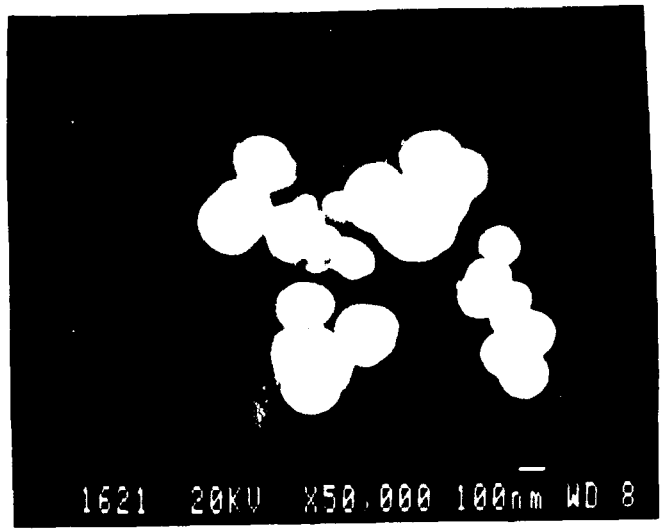

4-4B

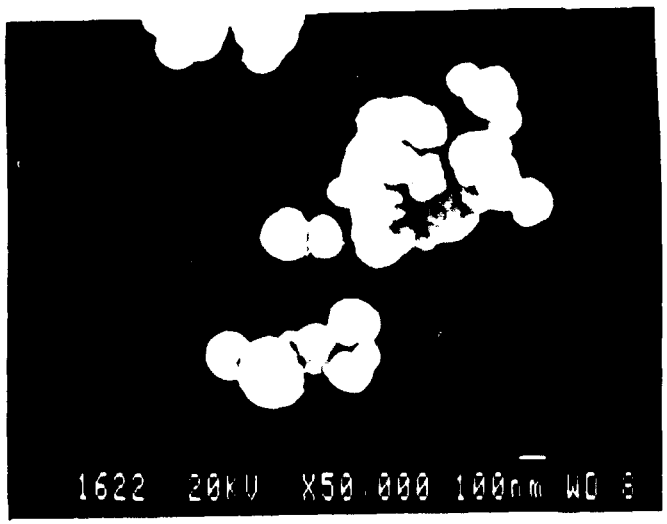

4-4B

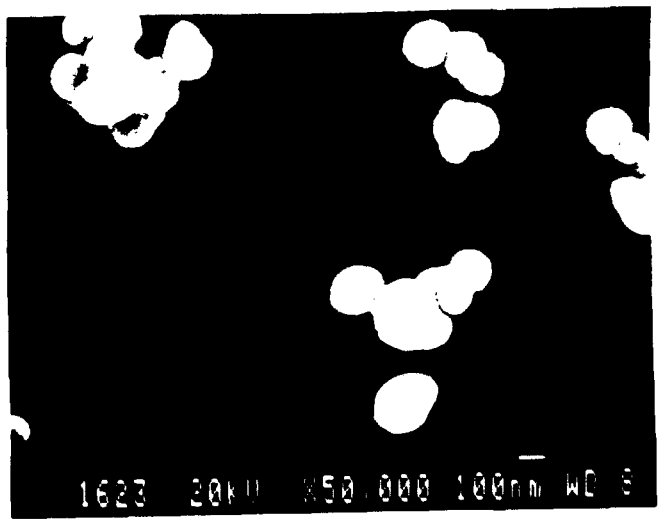

4-4B

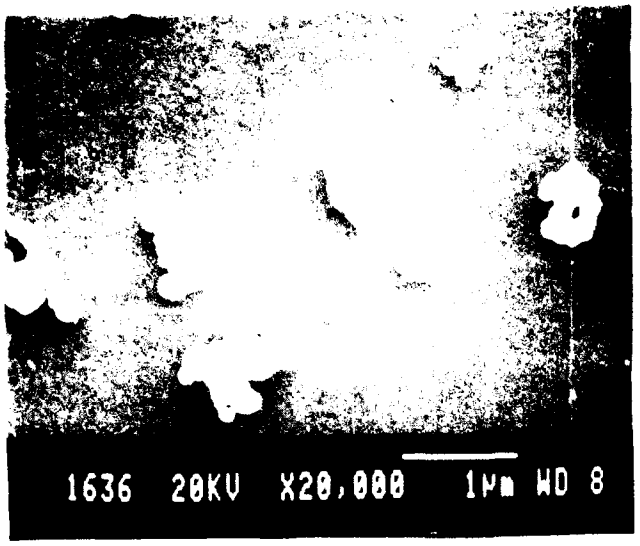

4-4P

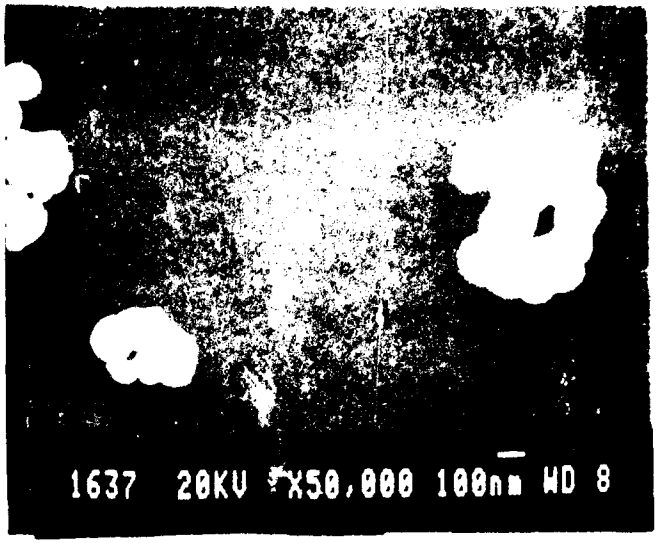

4-4P

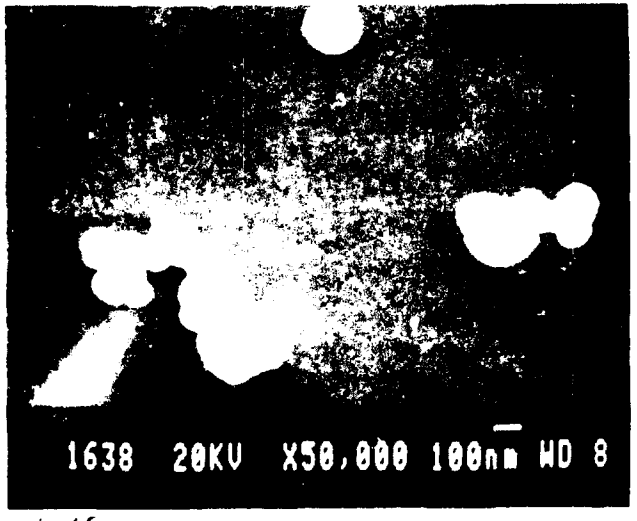

4-4P

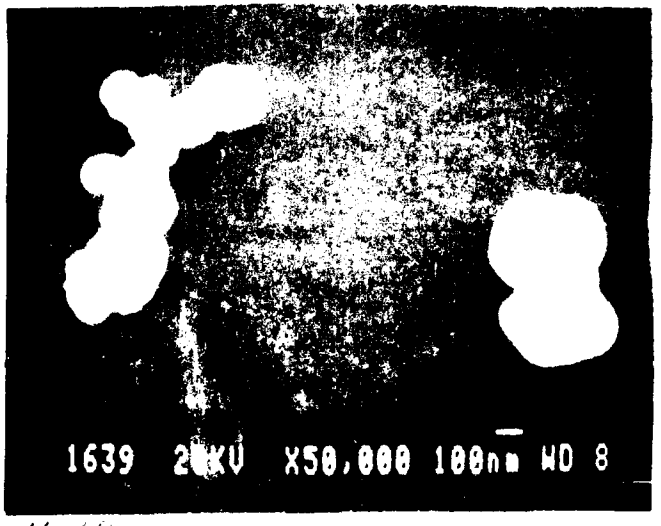

4-4P

5-1B

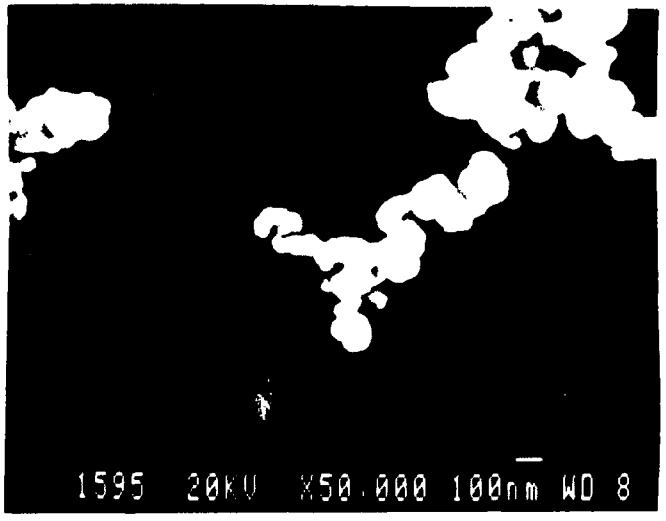

5-1B

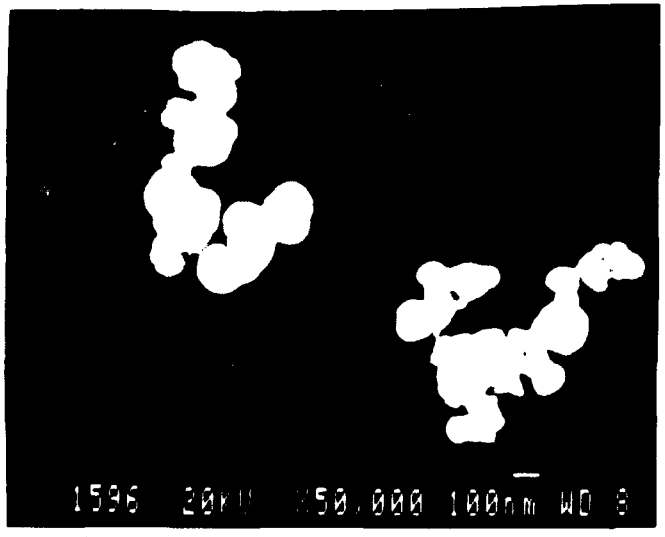

5-1B

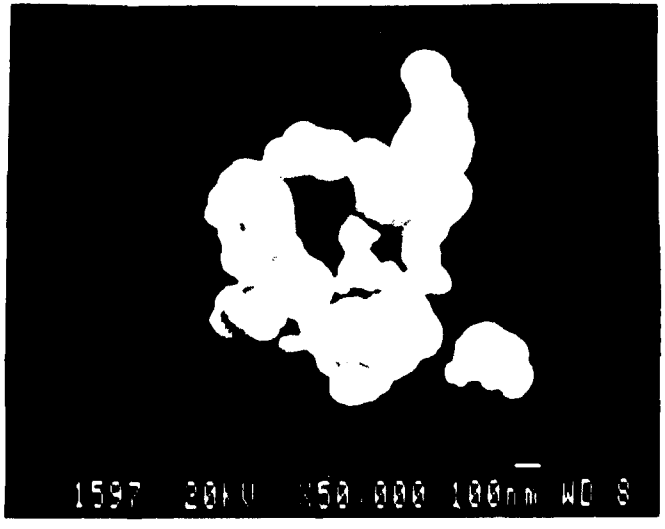

5-1B

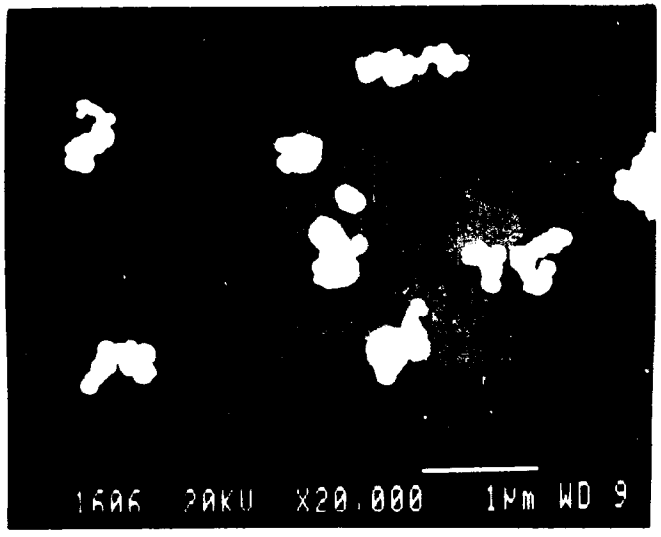

5-2B

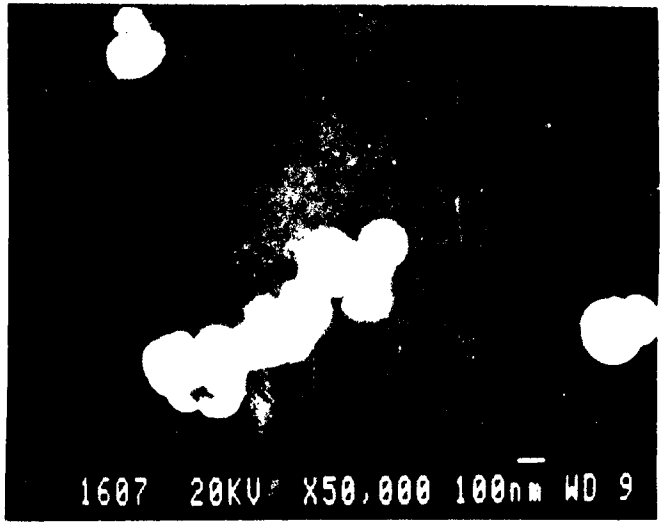

5-2B

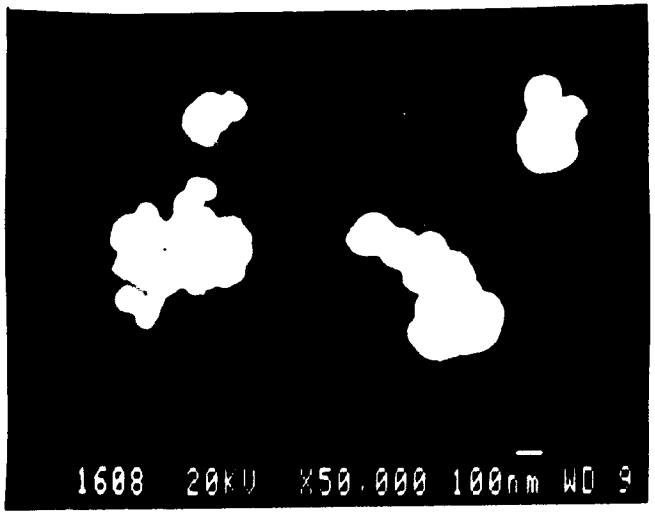

5-2B

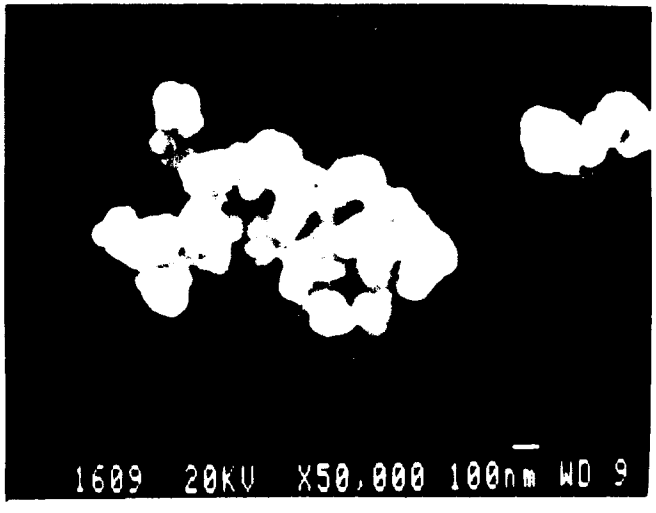

5-2B

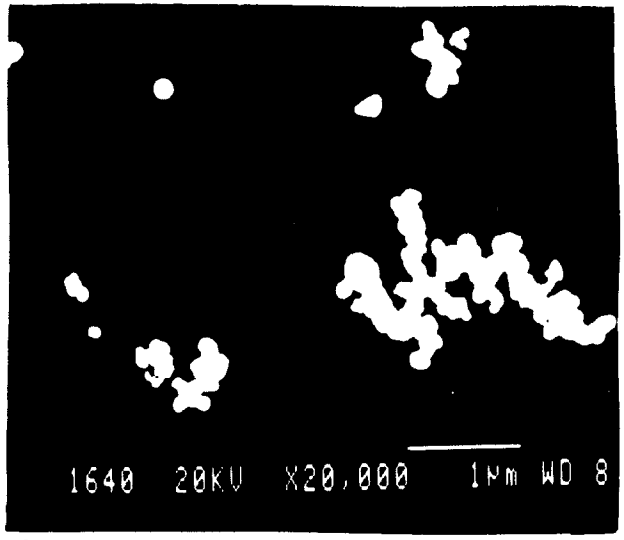

5-2P

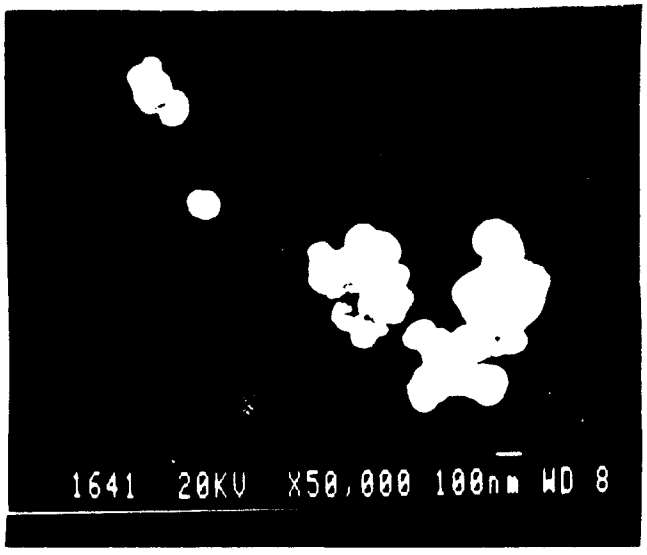

5-2P

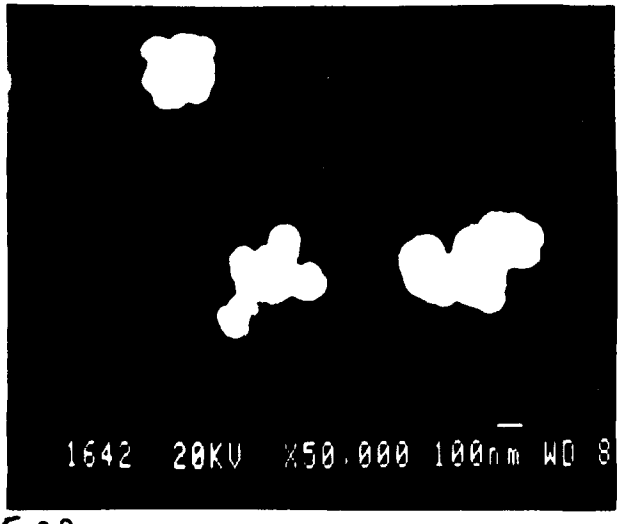

5-2P

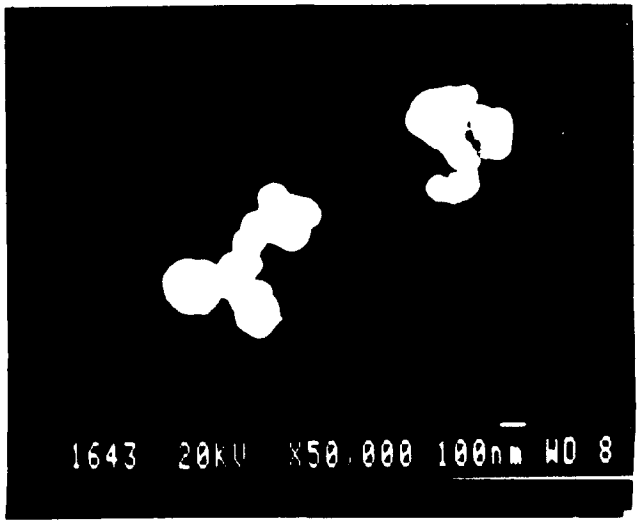

5-2P

5-3B

5-3B

5-3B

5-3B

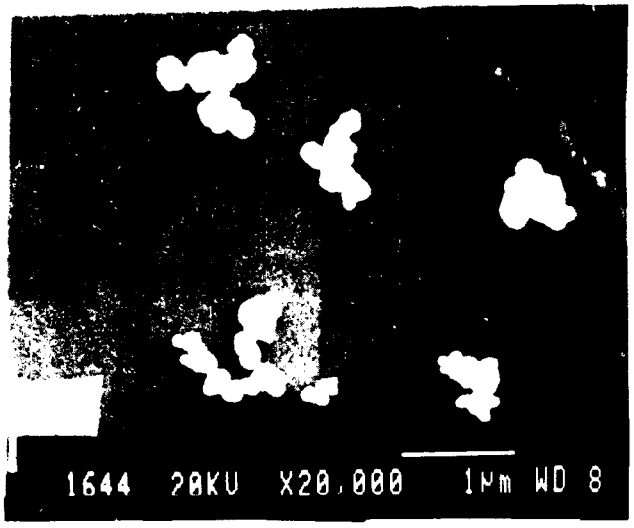
1644 20KU X20,000 1µm WD 8

-4B

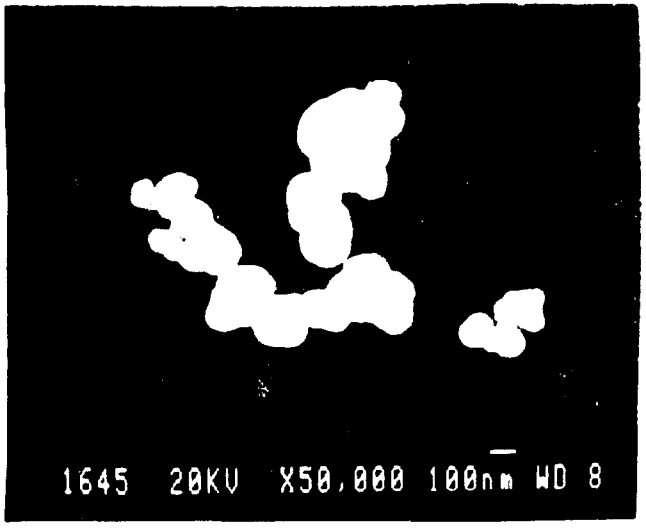
1645 20KU X50,000 100nm WD 8

5-4B

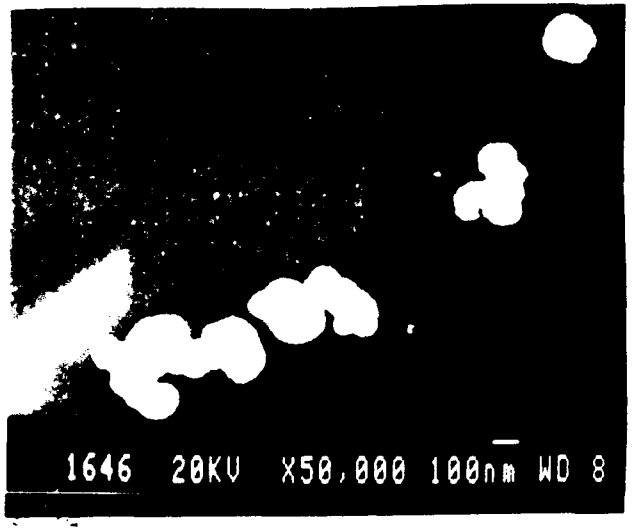
1646 20KU X50,000 100nm WD 8

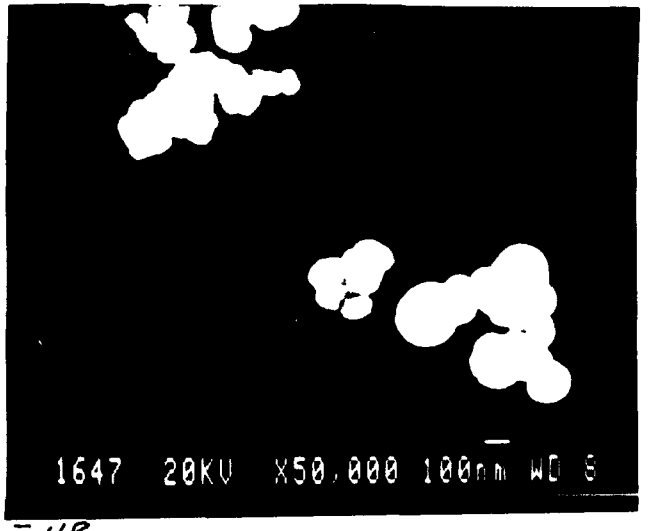
1647 20KU X50,000 100nm WD 8

5-4B

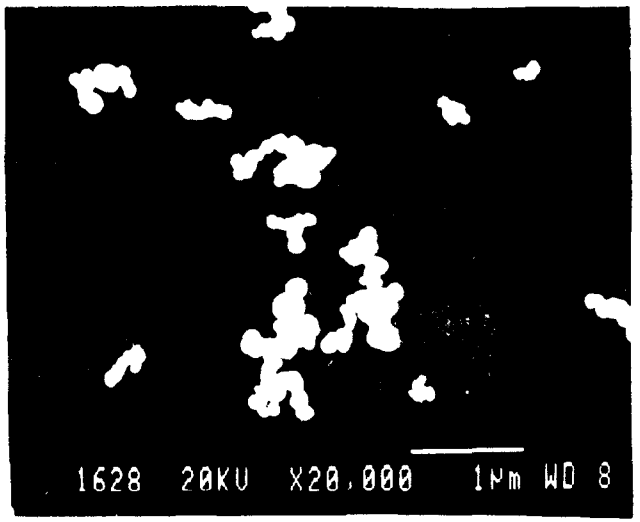

5-5B

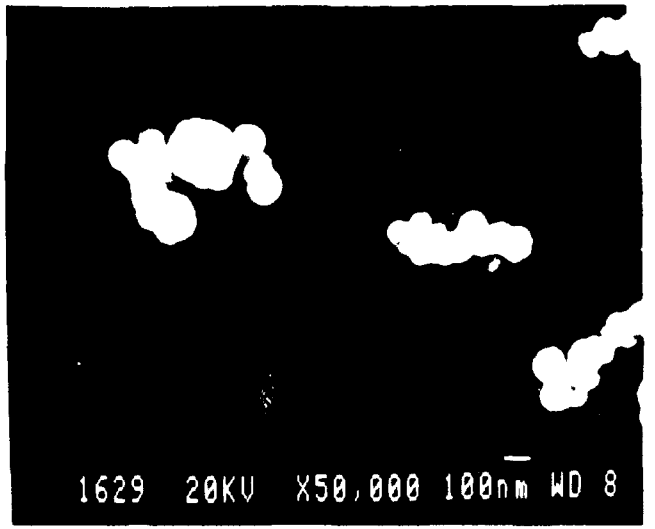

5-5B

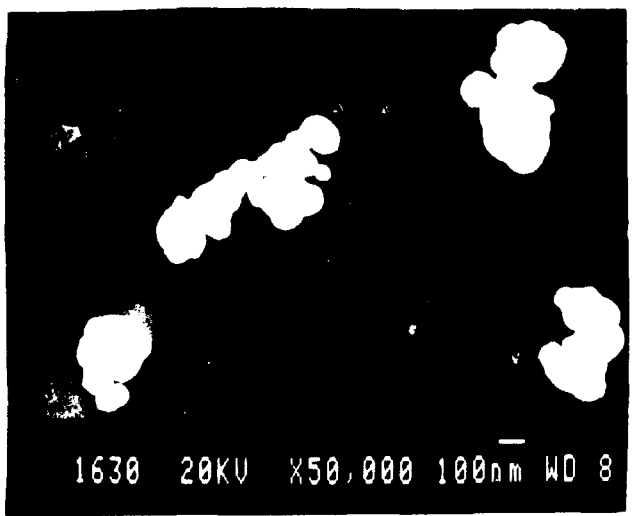

-5B

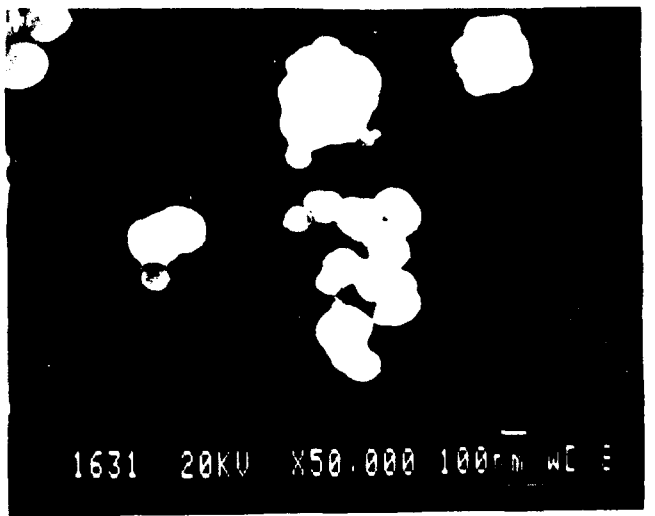

5-5B

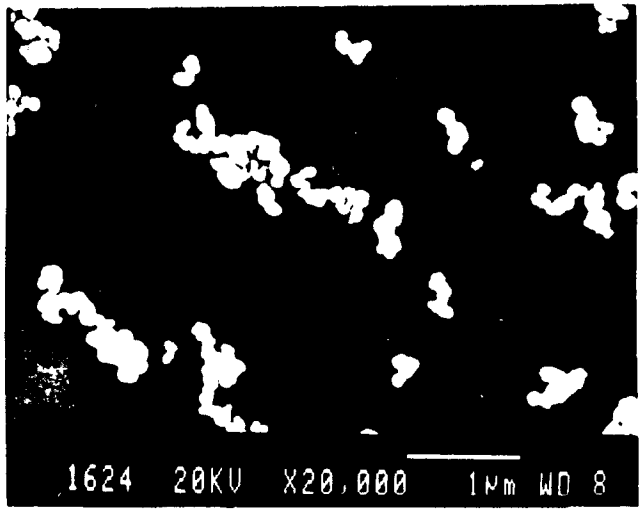

5.5B

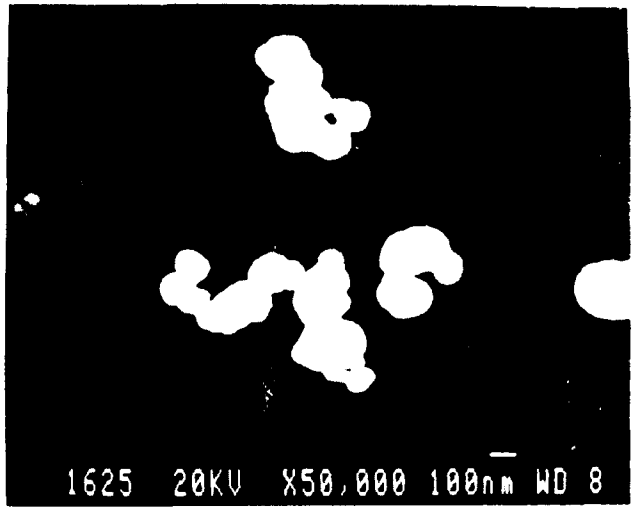

5.6B

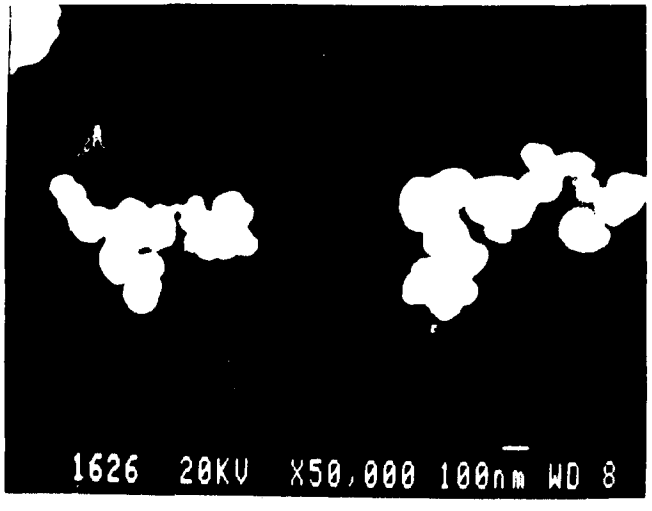

5.7B

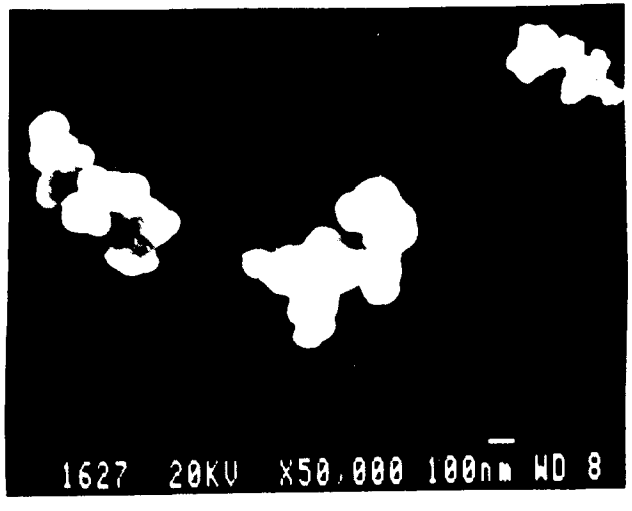

5.8B

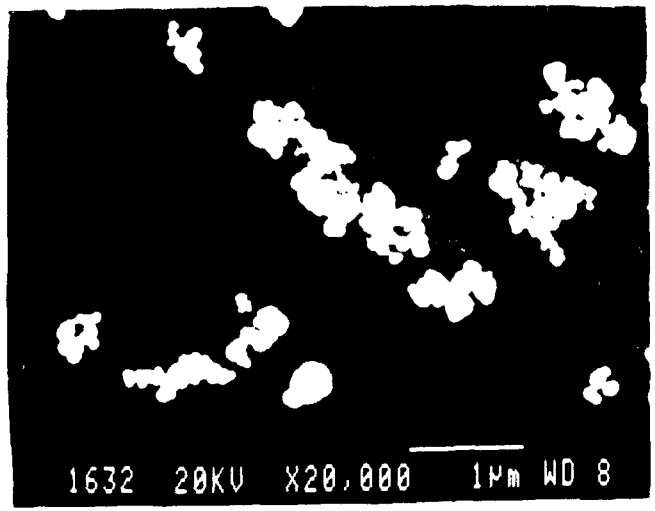

5-6P

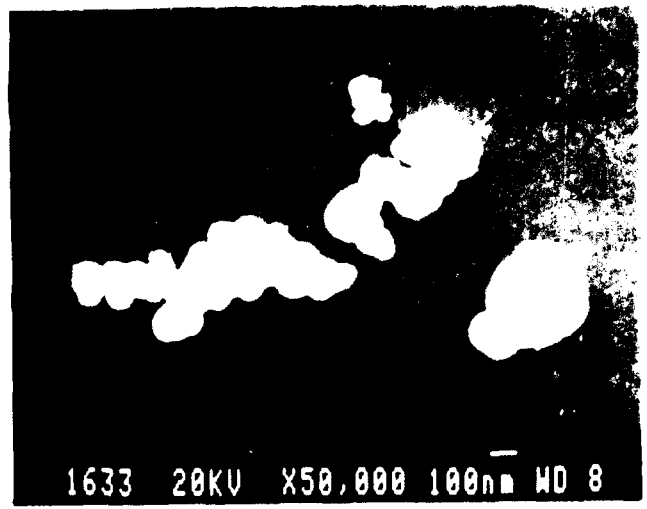

5-6P

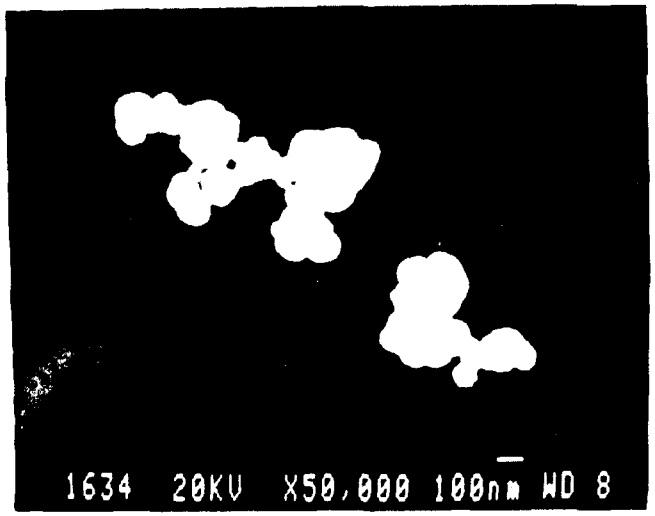

5-6P

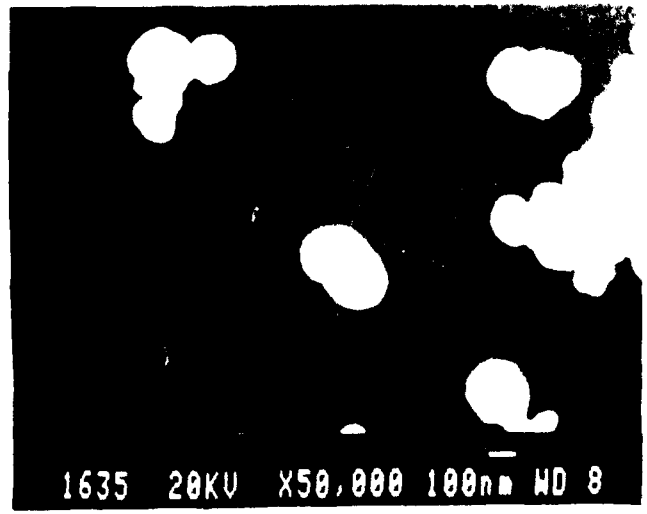

5-6P

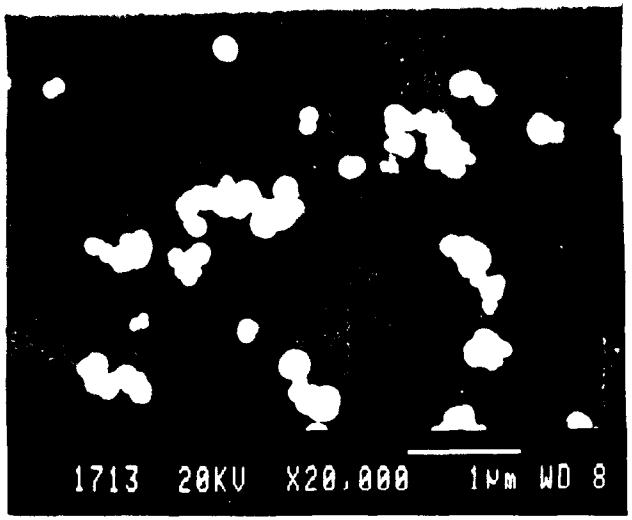
1713 20KV X20,000 1µm WD 8

6-1B

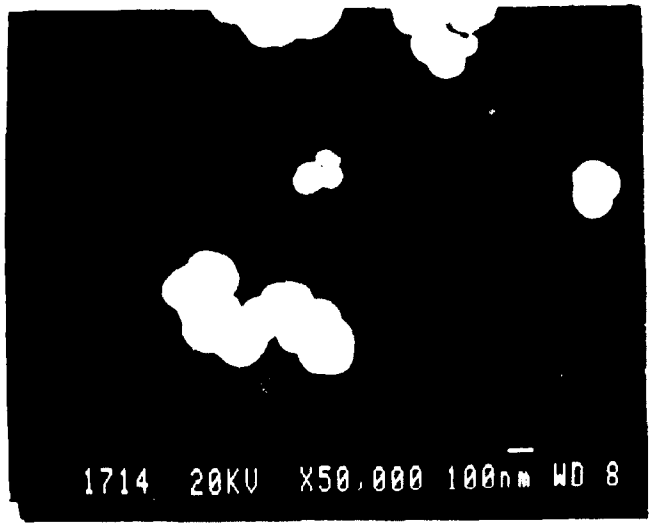
1714 20KV X50,000 100nm WD 8

6-1B

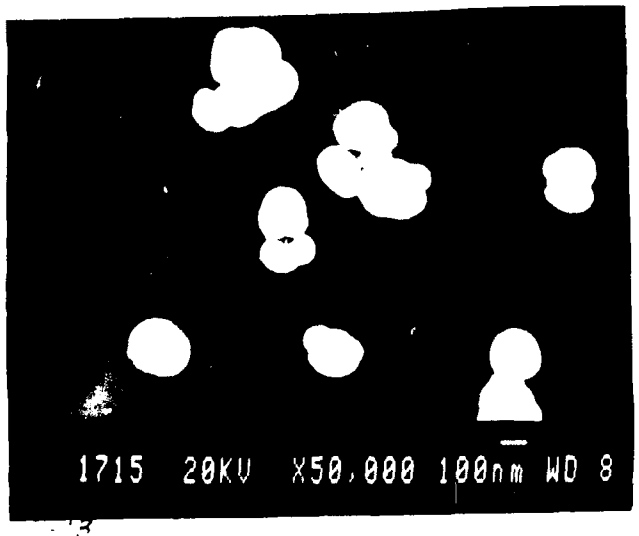
1715 20KV X50,000 100nm WD 8

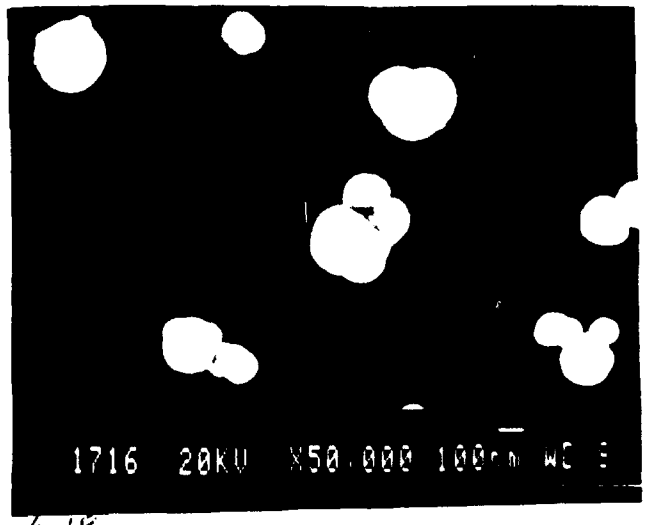
1716 20KV X50,000 100nm WD 8

6-1B

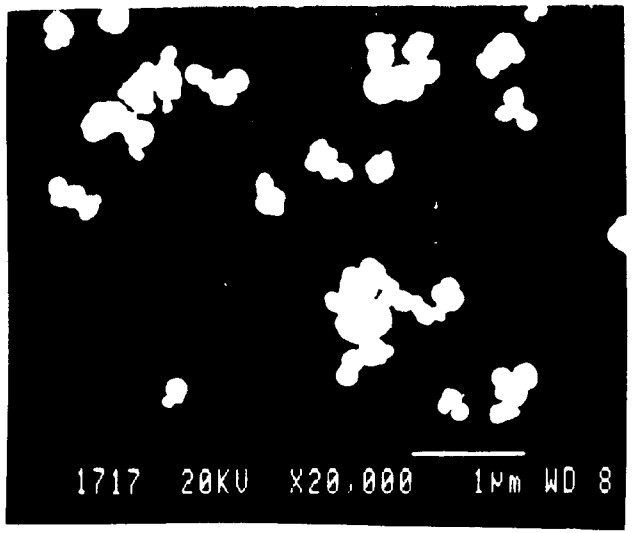

6-2B

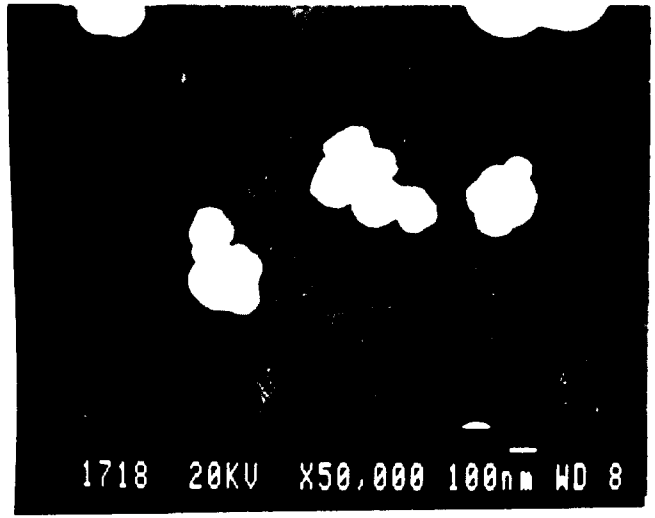

6-2B

250

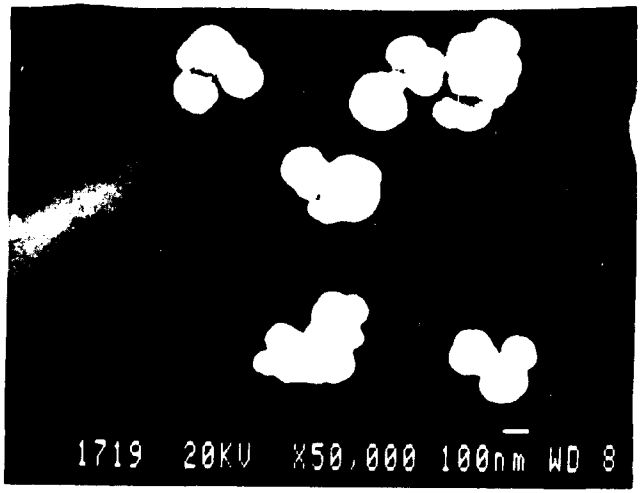

6-2A

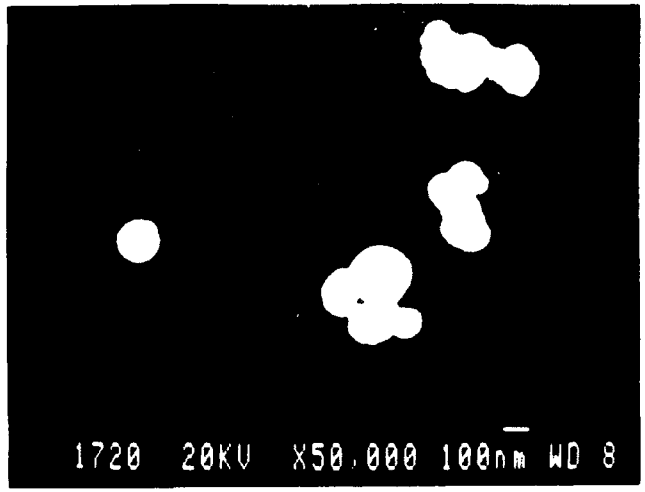

6-2A

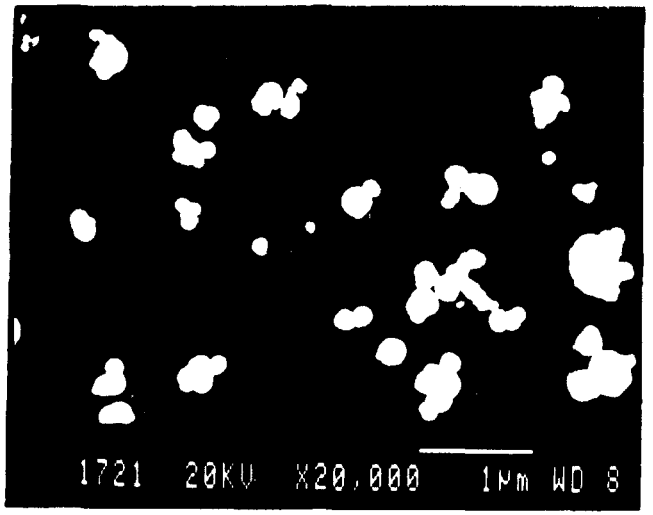

6-3B

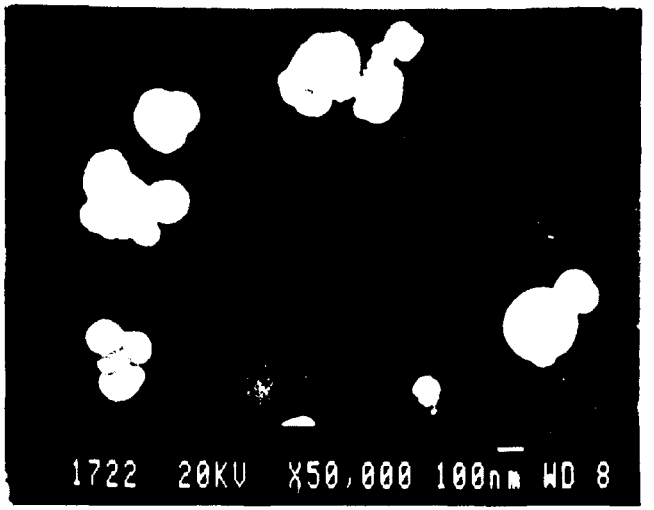

6-3B

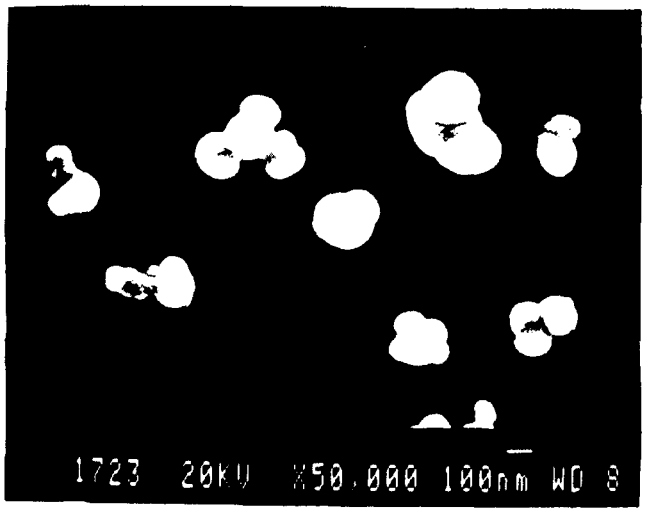

6-3B

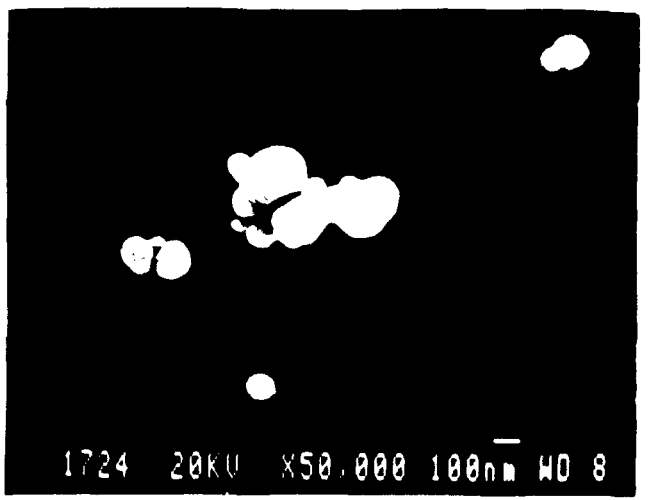

6-3B

231

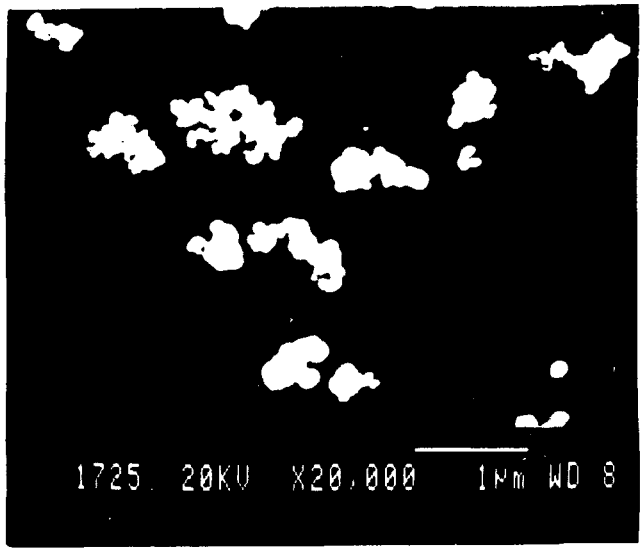

6-3P

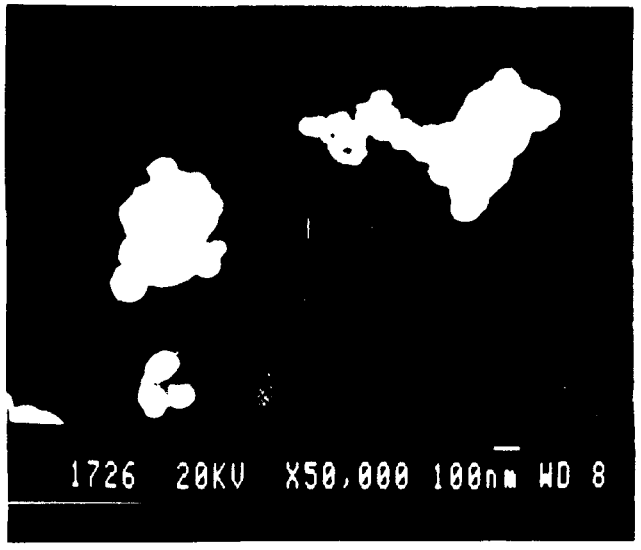

6-3P

232

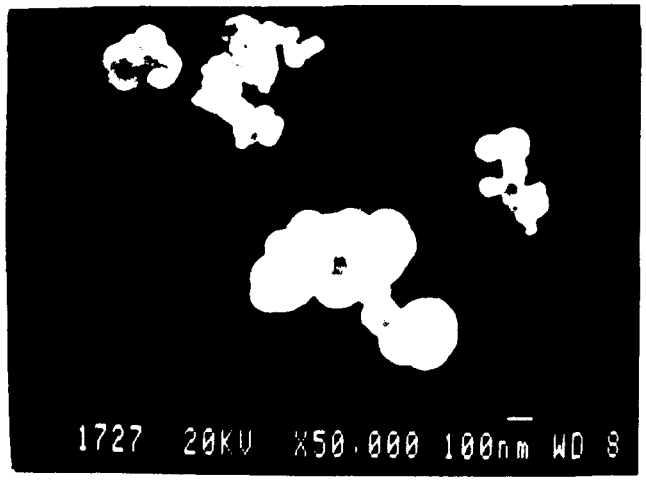

6-3P

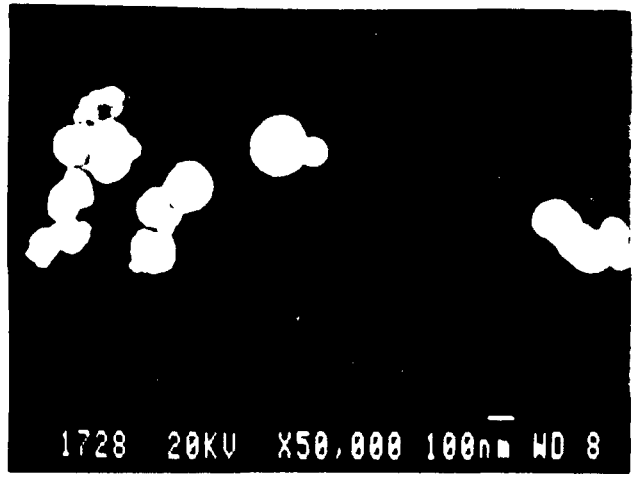

6-3P

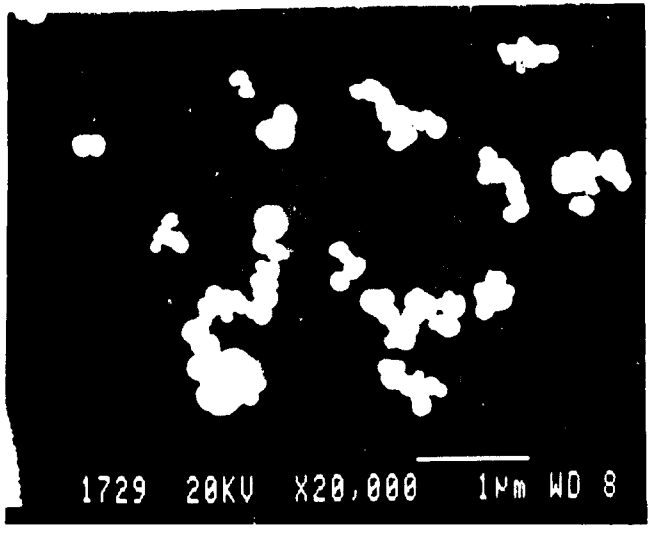

6-4B

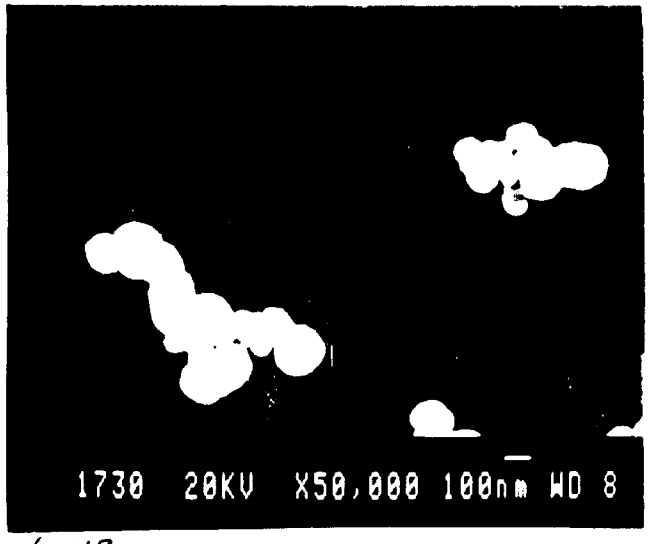

6-4B

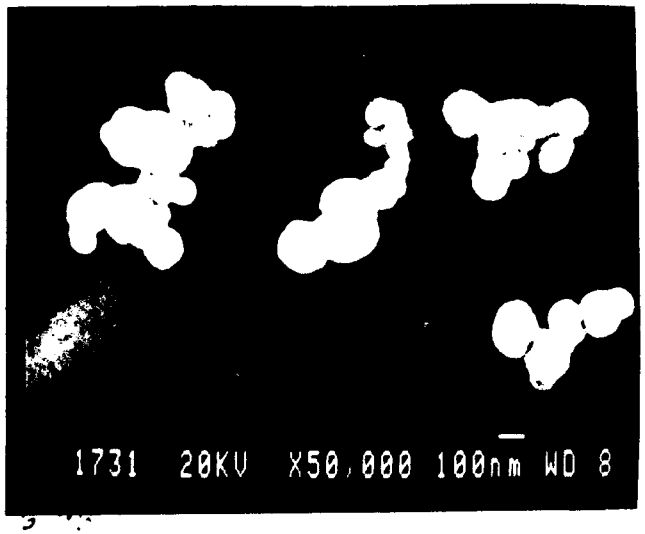

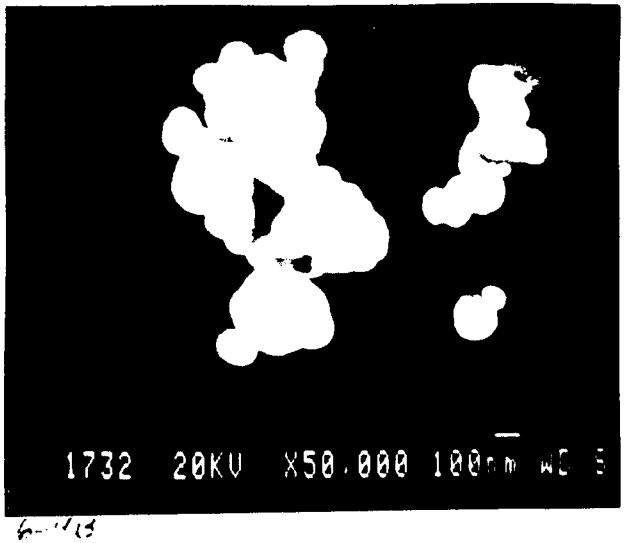

6-4B

233

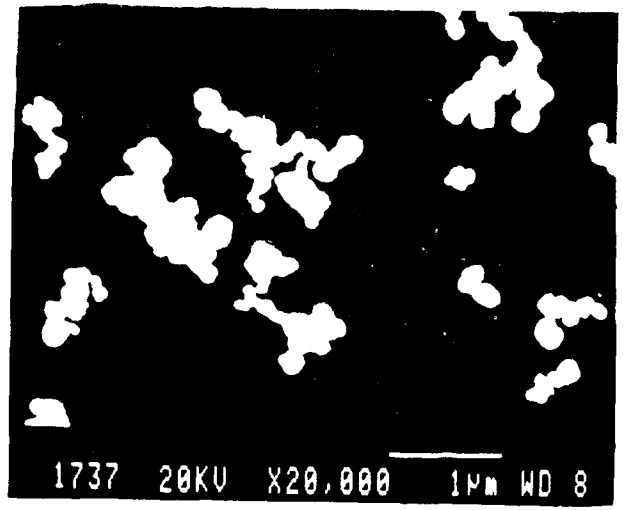
1737 20KV X20,000 1µm WD 8

6-5B

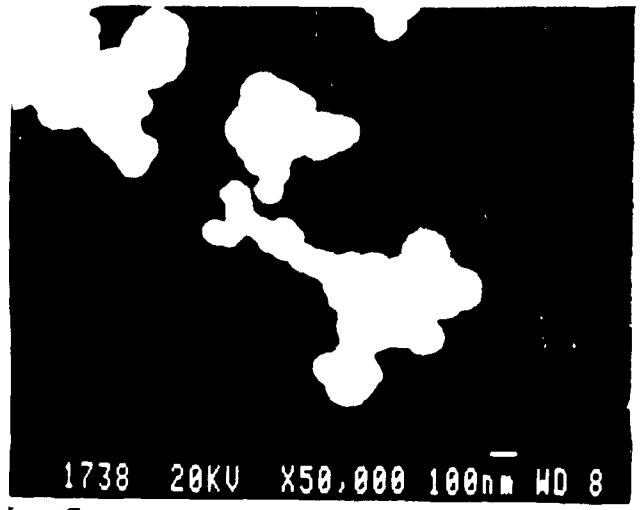
1738 20KV X50,000 100nm WD 8

6-5B

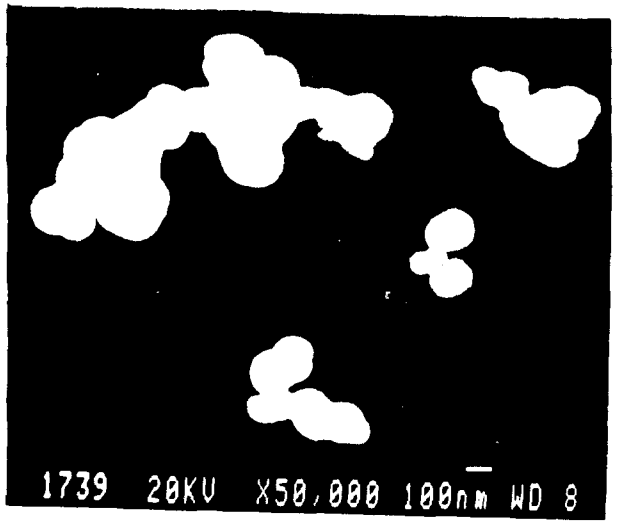
1739 20KV X50,000 100nm WD 8

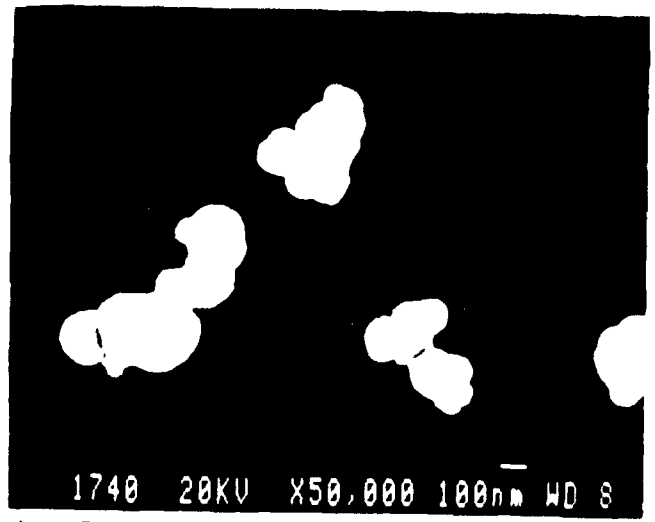
1740 20KV X50,000 100nm WD 8

6-5B

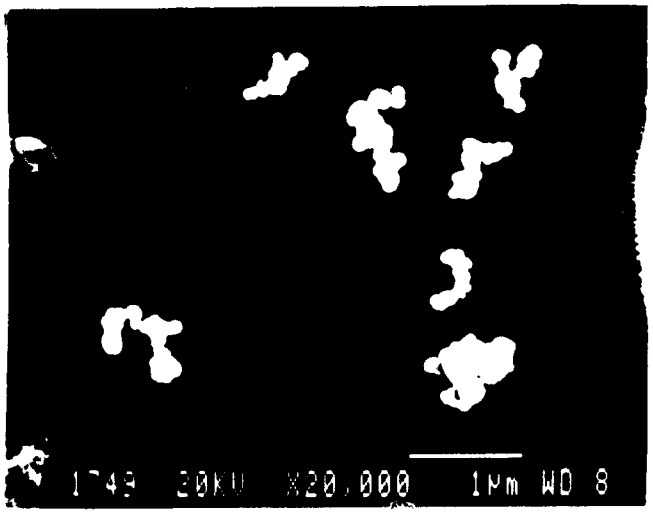

6-5P

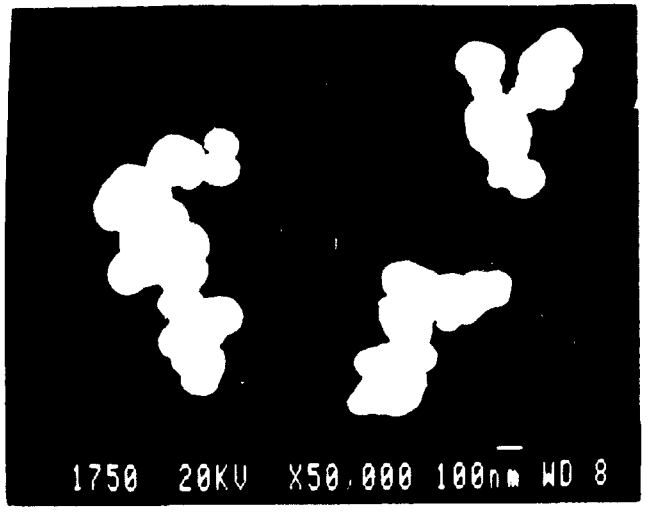

6 5P

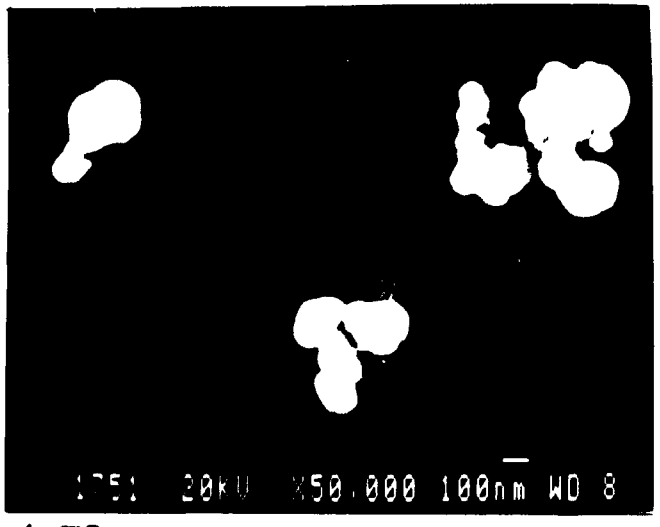

6-5P

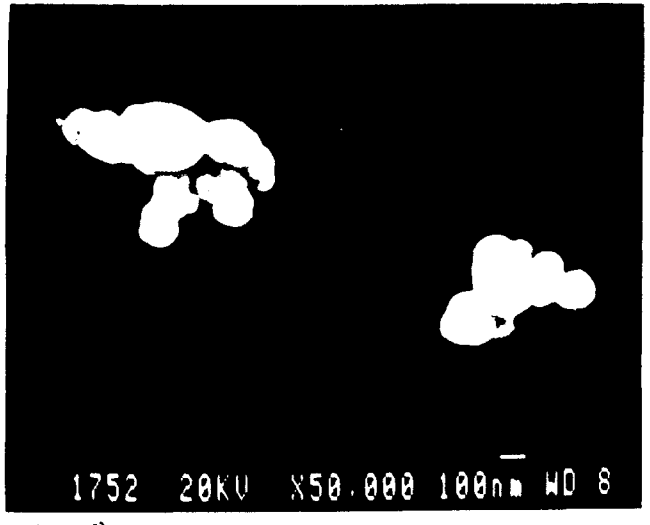

6-5P

a-6B

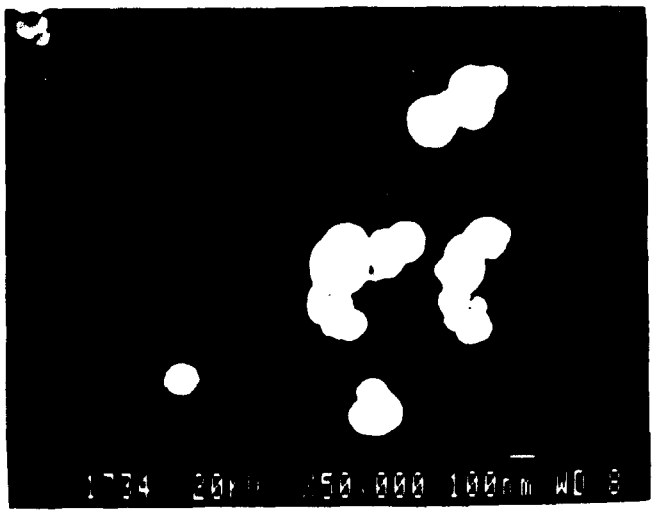

b-6B

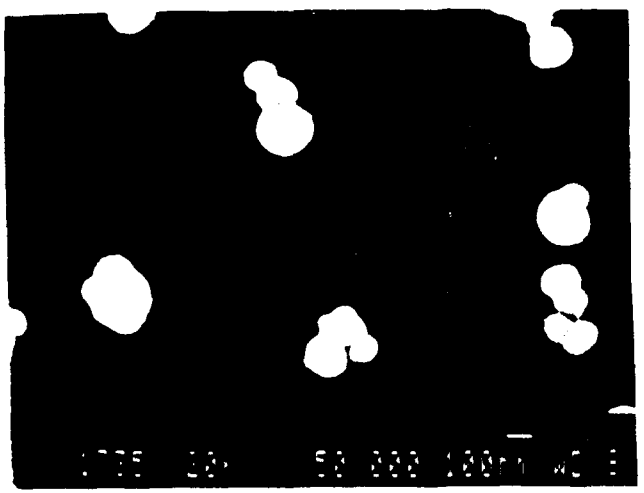

c-6B

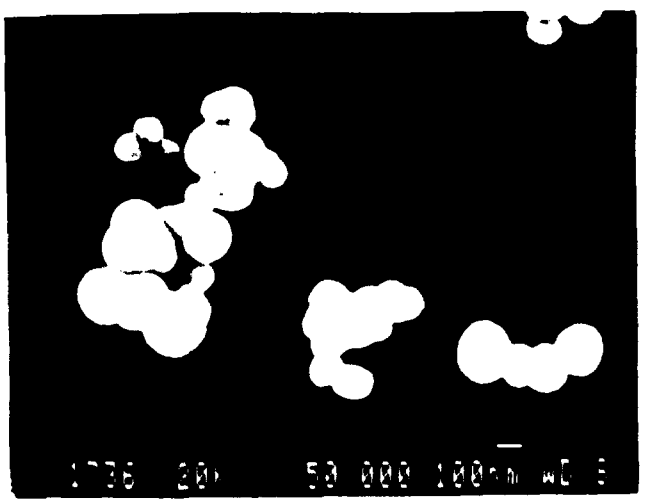

d-6B

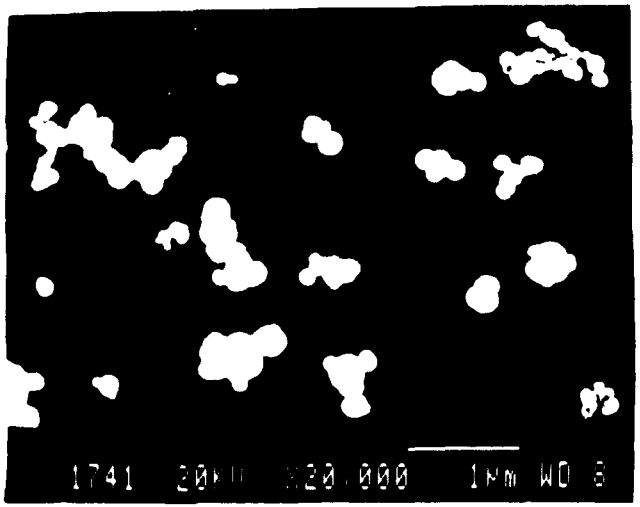

6-7B

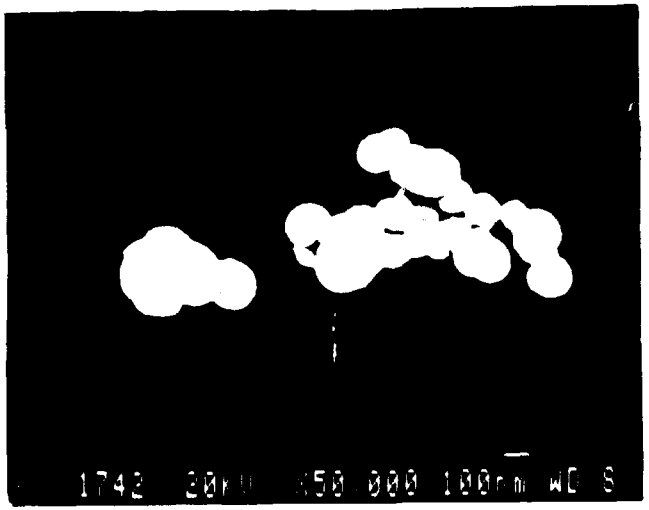

6-7B

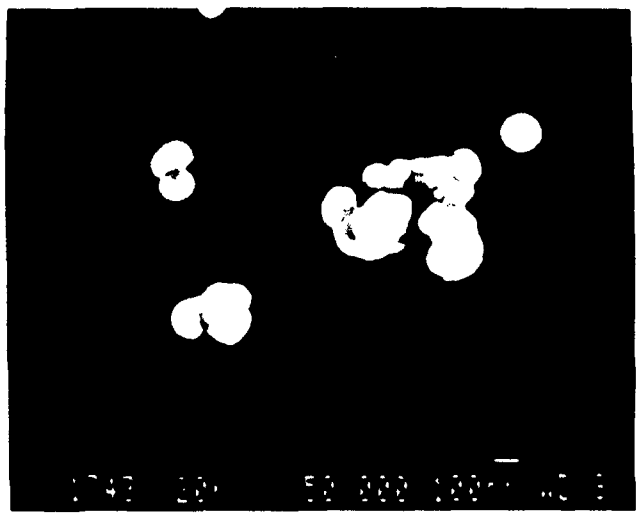

6-7B

6-7B

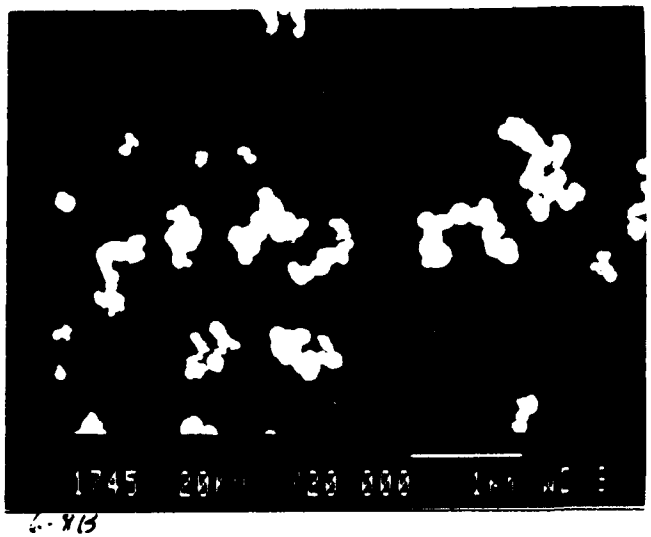

6-8B

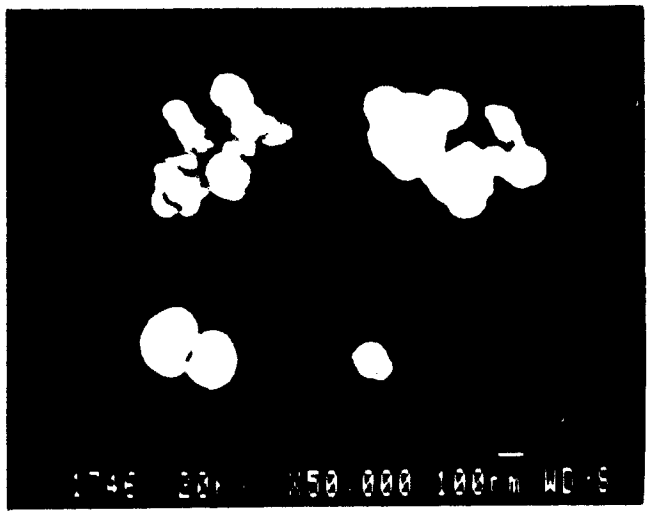

6-8B

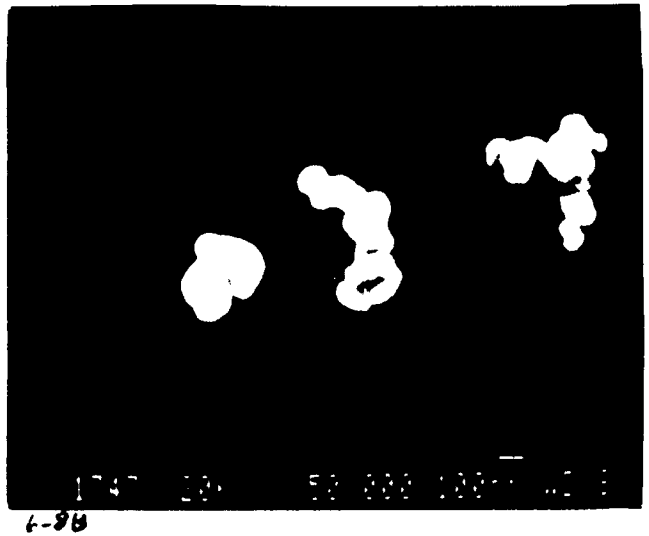

6-8B

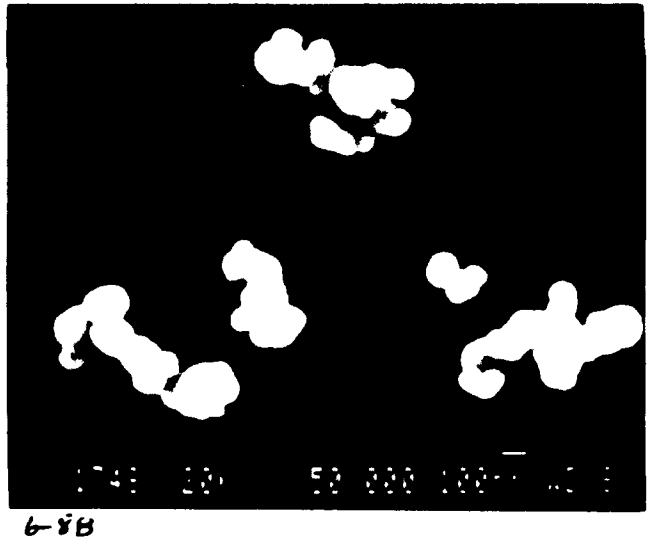

6-8B

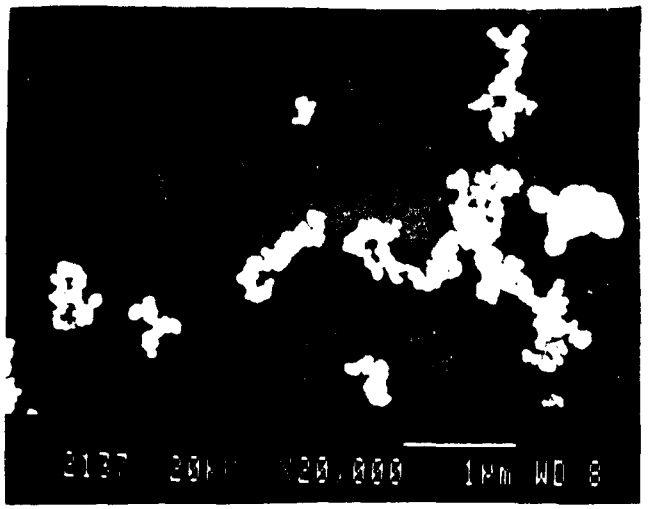

7-PB

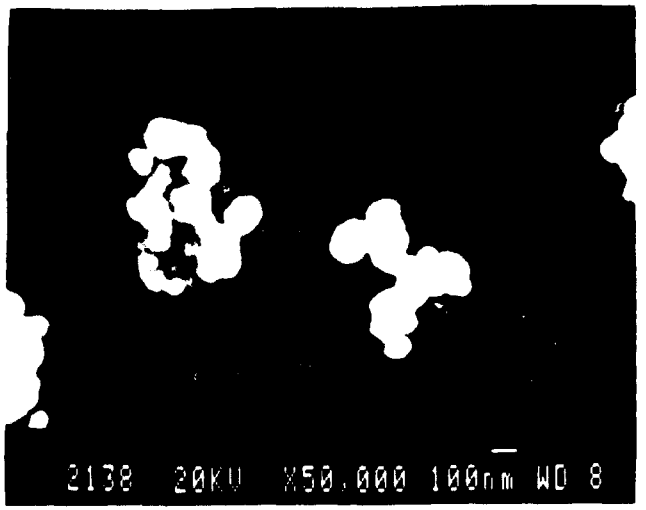

7-PB

7-PB

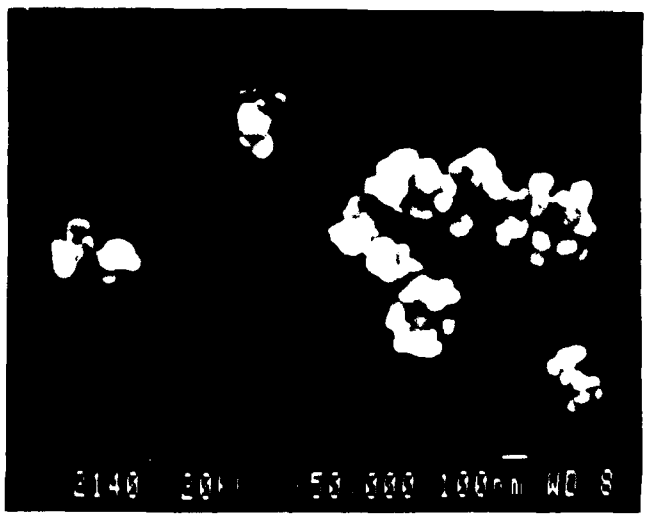

7-PB

7-1B

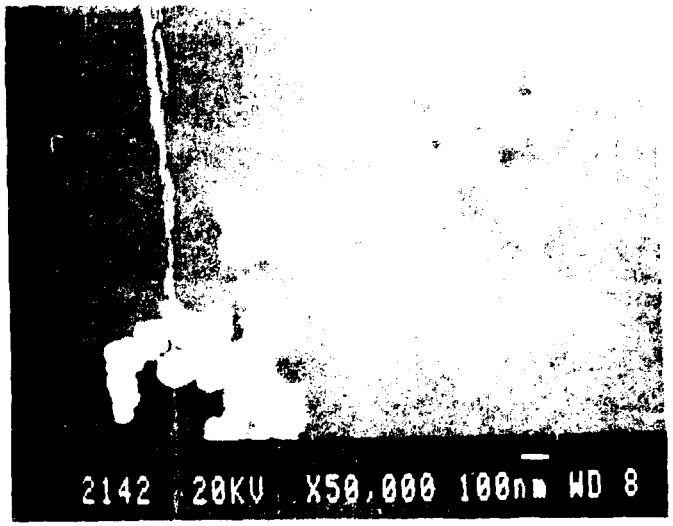

7-1B

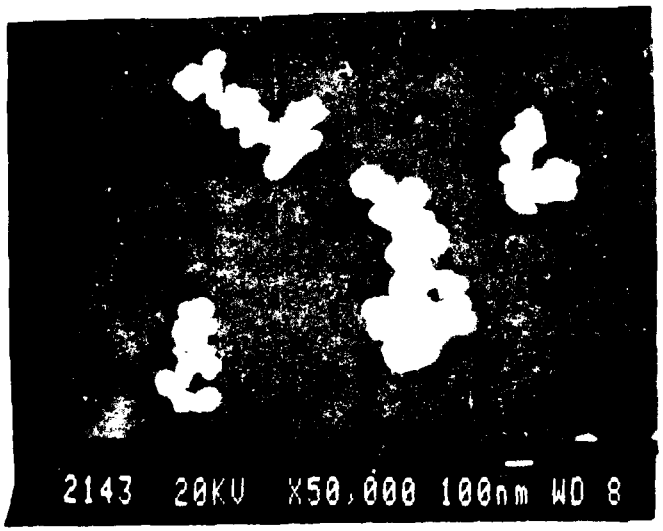

7-1B

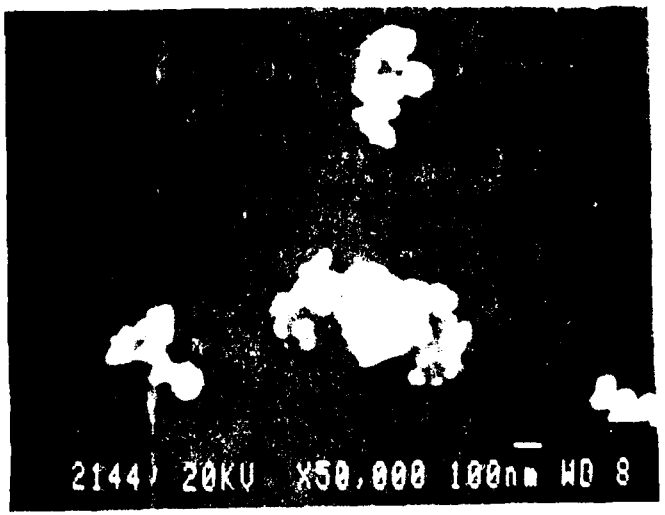

7-1B

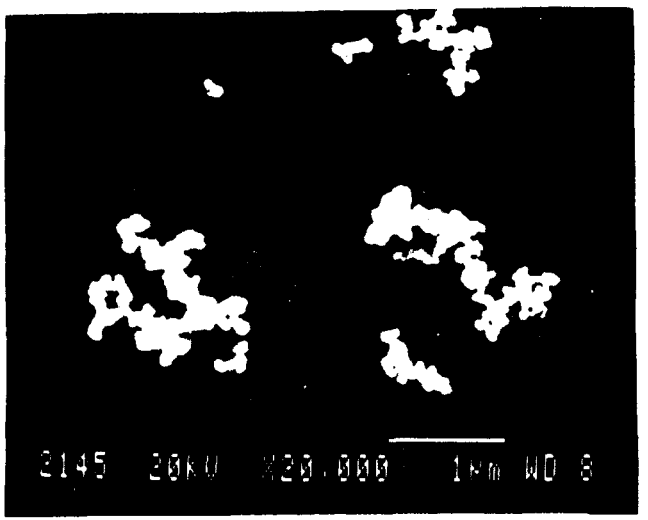

7-2B

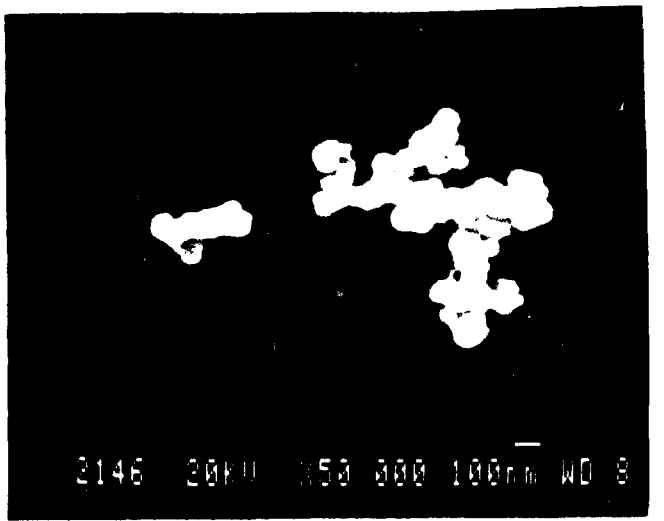

7-2B

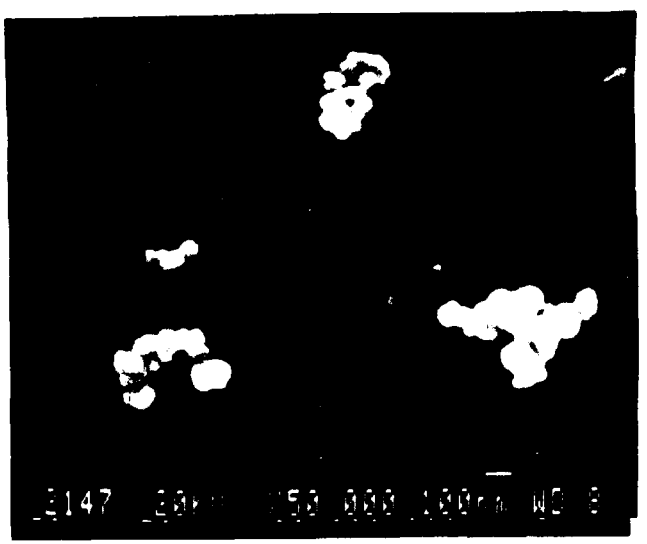

7-2B

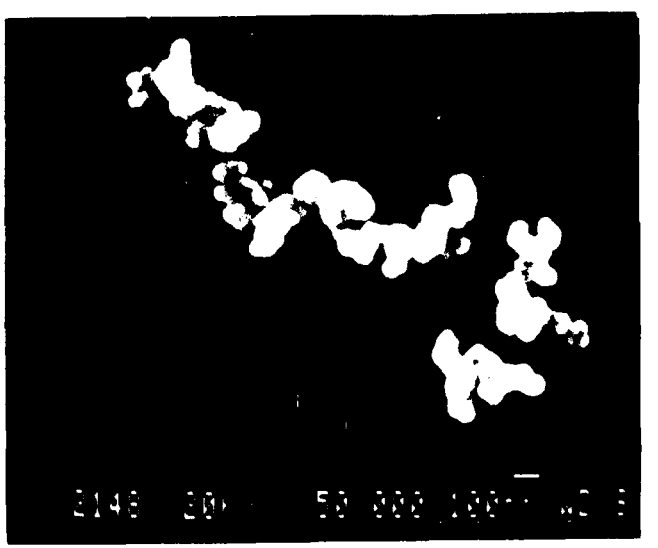

7-2B

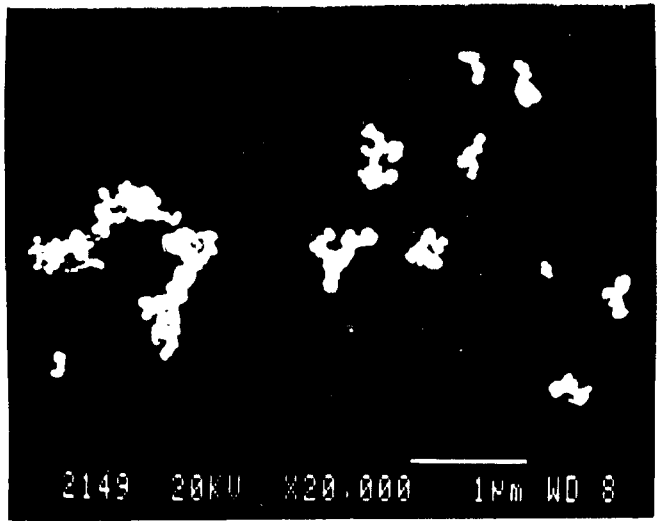

7-2P

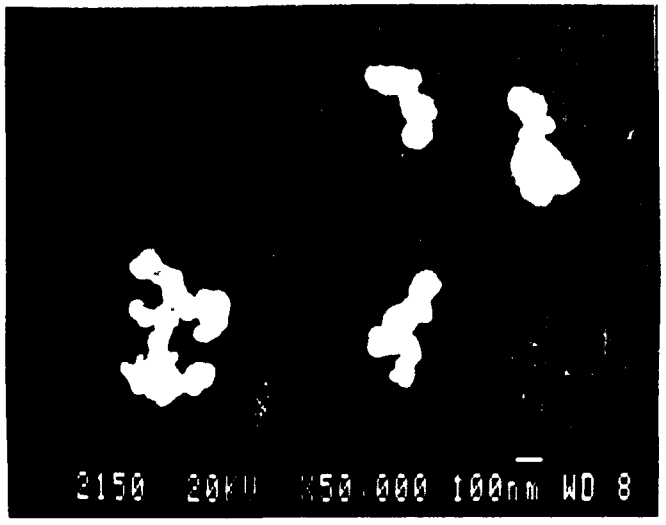

7-2P

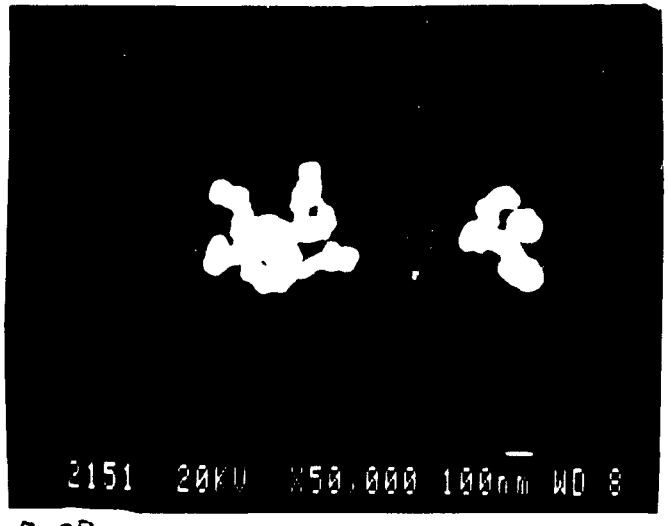

7-2P

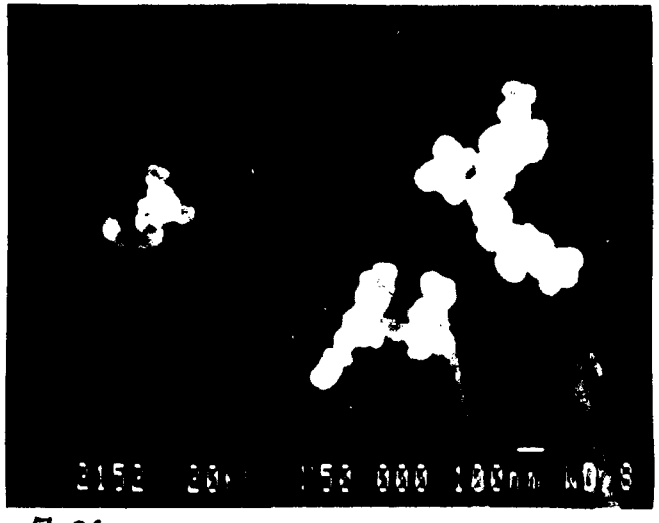

7-2P

242

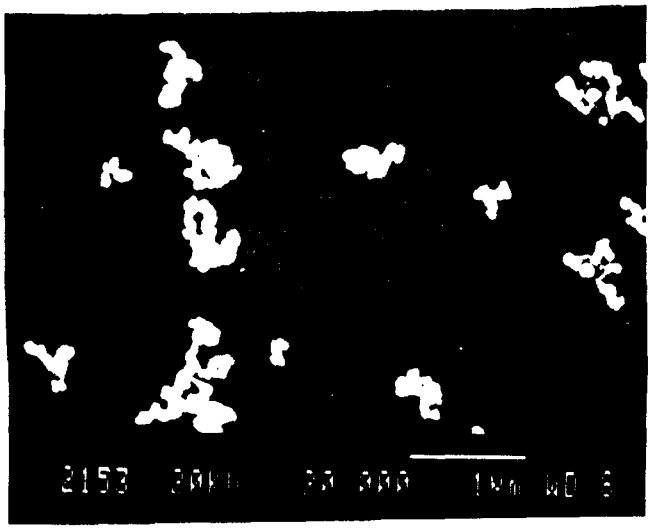

7-35

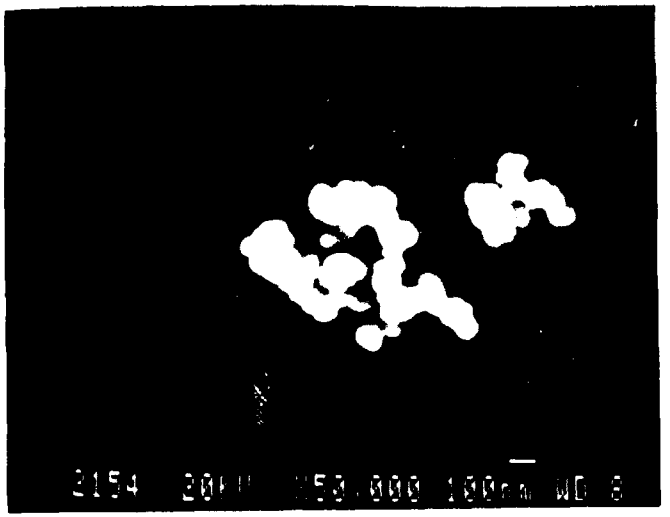

7-35

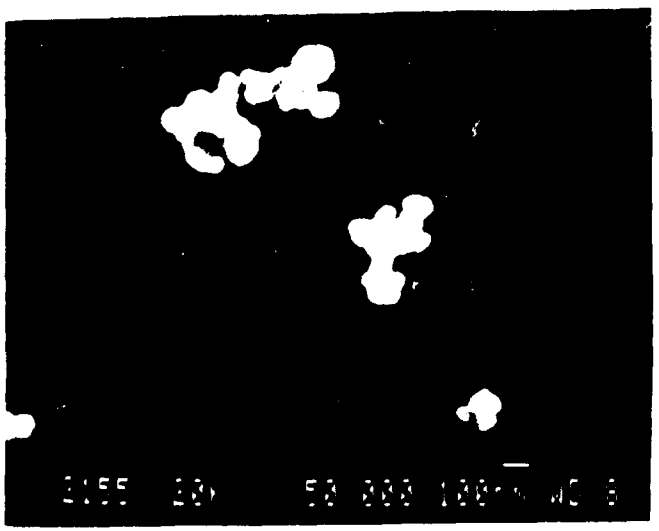

7-36

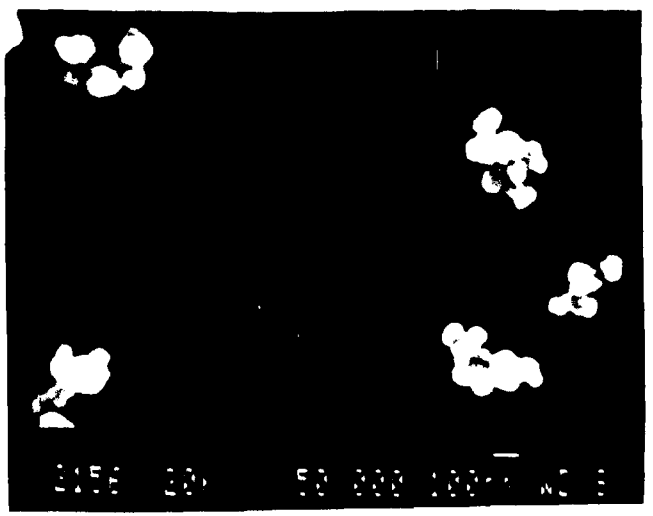

7-36

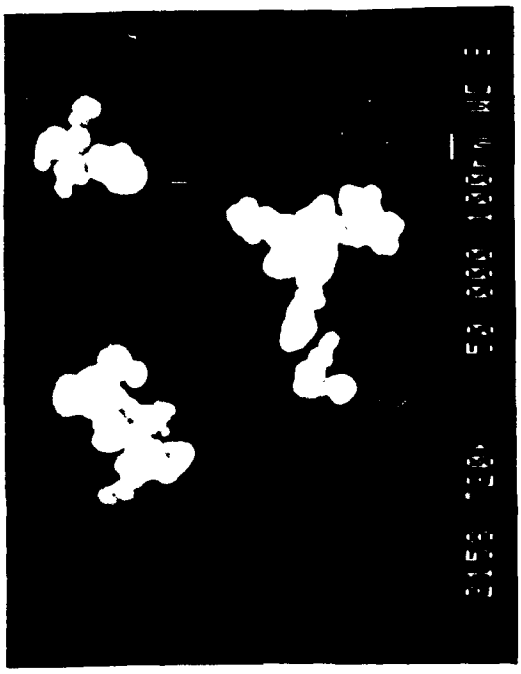

7-48

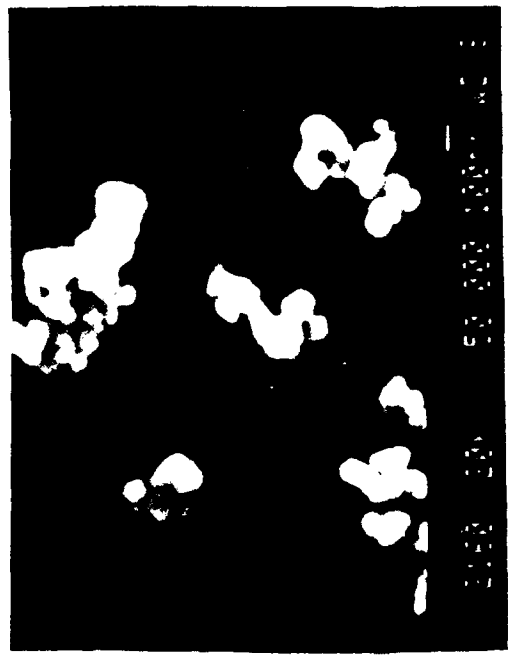

7-48

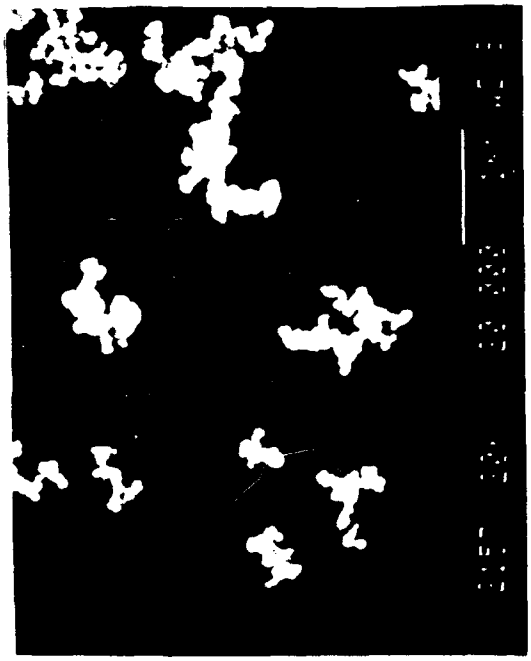

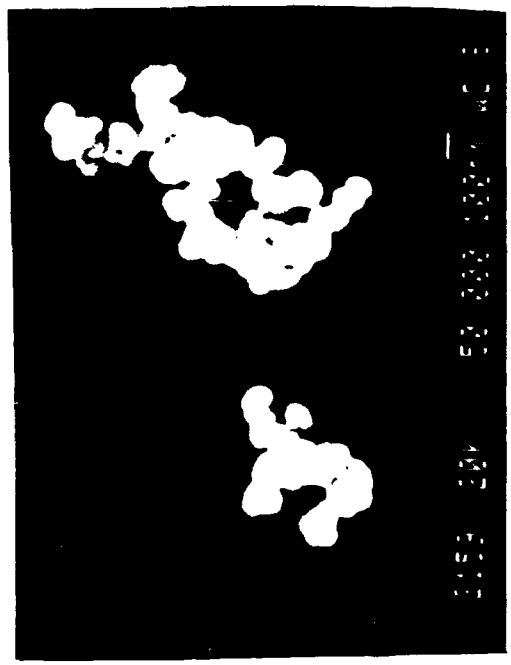

7-48

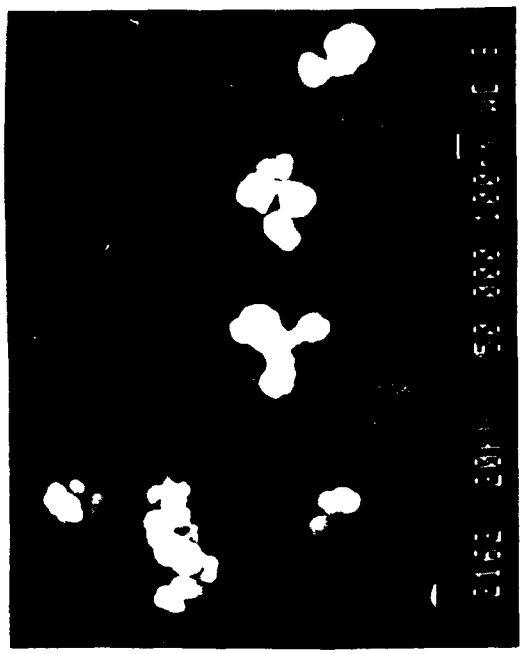

7-5B

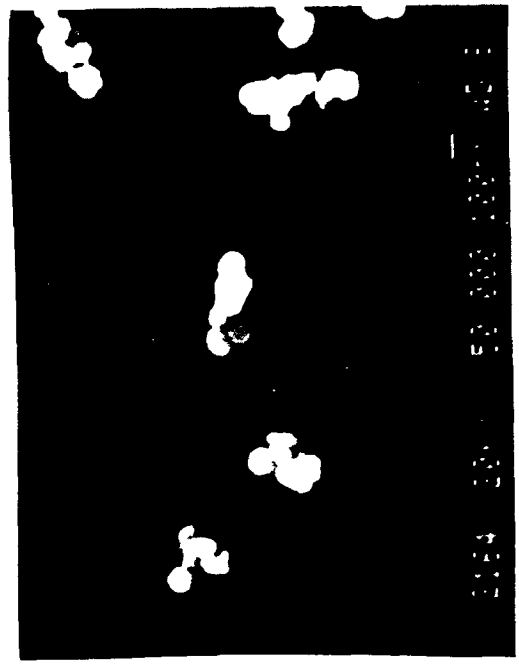

7-5A

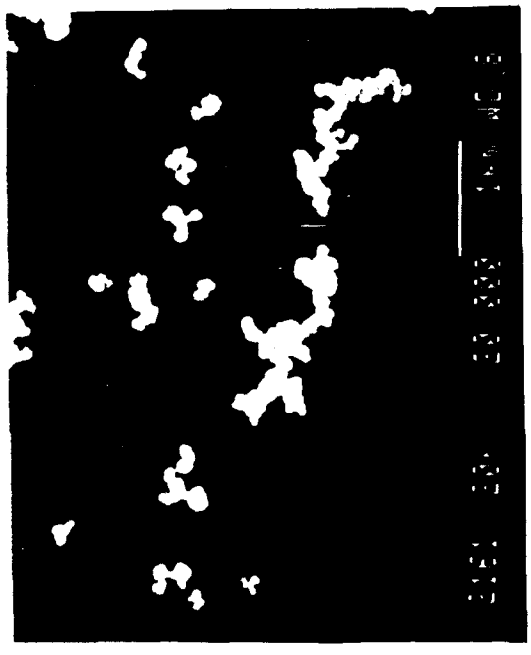

7-5D

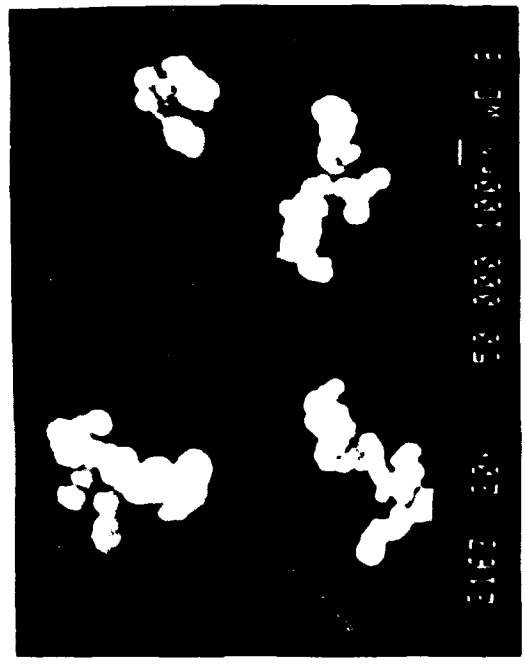

7-5C

2166 20KV X50,000 100nm WD 8

2168 20KV X50,000 100nm WD 8

2165 20KV X20,000 1μm WD 8

2167 20KV X50,000 100nm WD 8

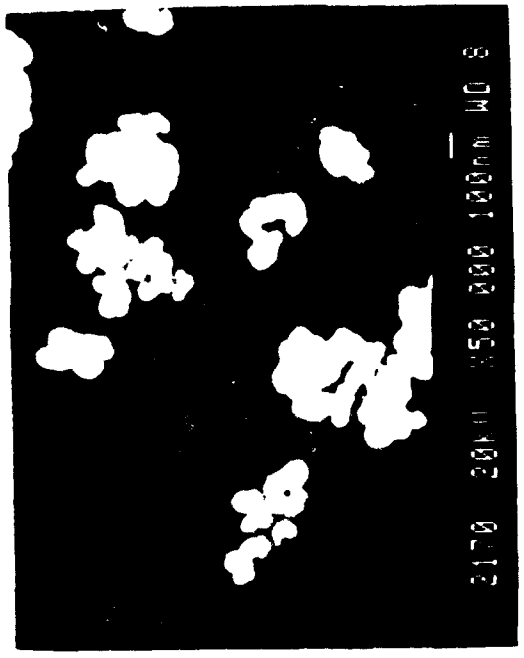

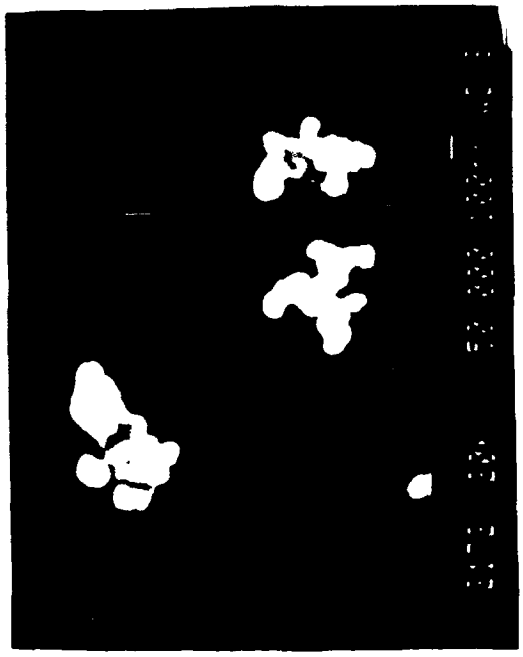

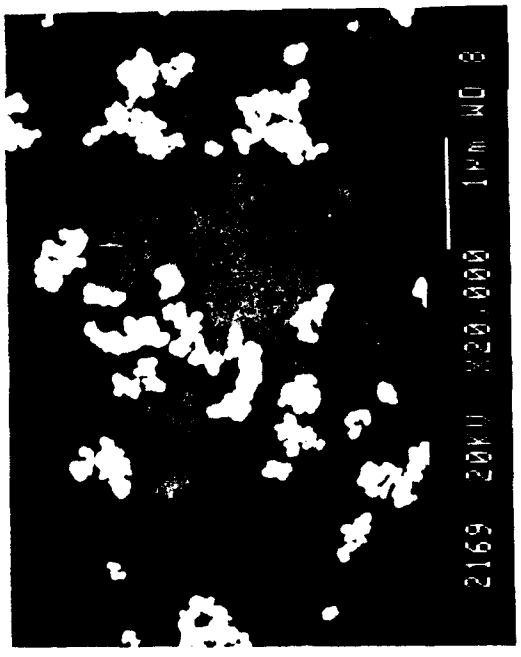

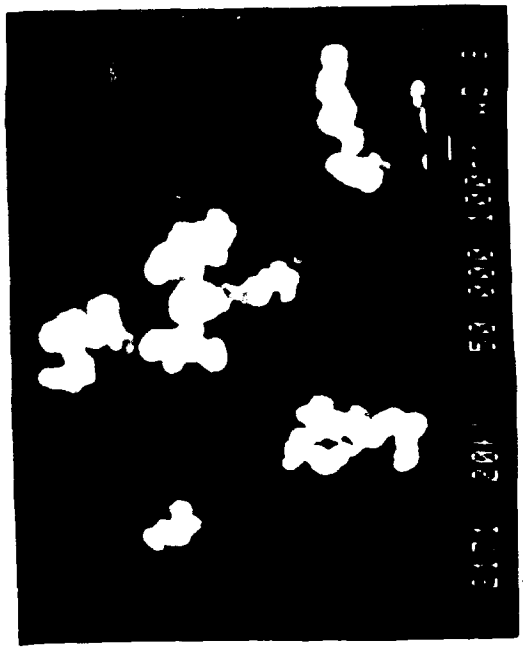

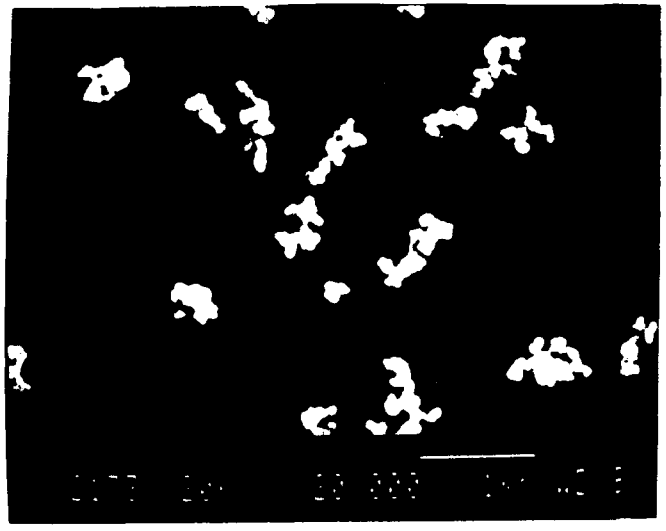

7-7B

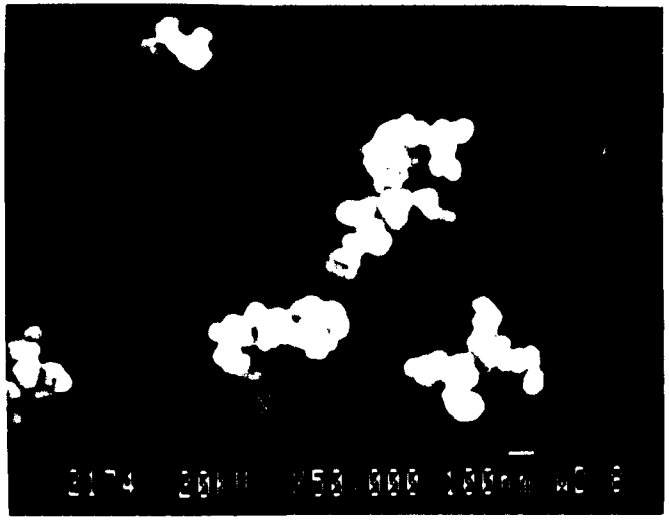

7-7B

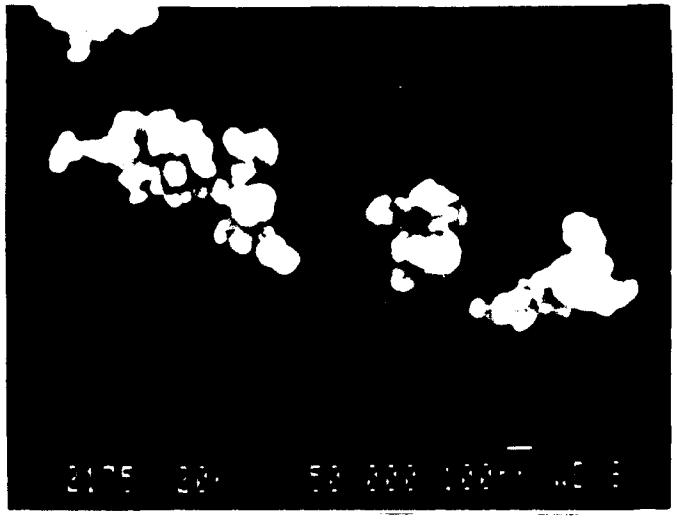

7-7B

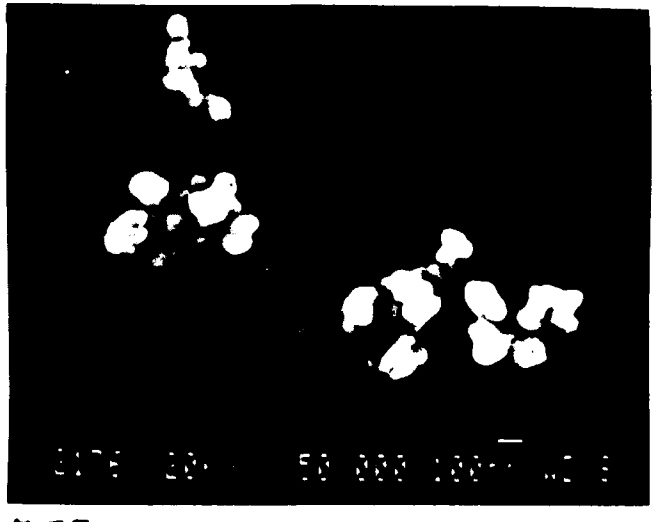

7-7B

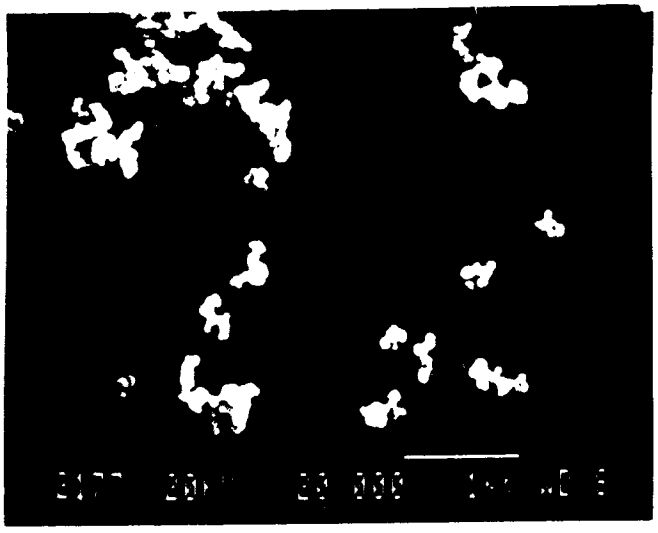

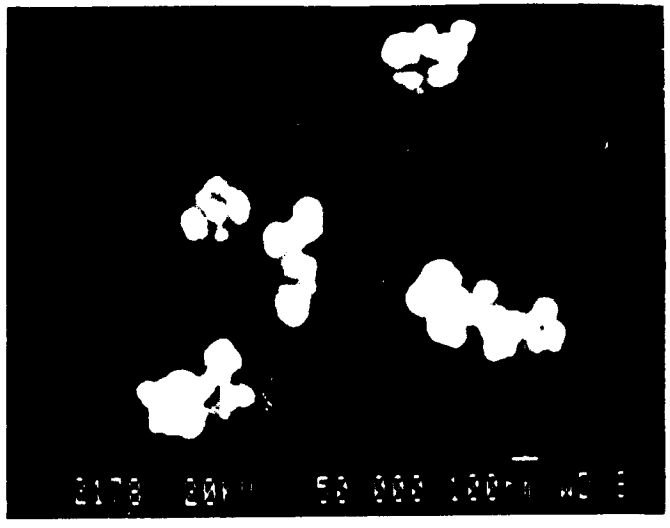

7-8B

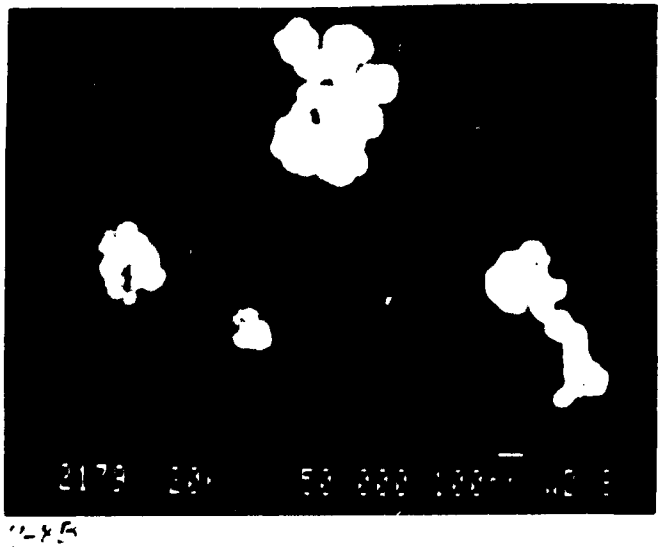

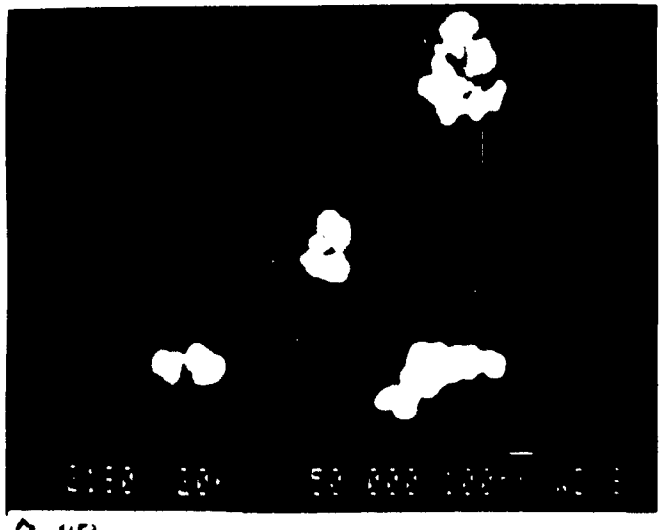

7-8B

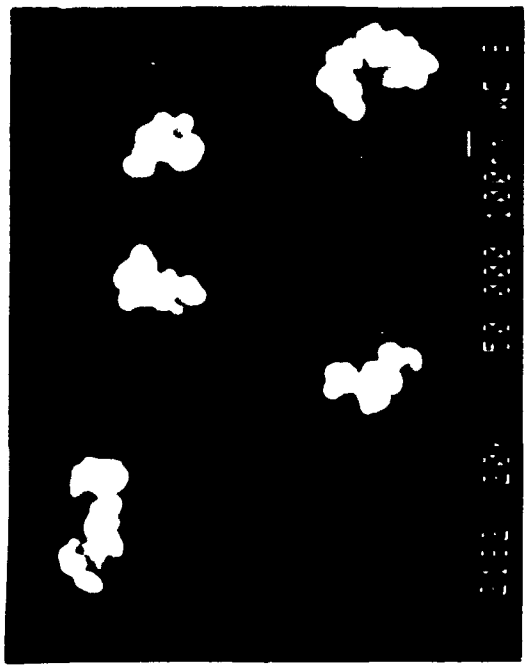

7-8P

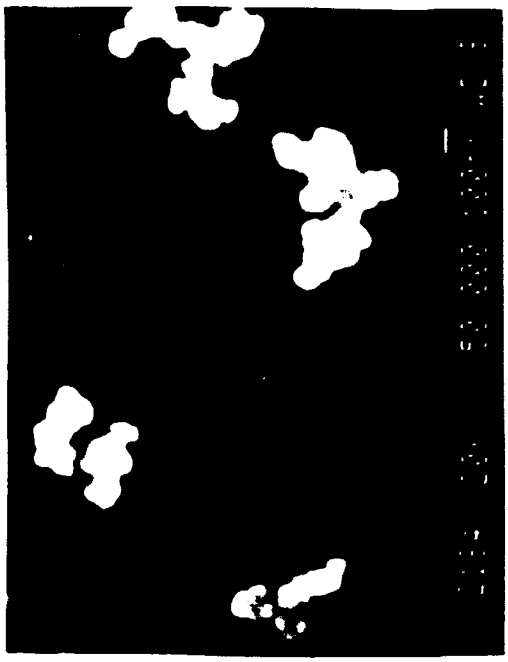

7-8P

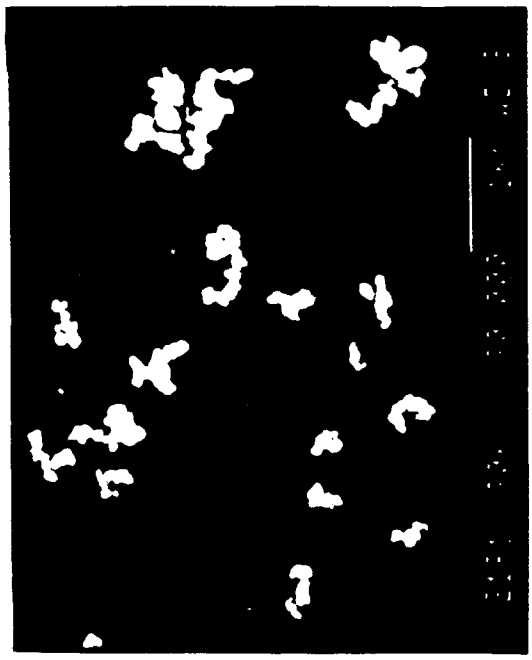

7-8O

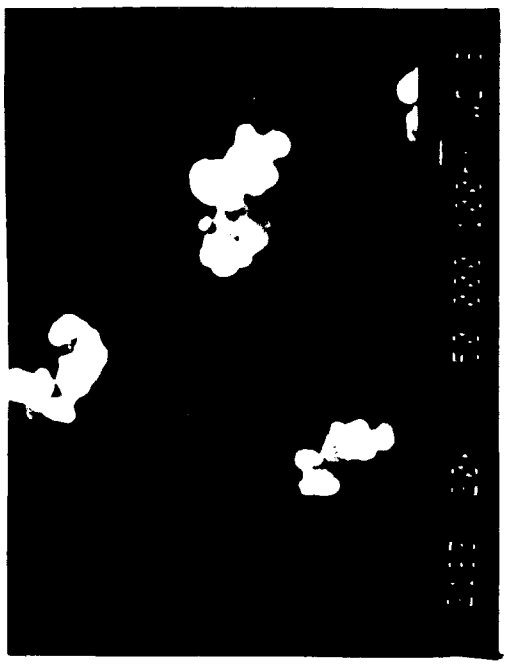

7-8P

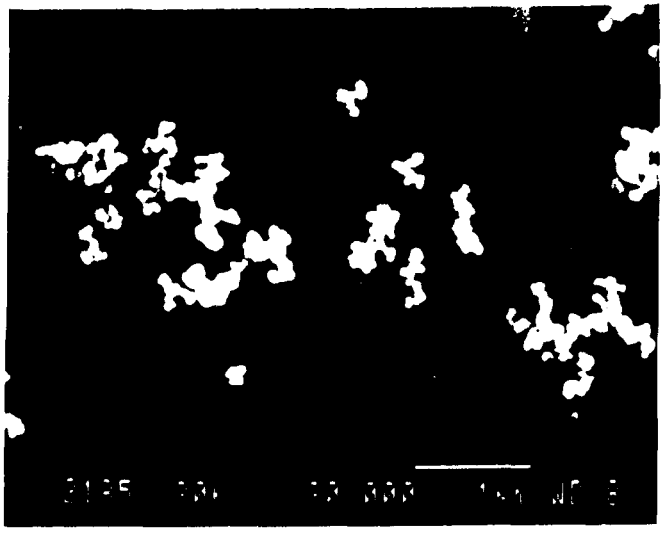

7-9B

7-9B

7-9B

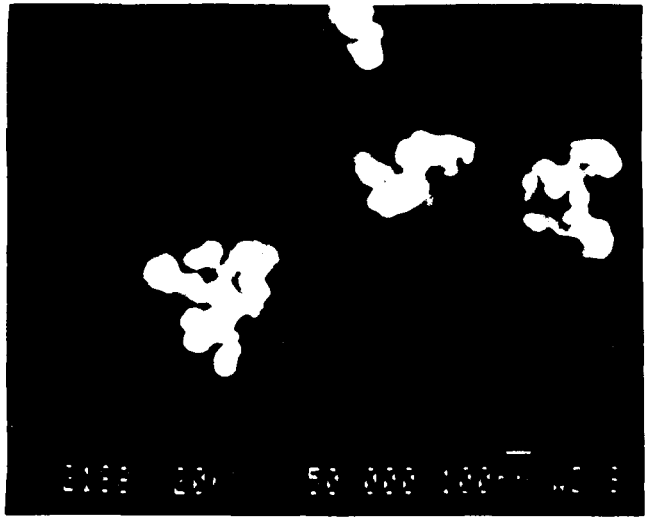

7-9B

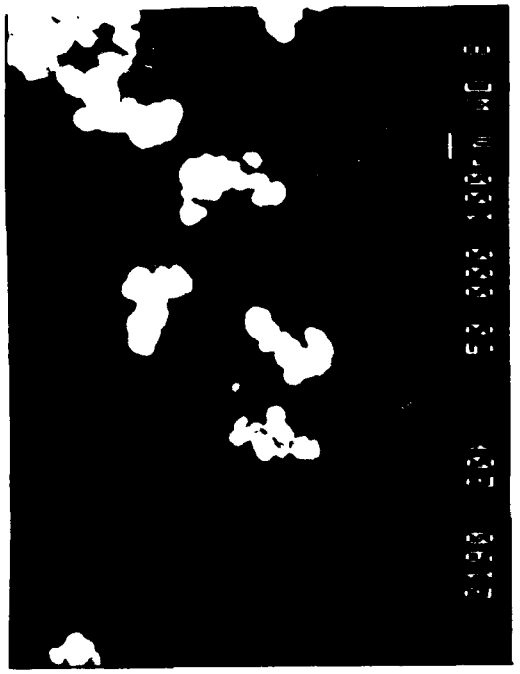

7-10B

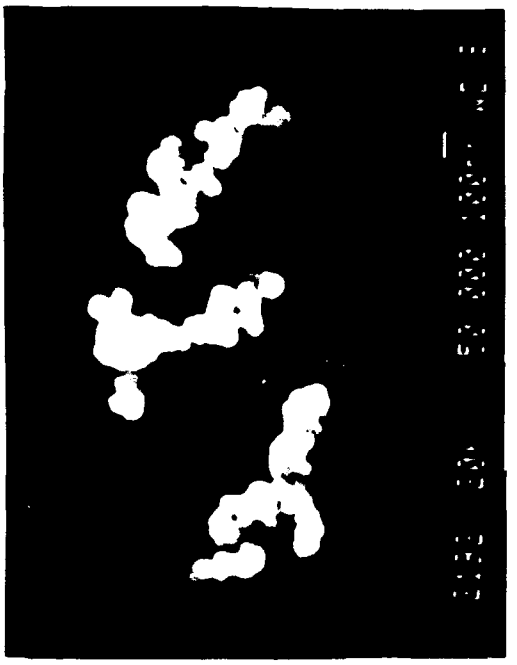

7-10B

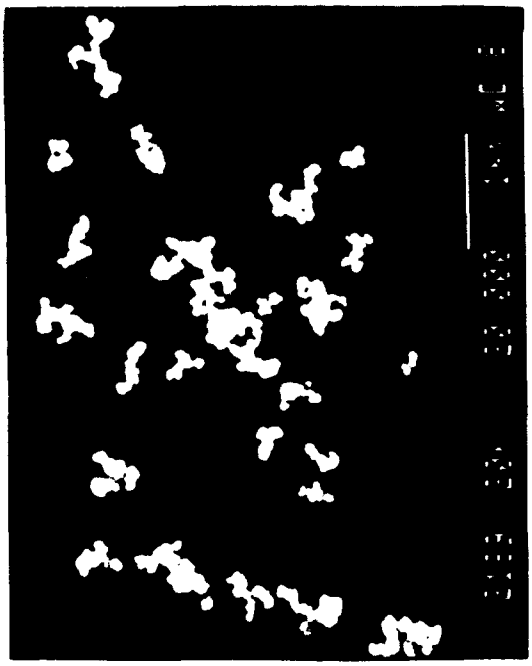

7-10B

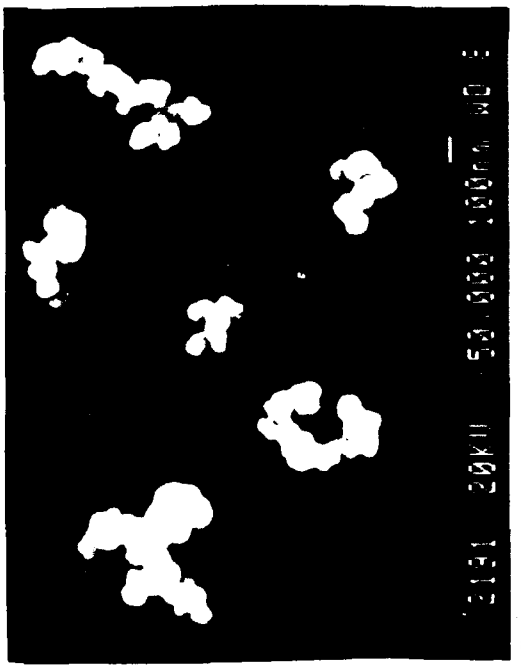

7-10B

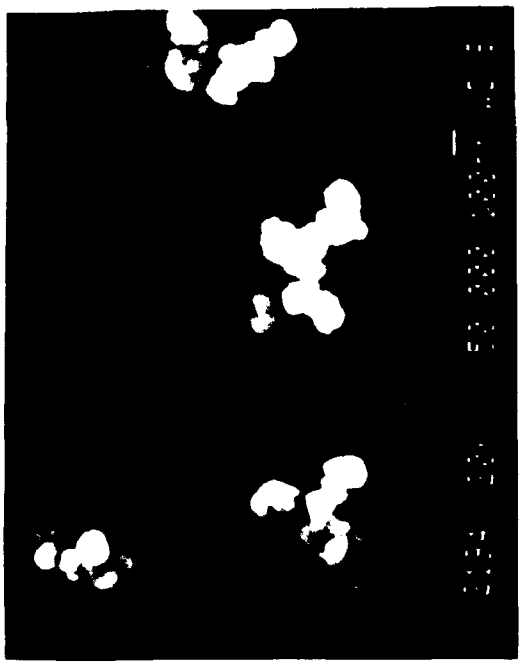

7-10P

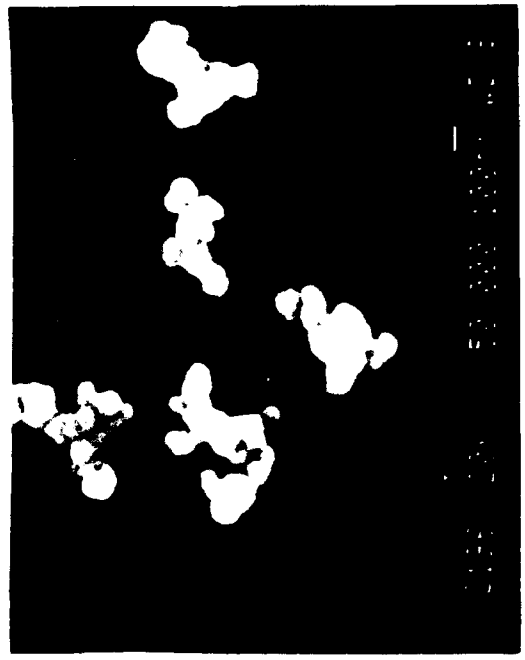

7-10P

7-10P

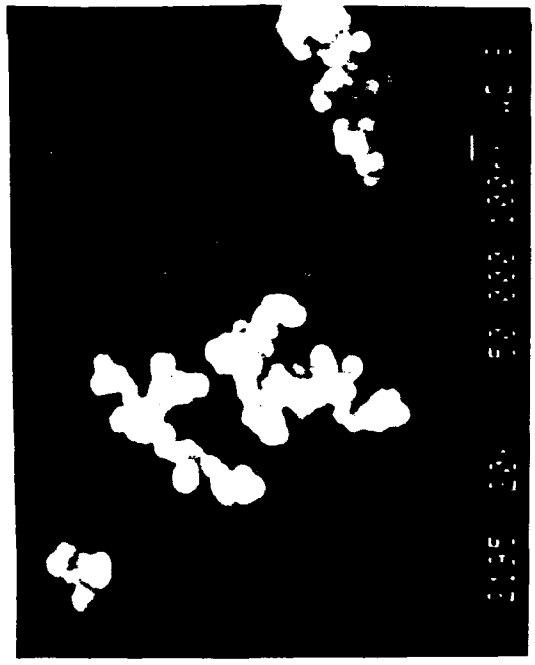

7-11P

*U.S. GOVERNMENT PRINTING OFFICE: 1991-548-076/44246 Region 5.